frontiers | Research Topics

Omics-based approaches in stroke research

Edited by
Shubham Misra and Pradeep Kumar

Published in
Frontiers in Neurology

FRONTIERS EBOOK COPYRIGHT STATEMENT

The copyright in the text of individual articles in this ebook is the property of their respective authors or their respective institutions or funders. The copyright in graphics and images within each article may be subject to copyright of other parties. In both cases this is subject to a license granted to Frontiers.

The compilation of articles constituting this ebook is the property of Frontiers.

Each article within this ebook, and the ebook itself, are published under the most recent version of the Creative Commons CC-BY licence. The version current at the date of publication of this ebook is CC-BY 4.0. If the CC-BY licence is updated, the licence granted by Frontiers is automatically updated to the new version.

When exercising any right under the CC-BY licence, Frontiers must be attributed as the original publisher of the article or ebook, as applicable.

Authors have the responsibility of ensuring that any graphics or other materials which are the property of others may be included in the CC-BY licence, but this should be checked before relying on the CC-BY licence to reproduce those materials. Any copyright notices relating to those materials must be complied with.

Copyright and source acknowledgement notices may not be removed and must be displayed in any copy, derivative work or partial copy which includes the elements in question.

All copyright, and all rights therein, are protected by national and international copyright laws. The above represents a summary only. For further information please read Frontiers' Conditions for Website Use and Copyright Statement, and the applicable CC-BY licence.

ISSN 1664-8714
ISBN 978-2-8325-5355-8
DOI 10.3389/978-2-8325-5355-8

About Frontiers

Frontiers is more than just an open access publisher of scholarly articles: it is a pioneering approach to the world of academia, radically improving the way scholarly research is managed. The grand vision of Frontiers is a world where all people have an equal opportunity to seek, share and generate knowledge. Frontiers provides immediate and permanent online open access to all its publications, but this alone is not enough to realize our grand goals.

Frontiers journal series

The Frontiers journal series is a multi-tier and interdisciplinary set of open-access, online journals, promising a paradigm shift from the current review, selection and dissemination processes in academic publishing. All Frontiers journals are driven by researchers for researchers; therefore, they constitute a service to the scholarly community. At the same time, the *Frontiers journal series* operates on a revolutionary invention, the tiered publishing system, initially addressing specific communities of scholars, and gradually climbing up to broader public understanding, thus serving the interests of the lay society, too.

Dedication to quality

Each Frontiers article is a landmark of the highest quality, thanks to genuinely collaborative interactions between authors and review editors, who include some of the world's best academicians. Research must be certified by peers before entering a stream of knowledge that may eventually reach the public - and shape society; therefore, Frontiers only applies the most rigorous and unbiased reviews. Frontiers revolutionizes research publishing by freely delivering the most outstanding research, evaluated with no bias from both the academic and social point of view. By applying the most advanced information technologies, Frontiers is catapulting scholarly publishing into a new generation.

What are Frontiers Research Topics?

Frontiers Research Topics are very popular trademarks of the *Frontiers journals series*: they are collections of at least ten articles, all centered on a particular subject. With their unique mix of varied contributions from Original Research to Review Articles, Frontiers Research Topics unify the most influential researchers, the latest key findings and historical advances in a hot research area.

Find out more on how to host your own Frontiers Research Topic or contribute to one as an author by contacting the Frontiers editorial office: frontiersin.org/about/contact

Omics-based approaches in stroke research

Topic editors

Shubham Misra — Yale University, United States

Pradeep Kumar — All India Institute of Medical Sciences, India

Citation

Misra, S., Kumar, P., eds. (2024). *Omics-based approaches in stroke research*. Lausanne: Frontiers Media SA. doi: 10.3389/978-2-8325-5355-8

Table of contents

frontiers | Frontiers in Neurology

TYPE Editorial
PUBLISHED 13 August 2024
DOI 10.3389/fneur.2024.1472912

Check for updates

OPEN ACCESS

EDITED AND REVIEWED BY
Jean-Claude Baron,
University of Cambridge, United Kingdom

*CORRESPONDENCE
Shubham Misra
shubham.misra30@gmail.com;
shubham.misra@yale.edu

RECEIVED 30 July 2024
ACCEPTED 01 August 2024
PUBLISHED 13 August 2024

CITATION
Misra S and Kumar P (2024) Editorial: Omics-based approaches in stroke research. *Front. Neurol.* 15:1472912. doi: 10.3389/fneur.2024.1472912

COPYRIGHT
© 2024 Misra and Kumar. This is an open-access article distributed under the terms of the Creative Commons Attribution License (CC BY). The use, distribution or reproduction in other forums is permitted, provided the original author(s) and the copyright owner(s) are credited and that the original publication in this journal is cited, in accordance with accepted academic practice. No use, distribution or reproduction is permitted which does not comply with these terms.

Editorial: Omics-based approaches in stroke research

Shubham Misra[1]* and Pradeep Kumar[2]

[1]Department of Neurology, Yale University School of Medicine, New Haven, CT, United States, [2]Clinical Research Unit, All India Institute of Medical Sciences, New Delhi, India

KEYWORDS

stroke, omics, biomarker, radiomics, management-healthcare

Editorial on the Research Topic
Omics-based approaches in stroke research

Stroke remains a leading cause of mortality and disability worldwide, posing substantial challenges to healthcare systems and necessitating innovative research approaches (1). Traditional epidemiological and clinical studies have provided significant insights into stroke risk factors and outcomes (2). However, the advent of omics technologies, including genomics, transcriptomics, proteomics, metabolomics, and radiomics, has revolutionized our ability to understand the molecular underpinnings of stroke (3–5). Omics-based studies have led to the discovery of potential biomarkers that can aid in early detection, risk stratification, and monitoring of stroke patients (6–9). Furthermore, these approaches can uncover novel therapeutic targets, facilitating personalized treatment strategies and the repurposing of existing drugs for stroke management (10).

The *Research Topic* "*Omics-based Approaches in Stroke Research*" in *Frontiers in Neurology* comprises nine articles that leverage omics technologies to advance stroke research. This editorial frames the goals and findings of this research, highlighting their contributions to our understanding of stroke risk, prognosis, and recovery.

Chen et al. used Mendelian randomization (MR) techniques (11) to investigate the causal associations of serum urate (SUA) with stroke risk and prognosis. They found that genetically predicted higher SUA levels increased the risk of any stroke and ischemic stroke (IS) while simultaneously improving post-stroke recovery outcomes. This dual effect was mediated, in part, by systolic and diastolic blood pressures, underscoring the intricate interplay between metabolic and cardiovascular factors in stroke pathophysiology. These findings highlight the importance of considering both the detrimental and protective roles of metabolic factors like SUA in stroke management and rehabilitation strategies. Hu et al. explored the causal relationship between the IgD-CD24-B cell absolute count (IgD-CD24-AC) and IS, along with the potential mediating role of ascorbic acid 2-sulfate (AA2S). Using an MR approach with Genome Wide Association Study data, they found that higher IgD-CD24-AC was associated with an increased IS risk. Additionally, AA2S was found to mediate a small portion of this effect, suggesting its involvement in the pathway linking IgD-CD24-AC and IS. These insights into the immune mechanisms underlying IS highlight potential targets for immune-based therapies in precision medicine. Wu et al. examined the causal relationship between hemoglobin concentration and stroke using a two-sample MR approach. Analyzing data from the UK Biobank, the FinnGen R9, and MEGASTROKE consortia, they found a negative association between hemoglobin levels and stroke risk. Specifically, higher hemoglobin was linked to a lower risk of overall stroke, IS, and cardiogenic stroke. These findings underscore the potential protective role

of hemoglobin concentration in stroke prevention and highlight the importance of managing hemoglobin levels in stroke risk reduction.

Zhang et al. investigated the role of peripheral T cells and their receptor repertoire in predicting outcomes of acute spontaneous intracerebral hemorrhage (SICH). Analyzing peripheral blood mononuclear cells from 45 ICH patients compared to healthy controls, they found that ICH was associated with reduced T cell abundance, heightened T cell activation, and altered T cell receptor (TCR) repertoire. Significant correlations between TCR diversity and clinical outcomes suggest that TCR repertoire profiling could serve as a potential biomarker for assessing ICH prognosis and highlight the need for further research into T cell mechanisms in brain injury and repair. Wang et al. explored the prognostic value of the albumin-corrected anion gap (ACAG) in patients with aneurysmal subarachnoid hemorrhage (aSAH). Comparing the predictive efficacy of ACAG and the standard anion gap (AG) in predicting 30-day mortality among 710 aSAH patients, they found that ACAG is positively correlated with mortality and performs better than AG alone in predicting outcomes. This comprehensive prognostic model showed improved predictive accuracy, suggesting that ACAG is a valuable tool for assessing risk and tailoring treatment strategies in aSAH patients. Stańczak et al. investigated whether circulating microRNA (miRNA) profiles could predict the hemorrhagic transformation (HT) risk after thrombolytic treatment in acute IS patients. Analyzing plasma samples from patients who developed HT and those who did not, they identified trends in miRNA expression changes. Notable findings included differential expression patterns that could potentially be used to predict HT risk, although further validation with larger samples is needed. This study highlights the potential of miRNA profiling, combined with additional biomarkers identified using other omics approaches, to enhance prediction models for thrombolysis-associated complications in stroke patients.

Li et al. evaluated the effectiveness of radiomics models derived from non-contrast CT (NCCT) and CT angiography (CTA) images in predicting early hematoma expansion (HE) in patients with SICH. Analyzing data from 182 patients, they created radiomics models based on NCCT and CTA images and found that these models exhibited superior performance compared to the CTA spot sign, a standard clinical marker. These results suggest that radiomics models based on NCCT and CTA are effective for predicting HE and may reduce the need for CTA, thereby lowering patient exposure to radiation and contrast agents. Nie et al. developed a radiomics model based on perivascular adipose tissue (PVAT) surrounding carotid plaques to differentiate symptomatic from asymptomatic plaques. Analyzing data from 203 patients with carotid plaques, they created a radiomics signature (RS) model that demonstrated high diagnostic performance, significantly outperforming traditional models. This RS model based on PVAT is a valuable tool for assessing plaque risk and could enhance risk stratification for carotid atherosclerotic disease.

Zhao et al. reviewed the significant advancements and applications of artificial intelligence in the neuroimaging and rehabilitation of IS patients. They highlighted that integrating radiomics with machine learning significantly enhances the predictive accuracy for acute IS outcomes. Radiomics models, utilizing imaging features from diffusion weighted imaging and NCCT, improve prognosis and risk assessment, especially after mechanical thrombectomy.

In summary, the Research Topic "*Omics-based approaches in stroke research*" provides a comprehensive overview of recent advancements in this field. The nine studies included in this topic highlight the potential of omics technologies to elucidate stroke mechanisms, discover new biomarkers, and enhance prognostic models. These findings emphasize the need for continued research to validate and implement these insights in clinical settings. We anticipate that this Research Topic will inspire further studies and contribute to the development of more personalized and effective stroke therapies and management strategies.

Author contributions

SM: Conceptualization, Methodology, Supervision, Writing – original draft, Writing – review & editing. PK: Validation, Writing – review & editing.

Funding

The author(s) declare that no financial support was received for the research, authorship, and/or publication of this article.

Acknowledgments

The authors are thankful to the contributors to this Research Topic as well as the Editorial support of the Journal.

Conflict of interest

The authors declare that the research was conducted in the absence of any commercial or financial relationships that could be construed as a potential conflict of interest.

Publisher's note

All claims expressed in this article are solely those of the authors and do not necessarily represent those of their affiliated organizations, or those of the publisher, the editors and the reviewers. Any product that may be evaluated in this article, or claim that may be made by its manufacturer, is not guaranteed or endorsed by the publisher.

References

1. GBD 2019 Stroke Collaborators. Global, regional, and national burden of stroke and its risk factors, 1990-2019: a systematic analysis for the Global Burden of Disease Study 2019. *Lancet Neurol.* (2021) 20:795–820. doi: 10.1016/S1474-4422(21)00252-0

2. O'Donnell MJ, Chin SL, Rangarajan S, Xavier D, Liu L, Zhang H, et al. Global and regional effects of potentially modifiable risk factors associated with acute stroke in 32 countries (INTERSTROKE): a case-control study. *Lancet.* (2016) 388:761–75. doi: 10.1016/S0140-6736(16)30506-2

3. Li W, Shao C, Zhou H, Du H, Chen H, Wan H, et al. Multi-omics research strategies in ischemic stroke: a multidimensional perspective. *Ageing Res Rev.* (2022) 81:101730. doi: 10.1016/j.arr.2022.101730

4. Jickling GC, Sharp FR. OMICs in stroke: insight into stroke through epigenomics, transcriptomics, proteomics, lipidomics, and metabolomics. In: Grotta JC, Albers GW, Broderick JP, Day AL, Kasner SE, Lo EH, editors. *Stroke*, 7th Edn. Philadelphia, PA: Elsevier (2022), p. 714–22.e2. doi: 10.1016/B978-0-323-69424-7.00050-8

5. Montaner J, Ramiro L, Simats A, Tiedt S, Makris K, Jickling GC, et al. Multilevel omics for the discovery of biomarkers and therapeutic targets for stroke. *Nat Rev Neurol.* (2020) 16:247–64. doi: 10.1038/s41582-020-0350-6

6. Misra S, Singh P, Nath M, Bhalla D, Sengupta S, Kumar A, et al. Blood-based protein biomarkers for the diagnosis of acute stroke: a discovery-based SWATH-MS proteomic approach. *Front Neurol.* (2022) 13:989856. doi: 10.3389/fneur.2022.989856

7. Misra S, Kawamura Y, Singh P, Sengupta S, Nath M, Rahman Z, et al. Prognostic biomarkers of intracerebral hemorrhage identified using targeted proteomics and machine learning algorithms. *PLoS ONE.* (2024) 19:e0296616. doi: 10.1371/journal.pone.0296616

8. Cheng S, Xu Z, Bian S, Chen X, Shi Y, Li Y, et al. The STROMICS genome study: deep whole-genome sequencing and analysis of 10K Chinese patients with ischemic stroke reveal complex genetic and phenotypic interplay. *Cell Discov.* (2023) 9:75. doi: 10.1038/s41421-023-00582-8

9. Balasubramanian R, Hu J, Guasch-Ferre M, Li J, Sorond F, Zhao Y, et al. Metabolomic profiles associated with incident ischemic stroke. *Neurology.* (2022) 98:e483–92. doi: 10.1212/WNL.0000000000013129

10. Hochrainer K, Yang W. Stroke proteomics: from discovery to diagnostic and therapeutic applications. *Circ Res.* (2022) 130:1145–66. doi: 10.1161/CIRCRESAHA.122.320110

11. Georgakis MK, Gill D. Mendelian randomization studies in stroke: exploration of risk factors and drug targets with human genetic data. *Stroke.* (2021) 52:2992–3003. doi: 10.1161/STROKEAHA.120.032617

frontiers | Frontiers in Neurology

TYPE Original Research
PUBLISHED 16 February 2024
DOI 10.3389/fneur.2024.1340202

Check for updates

OPEN ACCESS

EDITED BY
Shubham Misra,
Yale University, United States

REVIEWED BY
Huilin Zhao,
Shanghai Jiao Tong University, China
Arvind Bambhroliya,
University of Texas Health Science Center at Houston, United States
Yingwei Guo,
Northeastern University, China

*CORRESPONDENCE
Yu-Jin Zheng
37141116@qq.com
Qing-De Wu
wuqingde1@sohu.com

RECEIVED 17 November 2023
ACCEPTED 29 January 2024
PUBLISHED 16 February 2024

CITATION
Nie J-Y, Chen W-X, Zhu Z, Zhang M-Y, Zheng Y-J and Wu Q-D (2024) Initial experience with radiomics of carotid perivascular adipose tissue in identifying symptomatic plaque.
Front. Neurol. 15:1340202.
doi: 10.3389/fneur.2024.1340202

COPYRIGHT
© 2024 Nie, Chen, Zhu, Zhang, Zheng and Wu. This is an open-access article distributed under the terms of the Creative Commons Attribution License (CC BY). The use, distribution or reproduction in other forums is permitted, provided the original author(s) and the copyright owner(s) are credited and that the original publication in this journal is cited, in accordance with accepted academic practice. No use, distribution or reproduction is permitted which does not comply with these terms.

Initial experience with radiomics of carotid perivascular adipose tissue in identifying symptomatic plaque

Ji-Yan Nie[1,2], Wen-Xi Chen[1,2], Zhi Zhu[1,2], Ming-Yu Zhang[1,2], Yu-Jin Zheng[1]* and Qing-De Wu[1]*

[1]Department of Radiology, Shunde Hospital of Guangzhou University of Traditional Chinese Medicine, Shunde, China, [2]Graduate School, Guangzhou University of Chinese Medicine, Guangzhou, China

Background: Carotid atherosclerotic ischemic stroke threatens human health and life. The aim of this study is to establish a radiomics model of perivascular adipose tissue (PVAT) around carotid plaque for evaluation of the association between Peri-carotid Adipose Tissue structural changes with stroke and transient ischemic attack.

Methods: A total of 203 patients underwent head and neck computed tomography angiography examination in our hospital. All patients were divided into a symptomatic group (71 cases) and an asymptomatic group (132 cases) according to whether they had acute/subacute stroke or transient ischemic attack. The radiomic signature (RS) of carotid plaque PVAT was extracted, and the minimum redundancy maximum correlation, recursive feature elimination, and linear discriminant analysis algorithms were used for feature screening and dimensionality reduction.

Results: It was found that the RS model achieved the best diagnostic performance in the Bagging Decision Tree algorithm, and the training set (AUC, 0.837; 95%CI: 0.775, 0.899), testing set (AUC, 0.834; 95%CI: 0.685, 0.982). Compared with the traditional feature model, the RS model significantly improved the diagnostic efficacy for identifying symptomatic plaques in the testing set (AUC: 0.834 vs. 0.593; Z = 2.114, $p = 0.0345$).

Conclusion: The RS model of PVAT of carotid plaque can be used as an objective indicator to evaluate the risk of plaque and provide a basis for risk stratification of carotid atherosclerotic disease.

KEYWORDS

carotid atherosclerosis, perivascular adipose tissue, radiomics, stroke, transient ischemic attack

1 Introduction

Carotid atherosclerotic disease is the main cause of ischemic stroke, accounting for about 34% of ischemic stroke (1). The guidelines for the prevention and treatment of Stroke in China 2021 recommend carotid endarterectomy or carotid artery stenting for patients with more than 50% carotid artery stenosis to prevent stroke. However, the degree of carotid artery stenosis does not completely match the occurrence of stroke (2), and there is currently

a lack of objective indicators to assess the risk of stroke in carotid plaque. Head and neck computed tomography angiography (CTA) is the first line non-invasive imaging method for carotid atherosclerosis (3). Radiomics analysis of carotid plaques based on CTA has made some progress in identifying carotid plaques at high risk of stroke. However, automatic segmentation of carotid plaques is challenging due to the complex composition of plaques and the limited number of pixels in CTA images. As a consequence, the radiomic signature (RS) model derived from these segmentations often exhibits low performance and lacks universality (4). Vascular inflammation can drive atherosclerotic plaque rupture and thrombosis, leading to the occurrence of adverse cardiovascular and cerebrovascular events (5). A considerable body of recent research (6–10) has demonstrated that perivascular adipose tissue (PVAT) can be automatically segmented by applying a threshold range of −190 to -30HU on CTA, enabling the monitoring of vascular inflammation and identification of symptomatic plaques. Numerous studies (11–14) have also indicated that the pericoronary adipose tissue RS model exhibits excellent performance in identifying and predicting symptomatic plaques; however, there is limited literature available regarding carotid artery investigations.

In this study, we used radiomics analysis combined with machine learning methods to establish an RS model based on the PVAT of carotid plaques combined with traditional patient characteristics and investigated its performance in distinguishing symptomatic and asymptomatic carotid plaques.

2 Materials and methods

2.1 Study population

This was a retrospective study involving patients who underwent head and neck CTA at our hospital from April 2021 through February 2023 (Figure 1). All patients were divided into a symptomatic group and an asymptomatic group according to whether they had clinical symptoms within 2 weeks before CTA examination and/or whether a head MRI showed acute/subacute stroke (15). Clinical symptoms

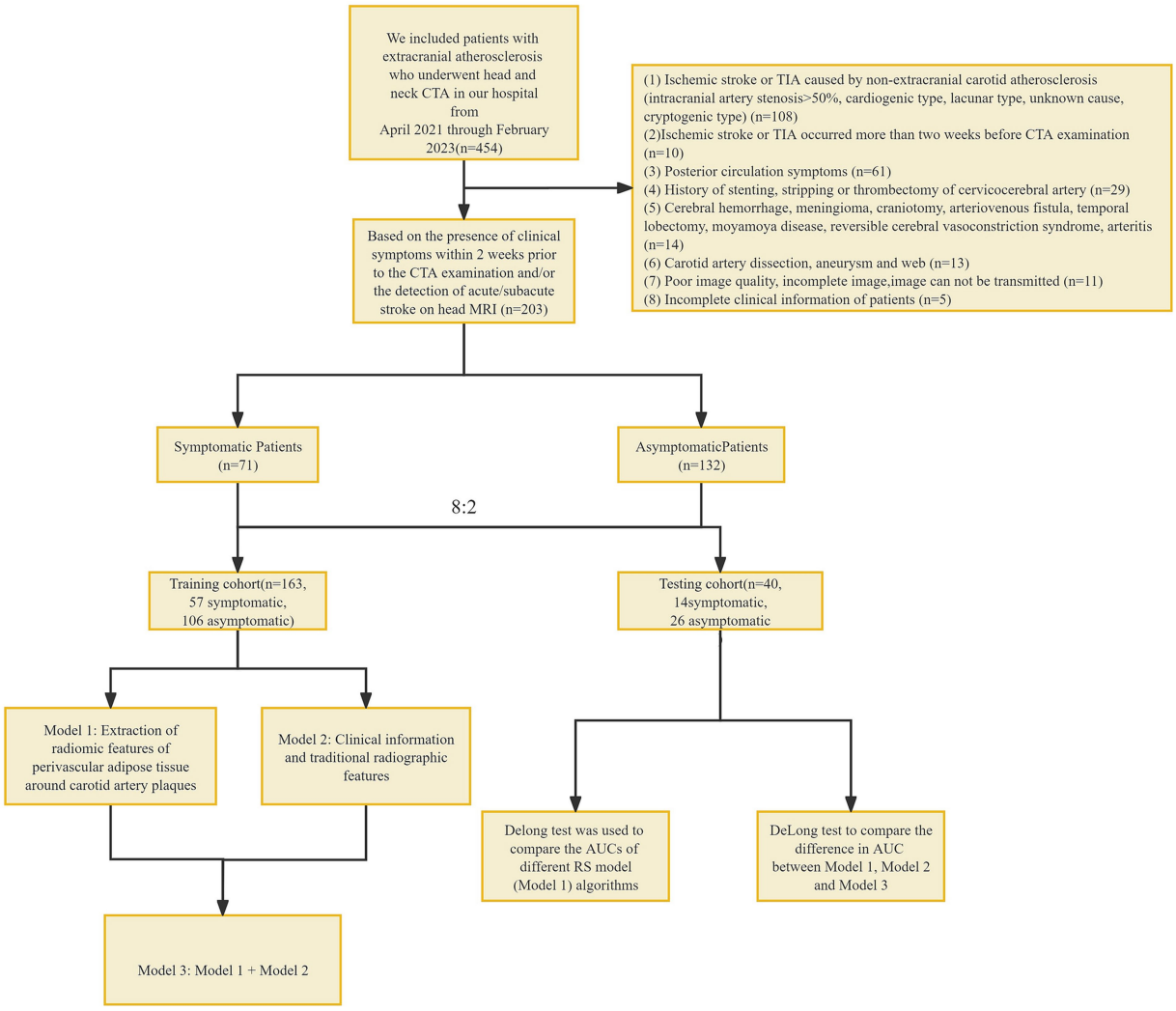

FIGURE 1
Flowchart. CTA, computed tomography angiography; TIA, transient ischemic attack, RS, radiomic signature.

included classic TIA (transient ischemic attack) and anterior circulation (carotid territory) ischemic stroke, as well as monocular symptoms ipsilateral (16) to the carotid plaque (amaurosis or retinal artery occlusion). Classic TIA is defined as an abnormal focal neurological deficit lasting less than 24 h. Complete ischemic stroke presents with the sudden onset of a focal neurologic deficit lasting >24 h (17). The patient's age, gender, body mass index (BMI), history of hypertension, diabetes, hyperlipidemia, smoking history, history of antihypertensive drugs, and history of antiplatelet drugs were collected.

Inclusion criteria: (1) extracranial carotid atherosclerosis; Exclusion criteria: (1) ischemic stroke or TIA caused by non-extracranial carotid atherosclerosis (intracranial arterial stenosis >50%, cardiogenic type, lacunar type, unknown cause, cryptogenic type) (18–24); (2) ischemic stroke or TIA occurred more than 2 weeks before CTA examination; (3) posterior circulation symptoms; (4) history of stenting, stripping or thrombectomy of cervicocerebral artery; (5) Cerebral hemorrhage, meningioma, craniotomy, arteriovenous fistula, temporal lobectomy, moyamoya disease, reversible cerebral vasoconstriction syndrome, arteritis; (6) Carotid artery dissection, aneurysm and web; (7) poor image quality, incomplete image, image cannot be transmitted; and (8) incomplete clinical information of patients. This study has been approved by the Ethics Committee of Shunde Hospital, Guangzhou University of Traditional Chinese Medicine (Ethics Review approval: KY-2022010).

2.2 CT scanning parameters

Head and neck CTA was performed using a third-generation dual-source CT (Somatom Force, Siemens). The patient was placed in a supine position with head advanced and calm breathing. The scanning direction was the foot–head direction, and the scanning range was from the level of the sternal Angle to the skull dome. A measure of 50 mL of ioversol (Bayer, Germany, iodine concentration 370 mg/mL) was injected via the cubital vein with a high pressure syringe at a rate of 5 mL/s, and 40 mL of normal saline was injected at the same flow rate. The ROI was drawn at the descending aortic arch using contrast agent tracking technology. The trigger threshold was 100HU, and the scan was delayed for 3–4 s after the trigger. The tube voltage was 90–100 KVp, and the tube current was adaptive.

2.3 Plaque data analysis

All CTA data were transferred to head and neck CTA AI system (Shukun Technology, Beijing, China) for plaque localization and analysis on curved planar reconstruction images. The symptomatic group selected the narrowest carotid plaque on the symptomatic side, and the asymptomatic group selected the narrowest carotid plaque. According to the location of the plaque, the plaque was divided into left carotid artery plaque and right carotid artery plaque. The degree of plaque stenosis was automatically calculated.

Plaque thickness was measured as the maximum axial size of the plaque on a single axial slice, representing its maximum thickness. Plaque length was defined as the distance from the origin of the plaque to the distal end. The remodeling index was calculated by averaging the maximum external vessel diameter of the plaque over the normal diameter of the proximal and distal regions.

Plaques were classified into three types based on the presence or absence of calcification: calcified plaque, non-calcified plaque, and mixed plaque. The presence of plaque ulceration was identified by the spread of a contrast agent deep into the plaque on multiple slices from different imaging perspectives. High-risk plaque is defined as having two or more of the following features: positive remodeling index >1.1, punctate calcification (with a diameter < 3 mm, occupying <1/4 of the lumen's diameter, and a CT value >130HU), low-density plaque (a non-calcified plaque with a CT value <30HU and an area of 1 mm^2 within the plaque), and the napkin ring sign (a contrast agent ring encircling a low-density plaque component, along with contrast agent in the surrounding vascular lumen).

2.4 Segmentation of plaque PVAT

ROI segmentation of the PVAT of extracranial carotid plaques was performed using perivascular fat analysis software (Shukun Technology, Beijing, China). The measurement was centered on the carotid bifurcation, extending 2 cm in the superior and inferior directions for a total length of 4 cm. The PVAT width was equivalent to the diameter of the carotid artery beyond the outer wall of the carotid artery vessel. The software automatically segmented adipose tissue with an attenuation value of −190 HU to −30 HU along the target length and width of the carotid artery vessel (25, 26) (Figure 2).

2.4.1 Fat attenuation index analysis of plaques

The Fat Attenuation Index (FAI) surrounding atherosclerotic plaques was assessed using specialized perivascular fat analysis software (Shukun Technology, Beijing, China). The length of "Stenosis FAI" is measured on the narrowest cross-sectional slice of the plaque, while the length of "Stenosis range FAI" is measured along the entire extent of the plaque, from its origin to the distal end. Both FAI measurements have a width equivalent to the diameter of the carotid artery beyond the outer wall of the carotid artery vessel. The software automatically segmented adipose tissue with an attenuation value of −190 HU to −30 HU along the target length and width of the carotid artery vessel, following which the software automatically computes the average density of the perivascular fat encompassing the plaque (Figure 2).

2.5 RS extraction and selection of plaque PVAT

2.5.1 RS extraction

ROI of all plaque PVAT was imported into Shukun AI Scientific Research Platform (Beijing, China) for RS extraction. A total of 1874 RS were extracted from the ROI of each plaque PVAT. These included 360 first-order features, 14 shape features, 480 gray level co-occurrence matrix (GLCM), 280 gray level dependence matrix (GLDM), 320 gray level run length matrix (GLRLM), 320 gray level size zone matrix (GLSZM), and 100 neighborhood gray tone difference matrix (NGTDM).

2.5.2 RS selection and model construction

All the extracted features were imported into uAI Research Portal software (version 1.1, United, China) for feature selection and model

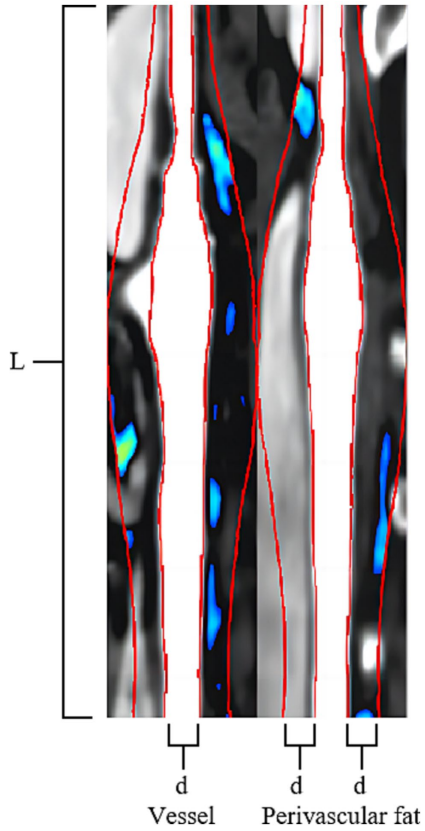

FIGURE 2
Carotid Plaque PVAT Segmentation Image. The Carotid Artery Straightening Image reveals a calcified plaque located at the bifurcation of the carotid artery. The red line was centered on the carotid bifurcation, extending 2 cm in the superior and inferior directions for a total length of 4 cm (L). The PVAT width of two red lines is equivalent to the diameter of the carotid artery beyond the outer wall of the carotid artery vessel (d). The software automatically segmented adipose tissue with an attenuation value of −190 HU to −30 HU along the target length and the width of the carotid artery vessel is visualized using a blue-green pseudocolored map.

construction. (1) The minimum redundancy maximum relevance (MRMR) algorithm is utilized to calculate the redundancy and relevance between each feature and the target variable, symptomatic plaques. Subsequently, 100 features are selected. A recursive feature elimination (RFE) algorithm selects feature subset by eliminating features with small contributions to prediction ability step by step. It determines the most important features for the prediction task by recursively training the model and evaluating feature importance. The RFE has been applied to select the most important features, resulting in 48 features, comprising 16 first-order features, 7 CLCM features, 6 GLDM features, 3 GLRLM features, 10 GLSZM features, 4 NGTDM features, and 2 shape features. (2) Linear discriminant analysis (LDA) is employed to reduce the dimensionality of the selected imaging features to 20 target dimensions. By using an mRMR algorithm, RFE algorithm, and LDA together, we can achieve several objectives: improving the effectiveness of feature selection, removing redundant and noisy features, extracting features with high classification ability, and reducing dimensionality. Through the comprehensive application of these methods, more robust and superior feature subsets can be obtained, which is helpful for better image-based radiomic analysis and model construction. (3) Machine learning models, including Bagging DecisionTree, XGBOOST, Random Forest, Support Vector Machine (SVM), and Quadratic Discriminant Analysis (QDA), are constructed Model 1 (RS model). The patients were divided into training set ($n = 163$) and test set ($n = 40$) according to the ratio of 8:2.

2.6 Statistical analysis

The data analysis was performed using SPSS 25.0, MedCalc 22.014, and uAI Research Portal software (version 1.1, United, China). Kolmogorov–Smirnov was used to test the normality of measurement data. Continuous variables were expressed as mean ± SDs or median and interquartile range as appropriate. Categorical variables were reported as count and percentage. Continuous variables were compared with the Student *t*-test or Mann–Whitney test. Categorical variables were compared using $\chi 2$ or the Fisher exact test. Univariate logistic regression was employed to analyze the correlation between the traditional features of each patient and symptomatic plaques. Features with $p < 0.05$ in the univariate logistic regression were included in the multivariate logistic regression analysis for further analysis.

In order to investigate if carotid PVAT imaging RS provides additional value in diagnosing symptomatic plaques compared to traditional plaque analysis, two models were developed. Model 2 (Traditional model) included different clinical and conventional CTA imaging features between symptomatic and asymptomatic patient groups in a multivariate logistic regression analysis. Model 3 (Combined model): Model 2 was enhanced by incorporating the Model 1. The machine learning algorithm parameters used in both models were identical to those in Model 1. Area Under the Curve (AUC) was used to evaluate the ability of the two groups of models to identify symptomatic plaques. The deLong test was used to compare the differences between AUCs. $p < 0.05$ was considered statistically significant (Figure 3).

3 Results

3.1 Characteristics of the study patients

This study included a total of 203 patients, with an average age of 71.87 ± 9.63 years and a total of 115 men. Among them, there were 71 cases in the symptomatic group and 132 cases in the asymptomatic group.

In the multivariate logistic regression analysis, it was found that the proportion of positive remodeling in the symptomatic group was higher than that in the asymptomatic group (97.2% vs. 84.8%, $p = 0.017$). Additionally, the proportion of statin use in the symptomatic group was significantly lower than that in the asymptomatic group (15.5% vs. 47%, $p < 0.001$).

Other factors such as age, gender, BMI, history of hypertension, diabetes mellitus, hyperlipidemia, smoking history, history of antihypertensive drugs, history of antiplatelet drugs, plaque location, degree of plaque stenosis, plaque length, plaque thickness,

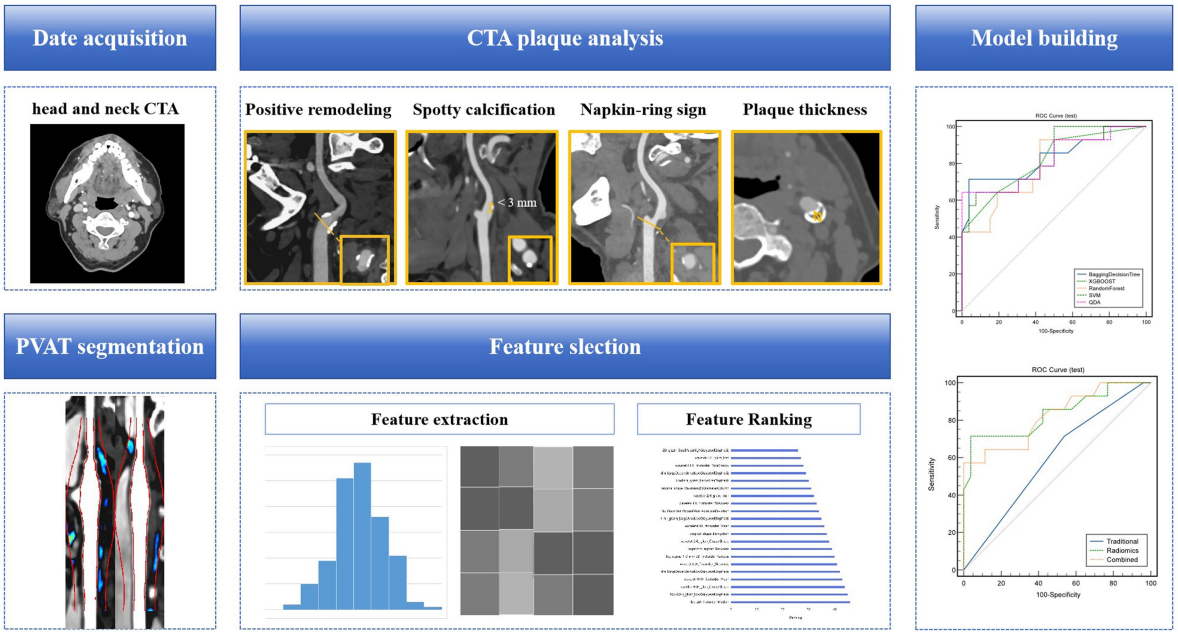

FIGURE 3
A flow chart of the model development process. Collect clinical and radiological information of patients, analyze and extract traditional features of carotid artery plaques. Based on head and neck CTA, segment the PVAT of carotid artery plaques, extract radiomics features, and use algorithms such as minimal redundancy maximal relevance, recursive feature elimination, and linear discriminant analysis for feature selection and dimensionality reduction. Construct a machine learning model for identifying symptomatic plaques using radiomics features, traditional features (clinical + traditional radiological features), and a combination of radiomics and traditional features. CTA, computed tomography angiography; PVAT, perivascular adipose tissue.

remodeling index, FAI at the most stenosis of the plaque, FAI within the stenosis of the plaque, conformal remodeling, low-density plaque, punctate calcification, napkin ring sign, and high-risk plaque distribution, plaque type, and plaque ulcer did not show statistically significant differences in the multivariate regression analysis ($p > 0.05$) (Table 1).

3.2 RS model of carotid PVAT

The RS model showed the highest diagnostic performance in identifying symptomatic plaques within the Bagging Decision Tree model, achieving an AUC of 0.837 (95%CI: 0.775, 0.899) in the training set and an AUC of 0.834 (95%CI: 0.685, 0.982) in the testing set. These results were significantly better than the performances of the XGBOOST, Random Forest, SVM, and QDA models ($p < 0.05$) (Figure 4; Table 2).

3.3 RS combined with the traditional model

Figure 5 depicts the diagnostic performance of traditional feature models and the RS model in identifying symptomatic plaques across different sets of data. In the training set, the traditional feature model achieved an AUC of 0.725 (95%CI: 0.695, 0.791), while in the testing set, the AUC was 0.593 (95%CI: 0.438, 0.749). Upon incorporating the RS model into the traditional feature model, the AUC in the training set improved to 0.831 (95%CI: 0.765, 0.896), and in the testing set, it reached 0.82 (95%CI: 0.675, 0.965).

Through the Delong test, it was determined that the combination of the RS model with the traditional feature model yielded a significantly higher AUC for distinguishing symptomatic plaques compared to using the traditional model alone (AUC: 0.82 vs. AUC: 0.593; $Z = 2.822$, $p = 0.0048$). Furthermore, when used independently, the RS model demonstrated a superior AUC in differentiating symptomatic plaques compared to the traditional model (AUC: 0.834 vs. AUC: 0.593; $Z = 2.114$, $p = 0.0345$).

4 Discussion

This study confirms that the RS model, based on carotid PVAT, has demonstrated significant improvement over the current traditional models in distinguishing symptomatic plaques. The RS model, relying on carotid PVAT, exhibited a higher AUC in the discrimination of symptomatic plaques (AUC: 0.834; 95% CI: 0.685, 0.982), compared to the traditional model (AUC: 0.593; 95% CI: 0.438, 0.749).

CT-based radiomics has been shown to be able to accurately classify diseases by extracting a large number of quantitative radiomics features that are invisible to the human eye (27). In this study, the diagnostic performance of the RS model, based on carotid PVAT, in distinguishing symptomatic plaques was evaluated in both the training set (AUC: 0.837; 95% CI: 0.775, 0.899) and the testing set (AUC: 0.834; 95% CI: 0.685, 0.982). In a study conducted by Chen et al. (4), which included 60 symptomatic and 84 asymptomatic individuals based on the occurrence of ischemic stroke or TIA within a 2 week period, the RS model based on carotid plaque PVAT demonstrated an AUC of 0.740 (95% CI: 0.644, 0.835) in the training set and 0.618 (95% CI:

10.3389/fneur.2024.1340202

TABLE 1 Traditional characteristics of the patient.

Characteristic	ALL patients	Symptomatic	Asymptomatic	Univariate analysis	Multivariate	
					OR (95% CI)	*p* value
Clinical characteristics						
Age, y, mean ± SD	71.87 ± 9.63	72.38 ± 9.54	71.59 ± 9.7	0.579		
No. of men, *n* (%)	115 (56.7)	39 (54.9)	76 (57.6)	0.717		
BMI, kg/m2, mean ± SD	23.34 ± 3.12	22.8 ± 2.83	23.63 ± 3.24	0.073		
Risk factors						
Hypertension, *n* (%)	155 (76.4)	55 (77.5)	100 (75.8)	0.785		
Diabetes mellitus, *n* (%)	72 (35.5)	28 (39.4)	44 (33.3)	0.386		
Hyperlipidemia, *n* (%)	50 (24.6)	19 (26.8)	31 (23.5)	0.605		
Smoking, *n* (%)	55 (27.1)	24 (33.8)	31 (23.5)	0.115		
History of medications						
Antihypertension use, *n* (%)	155 (76.4)	55 (77.5)	100 (75.8)	0.785		
Statin use, *n* (%)	73 (36)	11 (15.5)	62 (47)	< 0.001	4.950 (2.336, 10.492)	<0.001
Antiplatelet use, *n* (%)	90 (44.3)	32 (45.1)	58 (43.9)	0.877		
Quantitative plaque characteristics						
Diameter stenosis, %, mean ± SD	34.31 ± 22.95	32.08 ± 21.55	35.51 ± 23.67	0.31		
Lesion length, mm, mean ± SD	1.08 ± 7.68	1.02 ± 7.53	11.07 ± 7.78	0.462		
Plaque thickness, mm, mean ± SD	3.45 ± 1.47	3.25 ± 1.28	3.56 ± 1.56	0.154		
Remodeling index, mean ± SD	1.40 ± 0.25	1.43 ± 0.25	1.39 ± 0.25	0.224		
Stenosis FAI, HU, mean ± SD	−65.29 ± 13.83	−63.02 ± 14.31	−66.51 ± 13.46	0.087		
Stenosis range FAI, HU, mean ± SD	−66.06 ± 0.89	−63.99 ± 12.87	−67.18 ± 12.41	0.086		
Quantitative plaque characteristics						
Positive remodeling, *n* (%)	181 (89.2)	69 (97.2)	112 (84.8)	0.016	0.102 (0.016, 0.671)	0.017
Low-attenuation plaque, *n* (%)	23 (11.3)	10 (14.1)	13 (9.8)	0.366		
Spotty calcification, *n* (%)	129 (63.5)	54 (76.1)	75 (56.8)	0.007	0.220 (0.040, 1.205)	0.081
Napkin-ring sign, *n* (%)	10 (4.9)	3 (4.2)	7 (5.3)	0.736		
High-risk plaque, *n* (%)	126 (62.1)	54 (76.1)	72 (54.5)	0.003	1.839 (0.328, 10.308)	0.488
Plaque ulcer, *n* (%)	39 (19.2)	13 (18.3)	26 (19.7)	0.811		
Plaque location(L), *n* (%)	100 (49.3)	40 (56.3)	60 (45.5)	0.139		
Plaque Type, *n* (%)				0.773		
Calcified plaque, *n* (%)	114 (56.2)	42 (59.2)	72 (54.5)			
Non-calcified plaque, *n* (%)	14 (6.9)	4 (5.6)	10 (7.6)			
Mixed plaque, *n* (%)	75 (36.9)	25 (35.2)	50 (37.9)			

BMI, body mass index. Data are displayed as mean (SD) or number (percent).

0.440, 0.794) in the testing set (4). The relatively higher ROC performance observed in our study compared to Chen et al. may be attributed to the fact that Chen et al. extracted PVAT pixel values from the surrounding adipose tissue around the maximum stenosis level of the carotid plaque, resulting in fewer PVAT pixel values and a 2D image. Consequently, the performance of their RS model was relatively lower.

Recently, progress has been made in utilizing carotid plaque RS to differentiate symptomatic plaques. Xia et al. conducted a study on 179 patients with 219 carotid plaques, stratifying them into a

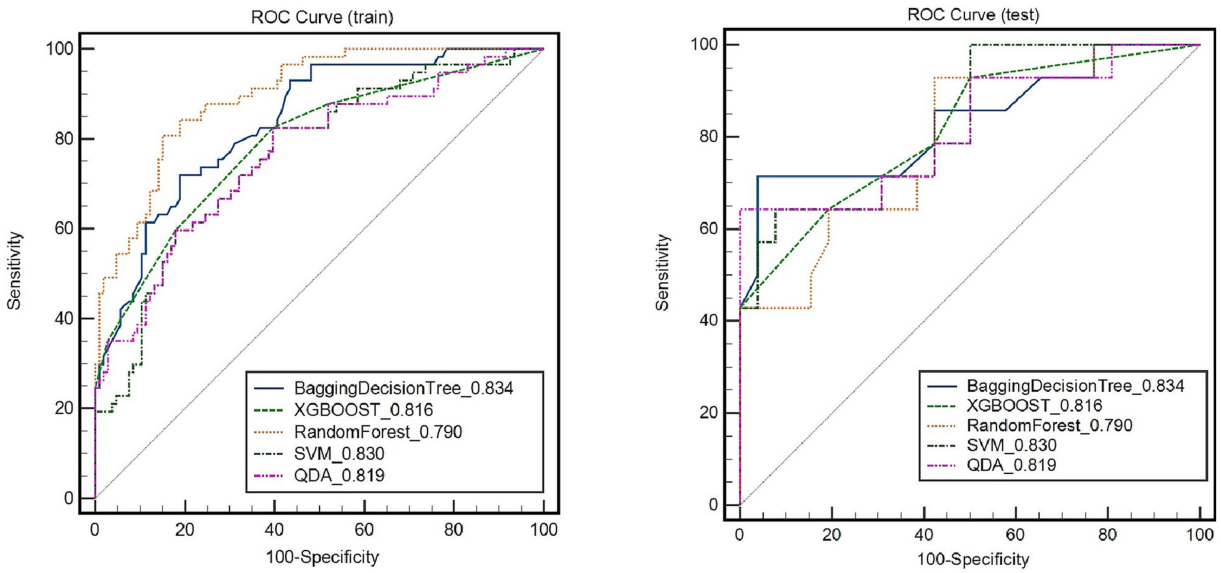

FIGURE 4
Receiver operating characteristic (ROC) curves of radiomic signature in identifying symptomatic plaques in different models.

TABLE 2 Predictive ability of all radiomics models.

Model	Training cohort				Testing cohort			
	AUC (95% CI)	SPE	SEN	ACC	AUC (95% CI)	SPE	SEN	ACC
Bagging decision-tree	0.837 (0.775, 0.899)	0.811	0.702	0.773	0.834 (0.685, 0.982)	0.731	0.714	0.725
XGBOOST	0.79 (0.717, 0.863)	0.821	0.596	0.742	0.816 (0.675, 0.957)	0.808	0.643	0.75
Random forest	0.897 (0.85, 0.944)	0.849	0.754	0.816	0.79 (0.64, 0.94)	0.808	0.643	0.75
SVM	0.762 (0.685, 0.839)	0.774	0.614	0.718	0.83 (0.694, 0.965)	0.643	0.769	0.725
QDA	0.765 (0.686, 0.843)	0.821	0.698	0.687	0.819 (0.665, 0.972)	0.714	0.692	0.7

AUC, area under the curve.

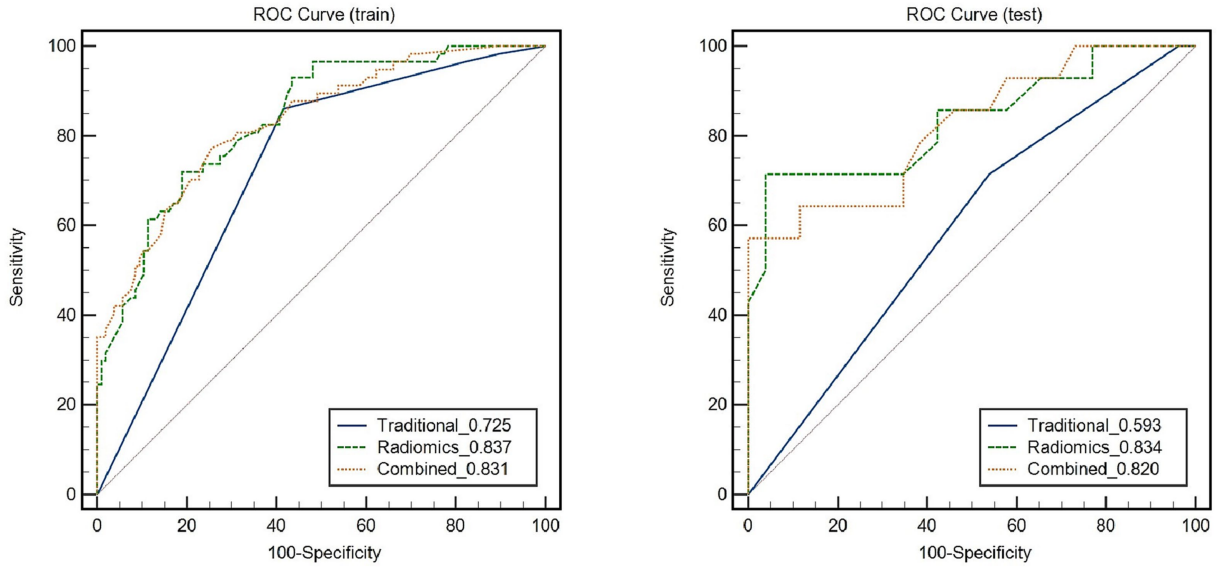

FIGURE 5
Receiver Operating Characteristic (ROC) curves demonstrate the diagnostic performance of symptomatic plaques in different feature sets.

TIA group and a non-TIA group according to the presence or absence of TIA after CTA examination (28). Their RS model for distinguishing the TIA group yielded a maximum AUC of 0.746 in the testing set. Our study shows an RS model based on carotid PVAT with a testing set AUC of 0.834, thus indicating superior diagnostic performance compared to Xia et al.'s study on a carotid plaque RS model. This suggests that the carotid PVAT-based RS model has the potential to provide additional benefits in identifying symptomatic plaques.

A large study showed (29) that long-term achievement of low LDL-C levels, as low as less than 20 mg per deciliter (<0.5 mmol per liter), was associated with a reduced risk of cardiovascular outcomes without significant safety concerns in patients with atherosclerotic cardiovascular and cerebrovascular disease. The lower proportion of statin use in the symptomatic group than in the asymptomatic group in this study may be due to the higher incidence of ischemic stroke or TIA in patients who do not receive statin therapy.

There was no significant difference in FAI at the narrowest point of the plaque and within the stenosis of the plaque between the two groups, which may be related to the fact that most of the patients in this study were elderly with an average age of 71.87 ± 9.63 years. FAI is used to dynamically monitor vascular inflammation (5) by measuring the mean density of adipose tissue on CT to reflect the change in lipid content. The patients in this study have a long history of atherosclerosis, PVAT of carotid plaque has gone into the chronic phase, lipid fibrosis and microvascular remodeling occur, and the dynamic change of lipid content is small (11, 30), so the ability of FAI to dynamically monitor vascular inflammation is limited (11). At the same time, Serum C reactive protein (CRP) is a marker of systemic inflammation and is associated with an increased risk of stroke and unstable carotid atherosclerotic plaques (31). However, high-sensitivity CRP is usually driven by other inflammatory conditions such as infection, arthritis, etc., and cannot specifically reflect the local inflammation of carotid atherosclerosis. PET is considered to be the most reliable non-invasive imaging modality for vascular inflammation. However, its clinical application is limited due to its low spatial resolution, high radiation exposure, and high cost. In our study, the RS of carotid PVAT was available, and the diagnostic efficacy of the RS model of carotid PVAT in identifying symptomatic plaques was 0.745. RS analysis can accurately capture the texture changes of PVAT and reflect the level of vascular inflammation.

The carotid plaque PVAT extracted in this study was extended 2 cm above and below the center of the carotid segment bifurcation, with a total of 4 cm as the longitudinal measurement distance. Because of the vascular shear stress (32), the vast majority of extracranial carotid plaques were distributed at the carotid bifurcation, and the plaques of the cases included in this study were distributed within 2 cm above and below the carotid bifurcation. Second, there was little fat distribution around the carotid artery, and the plaques of the cases included in this study were distributed in the range of 2 cm above and below the carotid bifurcation. This study referred to the method of extracting the proximal 4 cm PVAT of the coronary artery with pericoronary fat and appropriately increased the collection range of the PVAT of carotid plaques to ensure the accuracy of RS extraction in PVAT. Third, Oikonomou et al. (25) showed that perivascular FAI at 4 cm proximal to the right coronary artery can reflect global coronary inflammation and predict cardiac mortality. In our study, PVAT at 4 cm of the carotid bifurcation also has the potential to represent the risk of vascular inflammation at the carotid bifurcation plaque and the whole carotid artery segment.

This paper has the following limitations: (1) This paper adopts the mainstream method used in current related research to identify symptomatic plaques, but it lacks a gold standard. In the future, we aim to collect plaque samples through carotid artery stripping and other procedures to accurately identify culprit plaques; (2) The lack of external validation datasets to evaluate the diagnostic efficacy of machine learning models; and (3) As symptomatic and asymptomatic determination of plaques happens before CTA exams, it would have selection bias towards the model performance in the real clinical settings. In the next step of our research, we will conduct a prospective study on patients undergoing head and neck CTA to explore the association between PVAT imaging-based radiomics of carotid plaques and the occurrence of acute ischemic cerebrovascular events.

5 Conclusion

The RS model of carotid plaque PVAT, when combined with the traditional feature model, demonstrates a significant improvement in the diagnostic performance for identifying symptomatic plaques compared to the traditional feature model alone. This indicates that the RS model of carotid plaque PVAT can serve as an objective indicator for evaluating plaque risk, providing a basis for risk stratification, as well as the diagnosis and treatment of carotid atherosclerotic diseases.

Data availability statement

The raw data supporting the conclusions of this article will be made available by the authors, without undue reservation.

Ethics statement

The studies involving humans were approved by Shunde Hospital of Guangzhou University of Chinese Medicine. The studies were conducted in accordance with the local legislation and institutional requirements. The participants provided their written informed consent to participate in this study. Written informed consent was obtained from the individual(s) for the publication of any potentially identifiable images or data included in this article.

Author contributions

J-YN: Conceptualization, Data curation, Formal analysis, Investigation, Methodology, Writing – original draft. W-XC: Data curation, Formal analysis, Methodology, Writing – review & editing. ZZ: Writing – review & editing. M-YZ: Data curation, Formal analysis, Methodology, Writing – review & editing. Y-JZ: Data curation, Funding acquisition, Supervision, Writing – review & editing. Q-DW:

Conceptualization, Funding acquisition, Methodology, Writing – review & editing.

Funding

The author(s) declare financial support was received for the research, authorship, and/or publication of this article. This research was funded by dedicated project of Shunde Hospital, Guangzhou University of Chinese Medicine (Grant No. YNZX20220014), 2022 Foshan competitive Support Talent Project Special and Cultivation Project (Grant No. FSRC20220008) and Postgraduate project of Shunde Hospital, Guangzhou University of Chinese Medicine (Grant No. KY-2023072).

Conflict of interest

The authors declare that the research was conducted in the absence of any commercial or financial relationships that could be construed as a potential conflict of interest.

Publisher's note

All claims expressed in this article are solely those of the authors and do not necessarily represent those of their affiliated organizations, or those of the publisher, the editors and the reviewers. Any product that may be evaluated in this article, or claim that may be made by its manufacturer, is not guaranteed or endorsed by the publisher.

References

1. Smith-Bindman R, Bibbins-Domingo K. USPSTF recommendations for screening for carotid stenosis to prevent stroke-the need for more data. *JAMA Netw Open*. (2021) 4:e2036218. doi: 10.1001/jamanetworkopen.2020.36218

2. Brinjikji W, Huston J, Rabinstein AA, Kim GM, Lerman A, Lanzino G. Contemporary carotid imaging: from degree of stenosis to plaque vulnerability. *J Neurosurg*. (2016) 124:27–42. doi: 10.3171/2015.1.JNS142452

3. Giordano C, Morello A, Corcione N, Giordano S, Gaudino S, Colosimo C. Choice of imaging to evaluate carotid stenosis and guide management. *Minerva Med*. (2022) 113:1017–26. doi: 10.23736/S0026-4806.22.07996-4

4. Chen C, Tang W, Chen Y, Xu W, Yu N, Liu C, et al. Computed tomography angiography-based radiomics model to identify high-risk carotid plaques. *Quant Imaging Med Surg*. (2023) 13:6089–104. doi: 10.21037/qims-23-158

5. Antonopoulos AS, Sanna F, Sabharwal N, Thomas S, Oikonomou EK, Herdman L, et al. Detecting human coronary inflammation by imaging perivascular fat. *Sci Transl Med*. (2017) 9:eaal2658. doi: 10.1126/scitranslmed.aal2658

6. Adachi Y, Ueda K, Nomura S, Ito K, Katoh M, Katagiri M, et al. Beiging of perivascular adipose tissue regulates its inflammation and vascular remodeling. *Nat Commun*. (2022) 13:5117. doi: 10.1038/s41467-022-32658-6

7. Cheng CK, Ding H, Jiang M, Yin H, Gollasch M, Huang Y. Perivascular adipose tissue: fine-tuner of vascular redox status and inflammation. *Redox Biol*. (2023) 62:102683. doi: 10.1016/j.redox.2023.102683

8. Park K, Li Q, Lynes MD, Yokomizo H, Maddaloni E, Shinjo T, et al. Endothelial cells induced progenitors into Brown fat to reduce atherosclerosis. *Circ Res*. (2022) 131:168–83. doi: 10.1161/CIRCRESAHA.121.319582

9. Czamara K, Majka Z, Stanek E, Hachlica N, Kaczor A. Raman studies of the adipose tissue: current state-of-art and future perspectives in diagnostics. *Prog Lipid Res*. (2022) 87:101183. doi: 10.1016/j.plipres.2022.101183

10. Lee S, Sung JM, Andreini D, Al-Mallah MH, Budoff MJ, Cademartiri F, et al. Association between changes in perivascular adipose tissue density and plaque progression. *J Am Coll Cardiol Img*. (2022) 15:1760–7. doi: 10.1016/j.jcmg.2022.04.016

11. Oikonomou EK, Williams MC, Kotanidis CP, Desai MY, Marwan M, Antonopoulos AS, et al. A novel machine learning-derived radiotranscriptomic signature of perivascular fat improves cardiac risk prediction using coronary CT angiography. *Eur Heart J*. (2019) 40:3529–43. doi: 10.1093/eurheartj/ehz592

12. Ichikawa K, Miyoshi T, Osawa K, Nakashima M, Miki T, Nishihara T, et al. High pericoronary adipose tissue attenuation on computed tomography angiography predicts cardiovascular events in patients with type 2 diabetes mellitus: post-hoc analysis from a prospective cohort study. *Cardiovasc Diabetol*. (2022) 21:44. doi: 10.1186/s12933-022-01478-9

13. You H, Zhang R, Hu J, Sun Y, Li X, Hou J, et al. Performance of Radiomics models based on coronary computed tomography angiography in predicting the risk of major adverse cardiovascular events within 3 years: a comparison between the Pericoronary adipose tissue model and the Epicardial adipose tissue model. *Acad Radiol*. (2023) 30:390–401. doi: 10.1016/j.acra.2022.03.015

14. Antonopoulos AS, Angelopoulos A, Papanikolaou P, Simantiris S, Oikonomou EK, Vamvakaris K, et al. Biomarkers of vascular inflammation for cardiovascular risk prognostication: a meta-analysis. *J Am Coll Cardiol Img*. (2022) 15:460–71. doi: 10.1016/j.jcmg.2021.09.014

15. Li H, Liu J, Dong Z, Chen X, Zhou C, Huang C, et al. Identification of high-risk intracranial plaques with 3D high-resolution magnetic resonance imaging-based radiomics and machine learning. *J Neurol*. (2022) 269:6494–503. doi: 10.1007/s00415-022-11315-4

16. Olthuis SGH, Pirson FAV, Pinckaers FME, Hinsenveld WH, Nieboer D, Ceulemans A, et al. Endovascular treatment versus no endovascular treatment after 6-24 h in patients with ischaemic stroke and collateral flow on CT angiography (MR CLEAN-LATE) in the Netherlands: a multicentre, open-label, blinded-endpoint, randomised, controlled, phase 3 trial. *Lancet*. (2023) 401:1371–80. doi: 10.1016/S0140-6736(23)00575-5

17. Chun M, Qin H, Turnbull I, Sansome S, Gilbert S, Hacker A, et al. Heterogeneity in the diagnosis and prognosis of ischemic stroke subtypes: 9-year follow-up of 22,000 cases in Chinese adults. *Int J Stroke*. (2023) 18:847–55. doi: 10.1177/17474930231162265

18. Kopczak A, Schindler A, Sepp D, Bayer-Karpinska A, Malik R, Koch ML, et al. Complicated carotid artery plaques and risk of recurrent ischemic stroke or TIA. *J Am Coll Cardiol*. (2022) 79:2189–99. doi: 10.1016/j.jacc.2022.03.376

19. van Dam-Nolen DHK, Truijman MTB, van der Kolk AG, Liem MI, Schreuder FHBM, Boersma E, et al. Carotid plaque characteristics predict recurrent ischemic stroke and TIA: the PARISK (plaque at RISK) study. *J Am Coll Cardiol Img*. (2022) 15:1715–26. doi: 10.1016/j.jcmg.2022.04.003

20. Zhang X, Hua Z, Chen R, Jiao Z, Shan J, Li C, et al. Identifying vulnerable plaques: a 3D carotid plaque radiomics model based on HRMRI. *Front Neurol*. (2023) 14:1050899. doi: 10.3389/fneur.2023.1050899

21. Chen Y, Chen Z, Lin Y, Lin Z, Chen C, Yang M, et al. Stroke risk study based on deep learning-based magnetic resonance imaging carotid plaque automatic segmentation algorithm. *Front Cardiovasc Med*. (2023) 10:1101765. doi: 10.3389/fcvm.2023.1101765

22. Gao S, Wang YJ, Xu AD, Li YS, Wang DZ. Chinese ischemic stroke subclassification. *Front Neurol*. (2011) 2:6. doi: 10.3389/fneur.2011.00006

23. Saba L, Loewe C, Weikert T, Williams MC, Galea N, Budde RPJ, et al. State-of-the-art CT and MR imaging and assessment of atherosclerotic carotid artery disease: standardization of scanning protocols and measurements-a consensus document by the European Society of Cardiovascular Radiology (ESCR). *Eur Radiol*. (2023) 33:1063–87. doi: 10.1007/s00330-022-09024-7

24. Jickling GC, Stamova B, Ander BP, Zhan X, Tian Y, Liu D, et al. Profiles of lacunar and nonlacunar stroke. *Ann Neurol*. (2011) 70:477–85. doi: 10.1002/ana.22497

25. Oikonomou EK, Marwan M, Desai MY, Mancio J, Alashi A, Hutt Centeno E, et al. Non-invasive detection of coronary inflammation using computed tomography and prediction of residual cardiovascular risk (the CRISP CT study): a post-hoc analysis of prospective outcome data. *Lancet*. (2018) 392:929–39. doi: 10.1016/S0140-6736(18)31114-0

26. Zhang S, Yu X, Gu H, Kang B, Guo N, Wang X. Identification of high-risk carotid plaque by using carotid perivascular fat density on computed tomography angiography. *Eur J Radiol*. (2022) 150:110269. doi: 10.1016/j.ejrad.2022.110269

27. Xia H, Yuan L, Zhao W, Zhang C, Zhao L, Hou J, et al. Predicting transient ischemic attack risk in patients with mild carotid stenosis using machine learning and CT radiomics. *Front Neurol*. (2023) 14:1105616. doi: 10.3389/fneur.2023.1105616

28. Kotanidis CP, Xie C, Alexander D, Rodrigues JCL, Burnham K, Mentzer A, et al. Constructing custom-made radiotranscriptomic signatures of vascular inflammation from routine CT angiograms: a prospective outcomes validation study in COVID-19. *Lancet Digit Health*. (2022) 4:e705–16. doi: 10.1016/S2589-7500(22)00132-7

29. Gaba P, O'Donoghue ML, Park J, Wiviott SD, Atar D, Kuder JF, et al. Association between achieved low-density lipoprotein cholesterol levels and long-term cardiovascular and safety outcomes: an analysis of FOURIER-OLE. *Circulation*. (2023) 147:1192–203. doi: 10.1161/CIRCULATIONAHA.122.063399

30. Oikonomou EK, Antoniades C. The role of adipose tissue in cardiovascular health and disease. *Nat Rev Cardiol*. (2019) 16:83–99. doi: 10.1038/s41569-018-0097-6

31. Rost NS, Wolf PA, Kase CS, Kelly-Hayes M, Silbershatz H, Massaro JM, et al. Plasma concentration of C-reactive protein and risk of ischemic stroke and transient ischemic attack: the Framingham study. *Stroke*. (2001) 32:2575–9. doi: 10.1161/hs1101.098151

32. Kizhisseri M, Gharaie S, Schluter J. An analytical method informed by clinical imaging data for estimating outlet boundary conditions in computational fluid dynamics analysis of carotid artery blood flow. *Sci Rep*. (2023) 13:14973. doi: 10.1038/s41598-023-42004-5

frontiers | Frontiers in Neurology

TYPE Original Research
PUBLISHED 26 February 2024
DOI 10.3389/fneur.2024.1332509

Check for updates

OPEN ACCESS

EDITED BY
Shubham Misra,
Yale University, United States

REVIEWED BY
Jun Xu,
Capital Medical University, China
Qi Li,
Second Affiliated Hospital of Anhui Medical University, China

*CORRESPONDENCE
Hongying Zhang
✉ zhying11@aliyun.com

RECEIVED 03 November 2023
ACCEPTED 30 January 2024
PUBLISHED 26 February 2024

CITATION
Li Q, Li F, Liu H, Li Y, Chen H, Yang W, Duan S and Zhang H (2024) CT-based radiomics models predict spontaneous intracerebral hemorrhage expansion and are comparable with CT angiography spot sign. *Front. Neurol.* 15:1332509. doi: 10.3389/fneur.2024.1332509

COPYRIGHT
© 2024 Li, Li, Liu, Li, Chen, Yang, Duan and Zhang. This is an open-access article distributed under the terms of the Creative Commons Attribution License (CC BY). The use, distribution or reproduction in other forums is permitted, provided the original author(s) and the copyright owner(s) are credited and that the original publication in this journal is cited, in accordance with accepted academic practice. No use, distribution or reproduction is permitted which does not comply with these terms.

CT-based radiomics models predict spontaneous intracerebral hemorrhage expansion and are comparable with CT angiography spot sign

Qingrun Li[1], Feng Li[1], Hao Liu[2], Yan Li[3], Hongri Chen[3], Wenrui Yang[3], Shaofeng Duan[4] and Hongying Zhang[3]*

[1]Department of Radiology, Traditional Chinese Medicine Hospital of Dianjiang Chongqing, Chongqing, China, [2]Department of Research and Development, Yizhun Medical AI Co. Ltd., Beijing, China, [3]Department of Radiology, Northern Jiangsu People's Hospital, Yangzhou, Jiangsu, China, [4]Precision Health Institution, GE Healthcare, Shanghai, China

Background and purpose: This study aimed to investigate the efficacy of radiomics, based on non-contrast computed tomography (NCCT) and computed tomography angiography (CTA) images, in predicting early hematoma expansion (HE) in patients with spontaneous intracerebral hemorrhage (SICH). Additionally, the predictive performance of these models was compared with that of the established CTA spot sign.

Materials and methods: A retrospective analysis was conducted using CT images from 182 patients with SICH. Data from the patients were divided into a training set (145 cases) and a testing set (37 cases) using random stratified sampling. Two radiomics models were constructed by combining quantitative features extracted from NCCT images (the NCCT model) and CTA images (the CTA model) using a logistic regression (LR) classifier. Additionally, a univariate LR model based on the CTA spot sign (the spot sign model) was established. The predictive performance of the two radiomics models and the spot sign model was compared according to the area under the receiver operating characteristic (ROC) curve (AUC).

Results: For the training set, the AUCs of the NCCT, CTA, and spot sign models were 0.938, 0.904, and 0.726, respectively. Both the NCCT and CTA models demonstrated superior predictive performance compared to the spot sign model (all $P < 0.001$), with the performance of the two radiomics models being comparable ($P = 0.068$). For the testing set, the AUCs of the NCCT, CTA, and spot sign models were 0.925, 0.873, and 0.720, respectively, with only the NCCT model exhibiting significantly greater predictive value than the spot sign model ($P = 0.041$).

Conclusion: Radiomics models based on NCCT and CTA images effectively predicted HE in patients with SICH. The predictive performances of the NCCT and CTA models were similar, with the NCCT model outperforming the spot sign model. These findings suggest that this approach has the potential to reduce the need for CTA examinations, thereby reducing radiation exposure and the use of contrast agents in future practice for the purpose of predicting hematoma expansion.

KEYWORDS

intracerebral hemorrhage, hematoma expansion, radiomics, computed tomography, spot sign

Introduction

Spontaneous intracerebral hemorrhage (SICH) is a prevalent subtype of stroke, accounting for ∼10%−15% of all strokes. Unlike ischemic stroke, SICH leads to more severe disability and higher mortality rates, with nearly 40% mortality within the first month (1). Early hematoma expansion (HE) occurs in ∼30% of SICH patients and is strongly associated with unfavorable outcomes (2). Studies have shown that, for every 1 mL increase in bleeding, the risk of death or disability increases by ∼5% (3). Therefore, the accurate identification of patients at risk of HE is crucial in clinical settings.

Several imaging markers have been proven to serve as reliable predictors for determining HE: these include an irregular shape, the island sign, hypodensities within the hematoma, the blend sign, the black hole sign, and the swirl sign on non-contrast computed tomography (NCCT), as well as the spot sign on computed tomography angiography (CTA) (4–10). In particular, the CTA spot sign has been widely adopted as a benchmark for prediction of HE in clinical practice. However, these markers are susceptible to subjective interpretation influenced by the researcher's experience, and many lack sufficient sensitivity. For example, despite the promising performance of the CTA spot sign, the pooled sensitivity values reported in three previous meta-analyses are only 0.53, 0.62, and 0.57 (11–13). In other words, these predictors are suboptimal for accurately predicting HE. Therefore, in this study, we aimed to explore a more sensitive, objective, and convenient approach.

Radiomics, an emerging field of research, utilizes data mining algorithms to extract quantitative features from medical images (14). It has garnered significant attention in oncological investigations (15, 16). Recently, researchers have explored the potential of radiomics in predicting the expansion of intracerebral hemorrhage (17–19). Their studies have demonstrated the effectiveness of radiomics models in predicting HE, surpassing conventional radiological and clinical models. However, these previous studies have focused solely on NCCT data. In clinical practice, multimodal CT images, such as CTA images, are available for patient evaluation. CTA images not only reveal hidden vascular information within the hemorrhage but also enhance changes in the image construct. Considering these advantages, we hypothesized that a radiomics model based on CTA images would outperform models based on other image types. Therefore, in this study, we aimed to develop separate radiomics models based on NCCT and CTA images to predict HE. Additionally, we aimed to evaluate their predictive performance by comparing them with the established spot sign.

Abbreviations: AUC, area under the curve; CTA, computed tomography angiography; HE, hematoma expansion; ICC, intraclass correlation coefficient; LASSO, least absolute shrinkage and selection operation; LR, logistic regression; NCCT, non-contrast computed tomography; ROC, receiver operating characteristic; SICH, spontaneous intracerebral hemorrhage; VOI, volume of interest.

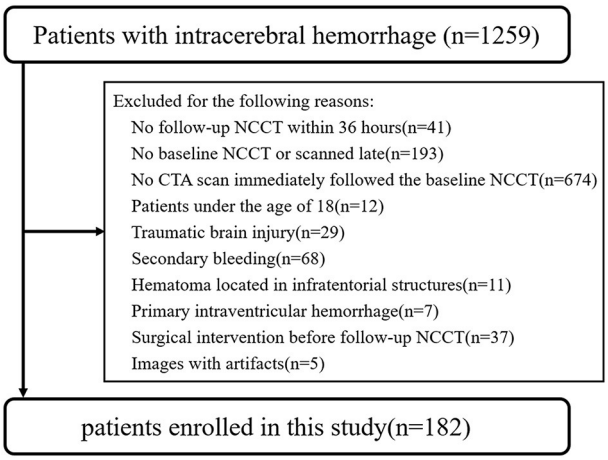

FIGURE 1
Flowchart of patient enrolment and exclusion criteria.

Materials and methods

Patients

This retrospective study enrolled patients with SICH who were admitted to Northern Jiangsu People's Hospital via the emergency department between December 2015 and December 2020. Patients eligible to participate were those with SICH aged 18 years or older who underwent initial NCCT followed by cranial CTA within 6 h of symptom onset and follow-up NCCT within 36 h. Patients with traumatic brain injury, secondary intracerebral hemorrhage resulting from an aneurysm, vascular malformation, brain tumor, or hemorrhagic transformation of infarction, as well as those with infratentorial hematoma or primary intraventricular hemorrhage, those who underwent surgical intervention before follow-up NCCT, and those with CT images with artifact, were excluded from the study. A flowchart illustrating the patient selection process is shown in Figure 1.

This retrospective study was approved by the hospital's ethics committee, and the requirement for informed consent was waived.

Image acquisition

Image acquisition was performed using a 64-row, 128-slice scanner (Optima CT660, GE Healthcare, Chicago, IL, USA) and an 80-row, 160-slice scanner (uCT 780, UIH, Shanghai, China). The scanning protocols for the Optima CT660 scanner consisted of a tube voltage of 120kV, automatic tube current, a collimation width of 64 mm, a scanning field of 250 mm, and slice thickness and interslice spacing of 5 mm and 0.625 mm for NCCT and CTA, respectively. For the uCT 780 scanner, the scanning protocols consisted of a tube voltage of 120kV, automatic tube current, a collimation width of 40 mm, a scanning field of 300 mm, and slice thickness and interslice spacing of 5 mm and 0.5 mm for NCCT and CTA, respectively. The scanning range extended from the base to the top of the skull. Test bolus technology was utilized to determine

the appropriate CTA acquisition time. During CTA, 50–70 mL of iodixanol (Xiansu, Yangtze River Pharmaceutical Co, Ltd, Jiangsu, China; 320 mg I/mL) was intravenously injected at a rate of 5 mL/s via a power injector through the antecubital vein. All images were transferred to the post-processing workstation AW4.7 (GE Healthcare, USA).

Radiological analysis

Automated hematoma recognition was performed on initial and follow-up CT images using the Stroke VCAR software package on the AW4.7 workstation; this assisted in segmenting hematoma areas and measuring hematoma volume. In this study, HE was defined as an increase in hematoma volume of $\geq$ 6 mL or $\geq$ 33% on follow-up CT compared to initial CT (20). Based on this criterion, all patients were categorized as either HE or non-HE. For SICH patients with intraventricular hemorrhage extension, the classification was independently verified by two physicians, one with 3 years and the other with 15 years of experience in radiodiagnosis, and their determinations were found to be consistent.

To evaluate the presence of the CTA spot sign in CTA images, two other neuroimaging diagnostic physicians, one with 2 years and the other with 20 years of experience, conducted independent assessments. Any discrepancies were resolved through joint discussion to reach a consensus. Both readers were blinded to all clinical information. Subsequently, a binary logistic regression (LR) model for the CTA spot sign (the spot sign model) was developed. The assessment included evaluating the location, shape, intraventricular hemorrhage extension, swirl sign, blend sign, black hole sign, and island sign, all of which were documented. Hematoma locations were classified as lobar or deep (involving the basal ganglia and/or thalamus) based on the location of the main body of the hematoma. The shape of the hematoma was recorded as either irregular or regular (5).

Radiomics analysis

Lesion segmentation

To mitigate the influence of varying slice thickness and interslice spacing across different CT scanners, as well as the distinctions between CTA and NCCT images, all original CTA images were reconstructed with a consistent slice thickness and interslice spacing of 5 mm, matching that of the NCCT images. Subsequently, both the NCCT and the reconstructed CTA images for the enrolled patients were exported in DICOM format and transferred to the DARWIN intelligent research platform (Yizhun Medical AI technology, Beijing, China, https://arxiv.org/abs/2009.00908). A volume of interest (VOI) for the hematoma was manually delineated and segmented layer by layer in the NCCT images, following the boundary of the hematoma from top to bottom. This delineation was then applied to the CTA images, with necessary adjustments made to derive the tailored VOI (Figure 2). Segmentation of the hematoma VOIs was independently carried out by the aforementioned two neuroimaging diagnosticians.

Feature extraction and selection

A total of 120 quantitative features were extracted from each VOI in the original images using the pyradiomics package (http://pyradiomics.readthedocs.io/en/latest/index.html). In addition, seven filters were employed to transform the original images to capture additional information. These filters included the exponential filter, gradient filter, local binary pattern filter, logarithm filter, square filter, square root filter, and wavelet filter. Collectively, these processes resulted in the extraction of 1,688 candidate features. The candidate features were then categorized into three groups based on their relevance to (1) shape, (2) first-order statistics (histogram features), and (3) second-order statistics (texture features). The intraclass correlation coefficient (ICC) was computed to assess the reproducibility of feature extraction. Only features with an ICC >0.75 were included for further analysis.

To address the issue of redundant features, ANOVA *F*-test statistic was employed to select the top 100 features. Prior to feature screening, all features were standardized using Z-scores. The selected features were sorted based on their F-values, with higher values indicating lower *p*-values. Subsequently, the least absolute shrinkage and selection operation (LASSO) LR algorithm was employed to further reduce data redundancy and identify stable features through the use of non-zero coefficients. To ensure an unbiased comparison between the two models, an equal number of features were also selected using LASSO. Considering the relationship between the sample size and the number of features, we set this number at 10 on empirical grounds.

Model construction

To ensure the integrity of the data distribution and minimize the introduction of bias during data processing, data from all patients were randomly stratified into a training set and a testing set in a ratio of 4:1. This approach maintained the consistency of data distribution between the two sets.

The features selected from both NCCT and CTA images were utilized to train the radiomics prediction models in conjunction with the widely used and effective LR machine learning classifier (21). The prediction capabilities of the constructed models were subsequently evaluated using an independent testing set. The predictive performances of the two radiomics models (the NCCT model and CTA model) were then compared with that of the spot sign model.

Statistical analysis

An independent samples *t*-test or Mann–Whitney *U*-test was employed for continuous variables, and the chi-squared test was adopted for categorical variables. Continuous variables are reported in the form of mean ± standard deviation, and categorical variables are summarized in the form of count (percentage). The predictive performance of each model in estimating hematoma enlargement was evaluated via receiver operating characteristic (ROC) curve analysis. The area under the curve (AUC) values of the ROC curves

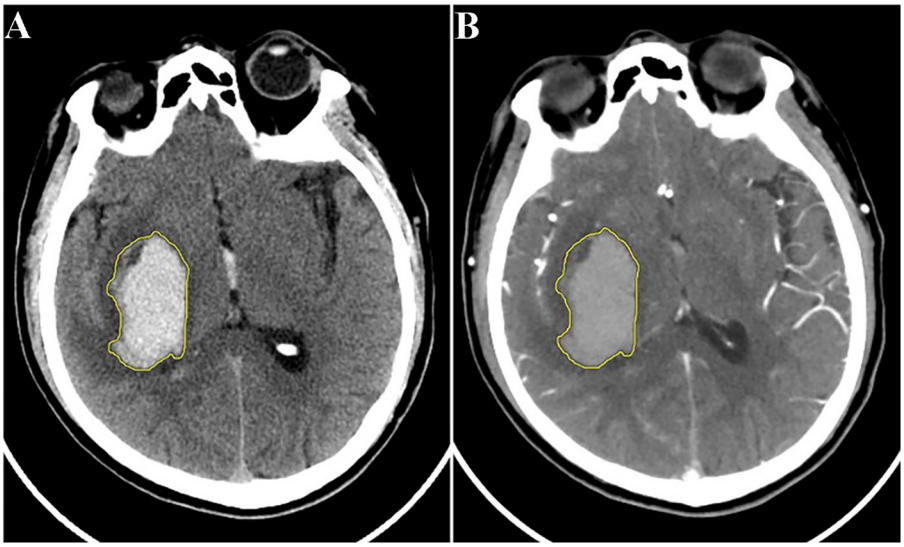

FIGURE 2
Schematic diagram of hematoma segmentation: **(A)** NCCT image; **(B)** reconstructed CTA image of the same patient. CTA, computed tomography angiography; NCCT, non-contrast computed tomography.

were compared using the DeLong test. Statistical significance was determined when the bilateral $p < 0.05$. All statistical analyses were conducted using the SPSS software package (version 25.0), and the MedCalc software package (version 18.11.3) was utilized to generate and compare the ROC curves.

Results

Patient characteristics

Following the aforementioned criteria, 182 patients diagnosed with SICH were included in this study. Based on the follow-up CT, these patients were categorized into the HE group (67 cases) or the non-HE group (115 cases). Table 1 presents the statistical analysis of relevant factors, revealing a significant difference between the HE group (4 cases) and the non-HE group (0 cases) in terms of the pre-onset use of anticoagulants (warfarin) ($P = 0.017$). However, no significant differences between the two groups were observed in terms of gender, age, systolic blood pressure, diastolic blood pressure, or the use of antiplatelet drugs (aspirin) (all $P > 0.05$).

Radiological characteristics and the spot sign model

Statistically significant differences between the HE and non-HE groups were observed in the initial volume, shape, swirl sign, blend sign, black hole sign, island sign, and CTA spot sign ($P < 0.05$). However, there was no significant disparity between the two groups in time from symptom onset to baseline CT ($P > 0.05$) (Table 1).

A random stratified sampling approach was employed to divide the data from the 182 patients into a training set (145 cases) and a testing set (37 cases). These sets were then submitted independently to univariate analysis, and no significant differences in radiological characteristics between them were found (all $P > 0.05$). In both the training set and the testing set, the HE group displayed larger initial volume and a higher likelihood of exhibiting the blend sign and the CTA spot sign (all $P < 0.05$). In the training set, irregular shape ($P = 0.015$), the swirl sign ($P = 0.046$), and the island sign ($P = 0.042$) were associated with hematoma enlargement. In the testing set, there was a significant difference between the two groups in terms of location of the hematoma ($P = 0.038$). However, when hematoma location and the black hole sign were examined within their respective sets, no statistically significant differences were found between the two groups within either the training set or the testing set (all $P > 0.05$). Detailed results are presented in Table 2.

A binary LR model was constructed to analyze the CTA spot sign as a predictor of HE. In the training set, the AUC, sensitivity, specificity, and accuracy were 0.726, 0.528, 0.924, and 0.779, respectively. In the testing set, the AUC, sensitivity, specificity, and accuracy were 0.720, 0.571, 0.870, and 0.757, respectively (Table 3).

Construction and validation of radiomics models

Following the aforementioned screening methods, 10 optimal radiomics features were extracted from the NCCT and CTA images (Figure 3 illustrates feature selection using LASSO regression). The remaining features were employed to construct radiomics models in combination with the LR machine learning classifier, using a five-fold cross-validation approach (Figure 4). In the training set, the NCCT model achieved an AUC of 0.938, sensitivity of 0.849, specificity of 0.924, and accuracy of 0.897. Similarly, the CTA model yielded an AUC of 0.904, sensitivity of 0.774, specificity of 0.902, and accuracy of 0.855. In the testing set, the NCCT model achieved

TABLE 1 Comparison of demographic, clinical, and baseline radiological characteristics between the HE group and the non-HE group.

	HE group ($n = 67$)	non-HE group ($n = 115$)	p-value
Gender (male/female)	45/22	73/42	0.615#
Age (y)	60.6 ± 13.0	59.1 ± 13.5	0.466*
Systolic blood pressure (mmHg)	160.2 ± 25.2	160.3 ± 24.5	0.968*
Diastolic blood pressure (mmHg)	91.4 ± 16.6	90.4 ± 14.1	0.685*
Use of anticoagulants (warfarin)	4 (6.0)	0 (0)	**0.017**#
Symptom onset to baseline CT (h)	3.17 ± 1.28	3.47 ± 1.37	0.226*
Use of antiplatelets (aspirin)	5 (7.5)	3 (2.6)	0.244#
Location (deep/lobe)	39/28	82/33	0.071#
Intraventricular hemorrhage extension	15 (22.4)	20 (22.1)	0.409#
Initial volume (mL)	43.3 ± 24.9	27.5 ± 17.1	<**0.001***
Shape, irregular	38 (56.7)	42 (36.5)	**0.008**#
Swirl sign	26 (38.8)	24 (20.9)	**0.009**#
Blend sign	24 (35.8)	15 (13.0)	<**0.001**#
Black hole sign	9 (13.4)	5 (4.3)	**0.027**#
Island sign	14 (20.9)	9 (7.8)	**0.010**#
CTA spot sign	36 (53.7)	10 (8.7)	<**0.001**#

#Chi-squared test, with percentages in parentheses. *Independent samples t-test or Mann–Whitney U-test; data reported are the mean ± standard deviation. Boldface indicates statistical significance. HE, hematoma expansion.

TABLE 2 Comparison of radiological characteristics between the HE group and the non-HE group in the training and testing sets.

	Training set ($n = 145$)			Testing set ($n = 37$)			p-value
	HE ($n = 53$)	non-HE ($n = 92$)	p-value	HE ($n = 14$)	non-HE ($n = 23$)	p-value	
Location (deep/lobe)	34/19	65/27	0.418#	5/9	17/6	**0.038**#	0.311#
Intraventricular hemorrhage extension	11 (20.8)	16 (17.4)	0.616#	4 (28.6)	4 (17.4)	0.445#	0.679#
Initial volume (mL)	42.6 ± 25.7	26.6 ± 16.1	<**0.001***	45.9 ± 22.1	31.1 ± 20.8	**0.048***	0.245*
Shape, irregular	30 (56.6)	33 (35.9)	**0.015**#	8 (57.1)	9 (39.1)	0.328#	0.785#
Swirl sign	21 (39.6)	22 (23.9)	**0.046**#	5 (35.7)	2 (8.7)	0.080#	0.192#
Blend sign	18 (34.0)	13 (14.1)	**0.005**#	6 (42.9)	2 (8.7)	**0.035**#	0.974#
Black hole sign	6 (11.3)	4 (4.3)	0.209#	3 (21.4)	1 (4.3)	0.142#	0.651#
Island sign	10 (18.9)	7 (7.6)	**0.042**#	4 (28.6)	2 (8.7)	0.173#	0.648#
CTA spot sign	28 (52.8)	7 (7.6)	<**0.001**#	8 (57.1)	3 (13.0)	**0.008**#	0.485#

#Chi-squared test, with percentages in parentheses. *Independent samples t-test or Mann–Whitney U test; data reported are the mean ± standard deviation. Boldface test statistical significance. CTA, computed tomography angiography; HE, hematoma expansion.

an AUC of 0.925, sensitivity of 0.786, specificity of 0.913, and accuracy of 0.865. Similarly, the CTA model resulted in an AUC of 0.873, sensitivity of 0.714, specificity of 0.913, and accuracy of 0.838 (Table 3).

Comparison of the models on predictive performance

As illustrated in Table 4 and Figure 5, for the training set, both the NCCT model and the CTA model resulted in significantly larger AUCs compared to the spot sign model (all $P < 0.001$), while no statistically significant difference was observed between the NCCT model and the CTA model ($P = 0.068$). For the testing set, the NCCT model resulted in a larger AUC than the spot sign model ($P = 0.041$), while no significant difference was found between the NCCT model and the CTA model, or between the CTA model and the spot sign model (all $P > 0.05$). Figure 6 showcases a comparison of two SICH cases (with and without the spot sign). The radiomics models could successfully predict HE, even in cases where the spot sign was absent.

Discussion

HE is a dynamic process influenced by active bleeding and serves as an important variable associated with clinical prognosis.

TABLE 3 Predictive performance of three models for HE in the training and testing sets.

		AUC (95% CI)	Sensitivity	Specificity	Accuracy
Training set	Spot sign model	0.726 (0.646, 0.797)	0.528	0.924	0.779
	NCCT model	0.938 (0.886, 0.971)	0.849	0.924	0.897
	CTA model	0.904 (0.844, 0.947)	0.774	0.902	0.855
Testing set	Spot sign model	0.720 (0.549, 0.855)	0.571	0.870	0.757
	NCCT model	0.925 (0.790, 0.986)	0.786	0.913	0.865
	CTA model	0.873 (0.722, 0.959)	0.714	0.913	0.838

AUC, area under the curve; CI, confidence interval; CTA, computed tomography angiography; HE, hematoma expansion; NCCT, non-contrast computed tomography.

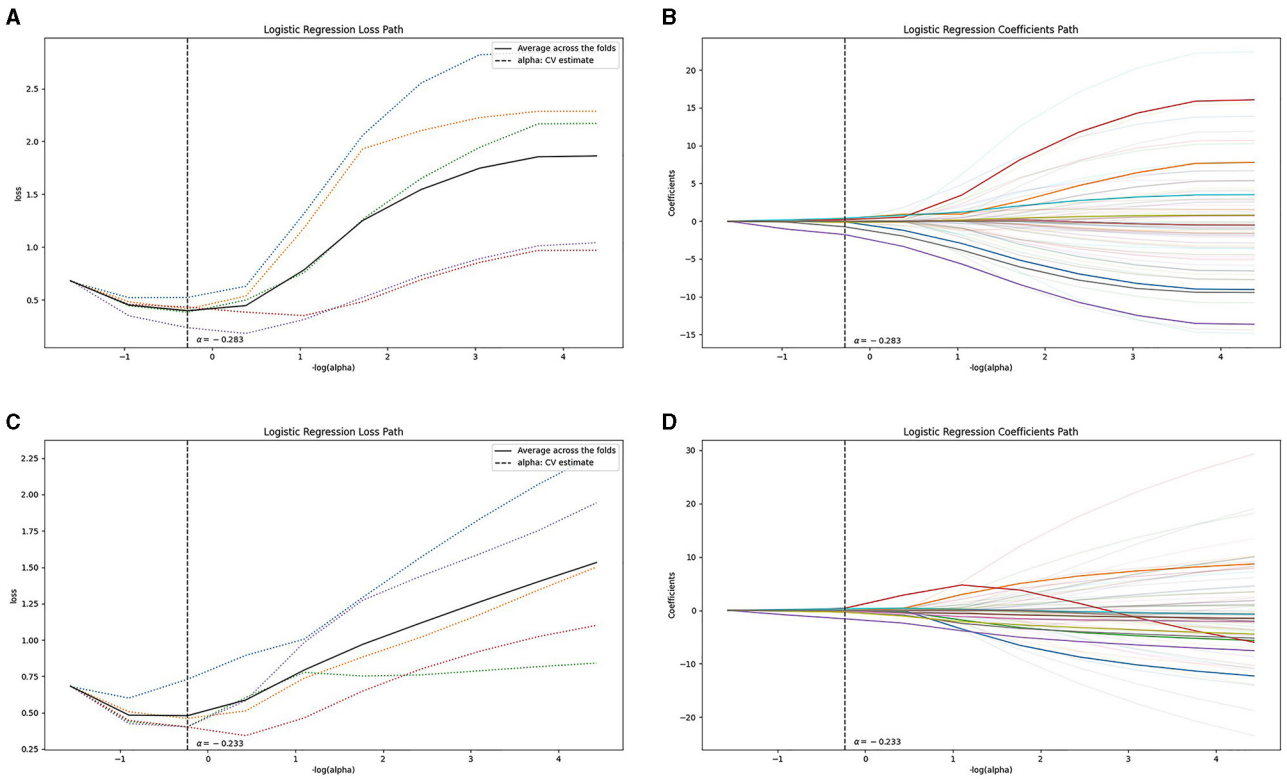

FIGURE 3
Feature selection using LASSO regression: the loss path of LASSO **(A, C)**, and the regression coefficients of LASSO **(B, D)**, for **(A, B)** the NCCT model and **(C, D)** the CTA model. CTA, computed tomography angiography; LASSO, least absolute shrinkage and selection operation; NCCT, non-contrast computed tomography.

In this study, we developed two radiomics models using NCCT and CTA images to anticipate HE and examined their performance in comparison to the CTA spot sign model. Our findings indicated that both radiomics models were effectively predictors of HE, demonstrating comparable performance. However, it is noteworthy that the NCCT radiomics model outperformed the traditional spot sign model in its predictive capabilities.

Initially, quantitative CT densitometry of hematoma through NCCT was utilized to predict ICH enlargement (22). However, this method provided limited information. Subsequently, dual-energy CT analysis of iodine concentration within the hematoma emerged as an improved approach for predicting HE. This analysis also led to the proposal of diffused leakage, indicating that the extravasation of contrast agents was not solely responsible for the aggregation observed within the hematoma (23). The advent of texture analysis and radiomics feature analysis in neuroimaging further contributed to the field. For instance, texture analysis parameters such as variance and uniformity demonstrated the ability to independently forecast HE following Laplacian of Gaussian operator filtering processing (24). Other researchers have subsequently demonstrated the predictive value of radiomics features for hematoma growth as well (17, 18).

Consistent with previous research findings (10, 25), our results reaffirmed the CTA spot sign as a well-established imaging marker for independently predicting HE in patients with ICH, demonstrating higher specificity than sensitivity. The appearance of the spot sign is believed to stem from contrast extravasation caused by ongoing bleeding from

10.3389/fneur.2024.1332509

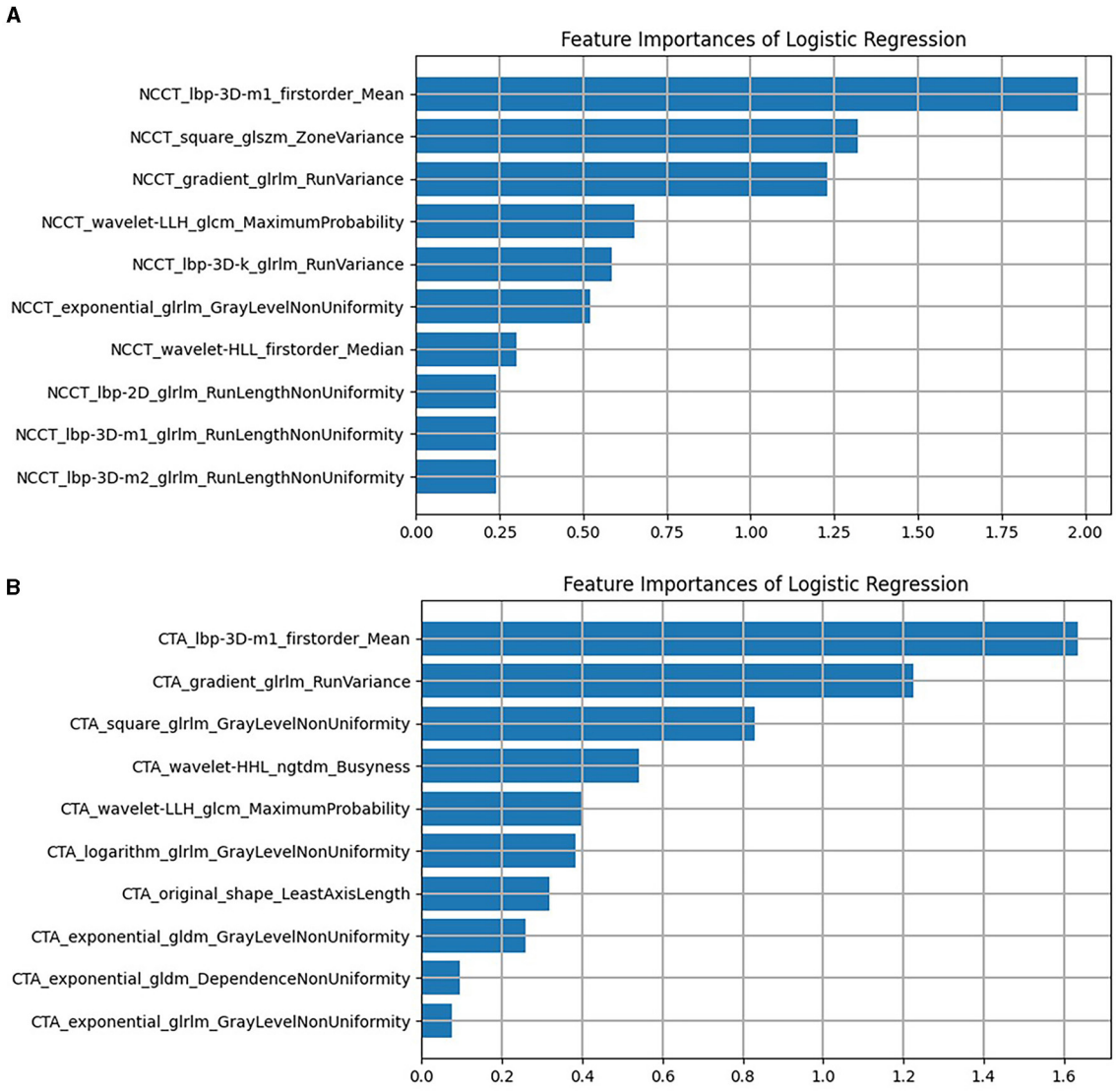

FIGURE 4
The remaining features of LASSO regression screening and the ranking of weight coefficients output by the corresponding LR classifier under **(A)** the NCCT model, **(B)** the CTA model. CTA, computed tomography angiography; LASSO, least absolute shrinkage and selection operation; LR, logistic regression; NCCT, non-contrast computed tomography.

TABLE 4 **Comparison of the three models on predictive performance for hematoma expansion.**

	Training set	Testing set
NCCT model vs. CTA model	0.068	0.440
NCCT model vs. Spot sign model	**<0.001**	**0.041**
CTA model vs. Spot sign model	**<0.001**	0.182

Boldface indicates statistical significance. CTA, computed tomography angiography; NCCT, non-contrast computed tomography.

ruptured blood vessels (26). Meta-analyses have indicated that the sensitivity of the spot sign is ∼53% (11), highlighting the fact that a significant portion of expanded hematomas may not exhibit this characteristic. Our study indicated that the radiomics models exhibited superior sensitivity to the spot sign.

In contrast to previous studies (17–19), our study utilized multimodal CT images and compared these with the spot sign. Prior research has demonstrated the superior predictive performance of the spot sign compared to NCCT signs (27), such as the blend sign. Hence, our initial assumption was that the CTA model would outperform the NCCT model. However, our findings contradicted this hypothesis. We speculate that these results may be attributed to the infiltration of contrast medium into hematomas during active bleeding, which occurs during CTA scans. Comparatively, the diffusion of contrast medium within the expanded hematoma weakens the disparities in CT values among each voxel, as well as the discrepancies in certain texture features. Consequently, the radiomics of the expanded

10.3389/fneur.2024.1332509

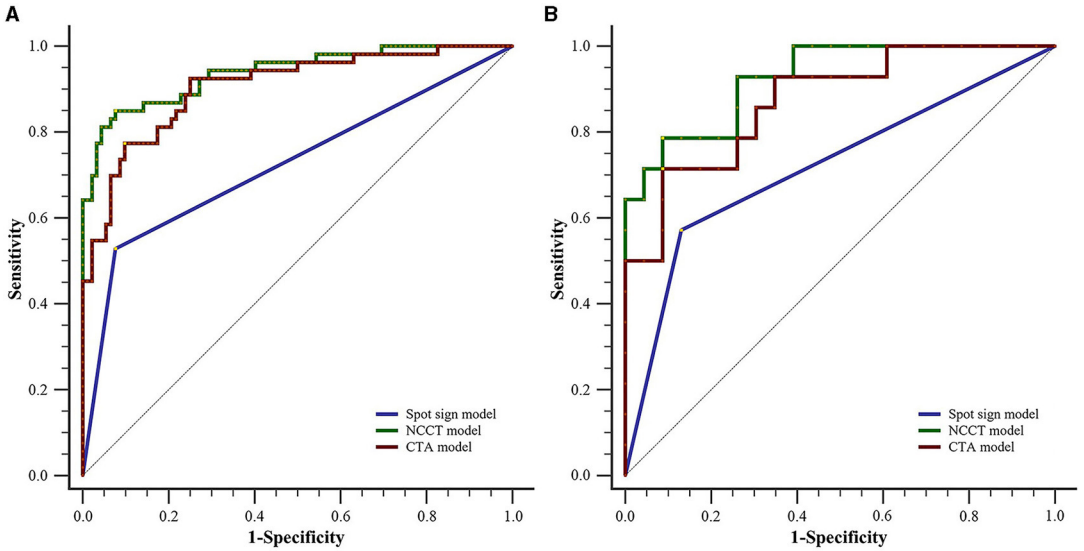

FIGURE 5
Comparison of ROC curves between the two radiomics models and the spot sign model for **(A)** the training set and **(B)** testing set. CTA, computed tomography angiography; NCCT, non-contrast computed tomography; ROC, receiver operating characteristic.

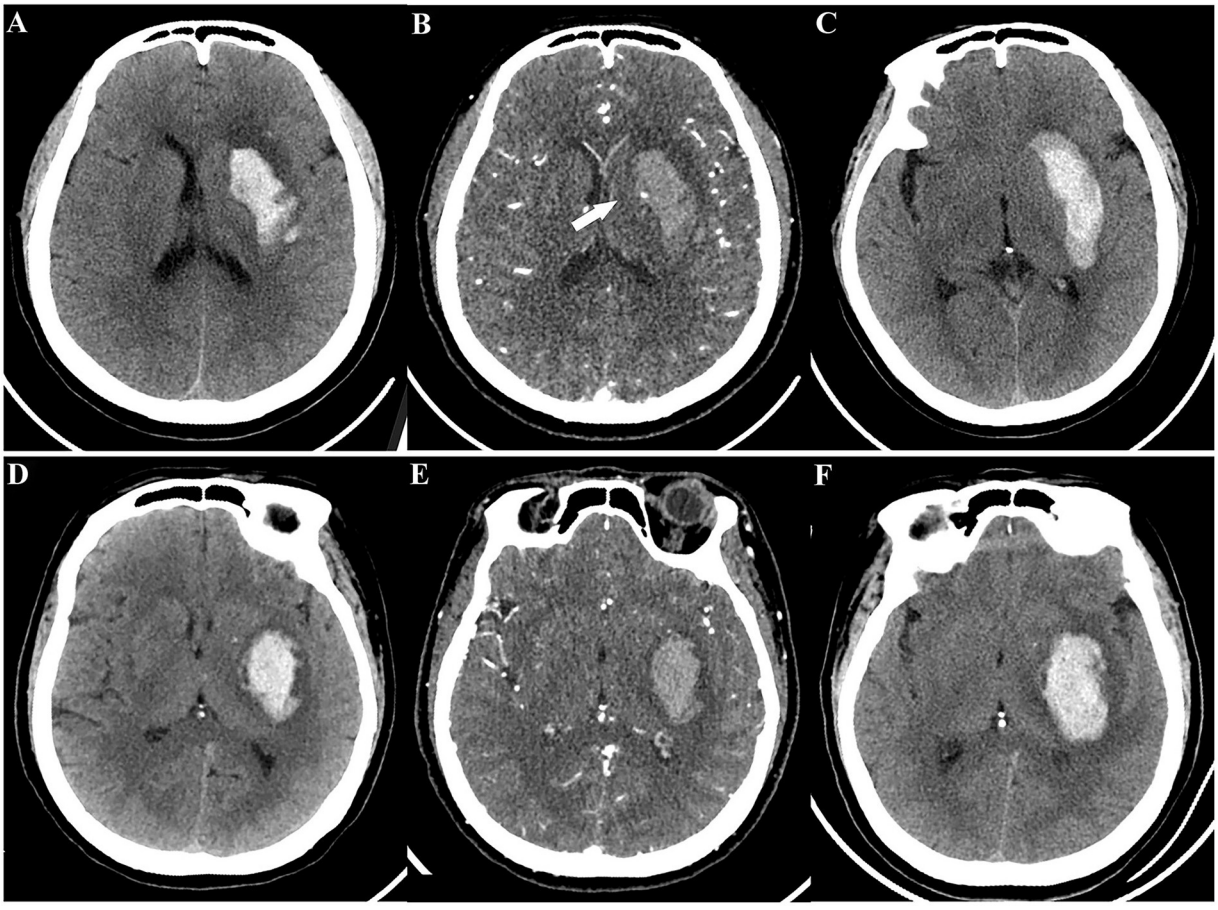

FIGURE 6
A comparison of two spontaneous intracerebral hemorrhage cases (with and without the spot sign) according to radiomics models. Case 1 with CTA spot sign, a 49-year-old woman: **(A)** initial NCCT; **(B)** CTA showed spot sign (white arrow); **(C)** follow-up CT revealed HE. Case 2 without CTA spot sign, a 55-year-old man: **(D)** initial NCCT; **(E)** CTA did not show spot sign; **(F)** follow-up CT still revealed HE. Both radiomics models provided successful predictions for these cases. HE, hematoma expansion; NCCT, non-contrast computed tomography; CTA, computed tomography angiography.

hematoma exhibited similarities to those of stable hematomas in the CTA model.

This study has elucidated the value of radiomics as a predictive tool for HE, particularly in the significant number of patients who lack the spot sign. Additionally, radiomics models offered objectivity and convenience, unlike the spot sign, determination of which may be influenced by experiential bias. Integrating radiomics into clinical practice, specifically by utilizing NCCT-based radiomics models, could yield commendable predictive efficacy for HE, potentially reducing the need for unnecessary CTA examinations. This approach could consequently mitigate radiation exposure and minimize contrast agent usage.

Several limitations should be noted with respect to our study. First, certain patients were excluded due to either having undergone surgical treatment before follow-up CT or displaying motion artifacts. This exclusion could potentially have introduced biases into the results. Second, although manual segmentation of VOIs showed good reproducibility, automatic segmentation techniques may offer increased speed and accuracy, especially for larger sample sizes. Third, our sample size was limited due to the relatively small number of patients who underwent concurrent NCCT and CTA examinations, necessitating further validation in multi-center studies with larger cohorts.

Conclusion

This study validated the predictive capability of radiomics models utilizing NCCT and CTA images for SICH expansion. Remarkably, our NCCT radiomics model exhibited superior performance compared to the spot sign model and was comparable to our CTA radiomics model. This has implications in terms of reducing the need for CTA examinations, thereby mitigating radiation exposure and contrast agent utilization. We firmly believe that radiomics analysis will play a crucial role in future clinical practice, aiding in treatment decisions for high-risk patients susceptible to HE.

Data availability statement

The raw data supporting the conclusions of this article will be made available by the authors, without undue reservation.

Ethics statement

The studies involving humans were approved by Ethics Committee of Northern Jiangsu People's Hospital. The studies were conducted in accordance with the local legislation and institutional requirements. Written informed consent for participation was not required from the participants or the participants' legal guardians/next of kin in accordance with the national legislation and institutional requirements.

Author contributions

QL: Conceptualization, Data curation, Investigation, Methodology, Writing – original draft, Writing – review & editing. FL: Methodology, Writing – review & editing. HL: Software, Visualization, Writing – review & editing. YL: Data curation, Formal analysis, Methodology, Writing – review & editing. HC: Methodology, Writing – review & editing. WY: Formal analysis, Writing – review & editing. SD: Writing – review & editing. HZ: Conceptualization, Funding acquisition, Investigation, Methodology, Resources, Supervision, Writing – original draft, Writing – review & editing.

Funding

The author(s) declare financial support was received for the research, authorship, and/or publication of this article. This work was supported by the National Natural Science Foundation of China (Grant No. 81471642) and the Opening Project of National Innovation Center for Advanced Medical Devices (NMED2021MS-01-006).

Conflict of interest

HL was employed by Yizhun Medical AI Co. Ltd. SD was employed by GE Healthcare.

The remaining authors declare that the research was conducted in the absence of any commercial or financial relationships that could be construed as a potential conflict of interest.

Publisher's note

All claims expressed in this article are solely those of the authors and do not necessarily represent those of their affiliated organizations, or those of the publisher, the editors and the reviewers. Any product that may be evaluated in this article, or claim that may be made by its manufacturer, is not guaranteed or endorsed by the publisher.

References

1. Keep RF, Hua Y, Xi G. Intracerebral haemorrhage: mechanisms of injury and therapeutic targets. *The Lancet Neurol.* (2012) 11:720–31. doi: 10.1016/S1474-4422(12)70104-7

2. Brouwers HB, Greenberg SM. Hematoma expansion following acute intracerebral hemorrhage. *Cerebrovascular Dis.* (2013) 35:195–201. doi: 10.1159/000346599

3. Delcourt C, Huang Y, Arima H, Chalmers J, Davis SM, Heeley EL, et al. Hematoma growth and outcomes in intracerebral hemorrhage: the INTERACT1 study. *Neurology.* (2012) 79:314–9. doi: 10.1212/WNL.0b013e318260cbba

4. Boulouis G, Morotti A, Brouwers HB, Charidimou A, Jessel MJ, Auriel E, et al. Association between hypodensities detected by computed tomography and hematoma

expansion in patients with intracerebral hemorrhage. *JAMA Neurol.* (2016) 73:961–8. doi: 10.1001/jamaneurol.2016.1218

5. Barras CD, Tress BM, Christensen S, MacGregor L, Collins M, Desmond PM, et al. Density and shape as CT predictors of intracerebral hemorrhage growth. *Stroke.* (2009) 40:1325–31. doi: 10.1161/STROKEAHA.108.536888

6. Li Q, Zhang G, Huang YJ, Dong MX, Lv FJ, Wei X, et al. Blend sign on computed tomography: novel and reliable predictor for early hematoma growth in patients with intracerebral hemorrhage. *Stroke.* (2015) 46:2119–23. doi: 10.1161/STROKEAHA.115.009185

7. Li Q, Zhang G, Xiong X, Wang XC, Yang WS, Li KW, et al. Black hole sign: novel imaging marker that predicts hematoma growth in patients with intracerebral hemorrhage. *Stroke.* (2016) 47:1777–81. doi: 10.1161/STROKEAHA.116.013186

8. Selariu E, Zia E, Brizzi M, Abul-Kasim K. Swirl sign in intracerebral haemorrhage: definition, prevalence, reliability and prognostic value. *BMC Neurol.* (2012) 12:1–6. doi: 10.1186/1471-2377-12-109

9. Li Q, Liu QJ, Yang WS, Wang XC, Zhao LB, Xiong X, et al. Island sign: an imaging predictor for early hematoma expansion and poor outcome in patients with intracerebral hemorrhage. *Stroke.* (2017) 48:3019–25. doi: 10.1161/STROKEAHA.117.017985

10. Demchuk AM, Dowlatshahi D, Rodriguez-Luna D, Molina CA, Blas YS, Dzialowski I, et al. Prediction of haematoma growth and outcome in patients with intracerebral haemorrhage using the CT-angiography spot sign (PREDICT): a prospective observational study. *The Lancet Neurol.* (2012) 11:307–14. doi: 10.1016/S1474-4422(12)70038-8

11. Du FZ, Jiang R, Gu M, He C, Guan J. The accuracy of spot sign in predicting hematoma expansion after intracerebral hemorrhage: a systematic review and meta-analysis. *PLoS ONE.* (2014) 9:e115777. doi: 10.1371/journal.pone.0115777

12. Xu X, Zhang J, Yang K, Wang Q, Xu B, Chen X. Accuracy of spot sign in predicting hematoma expansion and clinical outcome: a meta-analysis. *Medicine.* (2018) 97:e11945. doi: 10.1097/MD.0000000000011945

13. Phan TG, Krishnadas N, Lai VWY, Batt M, Slater LA, Chandra RV, et al. Meta-analysis of accuracy of the spot sign for predicting hematoma growth and clinical outcomes. *Stroke.* (2019) 50:2030–6. doi: 10.1161/STROKEAHA.118.024347

14. Lambin P, Rios-Velazquez E, Leijenaar R, Carvalho S, Van Stiphout RG, Granton P, et al. Radiomics: extracting more information from medical images using advanced feature analysis. *Eur J Cancer.* (2012) 48:441–6. doi: 10.1016/j.ejca.2011.11.036

15. Wakabayashi T, Ouhmich F, Gonzalez-Cabrera C, Felli E, Saviano A, Agnus V, et al. Radiomics in hepatocellular carcinoma: a quantitative review. *Hepatol Int.* (2019) 13:546–59. doi: 10.1007/s12072-019-09973-0

16. Takahashi S, Takahashi W, Tanaka S, Haga A, Nakamoto T, Suzuki Y, et al. Radiomics analysis for glioma malignancy evaluation using diffusion kurtosis and tensor imaging. *Int J Rad Oncol Biol Phys.* (2019) 105:784–91. doi: 10.1016/j.ijrobp.2019.07.011

17. Xie H, Ma S, Wang X, Zhang X. Noncontrast computer tomography–based radiomics model for predicting intracerebral hemorrhage expansion: preliminary findings and comparison with conventional radiological model. *Eur Radiol.* (2020) 30:87–98. doi: 10.1007/s00330-019-06378-3

18. Xu W, Guo H, Li H, Dai Q, Song K, Li F, et al. A non-contrast computed tomography-based radiomics nomogram for the prediction of hematoma expansion in patients with deep ganglionic intracerebral hemorrhage. *Front Neurol.* (2022) 13:974183. doi: 10.3389/fneur.2022.974183

19. Chen Q, Zhu D, Liu J, Zhang M, Xu H, Xiang Y, et al. Clinical-radiomics nomogram for risk estimation of early hematoma expansion after acute intracerebral hemorrhage. *Acad Radiol.* (2021) 28:307–17. doi: 10.1016/j.acra.2020.02.021

20. Dowlatshahi D, Demchuk AM, Flaherty ML, Ali M, Lyden PL, Smith EE. Defining hematoma expansion in intracerebral hemorrhage: relationship with patient outcomes. *Neurology.* (2011) 76:1238–44. doi: 10.1212/WNL.0b013e3182143317

21. Dong Y, Jiang Z, Li C, Dong S, Zhang S, Lv Y, et al. Development and validation of novel radiomics-based nomograms for the prediction of EGFR mutations and Ki-67 proliferation index in non-small cell lung cancer. *Quant Imaging Med Surg.* (2022) 12:2658. doi: 10.21037/qims-21-980

22. Barras CD, Tress BM, Christensen S, Collins M, Desmond PM, Skolnick BE, et al. Quantitative CT densitometry for predicting intracerebral hemorrhage growth. *Am J Neuroradiol.* (2013) 34:1139–44. doi: 10.3174/ajnr.A3375

23. Tan CO, Lam S, Kuppens D, Bergmans RH, Parameswaran BK, Forghani R, et al. Spot and diffuse signs: quantitative markers of intracranial hematoma expansion at dual-energy CT. *Radiology.* (2019) 290:179–86. doi: 10.1148/radiol.2018180322

24. Shen Q, Shan Y, Hu Z, Chen W, Yang B, Han J, et al. Quantitative parameters of CT texture analysis as potential markers for early prediction of spontaneous intracranial hemorrhage enlargement. *Eur Radiol.* (2018) 28:4389–96. doi: 10.1007/s00330-018-5364-8

25. Zheng J, Yu Z, Wang C, Li M, Wang X, You C, et al. Evaluating the predictive value of island sign and spot sign for hematoma expansion in spontaneous intracerebral hemorrhage. *World Neurosurg.* (2018) 117:e167–71. doi: 10.1016/j.wneu.2018.05.221

26. Brouwers HB, Raffeld MR, van Nieuwenhuizen KM, Falcone GJ, Ayres AM, McNamara KA, et al. CT angiography spot sign in intracerebral hemorrhage predicts active bleeding during surgery. *Neurology.* (2014) 83:883–9. doi: 10.1212/WNL.0000000000000747

27. Sporns PB, Schwake M, Kemmling A, Minnerup J, Schwindt W, Niederstadt T, et al. Comparison of spot sign, blend sign and black hole sign for outcome prediction in patients with intracerebral hemorrhage. *J Stroke.* (2017) 19:333. doi: 10.5853/jos.2016.02061

frontiers | Frontiers in Neurology

TYPE Original Research
PUBLISHED 14 March 2024
DOI 10.3389/fneur.2024.1371830

Check for updates

OPEN ACCESS

EDITED BY
Shubham Misra,
Yale University, United States

REVIEWED BY
Huaqiu Zhang,
Huazhong University of Science and Technology, China
Chaoran Xu,
Zhejiang University, China
Desheng Zhu,
Shanghai Jiao Tong University, China
Jiachen Liu,
Washington University in St. Louis, United States

*CORRESPONDENCE
Peng Wang
✉ qduwpeng@126.com

RECEIVED 17 January 2024
ACCEPTED 19 February 2024
PUBLISHED 14 March 2024

CITATION
Zhang R, Wang L, Zhang J, Zhang X and Wang P (2024) Peripheral T cell immune repertoire is associated with the outcomes of acute spontaneous intracerebral hemorrhage. *Front. Neurol.* 15:1371830. doi: 10.3389/fneur.2024.1371830

COPYRIGHT
© 2024 Zhang, Wang, Zhang, Zhang and Wang. This is an open-access article distributed under the terms of the Creative Commons Attribution License (CC BY). The use, distribution or reproduction in other forums is permitted, provided the original author(s) and the copyright owner(s) are credited and that the original publication in this journal is cited, in accordance with accepted academic practice. No use, distribution or reproduction is permitted which does not comply with these terms.

Peripheral T cell immune repertoire is associated with the outcomes of acute spontaneous intracerebral hemorrhage

Rui Zhang[1,2], Li Wang[1], Jiapo Zhang[2], Xiufang Zhang[2] and Peng Wang[1]*

[1]Department of Anesthesiology, The Affiliated Hospital of Qingdao University, Qingdao, Shandong, China, [2]Department of Emergency Medicine, Xiang'an Hospital of Xiamen University, School of Medicine, Xiamen University, Xiamen, Fujian, China

Systematic immune responses have been identified in patients with acute spontaneous intracerebral hemorrhage (ICH). T cells have been established to participate in central nervous system damage and repair following brain injury. However, their contribution to the prognosis of patients with ICH remains to be elucidated. In this study, peripheral blood mononuclear cells (PBMCs) were collected from 45 patients with acute spontaneous ICH (<24 h from symptom onset). Our results exposed significant negative correlations between hematoma volume/white blood cell (WBC) density and Glasgow Coma Scale (GCS) score. Contrastingly, lymphocyte density was negatively correlated with hematoma volume and positively correlated with GCS score. Moreover, flow cytometry determined that ICH activated T cells despite their proportion being lower in blood. Afterward, immune repertoire sequencing (IR-seq) revealed a significant decrease in VJ, VDJ usage, and TCR clonotypes in ICH patients. Finally, variations in the complementarity-determining region 3 (CDR3) amino acid (aa) were also detected in ICH patients. This study reveals the occurrence of peripheral T-cell diminishment and activation in response to acute hematoma. ICH lesion also alters the T cell receptor (TCR) immune repertoire, which is associated with patient prognosis.

KEYWORDS

intracerebral hemorrhage, T cell, T cell receptor, IR-seq, immune repertoire

Introduction

Acute spontaneous intracerebral hemorrhage (ICH) is a prevalent type of stroke (10%–15% of all strokes) that afflicts approximately 2 million people worldwide annually (1). It elevates intracranial pressure and induces neurologic deficits, leading to high morbidity and mortality due to limited therapeutic approaches, and only one-fifth of survivors regain their independence after 6 months (2). Accumulating evidence suggests that surgical removal of the blood clot does not benefit patients (2, 3). Consequently, there is an urgent need to discover novel approaches in order to enhance functional recovery.

Despite being "immune privileged," T cells are implicated in cognitive and social brain function under both physiological and pathological conditions (4). Hematoma formation disrupts the blood–brain barrier (BBB), resulting in inflammatory responses and lymphocyte extravasation from peripheral blood into the central nervous system (CNS), eventually

eliciting brain injury (5). Compelling evidence indicates that the activity of infiltrating T cells unequivocally contributes to the progression of neuroinflammation following CNS injury (6). However, the potential mechanisms underlying the infiltration and role of T cells in ICH are currently underexplored. Recent studies present two conflicting hypotheses (beneficial or harmful) regarding the effect of T cells after CNS injury, potentially attributed to the type of infiltrating T cells and the stage of the disease (5, 7, 8).

As is well documented, the levels of various T cell subsets (including regulatory T cells and helper T 17 cells) and cytokines (including IL-6, IL-17, IL-23, TNF-α, IL-4, IL-10, and TGF-β) are higher in the peripheral blood of ICH patients (9). However, the crosstalk between T cells, cytokines, and clinical outcomes in ICH patients remains elusive. The origin and type of T cells can be identified via T cell receptor (TCR) immune repertoire sequencing (IR-seq) using next-generation sequencing (NSG) (10). TCR is composed of variable (V), diversity (D), joining (J), and constant (C) domains, wherein the area from the terminus of the V domain to the beginning of the J domain is referred to as the complementarity-determining region 3 (CDR3) (11). CDR3 is a critical area that recognizes and binds specific antigens, thereby determining TCR specificity and clonotype (12, 13). Our previous studies inferred that T cells can sense external stimuli and preserve endogenous homeostasis, leading to the reconstitution of the TCR repertoire under disease status (14–16). Nevertheless, fluctuations in the TCR repertoire and its association with outcomes in ICH have not been elucidated so far.

According to the findings of previous studies, we hypothesized an essential evolution of the TCR repertoire in response to ICH-induced immune abnormalities. In the present study, the correlation between the total number of different peripheral blood cells and hematoma volume/Glasgow Coma Scale (GCS) score was initially assessed. Briefly, peripheral blood mononuclear cells (PBMCs) from patients with ICH and healthy controls were collected to measure the T cell state via flow cytometry. Then, NGS was utilized to monitor the profile of the TCR repertoire in ICH-associated PBMCs within 24 h from symptom onset. Our work identified a shift in the TCR repertoire in ICH, which is closely associated with patient prognosis.

Materials and methods

Subjects

This study belongs to basic experimental research. A total of 45 patients (26 male and 19 female; mean age = 59.9 ± 12.4 years) diagnosed with acute spontaneous ICH (<24 h from symptom onset) were admitted to the Department of Emergency Medicine, Xiang'an Hospital of Xiamen University from May 2021 to May 2022. All patients underwent head CT scan (Supplementary Figure S1) and GCS evaluation within 6 h of hospital admission. Exclusion criteria were (a) non-parenchymal hemorrhages (isolated subarachnoid hemorrhage, epidural or subdural hematoma), (b) ICH attributed to a clearly defined cause (trauma, structural vascular lesions, neoplasms, vasculitis, infection), (c) unavailable head CT scan within 6 h, (d) prior administration of drugs or surgical intervention before hospital admission, (e) infectious, autoimmune and chronic disease. The volume of the hematoma was calculated as previously described using CT images by two experienced neurologists (17). A major proportion (>90%) of patients belong to hypertension with basal ganglia hematoma. For biological experiments, the samples were randomly selected from these patients. Additionally, 10 healthy individuals (5 males and 5 females; mean age = 60.2 ± 7.8 years) without clinical signs of ICH were included as controls. The study protocol was approved by the Institutional Ethical Commission for the School of Medicine at Xiamen University. Written informed consent was obtained from all participants in accordance with the principles of the Declaration of Helsinki.

PBMCs collection and flow cytometry

Human blood samples were collected in EDTA-treated anticoagulant tubes from ICH patients within 24 h after ICH onset. For PBMC isolation, blood and Ficoll (Solarbio Life Sciences, Beijing, China) were mixed (volume ratio 1:1) and centrifuged at 1,000 g for 30 min. Then, the isolated cells were washed 3 times, followed by staining with fluorescently conjugated antibodies against FITC-CD3 (clone: OKT3) and PE-CD38 (clone: HIT2) from BioLegend. Lastly, the stained cells were examined using a BD Aria III machine and analyzed with FlowJo software 10.6.2 version (TreeStar).

Immune repertoire sequencing and data analysis

Total RNA was isolated from PBMCs using a SPARKeasy RNA Extraction Kit (Sparkiade Biotechnology Co., Ltd., Shandong, China) according to the manufacturer's specifications. A Transcriptor First Strand cDNA Synthesis Kit (LABLEAD, Beijing, China) was employed to reverse-transcribe RNA to cDNA using a T1000 Thermal Cycler (Bio-Rad Inc., Hercules, CA). For TCR immune repertoire library construction, a two-round nested amplicon PCR was performed using specific primers as previously described. Purified amplicons were paired-end sequenced (PE150) on the Illumina HiSeq X Ten platform (Illumina, San Diego, CA).

For immune repertoire data analysis, Blast Plus was utilized to identify TCR β chain V, D, and J genes in each sequence based on the TCR reference genome sourced from the International Immunogenetics Information System (IMGT)/GeneDB database. VDJmatch 1.2.2, VDJtools 1.2.1 package and VDJdb were used to identify the usage and clonotype of V, D, and J genes. The motif of CDR3 aa was identified using the ggseqlogo 0.1 package.

Statistical analysis

Statistical analyses were conducted using Prism 8.0 software (GraphPad Software), and data were presented as means ± standard deviations (SD). For immune repertoire data, a normality check has been done using Shapiro–Wilk test. The results showed that immune repertoire data (frequency, clonotypes, Chao1 and Gini coefficient) followed normal distribution. The two-tailed unpaired Student's *t*-test was used for the comparison of two independent groups. Correlation analysis was performed using Spearman's rank correlation test. p values less than 0.05 were considered statistically significant.

Results

Acute spontaneous ICH reduces T-cell abundance in PBMCs

Emerging evidence supports the notion that the hematoma volume reflects the severity and the prognosis of ICH. Indeed, our results demonstrated a negative correlation between GCS score and hematoma volume (Figure 1A). Interestingly, the GCS score was negatively correlated with the total count of WBC/neutrophils (Figures 1B,C) and positively correlated with lymphocyte counts (Figure 1D) in ICH-associated PBMCs. Similarly, a negative correlation was identified between hematoma volume and the lymphocyte count (Figure 1E). However, the total number of other cell subsets was not associated with GCS score or hematoma volume (Supplementary Figure S2). Moreover, flow cytometry determined a substantial decrease in the proportion of T cells and an increase in that of activated T cells (Figures 1F,G).

The patterns of V, D, and J genes in ICH

PBMC IR-seq from 10 control and 10 ICH patients were used to detect the TCR repertoire, yielding 4.35×10^6~7.93×10^6 productively TCR β chain blast reads per sample, with matching rates within the range of 65.03%~90.34% (Supplementary Table S1). A total of 52~58 V genes and 13~14 J genes were identified across all samples. Generally, the type and top usages of V/J were similar between the two groups (Figures 2A,B). On the other hand, significant differences were noted in the frequency of TRBV6-2, TRBV5-8, and TRBV6-9 (Figures 2C,D). Besides, the composition of paired VJ and VDJ usages was also analyzed. A total of 535~618 VJ usages and 821~1,107 VDJ usages were detected across all samples. Importantly, ICH significantly limited the frequency of several VJ and VDJ usages (Figures 2E,F). While a total of 32,123~76,735 CDR3 aa were identified, few CDR3 aa frequencies were significantly different between the control and ICH groups (Figure 2G).

ICH decreases the diversity of the T cell immune repertoire

The types of CDR3aa clonotype represent the diversity of the TCR immune repertoire. Of note, ICH markedly decreased the clonotype of V, J, VJ, VDJ, and CDR3aa despite their usage frequencies being comparable (Figures 3A–E). Subsequently, multiple parameters were used to evaluate the richness and diversity of the TCR immune repertoire. Chao1 index and Gini coefficient indicated a lower CDR3 aa abundance in ICH-associated PBMCs (Figures 3F–H). Likewise, Hill analysis, Rarefaction analysis, and Rank-Abundance analysis also identified a lower diversity of TCR clonotypes in PBMCs from ICH patients (Figures 3I–K). Furthermore, similar CDR3aa were clustered to compare their expression between the two groups. As anticipated, there was a significantly sparse distribution in the ICH group (Figure 3L).

TCR diversity is associated with the outcome of ICH

Principal component analysis revealed that ICH resulted in a significantly different CDR3 aa profile characterized by a

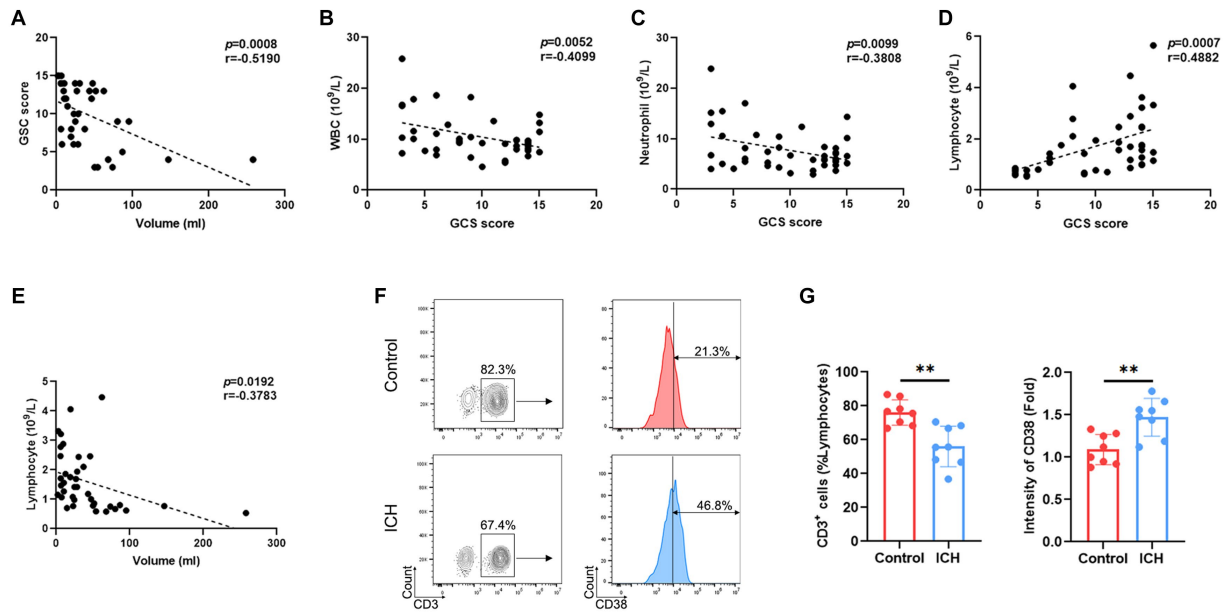

FIGURE 1
ICH leads to abnormal peripheral T-cell responses. **(A)** Correlation analysis between GCS score and hematoma volume. $n = 38$. **(B–D)** Correlation analysis between the count of WBCs/neutrophils/lymphocytes and GCS score. $n = 45$. **(E)** Correlation analysis between the lymphocyte count and hematoma volume. $n = 45$. **(F)** Representative flow cytometry image of CD3-positive cells and the expression levels of CD3-gated CD38. $n = 8$. **(G)** The percentage and CD38 fluorescence intensities of T cells. Data represent the results of three to five independent experiments. $^{**}p < 0.01$.

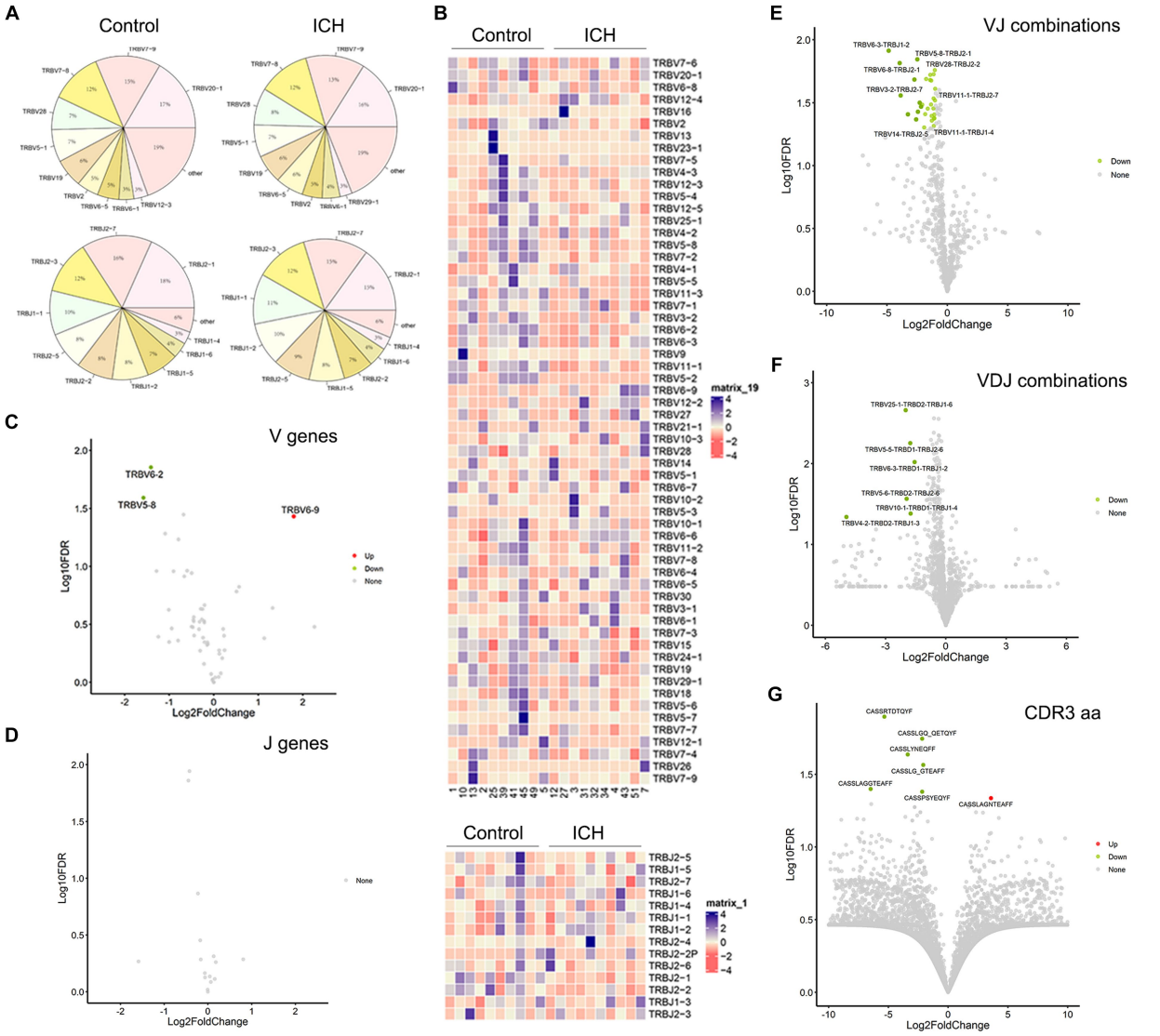

FIGURE 2
The usage of V gene, J gene and CDR3 aa. **(A)** The distribution of the top 10 V and J genes. $n = 10$. **(B)** Heatmaps of hierarchical clustering of V and J gene. $n = 10$. **(C,D)** Volcano plots of frequency of the V and J genes. $n = 10$. **(E–G)** Volcano plots of frequency of VJ combinations, VDJ combinations, and CDR3 aa. $n = 10$. Data represent the results of three to five independent experiments.

centralized distribution, signaling aberrant composition of CDR3 aa clonotypes (Figure 4A). Noteworthily, a substantial increase in CDR3 aa length was found after ICH, although the usages of V and J genes were similar across different CDR3 aa lengths (Figures 4B,C). Furthermore, the specific motif in high-frequency CDR3 aa (top 50%) was examined. Of note, a significantly different CDR3 motif was identified in the ICH group (Figure 4D). However, the proportion of high-frequency CDR3 aa was comparable between the two groups (Supplementary Figure S3). To investigate the correlation between the profile of CDR3 aa and outcomes of acute spontaneous ICH, correlation analyses of clonotype or chao1 of CDR3 aa and GCS score or hematoma volume were executed. On the one hand, a significant positive correlation was observed between CDR3 aa diversity and GCS score (Figures 5A,B). On the other hand, a negative correlation was identified between CDR3 aa diversity and hematoma volume (Figures 5C,D). These results collectively indicated that TCR diversity is a potential marker for assessing ICH prognosis.

Discussion

The CNS parenchyma is considered a lymphocyte-free organ, but T cells are found in the meninges and have been speculated to influence brain function. Emerging evidence insinuates that T cells extravasate from blood vessels into CNS through a chemokine gradient after ICH, similar to the mechanism by which they infiltrate peripheral tissues. Nonetheless, the precise role of T cells in brain function and recovery remains unknown. Earlier studies evinced that the TCR immune repertoire plays a pivotal role in monitoring the immune microenvironment. Accordingly, the identification of the TCR immune repertoire

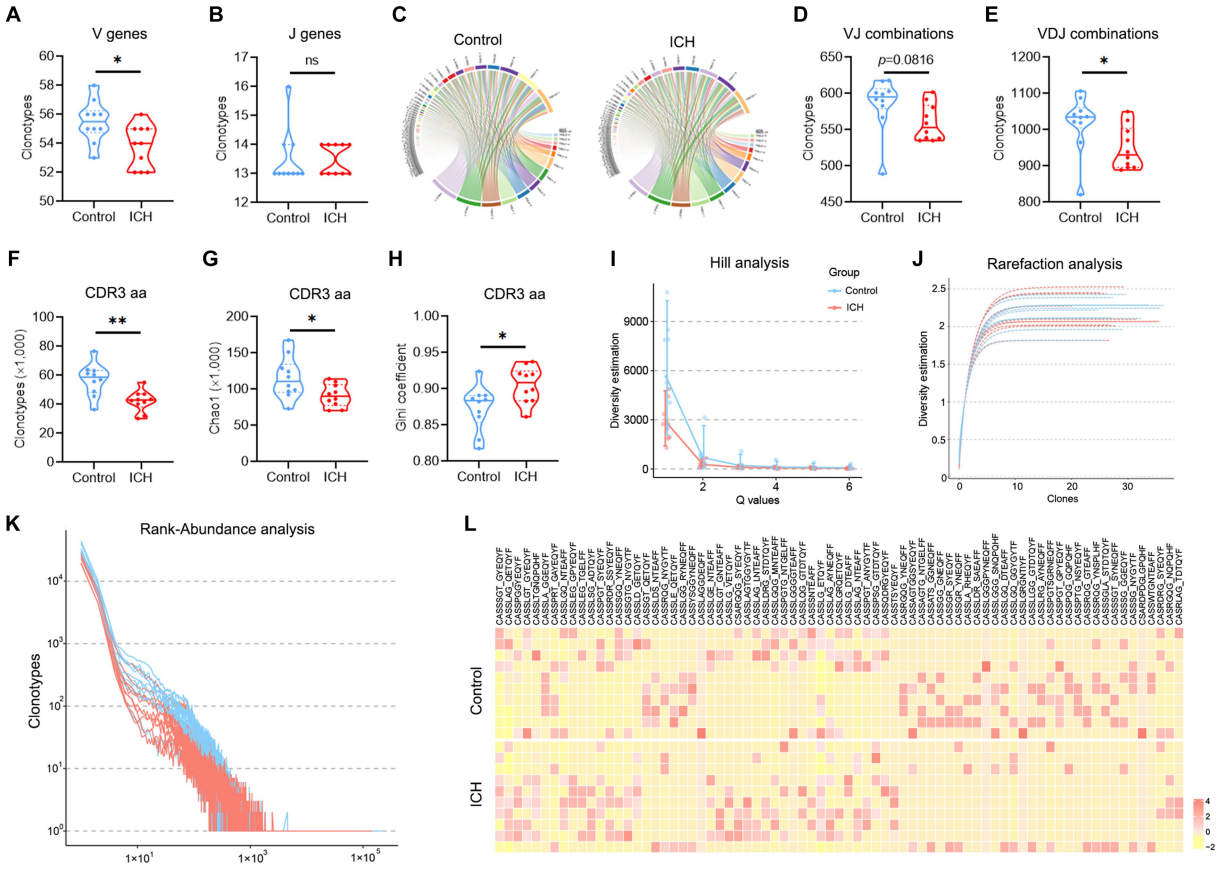

FIGURE 3
A significantly decreased TCR diversity was identified in ICH. **(A,B)** Clonotype of the V and J genes. $n = 10$. **(C)** Representative circle plot of paired VJ combinations. **(D,E)** Clonotype of VJ and VDJ combinations. $n = 10$. **(F–H)** Clonotype, Chao1, and Gini coefficient of CDR3 aa. $n = 10$. **(I–K)** Hill analysis, Rarefaction analysis, and Rank-Abundance analysis of CDR3 aa. $n = 10$. **(L)** Heatmap of the hierarchical clustering of similar CDR3 aa clusters. $n = 10$. $^*p < 0.05$, $^{**}p < 0.01$. Data represent the results of three to five independent experiments.

offers a strategy to track alterations in the peripheral immune microenvironment in ICH.

Herein, the immune response in ICH-associated blood was evaluated. The current study identified a significant correlation between the lymphocyte count and symptoms after the onset of ICH, suggesting that ICH can drive a shift in the distribution of peripheral T cells, consistent with the results of prior investigations (9, 18). Indeed, severe brain injury modulates the immune response. However, the precise mechanism by which neurogenic pathways are involved remains undefined. Lymphopenia may be ascribed to spleen shrinkage owing to the synergy between the sympathetic and hypothalamus-pituitary–adrenal axis (18).

A huge pool of evidence indicates that lymphocytes infiltrate into the brain immediately after a stroke (5). Nonetheless, to date, no specific cell population has been identified as a dominant pathogenetic initiator of stroke. While accumulating evidence supports the notion that T cells play a pathological role in brain injuries, the interactions between T cells and brain-intrinsic cells in the brain are poorly understood. Our results revealed the peripheral landscape of TCR change after ICH. Due to TCR tracking the origin of T cell development, the effect of ICH on adaptive immunity could be monitored by TCR repertoire. Moreover, we will find the more clues of the specific T cells in brain injury or repair. The deep mechanism that how the T cells modulate CNS pathological process can be investigated in our further work. A challenge in the identification of a specific T cell subset is determining the factor that triggers T cell diapedesis across the BBB into the lesion site. Recently, regulatory T cells, identified as an immunosuppressive T cell population, have been described as a central cerebroprotective modulator after stroke, targeting multiple inflammatory pathways via the IL-10 signaling pathway (19). Thus, it is of paramount importance to investigate T-cell transformation for the development of an effective immunotherapeutic strategy for ICH patients.

A recent study documented an antigen-independent mechanism of T cell neuroprotection after brain injury. A T cell adoptive treatment in major histocompatibility complex class II (MHC II)-deficient mice markedly alleviated neuronal damage after injury via MYD 88 and IL-4-mediated neuroprotection (20). Although the beneficial effect was independent of TCR-MHC II interaction, T cells may infiltrate the brain after CNS injury via multiple mechanisms (both antigen-dependent and antigen-independent). The availability of antigens or peptides released from the site of brain lesions has been theorized to endow T cells with neuroprotective functions (21). Therefore, tracking TCR repertoire after ICH may offer valuable insights into identifying the origin and function of T cells.

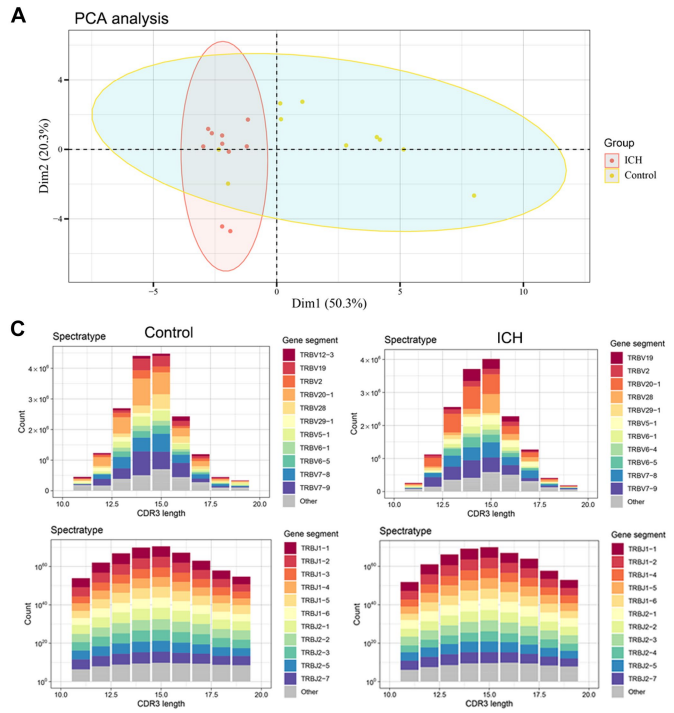

FIGURE 4
ICH results in CDR3 aa reconstitution. **(A)** PCA analysis of CDR3 aa. $n = 10$. **(B)** Comparison of clonotypes of different CDR3 aa lengths. $n = 10$. **(C)** The spectratype of the V and J genes in different CDR3 aa lengths. $n = 10$. **(D)** High-frequency (top 50%) CDR3 aa motifs. Data represent the results of three to five independent experiments.

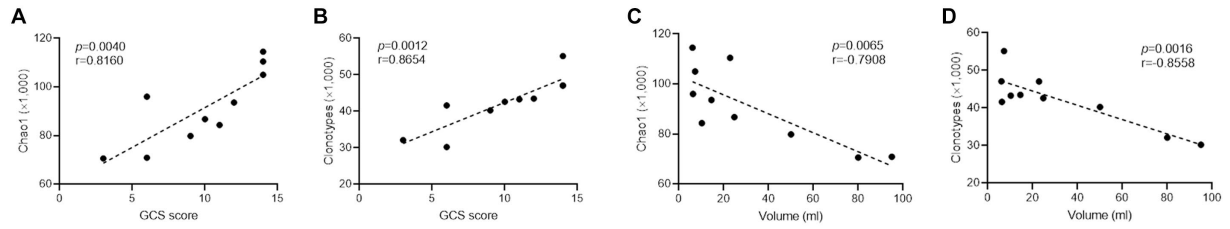

FIGURE 5
TCR diversity predicts ICH severity. **(A,B)** Correlation analysis between Chao1, clonotype of CDR3 aa, and GCS score. $n = 10$. **(C,D)** Correlation analysis between Chao1, clonotype of CDR3 aa, and hematoma volume. $n = 10$. Data represent the results of three to five independent experiments.

Our study revealed an intact TCR profile of V, J, VJ, VDJ, and CDR3 aa distribution in peripheral blood after ICH. Besides, a centralized clonotype and length CDR3 with chaotic CDR3 motif aa were found in the TCR repertoire, in line with the findings of previous studies reporting that ICH induced a significant decrease in the number of peripheral T cells. The shift in the TCR repertoire is indispensable for antigen recognition after ICH. In addition, notable relationships were discovered between CDR3 diversity and GCS score or hematoma volume, indicating that the TCR repertoire may serve as a biomarker for ICH symptoms and prognosis. Undoubtedly, the ICH-responsive TCR repertoire provides valuable clues on the origin of T cells, which enhances our understanding of the functions of T cells in brain injury. However, the mechanisms that govern TCR reconstitution in CNS damage and repair remain to be unraveled, warranting further studies.

Data availability statement

The data presented in the study are deposited in the NGDC GSA repository, accession number HRA006678, https://ngdc.cncb.ac.cn/gsa-human/.

Ethics statement

The studies involving humans were approved by Institutional Ethical Commission for the School of Medicine at Xiamen University. The studies were conducted in accordance with the local legislation and institutional requirements. The participants provided their written informed consent to participate in this study. Written informed consent was obtained from the

individual(s) for the publication of any potentially identifiable images or data included in this article.

Author contributions

RZ: Writing – original draft, Conceptualization, Data curation, Formal analysis, Funding acquisition, Investigation, Methodology, Project administration, Resources, Software, Supervision, Validation, Visualization. LW: Conceptualization, Data curation, Formal analysis, Funding acquisition, Investigation, Methodology, Project administration, Resources, Software, Supervision, Validation, Visualization, Writing – original draft. JZ: Resources, Validation, Visualization, Writing – original draft. XZ: Resources, Validation, Writing – original draft, Formal analysis. PW: Writing – original draft, Writing – review & editing.

Funding

The author(s) declare that no financial support was received for the research, authorship, and/or publication of this article.

Acknowledgments

The authors are grateful to MUSI biotech Co., Ltd. (Shanghai, China) and PUCG biotech Co., Ltd. (Shanghai, China) for technical support. We thank Home for Researchers editorial team (www.home-for-researchers.com) for language editing service.

Conflict of interest

The authors declare that the research was conducted in the absence of any commercial or financial relationships that could be construed as a potential conflict of interest.

Publisher's note

All claims expressed in this article are solely those of the authors and do not necessarily represent those of their affiliated organizations, or those of the publisher, the editors and the reviewers. Any product that may be evaluated in this article, or claim that may be made by its manufacturer, is not guaranteed or endorsed by the publisher.

Supplementary material

The Supplementary material for this article can be found online at: https://www.frontiersin.org/articles/10.3389/fneur.2024.1371830/full#supplementary-material

References

1. Krishnamurthi RV, Feigin VL, Forouzanfar MH, Mensah GA, Connor M, Bennett DA, et al. Global and regional burden of first-ever ischaemic and haemorrhagic stroke during 1990-2010: findings from the global burden of disease study 2010. *Lancet Glob Health*. (2013) 1:e259–81. doi: 10.1016/S2214-109X(13)70089-5

2. Cordonnier C, Demchuk A, Ziai W, Anderson CS. Intracerebral haemorrhage: current approaches to acute management. *Lancet*. (2018) 392:1257–68. doi: 10.1016/S0140-6736(18)31878-6

3. de Oliveira Manoel AL. Surgery for spontaneous intracerebral hemorrhage. *Crit Care*. (2020) 24:45. doi: 10.1186/s13054-020-2749-2

4. Ito M, Komai K, Mise-Omata S, Iizuka-Koga M, Noguchi Y, Kondo T, et al. Brain regulatory T cells suppress astrogliosis and potentiate neurological recovery. *Nature*. (2019) 565:246–50. doi: 10.1038/s41586-018-0824-5

5. Filiano AJ, Gadani SP, Kipnis J. How and why do T cells and their derived cytokines affect the injured and healthy brain? *Nat Rev Neurosci*. (2017) 18:375–84. doi: 10.1038/nrn.2017.39

6. Corps KN, Roth TL, McGavern DB. Inflammation and neuroprotection in traumatic brain injury. *JAMA Neurol*. (2015) 72:355–62. doi: 10.1001/jamaneurol.2014.3558

7. Krämer TJ, Hack N, Brühl TJ, Menzel L, Hummel R, Griemert EV, et al. Depletion of regulatory T cells increases T cell brain infiltration, reactive astrogliosis, and interferon-gamma gene expression in acute experimental traumatic brain injury. *J Neuroinflammation*. (2019) 16:163. doi: 10.1186/s12974-019-1550-0

8. Weitkamp JH. Gut-derived T cells might cause brain injury in NEC. *Nat Rev Gastroenterol Hepatol*. (2021) 18:291–2. doi: 10.1038/s41575-021-00432-6

9. Jiang C, Wang Y, Hu Q, Shou J, Zhu L, Tian N, et al. Immune changes in peripheral blood and hematoma of patients with intracerebral hemorrhage. *FASEB J*. (2020) 34:2774–91. doi: 10.1096/fj.201902478R

10. Liu H, Pan W, Tang C, Tang Y, Wu H, Yoshimura A, et al. The methods and advances of adaptive immune receptors repertoire sequencing. *Theranostics*. (2021) 11:8945–63. doi: 10.7150/thno.61390

11. Liang Q, Liu Z, Zhu C, Wang B, Liu X, Yang Y, et al. Intrahepatic T-cell receptor beta immune repertoire is essential for liver regeneration. *Hepatology*. (2018) 68:1977–90. doi: 10.1002/hep.30067

12. Glanville J, Huang H, Nau A, Hatton O, Wagar LE, Rubelt F, et al. Identifying specificity groups in the T cell receptor repertoire. *Nature*. (2017) 547:94–8. doi: 10.1038/nature22976

13. Hou XL, Wang L, Ding YL, Xie Q, Diao HY. Current status and recent advances of next generation sequencing techniques in immunological repertoire. *Genes Immun*. (2016) 17:153–64. doi: 10.1038/gene.2016.9

14. Li D, Hu L, Liang Q, Zhang C, Shi Y, Wang B, et al. Peripheral T cell receptor beta immune repertoire is promptly reconstituted after acute myocardial infarction. *J Transl Med*. (2019) 17:40. doi: 10.1186/s12967-019-1788-4

15. Liang Q, Zhang M, Hu Y, Zhang W, Zhu P, Chen Y, et al. Gut microbiome contributes to liver fibrosis impact on T cell receptor immune repertoire. *Front Microbiol*. (2020) 11:571847. doi: 10.3389/fmicb.2020.571847

16. Liu J, Liu Z, Zhu Y, Dong B, Cai Z, Liang Q, et al. T cell receptor immune repertoires are promptly reconstituted after methicillin-resistant *Staphylococcus aureus* infection. *Front Microbiol*. (2019) 10:2012. doi: 10.3389/fmicb.2019.02012

17. Sembolini A, Romoli M, Pannacci U, Gambaracci G, Floridi P, Acciarresi M, et al. Acute hematoma expansion after spontaneous intracerebral hemorrhage: risk factors and impact on long-term prognosis. *Neurol Sci*. (2020) 41:2503–9. doi: 10.1007/s10072-020-04356-y

18. Zhang J, Shi K, Li Z, Li M, Han Y, Wang L, et al. Organ- and cell-specific immune responses are associated with the outcomes of intracerebral hemorrhage. *FASEB J*. (2018) 32:220–9. doi: 10.1096/fj.201700324r

19. Liesz A, Suri-Payer E, Veltkamp C, Doerr H, Sommer C, Rivest S, et al. Regulatory T cells are key cerebroprotective immunomodulators in acute experimental stroke. *Nat Med*. (2009) 15:192–9. doi: 10.1038/nm.1927

20. Walsh JT, Hendrix S, Boato F, Smirnov I, Zheng J, Lukens JR, et al. MHCII-independent CD4+ T cells protect injured CNS neurons via IL-4. *J Clin Invest*. (2015) 125:699–714. doi: 10.1172/JCI76210

21. Shi Z, Yu P, Lin WJ, Chen S, Hu X, Chen S, et al. Microglia drive transient insult-induced brain injury by chemotactic recruitment of CD8(+) T lymphocytes. *Neuron*. (2023) 111:e9:696–710.e9. doi: 10.1016/j.neuron.2022.12.009

frontiers | Frontiers in Neurology

TYPE Review
PUBLISHED 28 March 2024
DOI 10.3389/fneur.2024.1367854

Check for updates

OPEN ACCESS

EDITED BY
Shubham Misra,
Yale University, United States

REVIEWED BY
Freda Werdiger,
The University of Melbourne, Australia
Giuseppe Miceli,
University of Palermo, Italy

*CORRESPONDENCE
Hongbo Wang
✉ sj_wanghb@163.com

RECEIVED 09 January 2024
ACCEPTED 08 March 2024
PUBLISHED 28 March 2024

CITATION
Zhao Z, Zhang Y, Su J, Yang L, Pang L, Gao Y and Wang H (2024) A comprehensive review for artificial intelligence on neuroimaging in rehabilitation of ischemic stroke.
Front. Neurol. 15:1367854.
doi: 10.3389/fneur.2024.1367854

COPYRIGHT
© 2024 Zhao, Zhang, Su, Yang, Pang, Gao and Wang. This is an open-access article distributed under the terms of the Creative Commons Attribution License (CC BY). The use, distribution or reproduction in other forums is permitted, provided the original author(s) and the copyright owner(s) are credited and that the original publication in this journal is cited, in accordance with accepted academic practice. No use, distribution or reproduction is permitted which does not comply with these terms.

A comprehensive review for artificial intelligence on neuroimaging in rehabilitation of ischemic stroke

Zijian Zhao[1], Yuanyuan Zhang[1], Jiuhui Su[2], Lianbo Yang[3], Luhang Pang[4], Yingshan Gao[4] and Hongbo Wang[5]*

[1]Rehabilitation Center, ShengJing Hospital of China Medical University, Shenyang, Liaoning Province, China, [2]Department of Orthopedics, Haicheng Bonesetting Hospital, Haicheng, Liaoning Province, China, [3]Department of Reparative and Reconstructive Surgery, The Second Hospital of Dalian Medical University, Dalian Liaoning Province, China, [4]Department of Radiology, Shengjing Hospital of China Medical University, Shenyang, Liaoning Province, China, [5]Department of Radiology, Shengjing Hospital of China Medical University, Shenyang, Liaoning Province, China

Stroke is the second leading cause of death worldwide, with ischemic stroke accounting for a significant proportion of morbidity and mortality among stroke patients. Ischemic stroke often causes disability and cognitive impairment in patients, which seriously affects the quality of life of patients. Therefore, how to predict the recovery of patients can provide support for clinical intervention in advance and improve the enthusiasm of patients for rehabilitation treatment. With the popularization of imaging technology, the diagnosis and treatment of ischemic stroke patients are often accompanied by a large number of imaging data. Through machine learning and Deep Learning, information from imaging data can be used more effectively. In this review, we discuss recent advances in neuroimaging, machine learning, and Deep Learning in the rehabilitation of ischemic stroke.

KEYWORDS

ischemic stroke, rehabilitation, artificial intelligence, MRI, CT

1 Introduction

1.1 Epidemiology of ischemic stroke

Stroke stands as the second leading cause of global mortality and a primary contributor to disability and cognitive impairment (1). Stroke is classified into ischemic stroke and hemorrhagic stroke. Among these, ischemic stroke prevails. Approximately 9.5 million cases of ischemic stroke were reported globally in 2016 (2). In addition, 2.7 million people succumbed to ischemic stroke each year worldwide (3). Thromboembolism remains the leading cause of most ischemic strokes, primarily attributed to large artery atherosclerosis and cardiac conditions, particularly atrial fibrillation (4).

1.2 The application of artificial intelligence in the field of stroke

Artificial Intelligence (AI) technology is a rapidly advancing field. In the realm of brain diseases, AI is widely employed for the detection, segmentation, classification, and

identification of large vessel occlusion (LVO) in both hemorrhagic and ischemic strokes. Tang et al. (5) proposed a computer-aided detection scheme that detects early-stage ischemic strokes with small lesions through image feature analysis. The use of this method was found to improve stroke detection by healthcare professionals. The diagnosis of LVO is particularly crucial for selecting patients suitable for mechanical thrombectomy. An artificial neural network (ANN) algorithm developed by Chen et al. (6) demonstrated a high predictive accuracy of 0.820 for LVO, surpassing other prehospital prediction models. Additionally, research suggests that radiomics scores serve as independent prognostic indicators for the outcomes of acute ischemic stroke (7). Pfaff et al. (8) indicated that the e-ASPECTS software can be utilized to predict adverse outcomes after mechanical thrombectomy. Furthermore, survivors of strokes often experience upper limb motor deficits and achieve limited functional recovery within 6 months post-stroke. Many studies suggest the widespread application of robots in assisting patients with motor function rehabilitation (9). The utilization of artificial intelligence for the accurate analysis of medical images and clinical data, enabling rapid and precise identification of cerebrovascular disease types and etiologies. This facilitates the development of personalized treatment and rehabilitation plans, ultimately leading to improved patient survival rates and quality of life (10).

1.2.1 Related research trends

As depicted in Figure 1, articles related to ischemic stroke have shown an upward trend in the past 15 years. With the rapid development and widespread application of Artificial Intelligence in the field of medicine, research in this area has experienced an explosive growth in the last 3 years. Furthermore, it is evident that there are only 337 articles specifically focused on evaluating the prognosis or rehabilitation of ischemic stroke, constituting a small fraction of the overall literature. In comparison to prognosis prediction, more studies are concentrated on the detection of ischemic stroke itself.

1.2.2 Detection modalities

As illustrated in Figure 2, articles pertaining to the application of Artificial Intelligence in ischemic stroke have been summarized and categorized based on different data types. It is noteworthy that the prediction of ischemic stroke using medical imaging data emerges as the most prominent area of focus. A significant proportion of articles also revolves around prognostic evaluations based on the mRS scale.

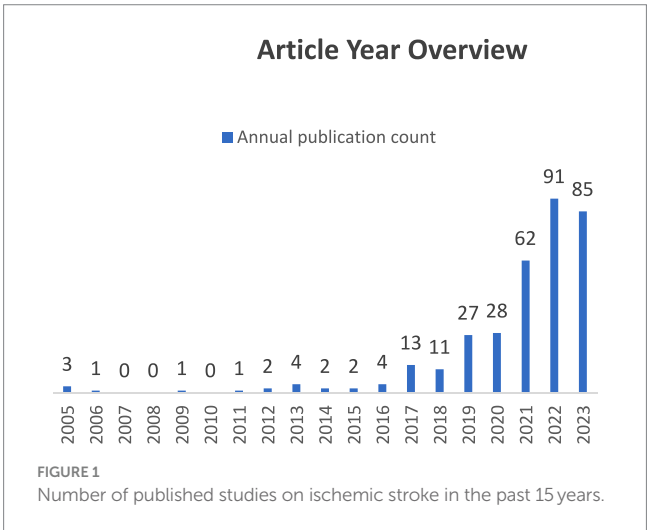

FIGURE 1
Number of published studies on ischemic stroke in the past 15 years.

1.3 Article retrieval

To gather relevant papers for our study, a comprehensive search strategy was devised, employing various combinations of the following keywords: "stroke," "ischemic stroke," "prognosis," "rehabilitation," "Deep Learning," "machine learning," and "Artificial Intelligence." Considering technological advancements and updates, we restricted the publication timeframe to the past 15 years. Using PubMed, Embase, Web of Science, and the Cochrane Library for the search, we initially included all articles reporting on ischemic stroke patients. This yielded 337 articles. After a meticulous review of abstracts and full texts, we first excluded articles not aligned with the research theme, then eliminated those without full texts, and finally removed articles not utilizing Artificial Intelligence for predicting ischemic stroke prognosis or rehabilitation. The selected literature focused on key technologies, resulting in a final set of 49 articles on Artificial Intelligence predictions of ischemic stroke prognosis or rehabilitation as our references. The paper selection process is illustrated in Figure 3.

1.4 The purpose of this article

While existing literature has summarized the research progress of AI in the field of ischemic stroke, most of it has focused primarily on pre-treatment prediction. For instance, Sheth et al. (11) provided an overview of common machine learning methods and their applications in detecting large vessel occlusion, intracranial hemorrhage, and infarct lesions. Soun et al. (12) systematically introduced AI methods in imaging and available public and commercial platforms, summarizing the applications of AI in acute stroke detection and prediction. Despite the detailed content, it did not address the prognosis of stroke patients, which is precisely the focal point of concern for most clinical professionals and patients. Ragoş et al. (13) summarized the evaluation of ischemic stroke outcomes using MRI radiomics and predictive models. However, relying solely on radiomic evaluation is too narrow, and the described imaging methods are not comprehensive enough. Shafaat et al. (14) evaluated the efficacy of machine learning in predicting the prognosis of ischemic stroke patients, overlooking research using methods such as Deep Learning and other AI techniques in this direction. Rüdiger von Kummer and colleagues summarized the progress of CT and MRI brain imaging technologies in acute ischemic stroke (15). This review focuses exclusively on CT/CTA and MRI/MRA imaging. With the advancement of Artificial Intelligence, many new technologies with greater potential applications have emerged. For instance, there is an urgent need to investigate the application value of CTP in ischemic stroke. Therefore, this article aims to systematically evaluate the potential applications of Artificial Intelligence in predicting the prognosis of ischemic stroke patients in the field of neuroimaging, primarily using CT and MR imaging.

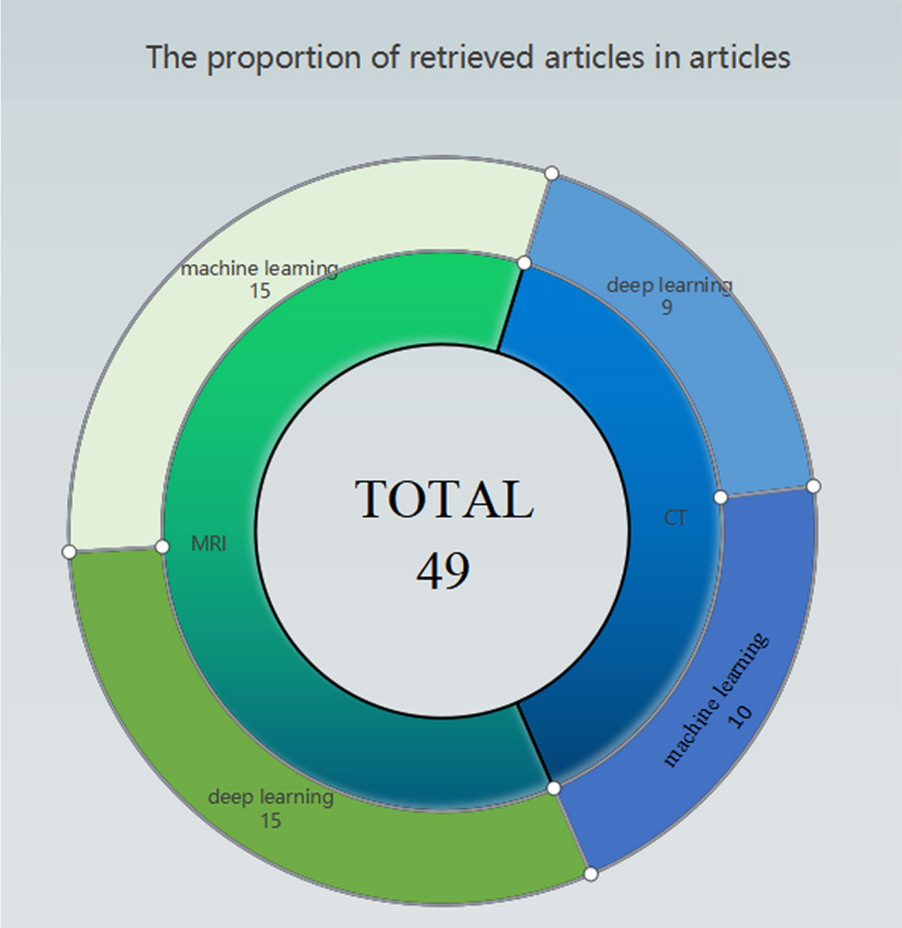

FIGURE 2
Pie chart of classes of studies included in this review.

2 Progress in predicting the rehabilitation of ischemic stroke based on artificial intelligence of neuroimaging

2.1 Radiological manifestations of ischemic stroke

The current diagnostic approach for stroke relies on CT and MRI imaging. MRI has higher sensitivity and specificity for diagnosing ischemic stroke, but due to factors such as longer imaging times and higher costs, CT-based imaging techniques remain the preferred method for diagnosing ischemic stroke. Vascular imaging through CT and MRI aids in identifying the extent of ischemia and the location of arterial occlusion. Furthermore, the results of radiological examinations play a crucial role in determining the treatment approach for ischemic stroke patients, providing support for interventions like thrombolysis and thrombectomy.

2.2 Ischemic stroke treatment

Treatment methods include intravenous thrombolysis, intra-arterial thrombolysis, mechanical thrombectomy, etc. (16). Currently, thrombolytic therapy is the most used treatment for ischemic stroke. The basic principle involves the activation of plasminogen into plasmin by the binding of the thrombus to fibrin, and plasmin breaks down fibrinogen and fibrin, dissolving the thrombus and allowing reperfusion of the ischemic brain (17). Intravenous thrombolysis is established for patients within 4.5 h of stroke onset. If symptoms appear within 6–8 h, mechanical vascular recanalization through stent retriever and/or thrombus aspiration is recommended.

2.3 Methods for evaluating prognosis in ischemic stroke

2.3.1 Modified Rankin scale

The modified Rankin Scale (mRS) is the most widely used measure for assessing the outcomes of acute ischemic stroke in research, clinical trials, and national and local quality improvement registries. It reflects the quality of life as assessed by both patients and healthcare professionals. In certain situations, an mRS score of 5 (bedridden, requiring constant care, and severe disability) is considered more severe than an mRS score of 6 (death) (18). However, studies indicate that among patients who have undergone hemicraniectomy, over 50% experience moderate to severe disability

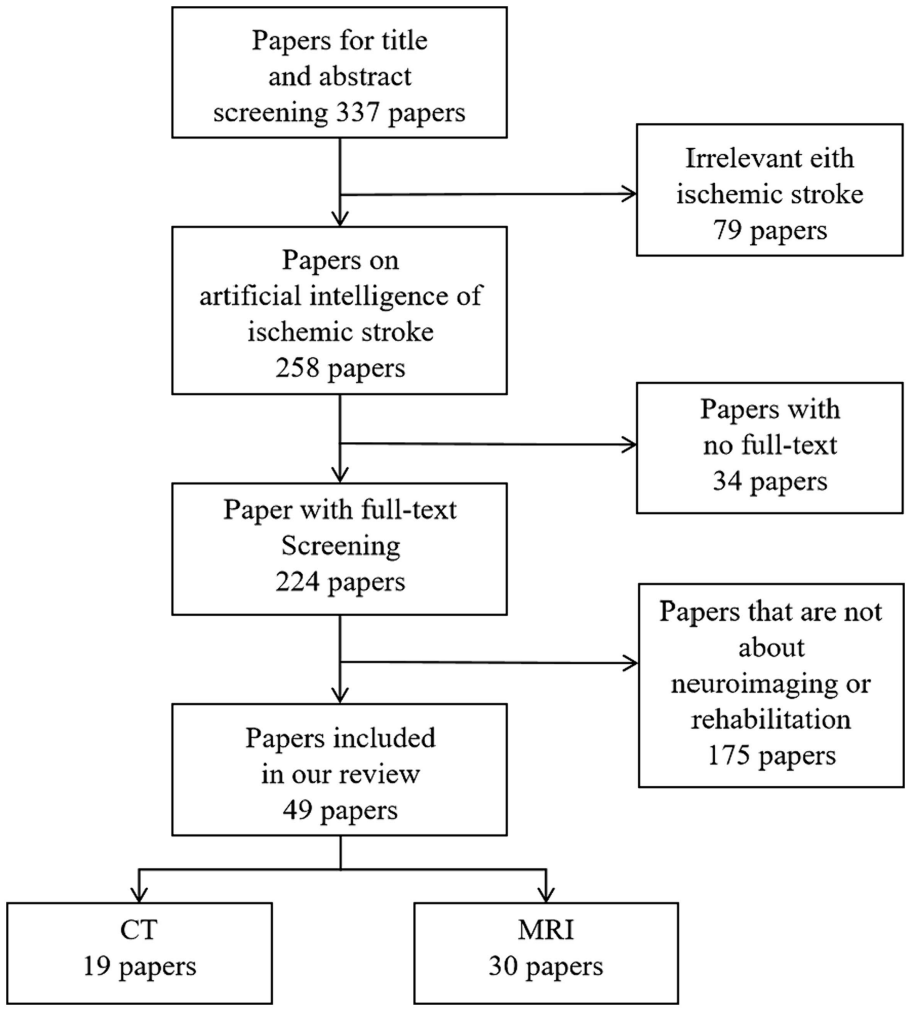

FIGURE 3
Flow chart of paper selection process.

postoperatively, yet remain satisfied with their life status (19). In clinical practice, achieving an mRS score between 0 and 2 (indicating functional independence) is generally considered a treatment success. Additionally, monitoring changes in the degree of disability is crucial. For instance, recovering to a mRS score of 3 is considered better than death or the need for nursing home care (mRS score of 5). Such transitions in disability levels can significantly reduce healthcare costs (4).

2.3.2 Muscle strength assessment

The severe impairment of limb function caused by stroke significantly affects the quality of life of stroke patients. The recovery of post-stroke patients is correlated with the location and size of the infarction. Among them, the primary issue is the motor dysfunction caused by damage to the corticospinal tract and brain motor centers (20). Therefore, improving the muscle strength of patients is an important indicator for assessing the quality of life of stroke patients. Li et al. developed a rehabilitation program for the self-care ability of Acute Ischemic Stroke (AIS) patients based on six levels of commonly used muscle pain assessment methods in clinical practice. This program showed improvement in patients' muscle strength, quality of life, and self-care ability by the third month (21). Fugl-Meyer and others devised a measurement method for functional recovery after cerebrovascular accidents, utilizing an accumulated numerical scoring system. They conducted a 1-year follow-up study on hemiplegic patients, ultimately achieving quantitative assessment of patients' physical functions. This made the scale suitable for statistical analysis in both research and clinical settings (22).

2.3.3 Imaging-based rehabilitation assessment

The degree of early ischemic changes on CT is correlated with stroke severity scores, such as NIHSS and serves as a predictive indicator of clinical outcomes. CTA and CT Perfusion (CTP) imaging are methods used to determine the collateral circulation blood flow status in patients, aiding in the selection of suitable candidates for intra-arterial treatment (23, 24). Patients with poor CTA collateral status tend to have a poorer prognosis even after reperfusion therapy (25). Early improvement in neurological function can often lead to a favorable prognosis, even without additional reperfusion therapy following intravenous tPA administration (26). The extent of collateral circulation may also help in selecting patients who benefit from reperfusion therapy beyond the current time windows for both

intravenous and intra-arterial treatments (27). Several studies indicate that positive results in DWI are associated with specific clinical features, including longer duration of symptoms, motor deficits, aphasia, and large vessel occlusion on Magnetic Resonance Angiography (MRA) (28–30). Importantly, research suggests that positive DWI results play a crucial role in prognosis. Specifically, these studies show a higher risk of recurrent ischemic events in patients with abnormal findings on DWI scans during transient ischemic attacks (TIA) compared to those without abnormalities (30).

2.4 Artificial intelligence-based prediction of stroke prognosis using CT

Distinguishing ischemic stroke from hemorrhagic stroke remains challenging solely through clinical means. Brain CT imaging becomes pivotal in aiding differential diagnosis. Non-enhanced CT scans swiftly and intuitively assist clinicians by showcasing distinct radiological features between ischemic and hemorrhagic strokes. Apart from aiding in the differential diagnosis of hemorrhagic stroke, non-enhanced CT scans are also useful in evaluating the extent of early ischemic damage. Early non-enhanced CT signs of ischemia encompass sulcal effacement and decreased attenuation (31), leading to a loss of gray-white matter differentiation. In some patients, early signs of cerebral ischemic changes, such as loss of gray-white matter differentiation, is suffice for diagnosing ischemic stroke. However, these changes are subtle, particularly within the initial few hours of stroke onset, making the loss of gray-white matter differentiation challenging to discern (4). In general, non-enhanced CT scans exhibit a sensitivity of approximately 52% in detecting substantial ischemic parenchymal changes (32).

CT angiography (CTA) is a perfusion contrast tracking technique capable of displaying major vessels from the aorta to the cranial apex within 15 s (33). CTA boasts superior spatial resolution, surpassing most MRI vascular imaging sequences. It reveals the location and size of occlusive thrombi and provides information regarding collateral blood supply to the ischemic area. CTA exhibits a sensitivity of 95–99% in detecting significantly narrowed or occluded vessels (34). It can determine occlusion locations within 24 h of symptom onset and aid in deciding the suitability for mechanical thrombectomy (35). Besides routine CTA, multiphase CTA, involving imaging before and after contrast passing through different arteries and veins in the brain, can assess collateral circulation status, aiding in evaluating patients suitable for mechanical thrombectomy (36). CTA facilitates assessment of cerebral blood flow and identification of tissue areas at risk of infarction and potential recovery zones (37).

CT perfusion imaging (CTP) is a medical imaging technique that utilizes continuous CT scans of the region of interest to observe changes in contrast agent concentration, thus obtaining time-density curves of the region of interest, indirectly reflecting changes in organ perfusion (38). CTP offers advantages of rapid imaging, effectively and quantitatively reflecting changes in local tissue blood perfusion, and is widely used clinically for the examination of cerebral ischemia (39). Therefore, CTP enables the evaluation of ischemic tissue, aiding in the timely restoration of normal blood supply.

The head CT scan is the preferred diagnostic method for the initial assessment of suspected stroke patients, as shown in Figure 4. Over time, CT can capture the difference in the image of the patient's brain. CT scans are widely available, cost-effective, and provide rapid results. Modern CT scanners can examine the entire brain in less than 1 s. However, it is difficult to differentiate between acute ischemic stroke (AIS) and intracerebral hemorrhage (ICH) based solely on clinical presentation. In CT images, acute ICH is characterized by a higher density shadow that appears brighter than normal brain tissue.

2.4.1 The application of machine learning in stroke

In 2019, Xie et al. incorporated CT, CTA, and perfusion CT data from 512 patients with acute ischemic stroke. Seven binomial GBM and XGB prediction models were developed using 23 features at admission, to predict patients' mRS scores at 90 days. After adding the 24-h NIHSS score, the results of the study showed that the predictive performance of the models was significantly improved with the addition of the 24-h NIHSS score, with AUCs ranging from 0.794 to 0.873 for the XGB model and 0.811 to 0.866 for the GBM model. The conclusions of the study suggest that machine learning can be used to predict the outcome of rehabilitation in stroke patients, with initial imaging information is sufficient, the inclusion of 24-h information improves accuracy, and consideration of recanalization status helps assess treatment risk and benefit (40).

In 2020, Wen et al. incorporated clinical information and NCCT and CTA data from January 30, 2017, to January 2, 2019. These data were obtained within 24 h after symptom onset in patients with MCA territory infarction. Their aim was to develop a model based on radiomic features to predict the development of malignant MCA infarction (mMCAi) in stroke patients. Patients were randomly divided into a training group ($n = 87$) and a validation group ($n = 39$). A total of 396 texture features were extracted from each NCCT image of 126 patients. Using least absolute shrinkage and selection operator regression analysis to reduce the feature dimensions, precise radiomic features were constructed based on the remaining texture features. Subsequently, a radiomic feature model was built using multivariate logistic regression, and its performance was evaluated using AUC. Decision curve analysis (DCA) was employed to assess the clinical efficiency of radiomic features in predicting mMCAi by calculating the net benefit within a threshold probability range. They then developed a model combining radiomic features and the Alberta Stroke Program Early CT Score (ASPECTS) based on NCCT to predict mMCAi. The predictive model demonstrated excellent performance, with AUCs of 0.917 and 0.913 for the training and validation sets, respectively. Furthermore, DCA validated the clinical effectiveness of the predictive model in distinguishing mMCAi and non-mMCAi patients within a threshold probability range of 0.067–1 in the training set and 0.046–1 in the validation set (41).

In 2021, Cheng et al. included CT and CTA data from 135 patients with large vessel occlusive stroke who underwent reperfusion therapy between 2015 and 2019. The aim was to explore the correlation between different CT-ASPECTS (Alberta Stroke Program Early CT Score) methods, follow-up CT-ASPECTS, and prognosis. Researchers calculated the relative differences in Hounsfield Units (HU) between different regions of the ischemic hemisphere and the average HU of the contralateral hemisphere, expressed as a percentage difference. The NCCT, CTA-arterial, and CTA-venous datasets were evaluated in a random order and validated by two expert readers after correctional segmentation. ROC curve analysis was used to assess the ability of different CT-ASPECTS patterns to identify patients with favorable outcomes. Researchers found that CTA-venous-ASPECTS was almost

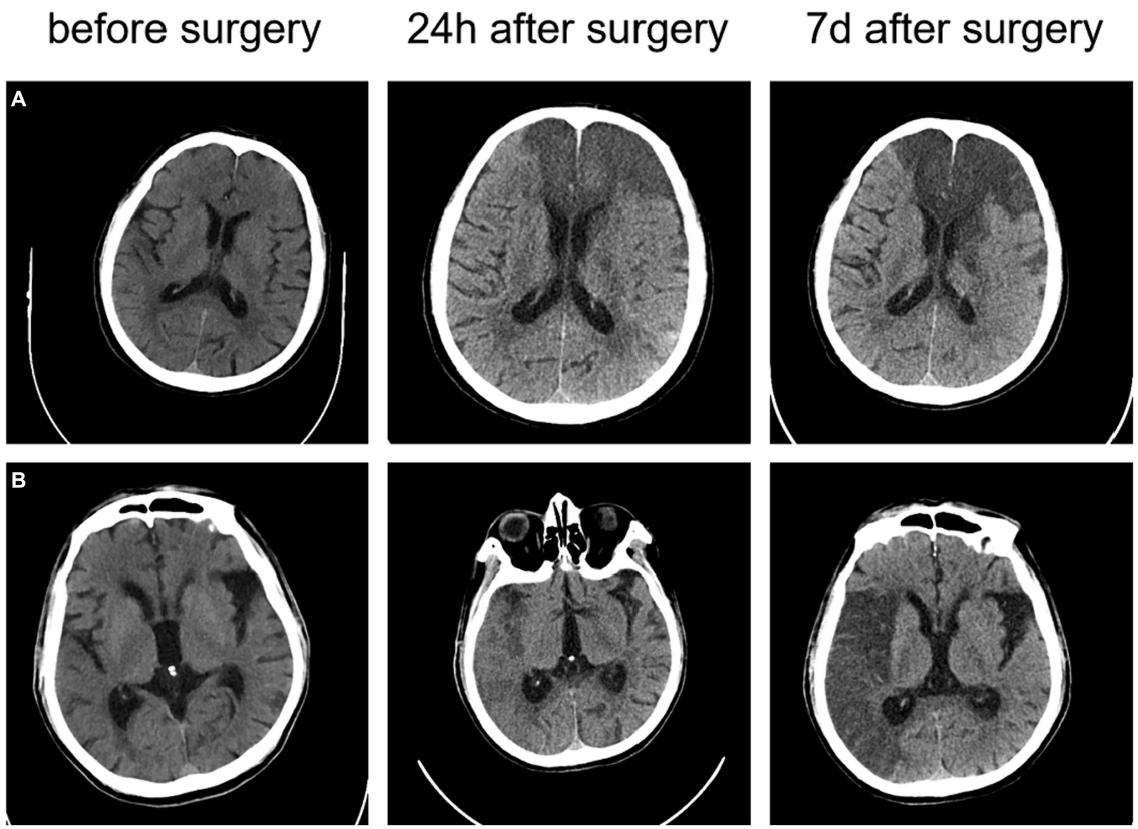

FIGURE 4
The CT images of two ischemic stroke patients undergoing thrombectomy **(A)** a 73-year-old male patient with an NIHSS score of 24 at the onset; and **(B)** a 78-year-old male patient with an NIHSS score of 14 at the onset.

perfectly correlated with follow-up CT-ASPECTS, outperforming other CT examinations. The 90-day mRS scores were significantly associated with CTA-venous-ASPECTS. ROC analysis defined the optimal accuracy and cutoff points for parameters related to the 90-day mRS score. The results indicated that CTA-venous-ASPECTS had the highest area under the curve (AUC: 0.82; 95%CI: 0.75–0.89; $p < 0.001$). This study suggests that CTA-venous-ASPECTS is almost perfectly correlated with the final infarct size and significantly associated with the 90-day mRS score (42).

In 2022, Potreck et al. included 136 stroke patients with major segment occlusion of MCA that occurred between March 2015 and December 2019. Two raters assessed ASPECTS on acute and follow-up NCCT, and a machine-learning algorithm evaluated the ASPECTS scale on NCCT (e-ASPECTS). A third radiologist used the MCA territory collateral score (also known as the Tan scoring system) to assess collateral status on the CT angiogram. The results indicate that inter-rater reliability depends on the duration of stroke symptoms in patients (OTI), with lower reliability observed in the hyperacute group, yielding ICC = 0.54, while higher reliability is seen in groups with longer time windows, yielding ICC = 0.74. The consistency between acute and follow-up ASPECTS improves with prolonged time, and there is a negative correlation between OTI time and ASPECTS. The collateral status serves as a predictor for favorable clinical outcomes, especially in hyperacute stroke. In conclusion, the accuracy and reliability of NCCT-ASPECTS are influenced by time, and collateral status on CT angiography may enhance the prediction of clinical outcomes (43).

In 2022, a study included data from 39 patients with AIS caused by LVO and poor reperfusion after mechanical thrombectomy (MT) from a stroke database between January 2015 and December 2019. The multimodal stroke protocol included non-contrast-enhanced computed tomography (NECT), CTP, and CTA in sequence. The ASPECTS score was used to assess whether early ischemic changes were present on baseline NECT. Three different automated perfusion software solutions (A: RAPID, B: Brainomix e-CTP, C: Syngo.via) were used to assess poor reperfusion. Low-perfusion volumes (HV) with Tmax >6 s were compared with the final infarct volume (FIV) on follow-up CT after futile reperfusion at 36–48 h. The study divided patients into high and low Hyperintense Rim (HIR) groups based on the median ratio of low-perfusion intensity (HIR, tissue volume ratio for Tmax >10 s and Tmax >6 s). Subgroup analyses of FIV (feature importance value) were conducted for favorable and unfavorable HIR. HIR was correlated with baseline clinical and outcome parameters using Pearson correlation. The study found a good correlation between HV and FIV with no significant difference. However, in cases with infarct volumes exceeding 150 mL, the performance of automated software solutions often declined. Subgroup analysis showed that patients with HIR ≥ 0.6 typically had underestimated FIV. However, in the subgroup with favorable HIR, there was a trend of overestimating FIV. Software packages A and B

showed good correlation between HV and FIV with no significant difference, while only software package C significantly overestimated FIV. The mRS score of 0–3 at 3 months was significantly higher in the favorable HIR group than in the unfavorable group. Lower HIR was associated with a higher Alberta Stroke Program Early CT Score (ASPECTS). In conclusion, the performance of automated perfusion software solutions in predicting FIV after futile reperfusion was good, with a decrease in accuracy for large infarcts exceeding 150 mL. However, FIV may be significantly overestimated or underestimated depending on HIR, and the Syngo software package showed the widest range of performance (44).

In 2023, Xiang et al. collected one-stop CTP imaging data from 54 patients with AIS at Handan Central Hospital. The data included non-contrast CT scans, CTA, T_{max} maps, and CBF maps before and after conservative treatment and mechanical thrombectomy. Among the 54 patients, 15 underwent both CTP and MRI examinations. The post-processing method involved transferring CTP data to Artificial Intelligence software to obtain pseudo-colored images, ischemic core volume, and areas of abnormal perfusion. Additionally, Artificial Intelligence software was utilized to acquire intracranial arterial CTA images. The results revealed that patients treated with mechanical thrombectomy guided by CTP imaging had significantly improved NIHSS scores compared to the conventional treatment group, and this difference was statistically significant ($p < 0.005$). In one case assessed with Artificial Intelligence-assisted CTP imaging, the ischemic core volume was greater than that displayed by DWI, while in the remaining 13 patients; the ischemic core volume was smaller than the DWI-displayed ischemic core volume. The team concluded that mechanical thrombectomy guided by CTP imaging can extend the treatment window for AIS-LVO patients. AI-assisted CTP diagnosis can facilitate rapid assessments independent of radiologists, but it may pose challenges in determining the ischemic core volume (45).

In 2023, Weng et al. included 97 stroke patients. The team extracted vascular structural features from CTA images and stroke location features from DWI images to comprehensively characterize the lesions. The 97 cases were randomly divided into a cross-validation set, independent test set 1, and independent test set 2 for model validation. The results showed that the proposed model achieved good predictive performance on two independent test sets, with classification accuracies of 85.19 and 81.25%, respectively (46).

In 2023, Zhang et al. collected clinical data and NCCT images from 240 patients with AIS. Using 3D Slicer, they manually segmented the infarct lesions and performed feature extraction on CT images and regions of interest (ROI). After normalizing clinical and radiological features, surplus features were eliminated using the Kruskal-Wallis test. Through triple cross-validation and grid search, the research team selected the optimal hyperparameters for the Support Vector Machine (SVM) model. The dataset was divided into 3-fold in each of the three cross-validation runs, forming three prediction models. The average performance metrics for these three models included accuracy, sensitivity, specificity, F1 score, and AUC. After an in-depth analysis of 1,454 texture features extracted from NCCT images of 240 AIS patients, it was found that the classification model integrating clinical and radiomic data performed the best, with an AUC of 0.857, accuracy of 84.8%, and sensitivity of 93.8%. In comparison, models using only clinical or radiomic features showed lower performance with AUCs of 0.705 and 0.643, respectively. These study results suggest that integrated models combining multiple types of data are more reliable in predicting clinical outcomes for AIS patients (47).

In 2023, Brugnara et al. conducted a study on acute ischemic stroke patients undergoing imaging examinations and EVT. They utilized e-ASPECTS (Brainomix) for automatic assessment of ASPECTS on 1 mm slices, and visual inspection was conducted by experienced radiologists (AE, with 2 years of experience) and committee-certified neuroradiologists (UN, with 8 years of clinical experience). Statistical analyses were performed using Logistic regression and ordinal Logistic regression. Model performance was evaluated through ROC curves, and the significance of differences between models was assessed using the DeLong test. Machine learning model performance was assessed through random forest variable importance. In the entire study cohort, 38% of patients exhibited favorable clinical outcomes, while 26% experienced adverse outcomes at 90 days. Multivariate regression model results indicated that cortical atrophy was independently predictive of favorable clinical outcomes. The predictive performance of the machine learning model significantly outperformed other models, achieving an AUC of 0.775. Further analysis validated the importance of cortical atrophy across different models. The study results suggest that cortical atrophy is an independent predictor of clinical prognosis in acute ischemic stroke patients (48).

In 2023, Shen et al. included 44 consecutive patients with AIS who underwent endovascular treatment. Clinical data, including baseline mCTA, mRS, and follow-up MRI after treatment, were collected. They utilized a multi-scale three-dimensional CNN, inputting NCCT, arterial phase peak CTA, and CTA+ images. The F-STROKE software was used to calculate subsequent infarct core (IC) volume based on DWI. Data analysis was conducted using SPSS and MedCalc software. Among the 44 AIS patients receiving endovascular treatment, 61.4% achieved a favorable outcome. The NIHSSpre at admission and mCTA-estimated IC volume were independently correlated with the functional outcome of AIS patients after mechanical thrombectomy. Patients with a favorable prognosis had lower NIHSSpre and smaller mCTA-estimated IC volume (20.3 ± 12.2 vs. 43.9 ± 23.5, $p = 0.001$), and a higher proportion of good collateral status (66.7 vs. 22.4%, $p = 0.016$). The integrated model showed the best performance, with an area under the ROC curve of 0.874. The mean onset-to-door time (ODT) and door-to-puncture time (DPT) were 75.6 and 16.3 min, respectively, with a successful reperfusion rate of 17.7%. Bland–Altman plots and intraclass correlation coefficient (ICC) assessment indicated an acceptable level of consistency between mCTA-estimated IC volume and follow-up IC volume. The optimal threshold for predicting performance was mCTA-estimated IC volume ≤ 40.3 mL. The study also focused on the handling of hemorrhagic transformation (HT) regions. Deep Learning techniques were employed to extract volume data from mCTA. The mCTA-estimated IC volume may have potential value in predicting follow-up infarct and clinical outcomes in AIS patients treated with endovascular therapy (49).

The main information of the above included literatures is shown in Table 1.

2.4.2 The application of deep learning in stroke

In 2019, Hilbert et al. collected CTA data from 1,526 ischemic stroke patients. Various preprocessing techniques were applied to the images, including dimension reduction using Maximum Intensity

Projections (MIPs) and rigid registration using Elastix software. Additionally, they developed a Structured Receptive Field Neural Network (RFNN) model and incorporated unsupervised pretraining in a stack denoising autoencoder (AE) experiment to learn the encoding part of the AE network. Machine learning models based on 20 radiographic biomarkers manually scored by experts from the MR CLEAN Registry core laboratory were constructed. Logistic regression (LR) models and random forest classifiers (RFC) were utilized and compared with standard Deep Learning (DL) models (ResNet). Three training methods were devised using four balanced groups for cross-validation in 1,301 patients. Gradient-weighted class activation mapping (Grad-CAM) was employed for visualization to elucidate the contribution of convolutional feature maps in the input space. Ultimately, two visualization models were developed for predicting mRS and mTICI outcomes. The Deep Learning models exhibited superior performance in the cross-validation folds of four functional outcomes, yielding an average AUC of 0.71, and achieved an average AUC of 0.65 across all reperfusion folds, surpassing models based on traditional radiographic biomarkers. The AUC values for LR and RFC methods were 0.68 and 0.66, respectively, for favorable functional outcomes. However, for reperfusion prediction, both LR and RFC yielded an AUC of 0.52. In conclusion, the RFNN-ResNet model achieved the highest average AUC without pretraining with emission, while RFNN-ResNet-AE fine-tuning excelled in mTICI prediction. Their Deep Learning methods outperformed traditional approaches and can predict stroke outcomes without necessitating image annotation, offering faster processing speed. By enhancing the model, interpretability of the predictions was improved (50).

In 2021, Hokkinen et al., included data from 117 suspected stroke patients with CTA and follow-up data after admission. Preprocessing was done using 3D Slicer images and a trained and validated 3D CNN, evaluating the accuracy of outputs for two clinical time windows (0–6 and 6–24 h). The accuracy of CNN was assessed through visual evaluation of ASPECTS anatomical regions, validating the matching accuracy of the CNN in lesion location and final infarct location, compared with ischemic changes marked by radiologists. Finally, the performance of CNN and CTP-RAPID in determining eligibility for Endovascular Treatment (EVT) was compared, considering factors such as ischemic core volume and patient age. Using a manually fitted linear model, the research team assessed the segmented volume output derived from CNN and CTP-RAPID ischemic core volume for predicting final infarct volume. Pearson correlation coefficients were used to assess the correlation between them, and Bland–Altman plots were used to show the agreement between estimated infarct volume and final infarct volume, as well as the volume derivation between CNN and CTP-RAPID. The results showed that in the early 0–6 h time window, CNN had a correlation of $r = 0.43$ ($p = 0.002$) with final infarct volume, while CTP-RAPID had a correlation of $r = 0.58$ ($p < 0.001$). In the late 6–24 h time window, both CNN ($r = 0.67$, slope 1.2, $p < 0.001$) and CTP-RAPID ($r = 0.82$, slope 1.4, $p < 0.001$) showed significantly increased correlation. Compared to CTP-RAPID, CNN had a sensitivity of 0.38 and specificity of 0.89. The study suggests that CTA-based CNN, in patients successfully receiving EVT treatment, can detect anterior circulation ischemic stroke in the late time window (6–24 h) and has a moderate correlation with final infarct volume (51).

In 2021, Hokkinen et al. included 83 patients who received thrombolytic treatment or supportive care for CTA. They saved the images to a server and performed precise segmentation of the infarct area using the 3DSlicer image processing and visualization platform. The accuracy of the lesion location predicted by CNN was evaluated in comparison with the ASPECTS anatomical regions, and a detailed comparison was made with the CTP-RAPID software. By calculating a linear regression model and Pearson correlation coefficient (r) between the two, the results showed that the sensitivity of the CNN output was 0.71, specificity was 0.87, and accuracy was 0.80. For patients who did not receive thrombolytic treatment, there was excellent correlation between the final infarct volume and the estimated values from CNN output and CTP-RAPID, with correlation coefficients of $r = 0.89$ (95% CI 0.80–0.95) and $r = 0.92$ (95% CI 0.83–0.97), respectively. There was also a good correlation between the CNN output and CTP-RAPID ischemic core volume ($r = 0.89$, 95% CI 0.82–0.94). The conclusion of the study is that CTA-based CNN software demonstrates good estimation capabilities for infarct core volume in follow-up imaging studies, and its output exhibits significant correlation with CTP-RAPID ischemic core volume (52).

In 2021, Hakim et al. summarized the results of the ISLES 2018 challenge, which was participated in by 24 teams, and which included CTP and DWI images of 103 patients with acute large artery occlusion and anterior circulation ischemic stroke. Of these 103 patients were divided into two groups, 40 for the lesion-free test set and 63 for the training set. The data consisted of (1) CTP source data; (2) perfusion maps post-processed using the standard thresholding method (RAPID), i.e., cerebral blood flow (CBF), cerebral blood volume, mean passage time, and time to peak; (3) DWI lesion segmentation in a binary form; and (4) the DWI images themselves. Teams used different thresholds to calculate the mean and standard deviation of the Dice similarity coefficient (DSC), the mean absolute volume difference (VD), the accuracy and recall, including the Dice score, the Hausdorff distance (HD), the mean and absolute lesion VD, the accuracy, the recall, and the mean symmetry plane distance. Comparisons of non-normally distributed data, including comparisons of HD and mean symmetric surface distance, were performed using the Wilcoxon signed rank test to identify the best performing cases for each team. Results showed that among the best performing cases, the median DWI capacity was 7.2 (IQR) and the median absolute VD was 26.41. The study conclusions suggest that CTP-based machine learning methods can more accurately predict infarcted tissue (53).

In 2022, Ramos et al. conducted a comprehensive analysis of CTA data from 3,279 patients who underwent acute ischemic stroke EVT. They utilized two training model approaches, one based on radiomics and another combining imaging with clinical information. After preprocessing the data, 1,260 features were computed in 70 regions of the brain map, which were then reduced to 68 features. Training was carried out using the ResNet10 architecture for up to 75 epochs, incorporating transfer learning with an additional 50 epochs, and enhancing weights by adding SE modules before the fully connected layer. The results revealed that 37% of patients exhibited modified Rankin Scale (mRS) ≤ 2 in terms of favorable functional outcomes, while 60% achieved improved Thrombolysis in Cerebral Infarction (eTICI) $\geq$ 2b in terms of reperfusion. At 90 days, 37% of patients had good functional outcomes, and 60% showed favorable reperfusion after treatment. In predicting functional outcomes, the radiomics method performed the best in clinical experiments, achieving an AUC of 0.81. The study suggests that a single Deep Learning method (ResNet10) performed relatively poorly in predicting favorable functional outcomes. The combined approach of

TABLE 1 Summary of papers on machine learning for CT on rehabilitation of Ischemic stroke.

PMID	30354266	32733197	34392005	34709408	35645395
YEAR	2019	2020	2021	2022	2022
LEARNING APPROACH	machine learning	machine learning	machine learning	machine learning	machine learning
PRIMARY AUTHOR	Xie Y	Wen X	Cheng X	A Potreck	Iris Muehlen
DISEASE	Acute Ischemic Stroke	Malignant middle cerebral artery infarction (mMCAi)	large-vessel occlusion stroke	Acute Stroke Symptom-onset	Large Vessel Occlusive Stroke and Poor Revascularization
DATA VOLUME	CT, CT angiography (CTA), and perfusion CT data from 512 patients.	A total of 396 texture features were extracted from each NCCT image from the 126 patients	135 patients undergoing reperfusion therapy.	136 patients with stroke involving occlusion of the main segment of the Middle Cerebral Artery (MCA)	39 patients underwent mechanical thrombectomy (MT) due to acute ischemic stroke (AIS) caused by anterior circulation large vessel occlusion (LVO) and impaired blood flow reconstruction.
DATA TYPE	Basis of Imaging, Demographic, and Clinical Information	NCCT、CTA	different CT modalities	NCCT	NECT、CTP、CTA
METHODS	Gradient Boosting Machine	model based on the radiomics signature and Alberta Stroke Program Early CT Score (ASPECTS) based on NCCT	Automated ASPECTS for multi-modality CT	NCCT-ASPECTS	Three Automated Perfusion Software Applications
RESULTS	In predicting mRS greater than 2, XGB and GBM have AUCs of 0.746 and 0.748, respectively. After incorporating the 24-hour NIHSS score, XGB's AUC increases to 0.884, and GBM's AUC increases to 0.877. Reperfusion status has a certain impact on predictions; XGB's AUC increases to 0.807 in non-reperfused patients but decreases to 0.670 in reperfused patients, while GBM's AUC increases to 0.781 in non-reperfused patients but decreases to 0.655 in reperfused patients. For predicting mRS greater than 0, XGB's AUC ranges from 0.794 to 0.873, and GBM's AUC ranges from 681.1 to 762.3. Considering the 24-hour NIHSS score, XGB's AUC ranges from 0.794 to 0.873, and GBM's AUC ranges from 0.811 to 0.866.	Their predictive model exhibits outstanding performance, with AUCs of 0.917 and 0.913 for the training and validation sets, respectively. Additionally, Decision Curve Analysis (DCA) validated the clinical effectiveness of the predictive model in distinguishing between mMCAi and non-mMCAi patients, with probability threshold ranges of 0.067–1 in the training set and 0.046–1 in the validation set.	Researchers found a nearly perfect correlation between CTA-venous-ASPECTS and follow-up CT-ASPECTS, which outperformed other CT scans. The 90-day Modified Rankin Scale (mRS) scores were significantly associated with CTA-venous-ASPECTS. ROC analysis defined the optimal accuracy and cutoff points for parameters associated with the 90-day MRS score.	In different time windows, there are variations in inter-rater reliability among patients. Consistency among professionals is highest for moderate treatment times. The presence of collateral circulation is associated with favorable treatment outcomes, and the pre-intervention ASPECTS is a crucial predictor, especially when treatment initiation exceeds 200 minutes. The Tan score is also effective for ultra-acute strokes (OTI < 100 min).	Overall, there was good correlation without significant differences between the HVs and the FIVs with package A ($r = 0.78$, $p < 0.001$) being slightly superior to B and C. However, levels of agreement were very wide for all software applications in Bland-Altman analysis. In cases of large infarcts exceeding 150 mL the performance of the automated software solutions generally decreased. Subgroup analysis revealed the FIV to be generally underestimated in patients with HIR ≥ 0.6 ($p < 0.05$). In the subgroup with favorable HIR, however, there was a trend towards an overestimation of the FIV. Nevertheless, packages A and B showed good correlation between the HVs and FIVs without significant differences ($p > 0.2$), while only package C significantly overestimated the FIV (-54.6 ± 56.0 mL, $p = 0.001$). The rate of modified Rankin Scale (mRS) 0–3 after 3 months was significantly higher in favorable vs. unfavorable HIR (42.1% vs. 13.3%, $p = 0.02$). Lower HIR was associated with higher Alberta Stroke Program Early CT Score (ASPECTS) at presentation and on follow-up imaging, lower risk of malignant edema, and better outcome ($p < 0.05$).

(Continued)

10.3389/fneur.2024.1367854

TABLE 1 (Continued)

CONCLUSIONS	Machine learning can be employed to predict the recovery outcomes of stroke patients. Initial imaging information is sufficient, and incorporating 24-hour information enhances accuracy. Considering reperfusion status aids in assessing treatment risks and benefits.	Imaging features from radiomics can serve as tools for predicting the risk of mMCAi.	CTA-venous-ASPECTS exhibits the highest area under the curve. This study indicates a nearly perfect correlation between CTA-venous-ASPECTS and the final infarct size, along with a significant association with the 90-day MRS score.	The sensitivity of NCCT in detecting rapid stroke progression decreases. In ASPECTS assessments based on both manual and machine learning approaches, the reliability and consistency of scores between acute and follow-up ASPECTS decrease during short-term OTIs. In cases of hyperacute stroke, the status of collateral circulation in CT angiography may contribute to improving the prediction of clinical outcomes and explaining the reasons for reperfusion failure.	HIR can serve as a valuable parameter for outcome prediction and aid in deciding whether to proceed with MT in delicate situations.
PMID	37287309	36934582	37437435	37581657	37607843
YEAR	2023	2023	2023	2023	2023
LEARNING APPROACH	machine learning	machine learning	machine learning	machine learning	machine learning
PRIMARY AUTHOR	Xiang S	Weng S	Zhang L	Brugnara G	Shen GC
DISEASE	Ischemic Stroke Patients with Large Vessel Occlusion beyond the Therapeutic Time Window	ischemic stroke	Acute ischemic stroke	acute ischemic stroke	estimated infarct core volume in the patients with acute ischaemic stroke
DATA VOLUME	54 patients were retrospectively divided into two groups based on the treatment methods: the mechanical thrombectomy group had 21 patients and the conservative treatment group had 33 patients	CTA and MRI images from 97 patients	Clinical data and NCCT (non-contrast computed tomography) images from 240 patients with acute ischemic stroke (AIS).	A total of 1103 consecutive patients, who underwent endovascular treatment (EVT) for occlusion in the territory of the middle cerebral artery, were included.	44 patients undergoing endovascular treatment.
DATA TYPE	CTA	CTA、DWI	Non-contrast computed tomography	native cranial computed tomography (NCCT)	mCTA
METHODS	machine learning model	machine learning model	Support vector machine	machine learning models	multi-scale three-dimensional convolutional neural network

(Continued)

10.3389/fneur.2024.1367854

TABLE 1 (Continued)

RESULTS	In patients treated with mechanical thrombectomy guided by CTP imaging, the post-treatment NIHSS scores were significantly better than those in the conventional treatment group, with statistical significance ($P < 0.005$). In one case assessed using artificial intelligence-assisted CTP imaging, the infarct core volume was larger than that shown by DWI, while in the remaining 13 patients, the infarct core volume was smaller than that indicated by DWI.	On two independent test sets, the accuracy (ACC) for the cross-validated dataset using the Adboost method was 0.8519, while the ACC for the independent test set using the SRC method was 0.8125.	A total of 1454 texture features were extracted from NCCT images. In the test cohort, ROC analysis revealed that the radiomics model and the fusion model exhibited AUCs of 0.705 and 0.857, respectively. The fusion model demonstrated an accuracy of 84.8% and sensitivity of 93.8%.	**38% of patients exhibited favorable clinical outcomes, while 26% experienced adverse outcomes at 90 days. The predictive performance of the machine learning model is significant, with an AUC of 0.775.**	The area under the ROC curve is 0.874. The mean onset-to-door time (ODT) and door-to-puncture time (DPT) are 75.6 and 16.3 minutes, respectively, with a successful reperfusion rate of 17.7%. The optimal threshold for predicting performance is an estimated infarct core volume ≤40.3 ml based on mCTA.
CONCLUSIONS	Artificial intelligence-assisted CTP diagnosis can facilitate rapid assessments independent of radiologists, but it may pose challenges in determining infarct core volumes.	This machine learning approach can effectively explore and accurately quantify features related to stroke prognosis, including vascular structure and stroke location.	The model based on NCCT radiomics and machine learning has high predictive efficiency for the prognosis of AIS patients receiving conventional treatment, which can be used to assist early personalized clinical therapy	Cortical atrophy emerges as an independent predictor of clinical prognosis in patients with acute ischemic stroke. The machine learning model demonstrates exceptional performance when comprehensively considering both clinical and imaging parameters.	mCTA-estimated IC volume might be promising for predicting the prognosis, and assisting in making individualized treatment decision in patients with AIS

10.3389/fneur.2024.1367854

clinical and radiomics data demonstrated good performance in predicting patient functional outcomes (54).

In 2022, Winder et al. conducted a study involving 145 patients with acute ischemic stroke who underwent ERASER thrombectomy or other treatments. The research utilized AnToNIa software for perfusion imaging analysis, processing CT perfusion maps (CTC), mean square deviation, and baseline average images. Block-cyclic singular value decomposition, truncation threshold at 15%, and automatically calculated arterial input function were employed for deconvolution to generate residue curves (RC), thereby creating perfusion parameter maps for CBF, cerebral blood volume (CBV), mean transit time (MTT), and time to peak (Tmax). Additionally, brain tissue masks were generated. NCCT images underwent segmentation using AnToNIa and ITK-SNAP software tools, and registration to the baseline average image was performed using the SimpleITK and ANTs software packages. In the machine learning phase, each dataset underwent masking of the ipsilateral hemisphere, and CTC and RC data were cropped to 32 time points of interest, followed by corresponding processing. The tissue outcome prediction phase included model training, model testing, binarization, and statistical evaluation steps. Using Deep Learning models, image analysis was performed on 222 patients from the I-KNOW multicenter and remote ischemic preprocessing, training with TensorFlow and Python. The study evaluated the radiological outcomes of a subset of patients receiving intravenous rtPA and compared the performance of different models. The results showed that, compared to other models, CNNdeep performed better with an AUC of 0.88 ± 0.12, demonstrating significant differences from GLM, CNNTmax, and ADCthres. Overall, using multiple biomarkers as inputs in Deep Learning models achieved better predictive performance (55).

In 2022, Jabal et al. included 443 patients with AIS who underwent thrombectomy. Quantitative imaging features were extracted from clinical information and CT images using the e-Stroke software. The features were categorized into four classes, and additional new features were extracted. Machine learning (ML) algorithms, including k-Nearest Neighbors, Random Forest (RF), Gradient Boosting (GB), and Extreme Gradient Boosting (XGBoost), were constructed using the Scikit-learn library. The algorithms were optimized through the Optuna framework to differentiate and segment ASPECTS and output the total volume, volume for each ASPECTS region, and total e-ASPECTS volume. Simultaneously, the e-CTA software was used to identify the location of large vessel occlusion and quantify the volume percentage of collateral circulation defects to the total volume, as well as the absolute volume of vascular density defects in the MCA region relative to the contralateral hemisphere. Results showed that 101 patients had a favorable functional outcome (mRS-90 $\leq$ 2), while 192 patients had an unfavorable functional outcome (mRS-90 > 2). Non-enhanced CT imaging features associated with a favorable outcome included larger e-ASPECTS, larger brain volume, smaller cortical cerebrospinal fluid volume, smaller lateral ventricle volume, smaller acute ischemic volume, and smaller non-acute ischemic volume. Regarding imaging features, the XGBoost model performed the best with an AUC of 79%. Considering both clinical and radiological features, XGBoost remained the optimal model with an AUC of 80%. After Bayesian hyperparameter tuning and 10-fold stratified cross-validation, the optimized XGBoost model demonstrated a final performance on the patient test set with an AUC of 84%, accuracy of 77%, F1 score (mRS $\leq$ 2) of 67%, and F1 score (mRS > 2) of 82% (56).

In 2022, Amador et al. conducted a study on acute ischemic stroke, retrospectively collecting baseline CTP images from 147 patients. They preprocessed the images using the AnToNIa perfusion analysis software, which included motion correction, baseline correction, time smoothing, and interpolation. Building upon the preprocessing, they employed a Deep Learning approach to automatically identify the arterial input function (AIF). This involved architectures such as U-Net and temporal convolutional networks, directly utilizing the raw 4D CTP images for spatiotemporal analysis to predict treatment-dependent lesion outcomes in AIS patients. The study employed a 10-fold cross-validation scheme and, based on follow-up lesion volumes, trained, and evaluated the proposed Deep Learning method alongside a Tmax thresholding approach. All Deep Learning models underwent training for 100 epochs, and three performance evaluation metrics proposed by Winzeck et al. (57) were used for analysis. The results indicated that the 3D + time model performed the best in predicting stroke lesions, with a DSC of 0.30, a HD of 9.5 mm, and a volume error of 3.0 mL. In contrast, the performance of the Tmax thresholding method was the poorest, with a DSC of 0.24, HD of 14.4 mm, and volume error of 86.8 mL. The 2D + time model and the baseline method exhibited slightly lower average performance but were still considered acceptable, with an average volume error of 21.9 mL (58).

In 2023, Wouters et al. included 228 acute ischemic stroke patients with 127 in the training set and 101 in the validation set. They utilized CTP data from the MRCLEAN trial-derived cohort for training a DL model, and internal validation was performed after integrating clinical data. External validation used an independent dataset from the CRISP study. The study compared the performance of the DL model with the RAPID software, which uses deconvolution/thresholding methods, in predicting final infarct volume. Additionally, analyses of patient reperfusion grades, lesion growth rates, and relevant statistical analyses were conducted. The results showed that, in the analysis of 108 patients based on baseline CTP and actual infarct volume using RAPID, the DL model outperformed the RAPID software, with a mean absolute difference (MAD) of 34.5 mL (SD 29.4), compared to RAPID software's MAD of 52.4 mL (SD 49.8) ($p < 0.01$). For the 19 patients with intermediate reperfusion in the MR CLEAN study, the DL model had a MAD of 36.7 mL (SD 38.3), with no significant difference compared to the fully or non-reperfused groups ($p = 0.64$). ROC curve analysis indicated an optimal threshold for infarct growth at 0.36, with a median growth rate of 2.7 mL/h in patients with HIR < 0.36 and 8.5 mL/h in patients with HIR $\geq$ 0.36 ($p < 0.01$) (59).

The main information of the above included literatures is shown in Table 2.

2.5 Artificial intelligence-based prediction of stroke prognosis using MRI

MRI has various imaging sequences, such as diffusion-weighted MRI, perfusion MRI, T2 sequences, etc., which can assess different structural and functional features of brain tissue. Diffusion MRI can detect cytotoxic edema, which is the most sensitive core indicator of ischemic stroke. In the region of cytotoxic edema, water molecules move from extracellular space to intracellular space, and diffusion is restricted. Diffusion-weighted imaging can detect ischemic injury within minutes after the onset of ischemic stroke, showing a significant

TABLE 2 Summary of papers on deep learning for CT on rehabilitation of Ischemic stroke.

PMID	31707199	34868662	34164743	33957774	35432171
YEAR	2019	2021	2021	2021	2022
LEARNING APPROACH	deep learning	deep learning	deep learning	deep learning	deep learning
PRIMARY AUTHOR	Hilbert A	Hokkinen L	Hokkinen L	Hakim A	Ramos LA
DISEASE	Acute Ischemic Stroke	anterior circulation ischemic stroke	anterior cerebral circulation ischaemic stroke	Acute Ischemia	Acute Ischemic Stroke
DATA VOLUME	the MR CLEAN Registry dataset with 1301 patients	117 suspected stroke patients.	83 consecutive stroke cases undergoing thrombolytic therapy or alternative treatments	Among 103 patients with acute anterior circulation ischemic stroke due to large vessel occlusion, 40 constituted the lesion-free test set, while the remaining 63 formed the training group.	3279patients from the MR CLEAN Registry
DATA TYPE	Clinical variables and radiological image biomarkers (including age, pre-stroke mRS, NIHSS, occlusion location, ASPECTS, etc.)	CTA	CTA	CTP、DWI	radiomics features、 images and the clinical data
METHODS	Residual Neural Network (ResNet)	Convolutional neural network(CNN)	convolutional neural network	Machine learning method	3D deep learning models、machine learning models
RESULTS	Deep learning models demonstrated superior performance in functional outcome (average AUC of 0.71) and reperfusion (average AUC of 0.65).	The final infarct volume correlation for the Convolutional Neural Network (CNN) was r=0.43, while for CTP-RAPID, it was r=0.58. Within the 6-24 hour time window, both CNN (r=0.67, slope 1.2) and CTP-RAPID (r=0.82, slope 1.4) showed a significantly increased correlation. Compared to CTP-RAPID, CNN demonstrated a sensitivity of 0.38 and specificity of 0.89.	The sensitivity, specificity, and accuracy of the CNN stand at 0.71, 0.87, and 0.80, respectively. The correlation coefficient with manual segmentation is 0.83. For patients not subjected to thrombolytic therapy, noteworthy correlations emerge between the CNN output and CTP-RAPID estimated values, with correlation coefficients of r=0.89 and r=0.92, respectively. Additionally, a robust correlation of r=0.89 is observed between the CNN output and CTP-RAPID ischemic core volume.	In the best-performing cases, the median DWI volume was 7.2 (IQR), with a median absolute vascular density (VD) of 26.41	Combining image data with clinical data did not yield a significant improvement in mRS prediction (mean AUC of 0.81 vs. 0.80) compared to using clinical data alone, irrespective of the approach. However, for predicting reperfusion, a significant enhancement was observed with the combination of image and clinical features (mean AUC of 0.54 vs. 0.61), with the deep learning approach achieving the highest AUC.
CONCLUSIONS	n our dataset, automated image analysis using deep learning methods demonstrates superior performance in predicting stroke outcomes, with the potential to enhance treatment selection.	A CTA-based CNN method had moderate correlation with final infarct volumes in the late time window in patients successfully treated with EVT.	The CNN software based on CTA can provide robust estimates of infarct core volume. The infarct volume derived from CNN exhibits a strong correlation with the ischemic core volume from CTP-RAPID.	Machine learning methods may predict infarcted tissue from CTP with improved accuracy compared with threshold-based methods used in clinical routine.	The integration of radiomics and deep learning image features with clinical data significantly improves the prediction of favorable reperfusion.
PMID	36408399	35665041	36103772	34587794	

(Continued)

10.3389/fneur.2024.1367854

TABLE 2 (Continued)

YEAR	2022	2022	2022	2023	
LEARNING APPROACH	deep learning	deep learning	deep learning	deep learning	
PRIMARY AUTHOR	Winder AJ	Jabal MS	Amador K	Wouters	
DISEASE	acute ischemic stroke	estimated infarct core volume in the patients with acute ischaemic stroke	spatio-temporal convolutional neural networks	Acute Ischemic Stroke	
DATA VOLUME	145 patients with acute ischemic stroke who underwent intravenous thrombolysis treatment, following the conventions of scientific literature	293 patients undergoing thrombectomy.	147 patients from the multicenter, prospective ERASER study	228 acute ischemic stroke patients with 127 in the training set and 101 in the validation set.	
DATA TYPE	CT	CT/CTA	CTP	CTP	
METHODS	DCN	multi-scale three-dimensional convolutional neural network	4D CT perfusion imaging using spatio-temporal convolutional neural networks	DL model with the RAPID software	
RESULTS	DCN: 0.287, RDF: 0.262, Tmax-thresholding: 0.249, deconvolved residual curves: 0.286, source concentration-time curves: 0.296	In a cohort of 101 patients, favorable outcomes (mRS-90 $\leq$ 2) were observed, while 192 patients experienced unfavorable outcomes (mRS-90 > 2). The XGBoost model demonstrated optimal performance when considering both imaging features and clinical considerations, achieving AUCs of 79% and 80%, respectively. Following optimization, the final performance of the XGBoost model on the patient test set was characterized by an AUC of 84%, accuracy of 77%, F1 score (mRS $\leq$ 2) of 67%, and F1 score (mRS > 2) of 82%.	The 3D+time model demonstrates optimal performance, boasting a Dice Similarity Coefficient (DSC) of 0.30, Hausdorff Distance (HD) of 9.5 mm, and a volume error of 3.0 mL. In contrast, the Tmax threshold method exhibits the least favorable performance, with a DSC of 0.24, HD of 14.4 mm, and a volume error of 86.8 mL. The 2D+time model, while displaying slightly lower average performance, still maintains acceptability, with an average volume error of 21.9 mL.	The results showed that, in the analysis of 108 patients based on baseline CTP and actual infarct volume using RAPID, the DL model outperformed the RAPID software, with a mean absolute difference (MAD) of 34.5 ml (SD 29.4), compared to RAPID software's MAD of 52.4 ml (SD 49.8) ($p < 0.01$). For the 19 patients with intermediate reperfusion in the MR CLEAN study, the DL model had a MAD of 36.7 ml (SD 38.3), with no significant difference compared to the fully or non-reperfused groups ($p = 0.64$).	
CONCLUSIONS	Through DCN, utilizing features optimized from source concentration-time curves, the best predictions for tissue outcomes are provided.	The value of machine learning lies in integrating essential clinical information and automated imaging features for predicting functional outcomes three months after mechanical thrombectomy.	4D CTP datasets include more predictive information than perfusion parameter maps, and that the proposed method is an efficient approach to make use of this complex data	ROC curve analysis indicated an optimal threshold for infarct growth at 0.36,	

10.3389/fneur.2024.1367854

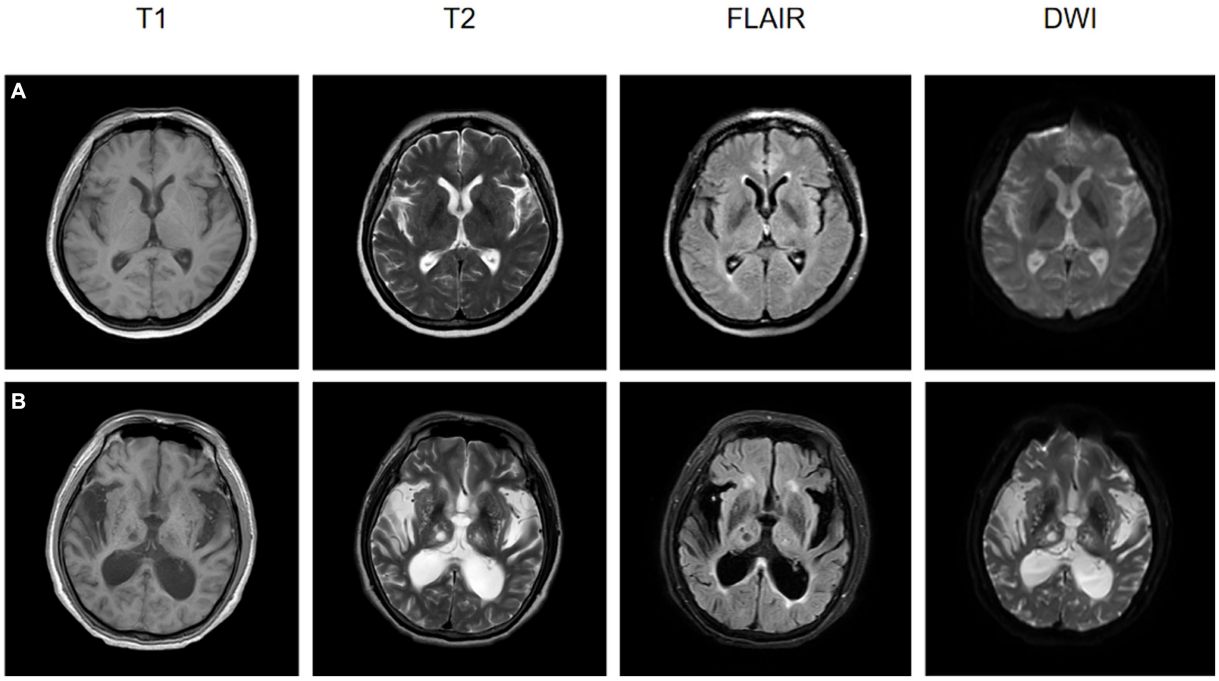

FIGURE 5
The MRI images at the onset of ischemic stroke for two patients, both of whom underwent rehabilitation training after their conditions stabilized, are presented. **(A)** A 57-year-old female patient, post-rehabilitation Berg Balance Scale score of 2, Functional Independence Measure (FIM) score of 6, and Modified Barthel Index of 3. **(B)** A 72-year-old male patient, post-rehabilitation Berg Balance Scale score of 0, FIM score of 1, and Modified Barthel Index of 0.

high signal (60). Studies have indicated that the sensitivity of MRI in diagnosing acute ischemic stroke is 83% (61). Traditional MRI sequences, such as T1, T2, and FLAIR, become sensitive to ischemic changes after a net increase in brain tissue water content, allowing detection of ischemic changes hours after symptom onset (62). Perfusion-weighted imaging (PWI) can provide an assessment of cerebral blood flow perfusion. By combining information from PWI and DWI sequences, the size and location of the ischemic penumbra can be evaluated.

MRI vascular imaging is a powerful tool for detecting vascular stenosis or occlusion, but it is more time-consuming than CTA and may not be available around the clock or in emergencies at all hospitals. Despite its limitations, MRA has unique advantages in diagnosing stenosis, occlusion, etc. In most studies, MRA has a sensitivity and specificity close to 100% for detecting carotid artery occlusion (63). If MRA shows no stenosis or stenosis less than 70%, further diagnostic evaluation is usually not necessary.

MRI has been used as a preferred modality for the treatment and secondary prevention of acute ischemic stroke, as show in Figure 5. While CT is most commonly employed for assessing acute stroke patients, the high signal-to-noise ratio and the ability to identify damaged brain tissue make MRI a crucial imaging modality for stroke diagnosis, prognosis, and prevention. Evaluation of ischemic stroke typically involves multiple imaging parameters, with changes in cerebral blood flow being a primary pathological alteration in ischemic stroke. MRI sequences, such as dynamic contrast-enhanced perfusion, can estimate the penumbral tissue, which is at risk of infarction without reperfusion treatment but has not yet undergone irreversible damage. Additionally, it can assess cerebral vascular reserve (CVR) to better select cerebrovascular intervention measures. CVR is defined as the ability to increase CBF in response to vascular dilation stimuli. In patients with reduced CVR, there is often an increased risk of stroke when CVR is diminished, especially in those with chronic cerebrovascular diseases. Arterial spin labeling (ASL) is an enhanced MRI sequence used to measure CBF, offering a promising technique for evaluating acute ischemic stroke and potentially identifying patients at higher risk of future strokes (64).

2.5.1 The application of machine learning in stroke

In 2005, Gottup et al. collected MRI data from 14 patients with acute stroke. The performance was measured using AUC. Three different implementations of the instance-based method—k-NN, Gaussian weighted, and constant radius search classification—were applied for data analysis. The results indicated that the performance of the optimal k-NN and Gaussian weighted algorithms did not shown a significant difference, but both were markedly superior to the constant radius implementation. Through a qualitative analysis of the distribution of instances in the feature space, it was observed that non-infarct instances tended to cluster together, while infarct instances were more dispersed in the feature space. Additionally, the analysis suggested the existence of feature space regions occupied exclusively by infarct instances, which were not present for non-infarct instances (65).

In 2015, Kim et al. enrolled 35 ischemic stroke patients with visual field defects (VFD) caused by posterior cerebral artery (PCA) infarction. All these patients underwent MRI scans. After transforming the lesion locations into standard maps, the ischemic lesion area range

(rEILs) for each cortical area was measured. Significant improvement in VFD was defined as a provisional improvement of 20% 3 months after the stroke. The performance of clinical and radiological variables in predicting significant improvement was measured using support vector machines. Clinical variables, baseline visual field scores, lesion volumes, and rEIL were compared between the significantly improved and less improved groups. Support vector machines with a linear kernel were employed to train and validate the prognostic classifier. The results showed that left PCA infarction, pre-stroke MRI time, and rEIL in the tongue, corpus callosum, and cuneal cortex were good prognostic indicators for lateralized VFD. Compared to clinical variables, the combination of rEIL in various cortical subregions demonstrated a better predictive effect on lateralized VFD. Adding rEIL to other variables improved the prognostic prediction of lateralized VFD (66).

In 2020, Grosse et al. included 99 patients with acute ischemic stroke for multi-parametric MRI data. They used the AnToNIa software tool for apparent diffusion coefficient (ADC) map calculation, intraslice motion correction of PWI sequences, and atlas-based methods for automatic extraction of arterial input functions, among other preprocessing steps. Perfusion parameter maps were computed using a block-circulant singular value decomposition method, and the FLAIR dataset was segmented. Image registration to the Montreal Neurological Institute (MNI) brain atlas was performed, and a combination of LR and RF algorithms was used for mixed tissue outcome prediction. Twenty-one prediction models were evaluated using Receiver Operating Characteristic Area Under the Curve (ROC AUC), Dice similarity index, sensitivity, and specificity. Single-sided paired *t*-tests were employed to assess Dice and ROC AUC values, and the average and median of local LR model coefficients were calculated for each MNI structural brain region. The study results demonstrated that the mixed LR model performed best in terms of the average ROC AUC value (0.872 ± 0.092), while the mixed RF model was optimal for the average Dice coefficient (0.353 ± 0.220). The mixed LR model showed the highest average values for ROC AUC and Dice coefficient, followed by the mixed RF model. The mixed model significantly improved the effect size at the 0.01 level, including ROC AUC and Dice values. The mixed LR model had the highest average values for ROC AUC, Dice coefficient, sensitivity, and specificity, followed by local LR, mixed, and local RF models, as well as global LR and RF models (67).

In 2021, Hamann et al. included clinical and imaging data from a cohort of 222 patients who underwent EVT for acute ischemic stroke caused by middle cerebral artery (MCA)-M1 occlusion at the Bern University Hospital between January 2012 and August 2017. The data used for predictive analysis was limited to diffusion-weighted and perfusion images. Imaging data underwent post-processing using the Acute Stroke Care plugin of Olea Sphere. A predictive model for favorable functional outcomes was developed using clinical variables and magnetic resonance imaging features based on regions of interest (ROIs). The study assessed the predictive capability of different patient characteristics and imaging variables, both individually and in combination, and evaluated overall performance based on the AUC values and Brier scores for the entire test set. The results indicated a successful revascularization rate of 78%, with 54% of patients achieving a favorable outcome (modified Rankin Scale score 0–2). Small infarct size was associated with a favorable functional outcome, while older age was related to a reduced chance of favorable outcomes and functional improvement. The use of isolated imaging information as a predictor for functional outcomes showed relatively poor performance. No significant differences were observed between the predictive variable sets when imaging variables were added to patient characteristics (68).

In 2022, Graaf et al. analyzed patients who had successful reperfusion in the MR CLEAN registry center from March 2014 to November 2017. Initially, they constructed a multivariable ordinal regression model to predict functional outcomes measured by the mRS at 90 days. Four groups of predictive factors were included: baseline patient factors, imaging factors, treatment factors, and postoperative factors (i.e., adverse events). Each group of predictive factors was incrementally added to the basic model, which only included baseline patient factors, and the overall explained variance of the most comprehensive model was subsequently evaluated. The results indicated that the most important predictive factors for mRS were baseline patient factors and postoperative factors. Among patients with successful reperfusion, the five most important individual predictive factors for functional outcomes at 90 days were pre-stroke mRS, baseline NIHSS, symptomatic intracranial hemorrhage (sICH), age, and pneumonia. Stroke patients with sICH had a 54% lower probability of functional independence compared to those without sICH, and patients with pneumonia had a 21% lower probability of functional independence than those without pneumonia. This study suggests that both patient and postoperative factors are crucial predictors of successful reperfusion outcomes in ischemic stroke patients (69).

In 2021, Abedi et al. developed classification models for six prediction windows by incorporating MRI data from 7,144 patients with acute ischemic stroke. Three algorithms, LR, XGB, and RF, were employed in the study. The research data were randomly split into 80: 20 training and testing sets, using RF and LR as baseline metrics. Ten repetitions of 5-fold cross-validation (CV) training were performed. Among the 7,144 patients meeting inclusion criteria, 5,347 did not experience a stroke after 2 years, 605 died within 1 month, 1,380 died within 1 year, and 1,797 died within 2 years. On the test dataset, the average Area Under the Receiver Operating Characteristic curve (AUROC) ranged from 0.76 to 0.81. The RF-based model performed best in the 1-month window (AUROC = 0.82), with the highest Negative Predictive Value (NPV) of 91.1 for shorter prediction windows. The RF model achieved the highest PPV at the 6-month window (0.92), while the XGB-based model had the highest accuracy (precision of 0.89) in the 1-month window. Age, hemoglobin levels, and BMI were identified as the top three relevant factors across different prediction windows, with average overall importance scores of 96.3, 68.2, and 55.5%, respectively (70).

In 2022, Elsaid et al. recruited 354 patients using a systematic random technique (every three admissions) from the Stroke and Intensive Care Unit (ICU) at Zagazig University Hospital in Egypt. The included data comprised routine MR and diffusion-weighted images for each patient. The team optimized several machines learning algorithms, including LRC, SVC, RFC, GBC, and MLPC. They evaluated the predictive performance of the models using ROC and explored the interactions among predictive factors using Generalized Additive Models (GAM). The results indicated a 19.8% occurrence rate of HT in ischemic stroke patients. Infarct size, cerebral microbleeds (CMB), and NIHSS were identified as the best predictors for HT. RFC and GBC outperformed LRC and MLPC

significantly. SVC performed better than LRC and MLPC but lacked statistical significance. There was no significant difference between LRC and MLPC (71).

In 2022, Guo et al. conducted a comprehensive analysis by including 156 patients with 88 DSC-PWI images. They preprocessed the DSC-PWI data and assessed the role of Dynamic R2* (DRF) in the diagnosis and prognosis prediction of ischemic stroke patients. The study segmented DSC-PWI images into N 3D images and calculated the performance of brain tissue DRF through four combination methods. Ten machine learning models, including SVM, Decision Tree (DT), Adaboost Classifier (Ada), Neural Network (NN), and others, were used for performance evaluation based on AUC, with AUC calculated using 10-fold cross-validation. Analysis of 78 DSC-PWI images detected 50 cases of ischemic stroke, including 60 patients with NIHSS scores of 95 and 66 patients with mRS scores less than 2 at 101 days. In terms of feature extraction, which included First_order, GLCM, GLDM, GLRLM, GLSZM, NGTDM, etc., the *p* values ranged from 0.0123 ± 0.0144. The *p* value for DRF significantly correlated with NIHSS assessment was 8324.0 ± 0232.0, totaling 156. For outcome prediction, 144 significant DRFs were extracted with a *p* value of 9203.0 ± 0238.0, including First_order, GLCM, GLDM, GLRRM, GLSZM, NGTDM, etc. Reduction in dimensions through PCA, ICA, t-SNE, IOSMAP, and UMAP methods resulted in *R* values of 0.110 ± 0.121, 0.140 ± 0.079, 0.110 ± 0.121, 0.294 ± 0.139, and 0.098 ± 0.133, respectively. The conclusion states that the study results indicate that different feature extraction and dimensionality reduction methods can achieve better performance in the detection, assessment, and outcome prediction of ischemic stroke. In some cases, features selected by Lasso demonstrated superior performance, increasing AUC for stroke detection by 19.4% (from 0.731 to 0.925), NIHSS assessment by 20.1% (from 0.652 to 0.853), and prognosis prediction by 14.9% (from 0.679 to 0.828) (72).

In 2022, Li et al., conducted a study involving 260 patients with acute ischemic stroke, incorporating a total of 620 DWI images. Initially, neuroradiologists selected ROIs, followed by ROI segmentation and normalization preprocessing. They integrated a SVM algorithm with a Least Absolute Shrinkage and Selection Operator (LASSO) regression model and optimized model parameters through 10-fold cross-validation. The predictive performance of the machine learning model was assessed using AUC of ROC curve. The study results revealed that among the 260 patients with acute ischemic stroke, there were 109 and 46 cases of favorable outcomes in the training and test sets, respectively. The LASSO regression model identified four features, with the highest-weighted coefficient attributed to "sqyareriit-IV." ROC curve analysis demonstrated that in the training set, the AUC for predicting the prognosis after mechanical thrombectomy was 0.945 (95% CI: 0.890–0.975), and in the test set, it was 0.920 (95% CI, 0.849–0.981) (73).

In 2023, Luo et al. conducted a study analyzing 132 patients with Basilar Artery Occlusion (ABAO), randomly dividing them into a training group ($n = 106$) and a test group ($n = 26$). They extracted 1,130 radiomic features from DWI images and employed the Least Absolute Shrinkage and Selection Operator (LASSO) regression method for feature selection. Radiomic and clinical models were constructed using SVM, and the models were evaluated using ROC and decision curves. The results indicated that AUC of the ROC curve for the radiomic-clinical model was 0.897 in the training group and 0.935 in the test group. The AUC for the radiomic model was 0.887 in the training group and 0.840 in the test group. The AUC for the clinical model was 0.746 in the training group and 0.766 in the test group. Importantly, the AUC of the radiomic-clinical model was significantly greater than that of the clinical model (74).

In 2023, Xu et al. included 314 patients with acute corpus callosum infarction (CC). Basic clinical and radiological information was obtained through the Electronic Medical Records (EMR) management system. Neuroimaging evidence was collected from MRI, MRA, or CTA. For patients diagnosed with CC infarction 1 year after onset, the team used the Behavioral Risk Factor Surveillance System (BRFSS) questionnaire to identify subjective cognitive decline (SCD). The team established seven machine learning models, including XGBoost, LR, LightGBM, AdaBoost, GNB, CNB, and SVM. They compared the predictive performance of these models using different metrics. The results indicated that the LR model outperformed the other six machine learning models in predicting SCD after CC infarction. Through LASSO and SHAP analyses, the team identified the top nine important predictive factors from the LR model output. Additionally, they discovered factors independently associated with cognitive outcomes (75).

In 2023, Wang et al. conducted a study involving 2015 patients who experienced ischemic strokes within 650 h. The study utilized MRI images and follow-up data. NeuBrainCARE software was employed to manually measure the infarct volume, represented by the ADC. Additionally, two radiologists assessed the burden of small vessel disease (SVD). The researchers employed a bidirectional stepwise regression method to select indicators in the LR model and applied three machine learning algorithms (Gaussian process regression, random forest, and extreme gradient boosting) to establish predictive models. The results indicated that the LR model (SVO-AIS) achieved an AUC of 0.86 [0.78–0.94] for favorable outcomes and an AUC of 0.88 [0.8–0.96] for good outcomes. The LR model (LAA-AIS) had AUC values of 0.73 [0.54–0.91] for favorable outcomes and 0.75 [0.59–0.91] for good outcomes. The GPR model (SVO-AIS) achieved an AUC of 0.86 [0.77–0.95] for favorable outcomes and an AUC of 0.86 [0.77–0.96] for good outcomes. The GPR model (LAA-AIS) had AUC values of 0.65 [0.47–0.83] for favorable outcomes and 0.66 [0.49–0.84] for good outcomes. The GOA-RF model (SVO-AIS) demonstrated an AUC of 0.85 [0.75–0.94] for favorable outcomes and 0.84 [0.74–0.94] for good outcomes. The GOA-RF model (LAA-AIS) achieved AUC values of 0.66 [0.49–0.84] for favorable outcomes and 0.68 [0.51–0.86] for good outcomes. The GOA-XGBoost model exhibited AUC values of 0.87 [0.79–0.96] for favorable outcomes and 0.85 [0.76–0.94] for good outcomes. In the LAA-AIS population, the AUC values were 0.91 [0.84–0.97] for favorable outcomes and 0.90 [0.83–0.97] for good outcomes (76).

In 2023, Yu et al. investigated the demographic characteristics, clinical data, and MR data of 180 patients with AIS. They manually delineated ROI for acute ischemic lesions on DWI images using MRIcron software. The data from all modalities, including ADC, FLAIR, SWI, and T1-2w, were aligned with the DWI images using SPM1 software. Radiomic analysis was performed on the MRI data of the five modalities, extracting a total of 946 features per image. Additionally, 14 shape features of the lesion regions were extracted. The scikit-learn package was utilized for feature selection using the recursive feature elimination (RFE) method. Ultimately, 16 image features were selected for training machine learning models, including SVM, RF, LightGBM, CatBoost, and XGBoost. Statistical analysis was

conducted using SPSS 21.0. The results showed that out of 148 patients, 83 (56.1%) had a favorable prognosis, while 65 (43.9%) had an unfavorable prognosis. For each MRI modality, three optimal radiomic features (DWI, ADC, FLAIR, SWI, and T1w) and one optimal feature related to lesion shape were selected as key features in the machine learning models. The accuracy of the models was as follows: SVM model, 79%; RF model, 82%; LightGBM model, 83%; CatBoost model, 81%; and XGBoost model, 80%. This study revealed the potential value of a multimodal radiomic approach in accurately predicting the clinical outcomes of patients with AIS (77).

In 2023, Lee et al. included 3,687 patients with acute ischemic stroke, along with their MRI and relevant clinical information. The Rankin scale, assessed by neurologists, was used for outcome evaluation. The team employed multiple imputation by chained equations (MICE) to handle outliers and missing data and normalized the data using MinMaxScaler. They developed models based on three algorithms: random forest, XGBoost, and LGBM. The TreeSHAP method was used to calculate interaction effects between features. Model performance was evaluated using AUC-ROC, revealing that 30.4% of patients had unfavorable outcomes, with external validation data showing rates of 37.2 and 29.1%. The AUROC for the internal test set, external validation sets A and B were 0.790, 0.791, and 0.873, respectively, while the Brier scores were 0.172, 0.202, and 0.141. In summary, the models demonstrated overall good performance (78).

In 2023, Weng et al. included 97 stroke patients with CTA and MRI images. Preprocessing of CTA and DWI images was conducted in MATLAB 2019. For CTA images, the processing involved feature extraction for 116 brain regions, image registration, segmentation of cerebral vessels using the Unet model, and calculation of vascular volume and length features. For DWI image processing, it included location feature extraction, image registration, and manual marking of stroke lesions by radiologists on the itk-snap platform. By multiplying the brain matrix and position matrix, the stroke regions for each area were obtained, and the proportion of stroke regions in the entire brain area was calculated. Subsequently, a machine learning model was established, utilizing a classification model based on the sparse representation method for feature selection and classification. The research results indicated that, on two independent test sets, the ACC of the cross-validation dataset using the Adboost method was 0.8519, while the ACC for the independent test set using the SRC method was 0.8125. This study suggests that the machine learning approach is effective in extracting and accurately quantifying features related to stroke prognosis, including vascular structure and stroke location (46).

The main information of the above included literatures is shown in Table 3.

2.5.2 The application of deep learning in stroke

In 2018, Nielsen et al. conducted a detailed analysis of a multi-center study involving 222 patients from the I-KNOW consortium and remote ischemic pre-conditioning for MRI. The study included a subgroup of patients receiving intravenous rtPA treatment ($n = 187$) and the imaging results of 35 untreated patients. In the training phase, a CNN was trained using TensorFlow 2.7.9 to automatically identify initial arterial input functions. Deconvolution was performed using concentration curve parameters to obtain average microvascular transit time and cerebral blood flow. CNNTmax was used to assess the accuracy of Tmax and was compared with regression methods using generalized linear models (GLM) to predict the risk of infarction at the individual voxel level. The final infarction prediction performance was evaluated by AUC from T2-FLAIR scans. Patients receiving intravenous treatment were divided into independent training (158 cases) and test sets (29 cases) to evaluate the model's performance in independent patients. Follow-up infarctions were assessed by four radiology experts 1 month after stroke. The 35 untreated patients underwent post-training, resulting in CNNdeep-rtPA. Differences were assessed through post-training of CNNdeep. The new model was evaluated on 29 patients in the trial group who received intravenous rtPA treatment, and AUC and final infarct area were compared. The results showed that CNNshallow tended to overestimate the final lesion volume, while CNNTmax predicted a lower risk of infarction. In contrast, CNNdeep provided better visual predictions. CNNdeep had an AUC of 0.88 ± 0.12, significantly better than CNNshallow (0.85 ± 0.11), GLM (0.78 ± 0.12), CNNTmax (0.72 ± 0.14), and ADCthres (0.66 ± 0.13). There was a significant difference between CNNdeep and GLM ($p = 0.005$), CNNTmax ($p < 0.003$), and ADCthres ($p < 0.0001$), while the difference between CNNdeep and CNNshallow was not significant ($p = 0.063$) (79).

In 2018, Pinto et al. included MRI images and clinical information from 75 ischemic stroke patients who underwent mechanical thrombectomy from the ISLES2017 dataset. Using a Deep Learning architecture that combines U-net with two-dimensional Gated Recurrent Units (GRU), the study integrated clinical information at the population level and analyzed it using the Thrombolysis in Cerebral Infarction (TICI) scale. The study experimented with cross-validation on the training set and compared its results with a baseline architecture that did not include any clinical metadata. This research innovatively combined imaging and non-imaging clinical data in a Deep Learning architecture and, through the development of a customized loss function, incorporated clinical information in both the learning and prediction phases. This approach more accurately predicted different outcome scenarios. The study evaluated the performance of the method using five metrics (Dice similarity coefficient, accuracy, recall, Hausdorff distance, and average symmetric surface distance). In the end, the method achieved a Dice score of 0.29 ± 0.22, Hausdorff distance of 47.17 ± 22.13, ASSD of 7.20 ± 4.14, precision of 0.26 ± 0.23, and recall of 0.61 ± 0.28 (80).

In 2019, King et al. included MR images from 444 patients. They employed a multi-atlas skull stripping algorithm for skull stripping. By aligning brain images to the centerline of the axial plane, the study proposed a Deep Learning model, compared it with several benchmark models, and introduced an improved model. The performance of these models was evaluated through multiple validations, using metrics such as AUC, accuracy, and overlap coefficient. Here are the AUC and overlap coefficient results: 2D CNN: AUC of 0.783 ± 0.030, overlap coefficient of 0.728. 3D CNN: AUC of 0.799 ± 0.029, overlap coefficient of 0.717. Unitary CNN-Opposite: AUC of 0.871 ± 0.024, overlap coefficient of 0.811.SR-KDA: AUC of 0.788 ± 0.031, overlap coefficient of 0.679. Results for accuracy and recall are as follows: 2D CNN: Accuracy of 0.211, recall of 0.700. 3D CNN: Accuracy of 0.220, recall of 0.693. Unitary CNN-Opposite: Accuracy of 0.222, recall of 0.799. SR-KDA: Accuracy of 0.671, recall of 0.171. Experimental evidence suggests its optimal performance when trained with opposite patches. Through visualizing the results of the deep CNN, the study provides a detailed analysis of the model's performance in large infarcts and specific scenarios. Overall, this deep

TABLE 3 Summary of papers on machine learning for MRI on rehabilitation of Ischemic stroke.

PMID	15811787	26606516	33152045	33220140	34266905
YEAR	2005	2015	2020	2021	2022
LEARNING APPROACH	machine learning	machine learning	machine learning	machine learning	machine learning
PRIMARY AUTHOR	Christian Gottrup	Bum Joon Kim	Grosser M	Janne Hamann	Rob A van de Graaf
DISEASE	Acute Strok	Cerebral Infarction	acute ischemic stroke	stroke patients with middle cerebral artery-M1 occlusions and early thrombectomy	ischemic stroke
DATA VOLUME	magnetic resonance imaging of 14 patients with acute stroke	Thirty-five cases of ischemic infarction patients with visual field defects (VFD) due to posterior cerebral artery (PCA) infarction	weighted MRI data from 99 patients.	222 patients with acute ischemic stroke due to middle cerebral artery (MCA)-M1 occlusion who received EVT	A cohort of 3180 patients who successfully underwent reperfusion
DATA TYPE	mri	MRI	weighted MRI datasets	magnetic resonance imaging features.	data from the MR CLEAN Registry
METHODS	k-NN, Gaussian weighted, and constant radius search classification.	Support Vector Machine	global machine learning model	different machine-learning models and	A multivariate ordinal regression model
RESULTS	Optimal k-NN and Gaussian weighted algorithms exhibit no significant performance difference, yet both are notably superior to the constant radius implementation	The occurrence of left PCA infarction, pre-onset MRI duration, and reil in the tongue, corpus callosum, and cuneal cortex are indicative of a favorable prognosis for lateral visual field defects (VFD). When compared to clinical variables, the combination of rEIL in various cortical subregions demonstrates a superior predictive effect for lateral VFD. The inclusion of rEIL in other variables improves the prognosis prediction for lateral VFD.	The ensemble LR model performed optimally with the highest mean ROC AUC value (0.872±0.092), while the ensemble RF model excelled with the highest mean Dice coefficient (0.353±0.220).	The successful reperfusion rate reached 78%, with favorable outcomes observed in 54% of patients (Modified Rankin Scale score 0-2).	
CONCLUSIONS	The team has concluded that the IB method can be employed for predicting the ultimate infarction in patients with acute ischemic stroke. However, further efforts are necessary to make it applicable in a clinical setting.	The team has derived estimates of rEIL that provide valuable information about the location of ischemic lesions. rEIL accurately predicts significant improvements in VFD, and the conclusion is reinforced when combined with other variables, enhancing predictive capabilities.	Compared to a single global machine learning model trained on voxel information independent of brain location, a locally trained machine learning model provides more accurate predictions of lesion outcomes.	There exists a correlation between small infarct lesions and favorable functional outcomes, while age is associated with decreased chances of favorable outcomes and functional improvement. Standalone radiological information as a predictor for functional outcomes exhibits relatively poor performance. Upon incorporating imaging variables into patient characteristics, no significant differences were observed among the predictive variable sets.	
PMID	34218182	36504664	36143010	36055039	36804312
YEAR	2021	2022	2022	2022	2023
LEARNING APPROACH	machine learning	machine learning	machine learning	machine learning	machine learning
PRIMARY AUTHOR	Abedi V	Ahmed F Elsaid	Guo Y	Li Y	Luo Y

(Continued)

10.3389/fneur.2024.1367854

TABLE 3 (Continued)

DISEASE	acute ischemic stroke	ischemic stroke	Ischemic Stroke	acute ischemic stroke	acute basilar artery occlusion
DATA VOLUME	Clinical data from a cohort of 7144 patients retrieved from the database.	360 ischemic stroke patients were enrolled, and a continued investigation was conducted with a subset of 354 individuals.	88 DSC-PWI images from 156 patients.	A total of 260 stroke patients undergoing mechanical thrombectomy at our hospital were randomly divided into a training set (n=182) and a test set (n=78) in a 7:3 ratio.	A total of 132 patients were randomly allocated into a training group (n = 106) and a test group (n = 26).
DATA TYPE	MRI	T2 diffusion-weighted MRI	DSC-PWI	DWI	dwi
METHODS	EHR	generalized additive modeling (GAM)	Ten machine learning models	Combining machine learning with radiomics features	radiomics-clinical machine learning model
RESULTS	The model's average AUROC ranges from 0.76 to 0.81, with the Random Forest model excelling in a one-month window (AUROC=0.82). Shorter prediction windows show high Negative Predictive Values (NPV), peaking at 91.1. The RF model has the highest Positive Predictive Value (PPV) in a six-month window (0.92), while the XGBoost-based model achieves the highest accuracy in a one-month window (precision of 0.89). Age, hemoglobin levels, and BMI consistently rank as the top three influential factors across different prediction windows, with average overall importance values of 96.3%, 68.2%, and 55.5%, respectively.	The rate of hemorrhagic transformation (HT) in ischemic stroke patients was 19.8%.	The R values of dimensionality reduction features (DRF) obtained through methods such as First_order, GLCM, GLDM, GLRRM, GLSZM, and NGTDM using PCA, ICA, t-SNE, ISOMAP, and UMAP were 0.110 ± 0.121, 0.140 ± 0.079, 0.110 ± 0.121, 0.294 ± 0.139, and 0.098 ± 0.133, respectively.	In the training set, the AUC for predicting post-mechanical thrombectomy outcomes was 0.945 (95% CI: 0.890–0.975), while in the test set, it was 0.920 (95% CI: 0.849–0.981).	The area under the ROC curve (AUC) of the radiomics-clinical model was 0.897 in the training group and 0.935 in the test group. For the radiomics model alone, the AUC was 0.887 in the training group and 0.840 in the test group. The clinical model achieved an AUC of 0.746 in the training group and 0.766 in the test group.
CONCLUSIONS	The machine learning model successfully predicted outcomes for stroke patients across different time periods and highlighted the crucial role of these factors in predicting mortality rates.	The team identified cerebral microbleeds, NIHSS, and infarct size as predictors of HT. The optimal predictive models were RFC and GBC, revealing the ability to capture non-linear interactions among predictive factors.	In the detection, assessment, and outcome prediction of ischemic stroke, employing various feature extraction and dimensionality reduction methods can achieve satisfactory performance.	A model based on radiomic and machine learning features exhibits high predictive efficiency for the prognosis of acute ischemic stroke after mechanical thrombectomy.	The radiomics-clinical machine learning model based on DWI demonstrated satisfactory performance in predicting preoperative ineffective reperfusion in ABAO patients.
PMID	37416313	36650639	36699499	37745661	36934582
YEAR	2023	2023	2023	2023	2023
LEARNING APPROACH	machine learning	machine learning	machine learning	machine learning	machine learning
PRIMARY AUTHOR	Xu Y	Wang X	Yu H	Lee J	Weng S
DISEASE	corpus callosum infarction	acute ischemic stroke	acute ischemic stroke	acute ischemic stroke	ischemic stroke

(Continued)

10.3389/fneur.2024.1367854

TABLE 3 (Continued)

DATA VOLUME	A total of 314 patients with acute corpus callosum infarction (CC)	A total of 573 patients were included in the study, comprising 398 with small-vessel occlusion (SVO) and 175 with large artery atherosclerosis (LAA) acute ischemic stroke (AIS).	148 patients with acute ischemic stroke due to anterior circulation artery occlusion.	3,687 patients were in one group, and there were 250 and 110 patients in the other two groups for validation.	CTA and MRI images from 97 patients
DATA TYPE	Neuroimaging modalities such as MRI, MRA, or CTA were employed for neuroimaging assessments	DWI	multi-modal MRI radiomics	MRI and associated clinical information.	CTA、DWI
METHODS	interpretable machine learning-derived early warning strategy	Logistic regression (LR) and machine learning (ML)	machine learning based on multi-modal MRI radiomics	ML algorithms	machine learning-based method
RESULTS	The predictive performance of the LR model for SCD after CC infarction surpasses that of the other six machine learning models. Through LASSO and SHAP analyses, nine key predictive factors were identified in the LR model output. Additionally, factors independently associated with cognitive outcomes were revealed.	In brief, the LR model for small-vessel occlusion acute ischemic stroke (SVO-AIS) demonstrated excellent outcome AUC of 0.86 [0.78–0.94] and good outcome AUC of 0.88 [0.8–0.96]. For the LR model in large artery atherosclerosis acute ischemic stroke (LAA-AIS), the AUCs were 0.73 [0.54–0.91] for excellent outcomes and 0.75 [0.59–0.91] for good outcomes. The GPR model for SVO-AIS exhibited AUCs of 0.86 [0.77–0.95] for excellent outcomes and 0.86 [0.77–0.96] for good outcomes, while the GPR model for LAA-AIS had AUCs of 0.65 [0.47–0.83] for excellent outcomes and 0.66 [0.49–0.84] for good outcomes. The GOA-RF model for SVO-AIS achieved AUCs of 0.85 [0.75–0.94] for excellent outcomes and 0.84 [0.74–0.94] for good outcomes. The GOA-RF model for LAA-AIS showed AUCs of 0.66 [0.49–0.84] for excellent outcomes and 0.68 [0.51–0.86] for good outcomes. The GOA-XGBoost model displayed AUCs of 0.87 [0.79–0.96] for excellent outcomes and 0.85 [0.76–0.94] for good outcomes, with AUCs of 0.91 [0.84–0.97] for excellent outcomes and 0.90 [0.83–0.97] for good outcomes in the LAA-AIS population.	Among 148 patients, 83 (56.1%) had a favorable prognosis, while 65 (43.9%) had an unfavorable prognosis. The accuracy of the SVM model was 79%, the RF model was 82%, the LightGBM model was 83%, the CatBoost model was 81%, and the XGBoost model was 80%.	In the patient cohort, 30.4% experienced unfavorable outcomes, with external validation data showing rates of 37.2% and 29.1%, respectively. The internal test set, external validation sets A and B demonstrated AUROC values of 0.790, 0.791, and 0.873, while the Brier scores were 0.172, 0.202, and 0.141, respectively.	On two independent test sets, the accuracy (ACC) for the cross-validated dataset using the Adboost method was 0.8519, while the ACC for the independent test set using the SRC method was 0.8125.
CONCLUSIONS	The combination of the LR model and SHAP interpreter can assist in achieving personalized risk predictions and, given its suboptimal long-term efficacy, may serve as a decision tool for early intervention.	Various small vessel disease (SVD) markers carry different prognostic weights in acute ischemic stroke (AIS) patients. Only the SVD burden accurately predicts the prognosis of small-vessel occlusion acute ischemic stroke (SVO-AIS) patients.	The potential value of a multimodal radiomic approach in accurately predicting clinical outcomes in patients with acute ischemic stroke (AIS). It aids in preventing mental disorders following a stroke.	With the aid of the SHAP method, we can attain an in-depth understanding of how critical features contribute to model predictions and how changes in these features influence such predictions	This machine learning approach can effectively explore and accurately quantify features related to stroke prognosis, including vascular structure and stroke location.

10.3389/fneur.2024.1367854

CNN is considered the best tissue outcome prediction model with significant performance advantages (81).

In 2020, Yu et al. included 182 patients with acute ischemic stroke for MRI analysis. Initially, segmentation of T2-weighted fluid-attenuated inversion recovery images was performed by neuroradiologists. Subsequently, image registration and normalization were carried out using SPM12 software, and preprocessing of images was done with the Tmax and ADC segmentation from RAPID software. The study employed a neural network with U-Net architecture and calculated various performance metrics, including DSC, Positive Predictive Value (PPV), sensitivity, specificity, lesion volume error, etc., for the Deep Learning model, Tmax, and ADC threshold methods. Data analysis was conducted using Stata version 0.70. In this study, the Deep Learning model exhibited a median area under the curve of 0.92 (IQR, 0.87–0.96). Using a threshold of 0.50, the median DSC overlap for this model was 0.53 (IQR, 0.31–0.68), with a sensitivity of 0.66 (IQR, 0.38–0.86), specificity of 0.97 (IQR, 0.94–0.99), PPV of 0.53 (IQR, 0.28–0.74), volume error of 9 mL (IQR, −14-29), and absolute volume error of 24 mL (IQR, 11–50). The study concluded that the Deep Learning model appears to successfully predict infarct lesions from baseline imaging without the need for reperfusion information and performs comparably to existing clinical methods (82).

In 2020, Debs et al. included 109 patients with cerebral arterial occlusion who underwent thrombectomy for MRI and follow-up FLAIR imaging. They employed Olea Sphere software for circular singular value decomposition, extracting parameter maps from DSC-PWI images. In image processing, FSL was used to remove the skull and normalize the images, ensuring standardization across patients. Experts manually labeled lesions on baseline DWI and final FLAIR images using 3D Slicer. Three models were established: a "universal" model trained on the entire cohort without considering reperfusion status, a "reperfusion" model trained only on reperfusion patients, and a "non-reperfusion" model. These models, based on the U-Net architecture, received five inputs (DWI, ADC, Tmax, CBF, and CBV) and generated probability maps for lesions, healthy tissue, and background. The final infarct was defined by setting a threshold of 0.5. Result assessments included metrics such as DSC, accuracy, recall, volume similarity (*VS*), HD, and AUC. In non-reperfusion patients, the non-reperfusion model predicted an infarct volume of 39.7 mL with a DSC of 68%. In reperfusion patients, the reperfusion model predicted an infarct volume of 17.5 mL with a DSC of 89%. CNN-based models demonstrated excellent AUC values, with 0.87 for reperfusion patients and 0.81 for non-reperfusion patients. The study concluded that incorporating reperfusion status into training enhances model performance, and CNN outperforms clinical models. Predicting the final infarct plays a crucial role in evaluating treatment efficacy (83).

In 2020, Osama et al. included DWI and PWI data from 43 patients with acute ischemic stroke. They constructed a neural network model based on multi-parameter feature embedding (PMFE-SN) and applied it to predict the outcomes of acute ischemic stroke treatment. By preprocessing the images and employing two twin convolutional neural networks to build Siamese networks, effective feature extraction for samples of the same or different categories was achieved. At the output layer, the extracted features were normalized using cosine similarity, and training was performed with the backpropagation algorithm and stochastic gradient descent to minimize the binary cross-entropy loss function. The study extensively used various evaluation metrics, including Mean Absolute Error (MAE), macro-average F1 (F1macro), macro-average precision (Pmacro), macro-average recall (Rmacro), Matthews Correlation Coefficient (MCC), and AUC. The results showed a significant improvement in evaluation metrics for PMFE-SN compared to traditional random forest methods. Pmacro increased from 0.152 to 0.258, Rmacro increased from 0.21 to 0.31, F1macro increased from 0.18 to 0.28, and MCC increased from 0.04 to 0.09. The overall AUC value increased from 0.50 for the random forest method to 0.81. The research conclusion explicitly stated that PMFE-SN demonstrated excellent performance in predicting categories with both few and numerous samples (84).

In 2021, Bo et al. randomly selected 50 patients admitted to the hospital from January 2019 to January 2021. They conducted an analysis of the impact features of MRI on critically ill patients with cerebral infarction using CNN and explored the clinical application of Artificial Intelligence-assisted systems in imaging. Additionally, they established a CNN Artificial Intelligence system for learning and training, utilizing the CNN system to extract data such as pixel grayscale statistics, regional feature descriptions, and local region gradient analysis. The data were then computed using computer technology. Comparing the segmentation results, it was found that the segmentation Dice coefficient of U-Net without additional supervision was 81.74 ± 0.40%, and P-Net's Dice coefficient was 86.39 ± 0.31%. In the first stage, DPA-UNet was 83.52 ± 0.31%, in the second stage, it was 88.29 ± 0.27%, and in the third stage, it was 91.74 ± 0.12%. There was no significant difference between the data sets. A higher Dice coefficient indicates more accurate segmentation. Through the analysis of T1WI, contrast-enhanced T1WI, and T2WI images, significant differences were found between GLSZM and ALL, GLRLM, MGLSZM, and GLSZM (85).

In 2021, Ma et al. selected 36 patients diagnosed with lacunar cerebral infarction (LCI) between February 2019 and June 2020 as the study subjects. The objective was to explore the MRI features using the fuzzy local information C-means clustering (FLICM) image segmentation method and to analyze the risk factors for recurrent stroke in patients with lacunar infarction. The study, based on the FLICM algorithm, introduced the Canny edge detection algorithm, and Fourier shape descriptors to optimize the algorithm. The research investigated the differences in Jaccard coefficient, Dice coefficient, peak signal-to-noise ratio (PSNR), structural similarity index measure (SSIM), processing time, and segmentation accuracy between the optimized FLICM algorithm and other algorithms when segmenting brain tissue MRI images. Patients were categorized into a control group (no recurrent stroke, 20 cases) and a stroke group (recurrent stroke, 16 cases) based on whether they experienced another stroke. The study compared the differences in MRI features between the two groups and utilized logistic multivariate regression analysis to identify risk factors for recurrent stroke after lacunar infarction. The results showed that, under the same noise conditions, the optimized FLICM algorithm exhibited higher Jaccard coefficient, Dice coefficient, PSNR, and SSIM values when segmenting brain tissue compared to other algorithms. Additionally, age and a history of hypertension were identified as risk factors for recurrent stroke after lacunar infarction (86).

In 2021, Tolhuisen et al. included 316 FU-DWI (Follow-Up Diffusion Weighted Imaging) data from the HERMES, ISLES, and MR CLEAN-NOIV databases. They transformed DWI images into

standard MNI space using the SPM8 toolbox. A Deepmedic network was trained on the DWI images from the HERMES dataset, with the data split into training set (70%), validation set (10%), and test set (20%). The trained network was then applied to other datasets. Simultaneously, they manually adjusted using ITK-SNAP, and developed and optimized a Convolutional Autoencoder (CAE) using the Keras library. The study aimed to accurately predict functional independence within 90 days using mRS scores. They optimized SVM by adjusting the kernel type, coefficient (gamma), and regularization parameter (C). Feature normalization was performed on all features using scikit-learn's "RobustScaler" function, with 80% of DWI images used for 5-fold cross-validation. The remaining 20% of images were used to test the final classifier's performance by evaluating AUC of ROC curve. DeLong's test was applied for pairwise comparisons and to test for statistical differences. The study results demonstrated that the AUC values for the CAE and radiomics feature-based classifier were 0.88 and 0.81, respectively, while the FIV-based classifier had an AUC value of 0.79. The SVM classifier based on radiomics features achieved the highest accuracy of 0.80, whereas the SVM classifier based on FIV had the highest recall of 0.73 (87).

In 2022, Zeng et al. included 711 ischemic stroke patients admitted between March 1, 2017, and December 31, 2020, as the training group. Additionally, they included 140 ischemic stroke patients admitted to the same hospital between January 1, 2021, and May 1, 2021, as the testing group. Patients were assessed with NIHSS scores on admission and on the seventh day (classified as stage 1 if NIHSS <5 and stage 2 if NIHSS ≥5). The testing group underwent MRI within 24 h to 7 days after a subacute stroke episode and received thrombolysis. The researchers converted DICOM DWI to NIfTI format, removed DWI artifacts, corrected image alignment using 3Dslicer, normalized images, and adjusted pixel size using SimpleITK. The data were divided into eight models (Models A-H) based on admission NIHSS and NIHSS on the seventh day. They employed 3D CNN models (Models E-G) based on input DWI with pixel and preprocessing strategies. The performance of different models was compared using the DeLong test ($p < 0.05$, statistically significant), and AUC was evaluated after exporting results. Model E demonstrated the highest AUC in the testing set, particularly in predicting NIHSS stage on admission. Model A performed best in predicting NIHSS stage on admission when a subsequent ischemic stroke occurred, with Model D correctly predicting all cases of subsequent ischemic stroke in later cycles. For predicting NIHSS stage on the seventh day of hospitalization, Model E had the highest AUC, with relatively higher AUC in predicting NIHSS stage on the seventh day in patients with anterior circulation ischemic stroke and relatively lower AUC in predicting NIHSS stage on the seventh day in patients with posterior circulation ischemic stroke (88).

In 2022, Wong et al. included 875 patients with acute ischemic stroke (700 in the training set and 175 in the testing set) with DWI and MRI data. They manually segmented acute infarct volumes using MRIcro, selecting eADC to confirm the diffusion-restricted portion of the infarct, and extracting image volumes in Matlab using SPM12 tools. Subsequently, they employed a Deep Learning model, training a group convolutional neural network with U-Net architecture and Dice loss function, incorporating augmentations like rotation and reflection for segmentation. Evaluation metrics such as Dice scores, precision, and recall were compared with manual labels. Additionally, a multivariate logistic regression model was constructed to assess the predictive impact of topological infarct volume on 90-day mRS outcomes. In the testing data, the model without data augmentation achieved a Dice score of 0.85, precision of 0.83, and recall of 0.89. The model with data augmentation had a Dice score of 0.84, precision of 0.84, and recall of 0.89. Using each output for 30 fine brain regions to predict the mRS achieved an AUC of 0.80 and accuracy of 0.75 (89).

In 2022, Nazari-Farsani et al. included 455 patients with acute ischemic stroke, and obtained DWI and PWI images. They initially preprocessed the images using SPM12 software and then applied a 3D Attention Gated (AG) U-net model with Rectified Linear Unit (ReLU) activation function and ADAM optimizer. The model was subjected to 5-fold cross-validation using a hybrid loss function. The evaluation metrics included AUC, sensitivity, specificity, DSC, volume error, absolute volume error, and Jaccard index. Statistical analysis was conducted using the Scipy package in Python. The results showed that the median AUC of the DCNN model was 0.91 (IQR: 0.84–0.96). Using a probability threshold of 0.5, the median sensitivity, specificity, and Jaccard index were 0.60 (IQR: 0.16–0.84), 0.97 (IQR: 0.93–0.99), and 0.50 (IQR: 0.21–0.70), respectively. The DCNN model's median DSC was 0.50, while the ADC threshold method had a median DSC of 0.18 ($p < 0.01$). The predicted volume by the model exhibited a high correlation with the actual lesion volume, with a correlation coefficient of 0.73 ($p < 0.001$) (90).

In 2022, Moulton et al. included patients suspected of large vessel occlusion and candidates for reperfusion therapy with DWI. They preprocessed the images using techniques such as skull stripping, manual correction, and normalization. High-level feature sets were generated using VGGNet, and the model was trained and evaluated through internal training-validation sets and LOCO cross-validation. Adam optimizer and binary cross-entropy loss function were employed during model training. The analysis involved 322 patients, with 113 from the Pitié-Salpêtrière registry, 94 from the Insulin Stroke Trial, and 115 from six centers in the ASTER trial. Significant differences were found in stroke-to-needle time ($p = 0.008$) and stroke side ($p < 0.001$). The Deep Learning ensemble model performed the best, with an accuracy of 0.79, AUC of 0.83, sensitivity of 0.67, specificity of 0.87, PPV of 0.79, and NPV of 0.78. The conclusion suggests that the model has potential applications in predicting long-term functional outcomes in stroke patients and could be used as a patient stratification strategy for neuroprotective and rehabilitation therapies (91).

In 2023, Lv et al. included 282 patients with 50% stenosis of the internal carotid artery for MRI 1 week later. They preprocessed DICOM images, applied convolution, utilized max-pooling layers, and fully connected layers to output images. Features from different modalities were concatenated, and a Fully Connected (FC) layer was created in the corresponding dimension of the channel to obtain classification results. In statistics, the loss function allows the evaluation of the difference between the true and predicted values. They measured the performance of common machine learning methods based on the random forest, logistic regression, and XGBoost concepts in predicting recurrent stroke. The models were trained to minimize the differences between model values and actual values. Results showed that the AUC values for four different modalities were 62.2, 68.9, 65.4, and 60.4%, respectively. The AUC for T2WI modality was 8.5% higher than that for the ADC modality. ADC modality performed relatively worse, being 11.6% lower than the FLAIR

modality, which exhibited better performance. The AUC values for the three algorithms were 50.6, 64.8, and 66.8%, with XGBoost achieving an AUC of 66.8% (92).

In 2023, Ye et al. conducted a study involving 441 patients with acute ischemic stroke. They utilized MRI and grouped the patients based on the prognosis NIHSS scores. The ITK-SNAP 6.0.3 software was employed to independently segment ROIs in the images, generating three-dimensional structural data of the lesions. Subsequently, radiomic features of each annotated lesion were extracted using radiomics analysis tools (Pyradiomics software package), resulting in a total of 17 clinical features and 851 radiomic features. After preprocessing steps such as data imputation, denoising, standardization, filtering, concatenation, and balancing, they constructed a multi-level cascaded Deep Learning ensemble (EDL) model, combining ensemble learning and Deep Learning. The optimized Deep Learning ensemble (OEDL) model was established by introducing the big bang optimization algorithm (BBOA). Model training was carried out on a Linux workstation equipped with a GPU, utilizing the Python 3.7 platform and TensorFlow 2.8 framework, with 70% of the data allocated for the training set and 30% for the test set. The statistical analysis of clinical, radiomic, performance prediction, and comparative results showed that Macro-AUC, ACC, Macro-R, Macro-P, and Macro-F1 achieved values of 97.89, 95.74, 94.75, 94.03, and 94.35%, respectively. In comparison, the EDL method demonstrated a Macro-AUC of 96.68% and ACC of 92.55%. The OEDL method achieved a Macro-AUC of 97.89% and ACC of 95.74%. The SMOTEENN-based mixed sampling method exhibited the best classification performance, with Macro-AUC, ACC, Macro-R, Macro-P, and Macro-F1 reaching 97.89, 95.74, 94.75, 94.03, and 94.35%, respectively (93).

The main information of the above included literatures is shown in Table 4.

2.6 The potential applications of other imaging modalities in ischemic stroke

2.6.1 Positron emission tomography

Positron emission tomography scans, employing oxygen-15 technology, provide information about glucose and oxygen metabolism abnormalities, ranging from the penumbra to ischemic tissue (94). With PET, it is possible to assess CBF reserve capacity in carotid atherosclerosis, aiding in the planning of future intervention strategies (95). In addition, TSPO PET can provide detailed information about metabolic and molecular changes during the neuroinflammatory phase after a stroke. However, the gold standard for TSPO PET quantification involves a 90-min scan and continuous arterial blood sampling, which is undoubtedly challenging in routine clinical practice. Artem Zatcepin and colleagues developed a machine learning-based algorithm to establish a simplified TSPO quantification method that can be easily implemented in clinical settings (96). Measurements of brain metabolism can provide new kinds of data for deep learning models, especially those based on computer vision. By combining metabolic and anatomic information, we can provide a more comprehensive picture of brain injury and build a more accurate predictive model of recovery. The detection of the brain metabolism of patients during rehabilitation can not only provide potential information support for the adjustment of rehabilitation measures, but also provide data sources for the construction of deep learning models containing temporal information.

2.6.2 Single photon emission computed tomography

Ongoing advancements in SPECT instrumentation have facilitated the clinical application of several new technologies, including semiconductor Cadmium Zinc Telluride (CZT) detectors, absolute quantification of radiopharmaceutical uptake, multi-bed position whole-body SPECT acquisition, and novel non-parallel-hole collimators (97). The application of SPECT allows for the detection of cerebral blood flow reserve capacity in patients with carotid atherosclerotic disease, aiding in the formulation of future intervention plans (95). Using the acetazolamide challenge test, SPECT can also assess the decline in vascular reserve function. This information can be used to predict whether patients undergoing carotid endarterectomy will experience ischemia. SPECT is capable of characterizing the content of atherosclerotic plaques, including oxidized low-density lipoprotein and apoptotic bodies (98). Furthermore, SPECT can provide detailed information about metabolic and molecular changes (99). Based on these characteristics, SPECT has long been used for the evaluation of brain ischemia recovery (100). SPECT is currently used to explore the mechanism by which thalamic injury leads to a decline in word retrieval ability during brain ischemia recovery (101). Similarly, SPECT is also used to assess mid-term motor recovery after cerebral infarction (102). In summary, AI models based on SPECT have the potential for quantitative assessment of recovery progress.

2.6.3 Dual-energy computed tomography

There has been some progress in the application of DECT in ischemic stroke. In a study by Na-Young Shin and colleagues, it was demonstrated that the collateral circulation status recorded by DECT could serve as a useful indicator for predicting the clinical prognosis of acute stroke patients (103). Additionally, Wang et al. (104) confirmed that DECT has certain value in the early diagnosis and prediction of intracranial hemorrhage after mechanical thrombectomy in patients with acute ischemic stroke. Furthermore, due to the advantages of dual-energy CT in measuring bone and muscle, it can be used to assess the recovery of motor function in stroke patients after rehabilitation therapy. This enables timely adjustments to the rehabilitation plan (105, 106).

3 Discussion

3.1 Existing methods

In current Artificial Intelligence-related research, due to clinical practical needs and challenges in data acquisition, researchers primarily utilize CT and MRI imaging modalities to assess ischemic stroke. Among these, MRI is undoubtedly the most widely used imaging modality. Although MRI has certain limitations for patients with metallic implants or claustrophobia, it can detect ischemic lesions earlier and more sensitively through diffusion-weighted imaging. The multiple imaging modalities of MRI also enable researchers to acquire more medical information, constructing more robust models. Another primary imaging modality without a doubt is CT. CT, as a simple,

TABLE 4 Summary of papers on deep learning for MRI on rehabilitation of ischemic stroke.

PMID	29720437	30568631	31131293	32163165
Year	2018	2018	2019	2020
Learning approach	Deep learning	Deep learning	Deep learning	Deep learning
Primary author	Nielsen A	Pinto A	Ho KC	Yu Y
Disease	Acute ischemic stroke	Stroke lesion	Ischemic stroke	Acute ischemic stroke
Data volume	A total of 222 patients were included, with 187 receiving rtPA treatment (recombinant tissue-type plasminogen activator).	75 ischemic stroke patients divided into two groups: training ($n = 43$) and testing ($n = 32$),	444 patient MR images were retrieved and examined from the University of California-Los Angeles picture archiving and communication system between December 2005 and December 2015.	182 patients with acute ischemic stroke, in accordance with the conventions of scientific literature.
Data type	MRI	MRI	MRI, Handcrafted features derived from perfusion images.	MRI
Methods	CNNdeep	Adopting a deep learning architecture that combines U-net with two-dimensional Gated Recurrent Units (GRU), following the pattern of nature.	Deep convolution neural networks (CNNs)	Neural network
Results	The AUC for CNNdeep is 0.88, surpassing the generalized linear model with an AUC of 0.78, CNNTmax with an AUC of 0.72, ADCthres with an AUC of 0.66, and substantially outperforming CNNshallow with an AUC of 0.85.	In accordance with the conventions of Nature: Dice Similarity Coefficient (DSC): Baseline 0.34 ± 0.22, Proposal 0.35 ± 0.22; Hausdorff Distance: Baseline 35.09 ± 17.27, Proposal 31.38 ± 15.81; Average Symmetric Surface Distance (ASSD) series: Baseline 6.08 ± 5.27, Proposal 5.55 ± 5.00; Precision: Baseline 0.37 ± 0.29, Proposal 0.41 ± 0.30; Recall: Baseline 0.54 ± 0.26, Proposal 0.47 ± 0.24.	Our deep CNN model improves feature learning, achieving an AUC of 0.871 ± 0.024, outperforming existing models for tissue fate.	The curve of 0.92, DSC of 0.53, and volume error of 9 mL.
Conclusions	The notable improvement in prediction accuracy enhances the potential for automated decision support, offering personalized treatment plan recommendations, surpassing the current state-of-the-art.	Leveraging deep learning for stroke outcome prediction, the study demonstrates promising outcomes on the ISLES 2017 dataset while indicating avenues for potential enhancements in clinical applications.	Our study utilizes deep learning techniques for predicting stroke tissue outcomes, advancing magnetic resonance imaging perfusion analysis toward becoming an operational decision support tool for guiding stroke treatment.	The deep learning model accurately predicted infarct lesions without reperfusion information, performing similarly to current clinical methods.
PMID	33450521	33105609	34385896	34887708
Year	2021	2020	2021	2021
Learning approach	Deep learning	Deep learning	Deep learning	Deep learning
Primary author	Debs N	Osama S	Bo Y	Chunli Ma
Disease	Acute ischemic stroke	Acute ischemic stroke	Cerebral infarction	Lacunar cerebral infarction
Data volume	109 patients, including 35 without reperfusion.	43 samples from the ISLES 2017 dataset.	50 patients with cerebral infarction were selected randomly.	36 patients with lacunar myosphere infarction (no recurrence in the control group, $n = 20$, recurrence in the stroke group, $n = 16$).

(Continued)

10.3389/fneur.2024.1367854

TABLE 4 (Continued)

PMID	29720437	30568631	31131293	32163165
Data type	Baseline diffusion and perfusion-weighted magnetic resonance imaging (MRI)	DWI、PWI	MRI	MRI
Methods	Convolutional neural networks (CNN)	Parallel multi-parametric feature embedded siamese network (PMFE-SN)	Convolutional neural network (CNN)	Deep learning algorithm
Results	The peak values of DSC (Dynamic Susceptibility Contrast) in reperfused and non-reperfused patients were 0.44 ± 0.25 and 0.47 ± 0.17, respectively. The Area Under the Curve (AUC) for reperfused patients was 0.87 ± 0.13, while for non-reperfused patients, it was 0.81 ± 0.13. The AUC for the perfusion-diffusion mismatch model was 0.73 ± 0.14.	PMFE-SN exhibits a significant improvement compared to traditional random forest methods. Pmacro increased from 0.152 to 0.258, Rmacro improved from 0.21 to 0.31, F1macro rose from 0.18 to 0.28, and MCC increased from 0.04 to 0.09. The overall AUC value elevated from 0.50 with the random forest method to 0.81.	In the absence of additional supervision, U-Net exhibited a segmentation Dice coefficient of 81.74 ± 0.40%, while P-Net demonstrated a Dice coefficient of 86.39 ± 0.31%. The first stage of DPA-UNet yielded a Dice coefficient of 83.52 ± 0.31%, the second stage achieved 88.29 ± 0.27%, and the third stage reached 91.74 ± 0.12%. There were no significant differences observed among the data sets.	The optimized FLICM algorithm, under the same noise conditions, exhibits higher Jaccard coefficient, Dice coefficient, PSNR, and SSIM values in the segmentation of brain tissues compared to other algorithms. Furthermore, age and a history of hypertension are identified as risk factors for recurrent strokes following lacunar infarction.
Conclusions	Utilizing a convolutional neural network (CNN)-based model demonstrates superior performance compared to the perfusion-diffusion mismatch model commonly employed in clinical settings.	PMFE-SN demonstrates exceptional performance in predicting categories with both fewer and more samples, delving into pre-and post-treatment clinical data. Exploring the use of additional similarity metrics in this context could contribute to a comprehensive enhancement of predictive accuracy for outcomes in acute ischemic stroke treatment.	Utilizing CNN to analyze features in MRI images of critically ill cerebral infarction patients, we have identified an image diagnostic method that mitigates subjective visual judgment errors to a certain extent. The introduction of a deep supervision mechanism enhances the recognition capabilities of U-Net, holding significant importance for the accurate extraction and reconstruction of MRI images in patients with cerebral infarction.	The optimized FLICM algorithm demonstrates effective segmentation of brain MRI images, with age and a history of hypertension identified as risk factors for recurrent strokes in lacunar infarction patients. This study provides valuable insights for the diagnosis and prognosis of lacunar infarction
PMID	35892499	35887776	35545938	36481696
Year	2022	2022	2022	2023
Learning approach	Deep learning	Deep learning	Deep learning	Deep learning
Primary author	Tolhuisen ML	Zeng Y	Wong KK	Nazari-Farsani S
Disease	Acute ischemic stroke	Ischemic stroke	Acute ischemic stroke	Ischemic stroke
Data volume	316 follow-up DWI datasets sourced from the HERMES, ISLES, and MR CLEAN-NOIV databases.	851 patients (711 in the training set and 140 in the test set)	875 patients ($n = 700$ in the training group, $n = 175$ in the test group)	445 patients
Data type	FU-DWI	DWI	MRI, DWI	PWI
Methods	Deep learning network	CNN	A rotation-reflection equivariant model was developed based on U-Net and grouped convolutions.	Deep convolutional neural network (DCNN)

(Continued)

10.3389/fneur.2024.1367854

TABLE 4 (Continued)

PMID	29720437	30568631	31131293	32163165
Results	The AUC values for the CAE and radiomic features classifier are 0.88 and 0.81, respectively, while the classifier based on FIV achieves an AUC value of 0.79. The SVM classifier based on radiomic features attains the highest accuracy at 0.80, whereas the SVM classifier based on FIV achieves the highest recall at 0.73.	Following the conventions of scientific writing: The proposed model exhibits improved performance in predicting NIHSS stages on the 7th day of hospitalization compared to admission (best AUC 0.895 vs. 0.846). Model D, trained on DWI images, achieved the best AUC of 0.846 in predicting NIHSS stages at admission. Model E, also trained on DWI images, achieved the best AUC of 0.895 in predicting NIHSS stages on the 32nd day of hospitalization. The model demonstrates favorable performance in predicting NIHSS stages on the 7th day of hospitalization for both anterior and posterior circulation strokes, with best AUCs of 7.0 and 905.0, respectively.	The segmentation model achieved Dice scores of 0.88 (training) and 0.85 (testing). The AUC for predicting modified Rankin Scale outcomes based on refined stroke volumes in 30 brain regions was 0.80, with an accuracy of 0.75.	The model achieved a median AUC of 0.91. Using a threshold of 0.5 for infarction probability, median sensitivity and specificity were 0.60 and 0.97 respectively, while the median DSC was 0.50, and the absolute volume error was 27 mL.
Conclusions	The prediction of functional outcomes should not solely rely on FIV; FU-DWI images should capture additional prognostic information	Our 3D-CNN model efficiently predicts stroke-related neurologic damage using DWI images, demonstrating outstanding performance in predicting NIHSS stages on the 7th day of hospitalization. It holds potential clinical decision-making value in subgroup analysis.	We developed a rotation-reflection equivariant deep learning model to effectively segment acute ischemic stroke lesions in diffusion-weighted imaging, showcasing competitive performance in well-balanced testing cases across different vascular territories. Moreover, when integrated with clinical factors, the model exhibited high accuracy and AUC in predicting 90-day modified Rankin Scale outcomes.	An AG-DCNN using diffusion information alone upon admission was able to predict infarct volumes at 3–7 days after stroke onset with comparable accuracy to models that consider both DWI and PWI.
PMID	36169033	36908778	37416306	
Year	2023	2023	2023	
Learning approach	Deep learning	Deep learning	Deep learning	
Primary author	Moulton E	Lv P	Ye W	
Disease	Post-stroke	Carotid atherosclerotic stenosis	Acute ischemic stroke	
Data volume	322 patients from the ASTER and INSULINFARCT trials as well as the Pitié-Salpêtrière registry.	Patients with 50% stenosis in 282 internal carotid arteries	441 patients with acute ischemic stroke, 17 clinical features and 19 radiomic features were included.	
Data type	DWI	MRI	Clinical and radiomics features	
Methods	Convolutional neural networks (CNN)	Multi-modality fused network	Optimized ensemble of deep learning (OEDL) method.	

(Continued)

10.3389/fneur.2024.1367854

TABLE 4 (Continued)

PMID	29720437	30568631	31131293	32163165
Results	The deep learning model demonstrated a notably superior performance with an area under the curve (AUC) of 0.83, surpassing lesion volume (AUC = 0.78) and ASPECT (AUC = 0.77). Upon aligning all classifiers with the specificity of the deep learning model (0.87), CNN's sensitivity (0.67) significantly outperformed lesion volume (0.48) and ASPECT (0.50).	The AUC values for four different modalities were 62.2, 68.9, 65.4, and 60.4% respectively, with the AUC for T2WI modality surpassing that of the ADC modality by 8.5%. The ADC mode exhibited relatively poorer performance, being 11.6% lower than the more favorable FLAIR mode. The AUC values for three algorithms were 50.6, 64.8, and 66.8%, with the XGBoost classification algorithm achieving an AUC of 66.8%	The OEDL method with combined features and mixed sampling achieved the best classification performance, with 97.89, 95.74, 94.75, 94.03, and 94.35% for Macro-AUC, ACC, Macro-R, Macro-P, and Macro-F1	
Conclusions	The attention mechanism revealed that the network learned to naturally attend to the lesion to predict outcome.	Deep learning models demonstrate enhanced predictive capability for clinical symptomatology and outcomes in stroke patients.	The proposed OEDL method significantly enhances stroke prognosis prediction, outperforming models based on individual clinical or radiomic features. The combined data modeling approach demonstrates superior effectiveness and holds promise for guiding interventions.	

feasible, and cost-effective diagnostic method, is widely favored among clinicians and emergency patients. CT enhancement or perfusion imaging methods performed on the basis of routine CT scans have been proven to have a powerful detection and evaluation effect.

Currently, the number of studies based on machine learning and deep learning is roughly equal. In terms of machine learning, modeling based on image texture features remains popular among researchers. Meanwhile, methods for extracting image texture features are applicable to various MRI sequences and facilitate the integration of information from different sequence images. However, this method requires the annotation of regions of interest (ROIs) to ensure consistency, leading to a significant amount of manual annotation and inspection of images, making it difficult to include a large number of samples in this type of research. Additionally, it is noteworthy that there are very few studies in rehabilitation-related machine learning research that adopt entirely new algorithms. Researchers still use several classical machine learning algorithms for modeling and determine the best model after comparing using a single evaluation parameter (usually AUC). Research related to deep learning has been rapidly growing in recent years. Both methods of data annotation are used by researchers. Firstly, studies based on deep learning can, like those based on texture analysis, use only ROIs for classification after re-annotation. This method constrains the data acquisition range through prior knowledge, which can effectively improve the model's accuracy under normal circumstances. Another method directly uses 3D brain images. Unlike the ROI annotation method, this method greatly expands the source of information. For strokes, this method incorporates not only information related to the severity of the injury within the ROI (usually the lesion) but also extracts information such as the relative extent and spatial location of the damage. This may predict the patient's recovery status by evaluating potential compensatory capabilities. More importantly, using 3D images to build models eliminates the need for manual annotation, greatly reducing the difficulty of expanding the sample size and helping to improve the robustness of the model. Although neural network structures are more flexible compared to machine learning, researchers still prefer to use neural networks that have shown good performance on other types of datasets, rarely adjusting the neural network structure based on task characteristics. This means that there is still significant room for improvement in stroke rehabilitation research based on deep learning.

3.2 Summary

Ischemic stroke can lead to serious consequences, including permanent brain damage and neurological deficits. Therefore, reducing and preventing neural damage caused by strokes has always been a focal point of research. Assessing the long-term and short-term recovery of patients through imaging enables the early identification of those requiring intervention and facilitates adjustments to rehabilitation plans based on imaging evaluation results, thereby enhancing patient quality of life. As one of the non-invasive diagnostic methods capable of acquiring a large amount of medical information, AI-based neuroimaging has demonstrated its ability to assess the long-term and short-term recovery of stroke patients. This suggests that AI-based neuroimaging holds potential for guiding rehabilitation programs. Therefore, conducting

neuroimaging follow-up during therapy and using AI methods to clarify the qualitative and quantitative relationships between rehabilitation interventions and neuroimaging is an area worthy of further exploration by researchers.

Author contributions

ZZ: Writing – original draft. YZ: Writing – original draft. JS: Writing – original draft. LY: Visualization, Writing – original draft. LP: Project administration, Writing – original draft. YG: Visualization, Writing – original draft. HW: Funding acquisition, Supervision, Writing – review & editing.

Funding

The author(s) declare financial support was received for the research, authorship, and/or publication of this article. This work was supported by the National Natural Science Foundation of China(82202280).

Conflict of interest

The authors declare that the research was conducted in the absence of any commercial or financial relationships that could be construed as a potential conflict of interest.

Publisher's note

All claims expressed in this article are solely those of the authors and do not necessarily represent those of their affiliated organizations, or those of the publisher, the editors and the reviewers. Any product that may be evaluated in this article, or claim that may be made by its manufacturer, is not guaranteed or endorsed by the publisher.

References

1. Feigin VL, Norrving B, Mensah GA. Global burden of stroke. *Circ Res*. (2017) 120:439–48. doi: 10.1161/CIRCRESAHA.116.308413

2. Lindsay MP, Norrving B, Sacco RL, Brainin M, Hacke W, Martins S, et al. World Stroke Organization (WSO): Global Stroke Fact Sheet 2019. *Int J Stroke*. (2019) 806–17. doi: 10.1177/1747493019881353

3. Malhotra K, Katsanos AH, Goyal N, Ahmed N, Strbian D, Palaiodimou L, et al. Safety and efficacy of dual antiplatelet pretreatment in patients with ischemic stroke treated with IV thrombolysis: a systematic review and meta-analysis. *Neurology*. (2020) 94:e657–66. doi: 10.1212/WNL.0000000000008961

4. Campbell BCV, De Silva DA, Macleod MR, Coutts SB, Schwamm LH, Davis SM, et al. Ischaemic stroke. *Nat Rev Dis Primers*. (2019) 5:70. doi: 10.1038/s41572-019-0118-8

5. Tang FH, Ng DK, Chow DH. An image feature approach for computer-aided detection of ischemic stroke. *Comput Biol Med*. (2011) 41:529–36. doi: 10.1016/j.compbiomed.2011.05.001

6. Chen Z, Zhang R, Xu F, Gong X, Shi F, Zhang M, et al. Novel prehospital prediction model of large vessel occlusion using artificial neural network. *Front Aging Neurosci*. (2018) 10:181. doi: 10.3389/fnagi.2018.00181

7. Zhou Y, Wu D, Yan S, Xie Y, Zhang S, Lv W, et al. Feasibility of a clinical-Radiomics model to predict the outcomes of acute ischemic stroke. *Korean J Radiol*. (2022) 23:811–20. doi: 10.3348/kjr.2022.0160

8. Pfaff J, Herweh C, Schieber S, Schönenberger S, Bösel J, Ringleb PA, et al. E-ASPECTS correlates with and is predictive of outcome after mechanical Thrombectomy. *AJNR Am J Neuroradiol*. (2017) 38:1594–9. doi: 10.3174/ajnr.A5236

9. Lee HC, Kuo FL, Lin YN, Liou TH, Lin JC, Huang SW. Effects of robot-assisted rehabilitation on hand function of people with stroke: a randomized, crossover-controlled, Assessor-blinded study. *Am J Occup Ther*. (2021) 75:7501205020p1. doi: 10.5014/ajot.2021.038232

10. Miceli G, Basso MG, Rizzo G, Pintus C, Cocciola E, Pennacchio AR, et al. Artificial intelligence in acute ischemic stroke subtypes according to toast classification: a comprehensive narrative review. *Biomedicine*. (2023) 11:1138. doi: 10.3390/biomedicines11041138

11. Sheth SA, Giancardo L, Colasurdo M, Srinivasan VM, Niktabe A, Kan P. Machine learning and acute stroke imaging. *J Neurointerv Surg*. (2023) 15:195–9. doi: 10.1136/neurintsurg-2021-018142

12. Soun JE, Chow DS, Nagamine M, Takhtawala RS, Filippi CG, Yu W, et al. Artificial intelligence and acute stroke imaging. *AJNR Am J Neuroradiol*. (2021) 42:2–11. doi: 10.3174/ajnr.A6883

13. Dragoş HM, Stan A, Pintican R, Feier D, Lebovici A, Panaitescu P, et al. MRI Radiomics and predictive models in assessing ischemic stroke outcome-a. *Syst Rev Diagnos*. (2023) 13:857. doi: 10.3390/diagnostics13050857

14. Shafaat O, Bernstock JD, Shafaat A, Yedavalli VS, Elsayed G, Gupta S, et al. Leveraging artificial intelligence in ischemic stroke imaging. *J Neuroradiol*. (2022) 49:343–51. doi: 10.1016/j.neurad.2021.05.001

15. von Kummer R, Dzialowski I, Gerber J. Therapeutic efficacy of brain imaging in acute ischemic stroke patients. *J Neuroradiol*. (2015) 42:47–54. doi: 10.1016/j.neurad.2014.10.004

16. Marsh JD, Keyrouz SG. Stroke prevention and treatment. *J Am Coll Cardiol*. (2010) 56:683–91. doi: 10.1016/j.jacc.2009.12.072

17. Murray V, Norrving B, Sandercock PA, Terént A, Wardlaw JM, Wester P. The molecular basis of thrombolysis and its clinical application in stroke. *J Intern Med*. (2010) 267:191–208. doi: 10.1111/j.1365-2796.2009.02205.x

18. Chaisinanunkul N, Adeoye O, Lewis RJ, Grotta JC, Broderick J, Jovin TG, et al. Adopting a Patient-centered approach to primary outcome analysis of acute stroke trials using a utility-weighted modified rankin scale. *Stroke* (2015) 46:2238–43. doi: 10.1161/STROKEAHA.114.008547

19. Ragoschke-Schumm A, Junk C, Lesmeister M, Walter S, Behnke S, Schumm J, et al. retrospective consent to hemicraniectomy after malignant stroke among the elderly, despite impaired functional outcome. *Cerebrovasc Dis*. (2015) 40:286–92. doi: 10.1159/000441194

20. Pramanick J, Uchat U, Chattopadhyay A, Mir AA, Koley M, Saha S. An open-label randomized pragmatic non-inferiority pilot trial comparing the effectiveness of curare 30CH against individualized homeopathic medicines in post-stroke hemiparesis. *Adv Integrat Med*. (2020) 7:79–88. doi: 10.1016/j.aimed.2019.06.002

21. Li Y, Wang Q, Liu XL, Hui R, Zhang YP. Effect of the physical rehabilitation program based on self-care ability in patients with acute ischemic stroke: a quasi-experimental study. *Front Neurol*. (2023) 14:1181651. doi: 10.3389/fneur.2023.1181651

22. Fugl-Meyer AR, Jääskö L, Leyman I, Olsson S, Steglind S. The post-stroke hemiplegic patient. 1. A method for evaluation of physical performance. *Scand J Rehabil Med*. (1975) 7:13–31. doi: 10.2340/1650197771331

23. Liebeskind DS, Jahan R, Nogueira RG, Zaidat OO, Saver JL. Impact of collaterals on successful revascularization in solitaire FR with the intention for thrombectomy. *Stroke*. (2014a) 45:2036–40. doi: 10.1161/strokeaha.114.004781

24. Liebeskind DS, Tomsick TA, Foster LD, Yeatts SD, Carrozzella J, Demchuk AM, et al. Collaterals at angiography and outcomes in the interventional Management of Stroke (IMS) III trial. *Stroke*. (2014b) 45:759–64. doi: 10.1161/strokeaha.113.004072

25. Nambiar V, Sohn SI, Almekhlafi MA, Chang HW, Mishra S, Qazi E, et al. CTA collateral status and response to recanalization in patients with acute ischemic stroke. *AJNR Am J Neuroradiol*. (2014) 35:884–90. doi: 10.3174/ajnr.A3817

26. Kharitonova TV, Melo TP, Andersen G, Egido JA, Castillo J, Wahlgren N. Importance of cerebral artery recanalization in patients with stroke with and without neurological improvement after intravenous thrombolysis. *Stroke*. (2013) 44:2513–8. doi: 10.1161/strokeaha.111.000048

27. Ribo M, Flores A, Rubiera M, Pagola J, Sargento-Freitas J, Rodriguez-Luna D, et al. Extending the time window for endovascular procedures according to collateral pial circulation. *Stroke*. (2011) 42:3465–9. doi: 10.1161/strokeaha.111.623827

28. Crisostomo RA, Garcia MM, Tong DC. Detection of diffusion-weighted MRI abnormalities in patients with transient ischemic attack: correlation with clinical characteristics. *Stroke*. (2003) 34:932–7. doi: 10.1161/01.Str.0000061496.00669.5e

29. Kidwell CS, Alger JR, Di Salle F, Starkman S, Villablanca P, Bentson J, et al. Diffusion MRI in patients with transient ischemic attacks. *Stroke*. (1999) 30:1174–80. doi: 10.1161/01.str.30.6.1174

30. Purroy F, Montaner J, Rovira A, Delgado P, Quintana M, Alvarez-Sabín J. Higher risk of further vascular events among transient ischemic attack patients with diffusion-weighted imaging acute ischemic lesions. *Stroke*. (2004) 35:2313–9. doi: 10.1161/01.Str.0000141703.21173.91

31. Wannamaker R, Buck B, Butcher K. Multimodal CT in acute stroke. *Curr Neurol Neurosci Rep*. (2019) 19:63. doi: 10.1007/s11910-019-0978-z

32. von Kummer R, Allen KL, Holle R, Bozzao L, Bastianello S, Manelfe C, et al. Acute stroke: usefulness of early CT findings before thrombolytic therapy. *Radiology*. (1997) 205:327–33. doi: 10.1148/radiology.205.2.9356611

33. Pomerantz SR, Harris GJ, Desai HJ, Lev MH. Computed tomography angiography and computed tomography perfusion in ischemic stroke: a step-by-step approach to image acquisition and three-dimensional postprocessing. *Semin Ultrasound CT MR*. (2006) 27:243–70. doi: 10.1053/j.sult.2006.03.001

34. Wintermark M, Rowley HA, Lev MH. Acute stroke triage to intravenous thrombolysis and other therapies with advanced CT or MR imaging: pro CT. *Radiology*. (2009) 251:619–26. doi: 10.1148/radiol.2513081073

35. Mendelson SJ, Prabhakaran S. Diagnosis and management of transient ischemic attack and acute ischemic stroke: a review. *JAMA*. (2021) 325:1088–98. doi: 10.1001/jama.2020.26867

36. Goyal M, Demchuk AM, Menon BK, Eesa M, Rempel JL, Thornton J, et al. Randomized assessment of rapid endovascular treatment of ischemic stroke. *N Engl J Med*. (2015) 372:1019–30. doi: 10.1056/NEJMoa1414905

37. Campbell BC, Purushotham A, Christensen S, Desmond PM, Nagakane Y, Parsons MW, et al. The infarct core is well represented by the acute diffusion lesion: sustained reversal is infrequent. *J Cereb Blood Flow Metab*. (2012) 32:50–6. doi: 10.1038/jcbfm.2011.102

38. Allmendinger AM, Tang ER, Lui YW, Spektor V. Imaging of stroke: part 1, perfusion ct??? Overview of imaging technique, interpretation pearls, and common pitfalls. *Am J Roentgenol*. (2012) 198:52–62. doi: 10.2214/AJR.10.7255

39. Cremers CH, Van Der Schaaf IC, Wensink E, Greving JP, Rinkel GJ, Velthuis BK, et al. CT perfusion and delayed cerebral ischemia in aneurysmal subarachnoid hemorrhage: a systematic review and meta-analysis. *J Cereb Blood Flow Metab*. (2014) 34:200–7. doi: 10.1038/jcbfm.2013.208

40. Xie Y, Jiang B, Gong E, Li Y, Zhu G, Michel P, et al. JOURNAL CLUB: use of gradient boosting machine learning to predict patient outcome in acute ischemic stroke on the basis of imaging, demographic, and clinical information. *AJR Am J Roentgenol*. (2019) 212:44–51. doi: 10.2214/ajr.18.20260

41. Wen X, Li Y, He X, Xu Y, Shu Z, Hu X, et al. Prediction of malignant acute middle cerebral artery infarction via computed tomography Radiomics. *Front Neurosci*. (2020) 14:708. doi: 10.3389/fnins.2020.00708

42. Cheng X, Shi J, Wu H, Dong Z, Liu J, Lu M, et al. Automated ASPECTS for multi-modality CT predict infarct extent and outcome in large-vessel occlusion stroke. *Eur J Radiol*. (2021) 143:109899. doi: 10.1016/j.ejrad.2021.109899

43. Potreck A, Weyland CS, Seker F, Neuberger U, Herweh C, Hoffmann A, et al. Accuracy and prognostic role of NCCT-ASPECTS depend on time from acute stroke symptom-onset for both human and machine-learning based evaluation. *Clin Neuroradiol*. (2022) 32:133–40. doi: 10.1007/s00062-021-01110-5

44. Muehlen I, Borutta M, Siedler G, Engelhorn T, Hock S, Knott M, et al. Prognostic accuracy of CTP summary maps in patients with large vessel occlusive stroke and poor revascularization after mechanical thrombectomy—comparison of three automated perfusion software applications. Tomography. (2022) 8:1350–62.

45. Xiang SF, Su Y, Li SY, Yang SJ, Wu YP. Application of computed tomography perfusion imaging-guided mechanical Thrombectomy in ischemic stroke patients with large vessel occlusion beyond the therapeutic time window. *Curr Med Imag*. (2023) 20. doi: 10.2174/1573405620666230608091800

46. Weng S, Sun X, Wang H, Song B, Zhu J. A new method for predicting the prognosis of ischemic stroke based vascular structure features and lesion location features. *Clin Imaging*. (2023) 98:1–7. doi: 10.1016/j.clinimag.2023.03.006

47. Zhang L, Wu J, Yu R, Xu R, Yang J, Fan Q, et al. Non-contrast CT radiomics and machine learning for outcomes prediction of patients with acute ischemic stroke receiving conventional treatment. *Eur J Radiol*. (2023) 165:110959. doi: 10.1016/j.ejrad.2023.110959

48. Brugnara G, Engel A, Jesser J, Ringleb PA, Purrucker J, Möhlenbruch MA, et al. Cortical atrophy on baseline computed tomography imaging predicts clinical outcome in patients undergoing endovascular treatment for acute ischemic stroke. *Eur Radiol*. (2023) 34:1358–66. doi: 10.1007/s00330-023-10107-2

49. Shen GC, Hang Y, Ma G, Lu SS, Wang C, Shi HB, et al. Prognostic value of multiphase CT angiography: estimated infarct core volume in the patients with acute ischaemic stroke after mechanical thrombectomy. *Clin Radiol*. (2023) 78:e815–22. doi: 10.1016/j.crad.2023.07.015

50. Hilbert A, Ramos LA, van Os HJA, Olabarriaga SD, Tolhuisen ML, Wermer MJH, et al. Data-efficient deep learning of radiological image data for outcome prediction after endovascular treatment of patients with acute ischemic stroke. *Comput Biol Med*. (2019) 115:103516. doi: 10.1016/j.compbiomed.2019.103516

51. Hokkinen L, Mäkelä T, Savolainen S, Kangasniemi M. Computed tomography angiography-based deep learning method for treatment selection and infarct volume prediction in anterior cerebral circulation large vessel occlusion. *Acta Radiol Open*. (2021a) 10:20584601211060347. doi: 10.1177/20584601211060347

52. Hokkinen L, Mäkelä T, Savolainen S, Kangasniemi M. Evaluation of a CTA-based convolutional neural network for infarct volume prediction in anterior cerebral circulation ischaemic stroke. *Eur Radiol Exp*. (2021b) 5:25. doi: 10.1186/s41747-021-00225-1

53. Hakim A, Christensen S, Winzeck S, Lansberg MG, Parsons MW, Lucas C, et al. Predicting infarct Core from computed tomography perfusion in acute ischemia with machine learning: lessons from the ISLES challenge. *Stroke*. (2021) 52:2328–37. doi: 10.1161/strokeaha.120.030696

54. Ramos LA, van Os H, Hilbert A, Olabarriaga SD, van der Lugt A, Roos Y, et al. Combination of radiological and clinical baseline data for outcome prediction of patients with an acute ischemic stroke. *Front Neurol*. (2022) 13:809343. doi: 10.3389/fneur.2022.809343

55. Winder AJ, Wilms M, Amador K, Flottmann F, Fiehler J, Forkert ND. Predicting the tissue outcome of acute ischemic stroke from acute 4D computed tomography perfusion imaging using temporal features and deep learning. *Front Neurosci*. (2022) 16:1009654. doi: 10.3389/fnins.2022.1009654

56. Jabal MS, Joly O, Kallmes D, Harston G, Rabinstein A, Huynh T, et al. Interpretable machine learning modeling for ischemic stroke outcome prediction. *Front Neurol*. (2022) 13:884693. doi: 10.3389/fneur.2022.884693

57. Winzeck S, Hakim A, McKinley R, Pinto J, Alves V, Silva C, et al. ISLES 2016 and 2017-benchmarking ischemic stroke lesion outcome prediction based on multispectral MRI. *Front Neurol*. (2018) 9:679. doi: 10.3389/fneur.2018.00679

58. Amador K, Wilms M, Winder A, Fiehler J, Forkert ND. Predicting treatment-specific lesion outcomes in acute ischemic stroke from 4D CT perfusion imaging using spatio-temporal convolutional neural networks. *Med Image Anal*. (2022) 82:102610. doi: 10.1016/j.media.2022.102610

59. Wouters A, Robben D, Christensen S, Marquering HA, Roos Y, van Oostenbrugge RJ, et al. Prediction of stroke infarct growth rates by baseline perfusion imaging. *Stroke*. (2022) 53:569–77. doi: 10.1161/strokeaha.121.034444

60. Hjort N, Christensen S, Sølling C, Ashkanian M, Wu O, Røhl L, et al. Ischemic injury detected by diffusion imaging 11 minutes after stroke. *Ann Neurol*. (2005) 58:462–5. doi: 10.1002/ana.20595

61. Chalela JA, Kidwell CS, Nentwich LM, Luby M, Butman JA, Demchuk AM, et al. Magnetic resonance imaging and computed tomography in emergency assessment of patients with suspected acute stroke: a prospective comparison. *Lancet*. (2007) 369:293–8. doi: 10.1016/s0140-6736(07)60151-2

62. Arsava EM. The role of MRI as a prognostic tool in ischemic stroke. *J Neurochem*. (2012) 123:22–8. doi: 10.1111/j.1471-4159.2012.07940.x

63. Debrey SM, Yu H, Lynch JK, Lövblad KO, Wright VL, Janket SJ, et al. Diagnostic accuracy of magnetic resonance angiography for internal carotid artery disease: a systematic review and meta-analysis. *Stroke*. (2008) 39:2237–48. doi: 10.1161/strokeaha.107.509877

64. Yu Y, Heit JJ, Zaharchuk G. Improving ischemic stroke care with MRI and deep learning artificial intelligence. *Top Magn Reson Imaging*. (2021) 30:187–95. doi: 10.1097/RMR.0000000000000290

65. Gottrup C, Thomsen K, Locht P, Wu O, Sorensen AG, Koroshetz WJ, et al. Applying instance-based techniques to prediction of final outcome in acute stroke. *Artif Intell Med*. (2005) 33:223–36. doi: 10.1016/j.artmed.2004.06.003

66. Kim BJ, Kim Y-H, Kim N, Kwon SU, Kim SJ, Kim JS, et al. Lesion location-based prediction of visual field improvement after cerebral infarction. *PLoS One*. (2015) 10:e0143882. doi: 10.1371/journal.pone.0143882

67. Grosser M, Gellißen S, Borchert P, Sedlacik J, Nawabi J, Fiehler J, et al. Localized prediction of tissue outcome in acute ischemic stroke patients using diffusion-and perfusion-weighted MRI datasets. *PLoS One*. (2020) 15:e0241917. doi: 10.1371/journal.pone.0241917

68. Hamann J, Herzog L, Wehrli C, Dobrocky T, Bink A, Piccirelli M, et al. Machine-learning-based outcome prediction in stroke patients with middle cerebral artery-M1 occlusions and early thrombectomy. *Eur J Neurol*. (2021) 28:1234–43. doi: 10.1111/ene.14651

69. van de Graaf RA, Samuels N, Chalos VA, Nijeholt GJL, van Beusekom H, Yoo AJ, et al. Predictors of poor outcome despite successful endovascular treatment for ischemic stroke: results from the MR CLEAN registry. *J Neuro Intervent Surg*. (2022) 14:660–5. doi: 10.1136/neurintsurg-2021-017726

70. Abedi V, Avula V, Razavi S-M, Bavishi S, Chaudhary D, Shahjouei S, et al. Predicting short and long-term mortality after acute ischemic stroke using EHR. *J Neurol Sci*. (2021) 427:117560. doi: 10.1016/j.jns.2021.117560

71. Elsaid AF, Fahmi RM, Shehta N, Ramadan BM. Machine learning approach for hemorrhagic transformation prediction: capturing predictors' interaction. *Front Neurol*. (2022) 13:951401. doi: 10.3389/fneur.2022.951401

72. Guo Y, Yang Y, Cao F, Wang M, Luo Y, Guo J, et al. A focus on the role of DSC-PWI dynamic radiomics features in diagnosis and outcome prediction of ischemic stroke. *J Clin Med*. (2022) 11:5364. doi: 10.3390/jcm11185364

73. Li Y, Liu Y, Hong Z, Wang Y, Lu X. Combining machine learning with radiomics features in predicting outcomes after mechanical thrombectomy in patients with acute

ischemic stroke. *Comput Methods Prog Biomed*. (2022) 225:107093. doi: 10.1016/j.cmpb.2022.107093

74. Luo Y, Sun X, Kong X, Tong X, Xi F, Mao Y, et al. A DWI-based radiomics-clinical machine learning model to preoperatively predict the futile recanalization after endovascular treatment of acute basilar artery occlusion patients. *Eur J Radiol*. (2023) 161:110731. doi: 10.1016/j.ejrad.2023.110731

75. Xu Y, Sun X, Liu Y, Huang Y, Liang M, Sun R, et al. Prediction of subjective cognitive decline after corpus callosum infarction by an interpretable machine learning-derived early warning strategy. *Front Neurol*. (2023) 14:1123607. doi: 10.3389/fneur.2023.1123607

76. Wang X, Lyu J, Meng Z, Wu X, Chen W, Wang G, et al. Small vessel disease burden predicts functional outcomes in patients with acute ischemic stroke using machine learning. *CNS Neurosci Ther*. (2023) 29:1024–33. doi: 10.1111/cns.14071

77. Yu H, Wang Z, Sun Y, Bo W, Duan K, Song C, et al. Prognosis of ischemic stroke predicted by machine learning based on multi-modal MRI radiomics. *Front Psychol*. (2023) 13:1105496. doi: 10.3389/fpsyt.2022.1105496

78. Lee J, Park KM, Park S. Interpretable machine learning for prediction of clinical outcomes in acute ischemic stroke. *Front Neurol*. (2023) 14:1234046. doi: 10.3389/fneur.2023.1234046

79. Nielsen A, Hansen MB, Tietze A, Mouridsen K. Prediction of tissue outcome and assessment of treatment effect in acute ischemic stroke using deep learning. *Stroke*. (2018) 49:1394–401. doi: 10.1161/STROKEAHA.117.019740

80. Pinto A, Mckinley R, Alves V, Wiest R, Silva CA, Reyes M. Stroke lesion outcome prediction based on MRI imaging combined with clinical information. *Front Neurol*. (2018) 9:1060. doi: 10.3389/fneur.2018.01060

81. Ho KC, Scalzo F, Sarma KV, Speier W, El-Saden S, Arnold C. Predicting ischemic stroke tissue fate using a deep convolutional neural network on source magnetic resonance perfusion images. *J Med Imag*. (2019) 6:026001. doi: 10.1117/1.JMI.6.2.026001

82. Yu Y, Xie Y, Thamm T, Gong E, Ouyang J, Huang C, et al. Use of deep learning to predict final ischemic stroke lesions from initial magnetic resonance imaging. *JAMA Netw Open*. (2020) 3:e200772. doi: 10.1001/jamanetworkopen.2020.0772

83. Debs N, Cho T-H, Rousseau D, Berthezène Y, Buisson M, Eker O, et al. Impact of the reperfusion status for predicting the final stroke infarct using deep learning. *NeuroImage Clin*. (2021) 29:102548. doi: 10.1016/j.nicl.2020.102548

84. Osama S, Zafar K, Sadiq MU. Predicting clinical outcome in acute ischemic stroke using parallel multi-parametric feature embedded Siamese network. *Diagnostics*. (2020) 10:858. doi: 10.3390/diagnostics10110858

85. Bo Y, Xie J, Zhou J, Li S, Zhang Y, Zhou Z. Magnetic resonance imaging features of cerebral infarction in critical patients based on convolutional neural network. *Contrast Media Mol Imag*. (2021) 2021:1–7. doi: 10.1155/2021/4095433

86. Ma C, Li H, Zhang K, Gao Y, Yang L. Risk factors of restroke in patients with lacunar cerebral infarction using magnetic resonance imaging image features under deep learning algorithm. *Contrast Media Mol Imag*. (2021) 2021:1–11. doi: 10.1155/2021/2527595

87. Tolhuisen ML, Hoving JW, Koopman MS, Kappelhof M, van Voorst H, Bruggeman AE, et al. Outcome prediction based on automatically extracted infarct core image features in patients with acute ischemic stroke. *Diagnostics*. (2022) 12:1786. doi: 10.3390/diagnostics12081786

88. Zeng Y, Long C, Zhao W, Liu J. Predicting the severity of neurological impairment caused by ischemic stroke using deep learning based on diffusion-weighted images. *J Clin Med*. (2022) 11:4008. doi: 10.3390/jcm11144008

89. Wong KK, Cummock JS, Li G, Ghosh R, Xu P, Volpi JJ, et al. Automatic segmentation in acute ischemic stroke: prognostic significance of topological stroke volumes on stroke outcome. *Stroke*. (2022) 53:2896–905. doi: 10.1161/STROKEAHA.121.037982

90. Nazari-Farsani S, Yu Y, Armindo RD, Lansberg M, Liebeskind DS, Albers G, et al. Predicting final ischemic stroke lesions from initial diffusion-weighted images using a deep neural network. *NeuroImage Clin*. (2023) 37:103278. doi: 10.1016/j.nicl.2022.103278

91. Moulton E, Valabregue R, Piotin M, Marnat G, Saleme S, Lapergue B, et al. Interpretable deep learning for the prognosis of long-term functional outcome post-stroke using acute diffusion weighted imaging. *J Cereb Blood Flow Metab*. (2023) 43:198–209. doi: 10.1177/0271678X221129230

92. Lv P, Yang J, Wang J, Guo Y, Tang Q, Magnier B, et al. Ischemic stroke prediction of patients with carotid atherosclerotic stenosis via multi-modality fused network. *Front Neurosci*. (2023) 17:1118376. doi: 10.3389/fnins.2023.1118376

93. Ye W, Chen X, Li P, Tao Y, Wang Z, Gao C, et al. OEDL: an optimized ensemble deep learning method for the prediction of acute ischemic stroke prognoses using union features. *Front Neurol*. (2023) 14:1158555. doi: 10.3389/fneur.2023.1158555

94. Baron J-C. Mapping the ischaemic penumbra with PET: implications for acute stroke treatment. *Cerebrovasc Dis*. (1999) 9:193–201. doi: 10.1159/000015955

95. Matsubara S, Moroi J, Suzuki A, Sasaki M, Nagata K, Kanno I, et al. Analysis of cerebral perfusion and metabolism assessed with positron emission tomography before and after carotid artery stenting. *J Neurosurg*. (2009) 111:28–36. doi: 10.3171/2008.09.17663

96. Zatcepin A, Kopczak A, Holzgreve A, Hein S, Schindler A, Duering M, et al. Machine learning-based approach reveals essential features for simplified TSPO PET quantification in ischemic stroke patients. *Z Med Phys*. (2023). doi: 10.1016/j.zemedi.2022.11.008

97. Ritt P. (2022). "Recent developments in SPECT/CT" in Seminars in Nuclear Medicine. Elsevier, 276–285.

98. Jaffer FA, Libby P, Weissleder R. Molecular and cellular imaging of atherosclerosis: emerging applications. *J Am Coll Cardiol*. (2006) 47:1328–38. doi: 10.1016/j.jacc.2006.01.029

99. Grotta JC, Alexandrov AV. tPA-associated reperfusion after acute stroke demonstrated by SPECT. *Stroke*. (1998) 29:429–32. doi: 10.1161/01.STR.29.2.429

100. Hodics T, Cohen LG, Cramer SC. Functional imaging of intervention effects in stroke motor rehabilitation. *Arch Phys Med Rehabil*. (2006) 87:36–42. doi: 10.1016/j.apmr.2006.09.005

101. Obayashi S. The supplementary motor area responsible for word retrieval decline after acute thalamic stroke revealed by coupled SPECT and near-infrared spectroscopy. *Brain Sci*. (2020) 10:247. doi: 10.3390/brainsci10040247

102. Choi JW, Kim MH, Park SA, Sin DS, Kim MS. Neural correlates of motor recovery measured by SPECT at six months after basal ganglia stroke. *Ann Rehabil Med*. (2017) 41:905–14. doi: 10.5535/arm.2017.41.6.905

103. Shin N-Y, Kim K-E, Park M, Kim YD, Kim DJ, Ahn SJ, et al. Dual-phase CT collateral score: a predictor of clinical outcome in patients with acute ischemic stroke. *PLoS One*. (2014) 9:e107379. doi: 10.1371/journal.pone.0107379

104. Wang Z, Chen W, Lin H, Luo S, Liu Y, Lin Y, et al. Early diagnosis and prediction of intracranial hemorrhage using dual-energy computed tomography after mechanical thrombectomy in patients with acute ischemic stroke. *Clin Neurol Neurosurg*. (2021) 203:106551. doi: 10.1016/j.clineuro.2021.106551

105. Borschmann K, Iuliano S, Ghasem-Zadeh A, Churilov L, Pang MYC, Bernhardt J. Upright activity and higher motor function may preserve bone mineral density within 6 months of stroke: a longitudinal study. *Arch Osteoporos*. (2018) 13:5. doi: 10.1007/s11657-017-0414-4

106. Lam FM, Pang MY. Correlation between tibial measurements using peripheral quantitative computed tomography and hip areal bone density measurements in ambulatory chronic stroke patients. *Brain Inj*. (2016) 30:199–207. doi: 10.3109/02699052.2015.1090625

frontiers | Frontiers in Neurology

TYPE Original Research
PUBLISHED 02 April 2024
DOI 10.3389/fneur.2024.1359292

Check for updates

OPEN ACCESS

EDITED BY
Shubham Misra,
Yale University, United States

REVIEWED BY
Lin Li,
The First Affiliated Hospital of Yangtze University, China
Sun Ha Jee,
Yonsei University, Republic of Korea

*CORRESPONDENCE
Jing Ji
✉ jjing@alu.zcmu.edu.cn

RECEIVED 03 January 2024
ACCEPTED 12 March 2024
PUBLISHED 02 April 2024

CITATION
Chen S, Chen Z, Xu Q, Jiang X, Lin C and Ji J (2024) Dual effects of serum urate on stroke risk and prognosis: insights from Mendelian randomization.
Front. Neurol. 15:1359292.
doi: 10.3389/fneur.2024.1359292

COPYRIGHT
© 2024 Chen, Chen, Xu, Jiang, Lin and Ji. This is an open-access article distributed under the terms of the Creative Commons Attribution License (CC BY). The use, distribution or reproduction in other forums is permitted, provided the original author(s) and the copyright owner(s) are credited and that the original publication in this journal is cited, in accordance with accepted academic practice. No use, distribution or reproduction is permitted which does not comply with these terms.

Dual effects of serum urate on stroke risk and prognosis: insights from Mendelian randomization

Shixuan Chen[1], Zhenzhen Chen[2], Qingqing Xu[1], Xia Jiang[1], Chuyong Lin[1] and Jing Ji[1]*

[1]Department of Rehabilitation Medicine, Wenzhou Hospital of Integrated Traditional Chinese and Western Medicine, Zhejiang Chinese Medical University, Wenzhou, China, [2]Department of Nursing, Wenzhou Hospital of Integrated Traditional Chinese and Western Medicine, Zhejiang Chinese Medical University, Wenzhou, China

Background: To investigate the causal associations of serum urate (SUA) with stroke risk and prognosis using Mendelian randomization (MR) and the potential mediating role of stroke risk factors in the causal pathways.

Methods: We used the random-effects inverse variance weighting (IVW) as our primary method. We initially performed two-sample univariable MR (UVMR) to identify the causal associations of SUA (n = 437,354) with any stroke (AS, FinnGen: n = 311,635; MEGASTROKE: n = 446,696), ischemic stroke (IS, FinnGen: n = 212,774; MEGASTROKE: n = 440,328), intracranial hemorrhage (ICH, FinnGen: n = 343,663; ISGC: n = 3,026), functional outcome after ischemic stroke at 90d (n = 4,363), and motor recovery within 24 months after stroke (n = 488), and then multivariable MR (MVMR) to estimate the direct causal effects of SUA on these outcomes, adjusting for potential confounders. Finally, we further conducted a two-step MR to investigate the potential mediating role of body mass index (BMI), systolic blood pressure (SBP), diastolic blood pressure (DBP), and estimated glomerular filtration rate (eGFR) in the identified causal pathways.

Results: Genetically predicted elevated SUA levels were significantly associated with increased risk of AS (meta-analysis: OR = 1.09, 95% CI [1.04–1.13], p = 3.69e-05) and IS (meta-analysis: OR = 1.10, 95% CI [1.01–1.19], p = 0.021) and with improved poor functional outcome after ischemic stroke at 90d (OR = 0.81, 95% CI [0.72–0.90], p = 1.79e-04) and motor recovery within 24 months after stroke (OR = 1.42, 95% CI [1.23–1.64], p = 2.15e-06). In MVMR, SBP and DBP significantly attenuated the causal effects of SUA on AS, IS, and functional outcome after ischemic stroke at 90d and motor recovery within 24 months after stroke. Further mediation analyses showed that SBP mediated 52.4 and 34.5% of the effects of SUA on AS and IS, while DBP mediated 28.5 and 23.4% of the causal effects, respectively.

Conclusion: This study supports the dual role of genetically predicted SUA in increasing stroke risk, especially ischemic stroke risk, and in improving functional outcome and motor recovery. SBP and DBP are key mediators lying on the causal pathways of SUA with AS and IS.

KEYWORDS

uric acid, stroke, blood pressure, genetic instrumental variables, Mendelian randomization

1 Introduction

Stroke is the major cause of mortality and disability worldwide, imposing a substantial challenge to human health. Despite considerable efforts dedicated to stroke prevention and treatment, its prevalence and disability rates remain high, signaling ongoing gaps in understanding and management strategies for stroke. Serum urate (SUA), the final output of purine metabolism, possesses pro-oxidant and antioxidant dual properties and may exert complex biological effects in our body. Observational studies showed that high SUA levels may indirectly contribute to stroke by inducing inflammatory responses, promoting oxidative stress, and triggering endothelial dysfunction (1–3). Additionally, SUA is also implicated in increasing thrombosis risk, which may impact the occurrence of cardiovascular disease (4). However, some studies have argued that the link between SUA and stroke is still a "pseudo-association" as hyperuricemia is closely associated with other stroke risk factors such as hypertension and obesity; thus, whether or not SUA affects stroke is controversial (5, 6). Furthermore, interventions aimed at reducing SUA did not prevent the onset and progression of cardiovascular disease, which further raises doubts about a direct link between SUA and stroke (7). On the other hand, there are conflicting findings regarding the influence of SUA on stroke prognosis (8–10). Therefore, it is necessary to conduct a more in-depth investigation into the causal association of SUA with stroke risk and prognosis as well as to unravel their precise mechanisms.

Conventional epidemiologic studies are susceptible to unaccounted confounders, excessive adjustment for mediators, or reverse causality, potentially leading to bias in the established causal associations. Mendelian randomization (MR) is an emerging approach for causal inference assessment that cleverly exploits the random distribution of genetic variants as instrumental variables (IVs) at conception to simulate the "random assignment" of participants in randomized controlled trials (RCTs) and aims to identify the differential risk of disease between genetic variant carriers and non-carriers (11). Due to genetic variation being inherited at birth and remaining stable throughout our lifespan, associations obtained from MR are less susceptible to causal inversions and unaccounted confounders compared to traditional observational studies. This study employed a two-sample MR to identify causal associations of SUA with stroke, post-stroke functional outcome, and motor recovery. Additionally, we further performed a two-step MR to explore the potential mediating roles of mediators in the identified causal pathways, which may contribute to enhancing our understanding of the mechanisms linking SUA to stroke risk and prognosis.

2 Methods

2.1 Study design

The workflow is visually presented in Figure 1. We initially performed a two-sample univariable MR (UVMR) to identify potential causal associations of SUA levels with stroke, post-stroke functional outcome, and motor recovery. A multivariable MR (MVMR) was then utilized to estimate the direct causal effects of SUA on these outcomes, adjusting for potential confounders. Moreover, we conducted a two-step MR to investigate the potential mediating role of body mass index (BMI), systolic blood pressure (SBP), diastolic blood pressure (DBP), and estimated glomerular filtration rate (eGFR) in the identified causal pathway. This MR study is based on publicly available published GWAS summary statistics, and all necessary ethical approval and informed consent were obtained for the original study.

2.2 Genetic instrument selection

SUA was included as exposure in this study, with its genome-wide association study (GWAS) dataset obtained from Barton AR et al.'s further analysis of the UK Biobank data involving 437,354 individuals of European ancestry (12). The SUA levels were measured by uricase PAP analysis, and the processed data were expressed as per standard deviation (1-SD = 80.3 μmol/L) of increase. We selected significant ($p < 5 \times 10^{-8}$) and independent ($r^2 < 0.001$ and a distance window of 10,000 kb) single nucleotide polymorphisms (SNPs) as genetic IVs for SUA. Subsequently, SNPs in palindromes and those that were closely linked to outcome ($p < 5 \times 10^{-5}$) were excluded. We further filtered out the SNPs with the MR Steiger test, which primarily affected the outcomes, rather than the exposures. Moreover, we calculated F-statistics to evaluate the potential bias caused by weak instruments using the following formula: $F = (N - k - 1)/k \times R^2 \diagup (1 - R^2)$, where N, k, and R^2 are sample size, number of IVs, and variance explained by all IVs, respectively (13). $R^2 = 2 \times EAF \times (1 - EAF) \times beta^2$, where EAF are effect allele frequency and *beta* are exposure effect. Any IV with an *F*-value below 10 suggests weakness and was excluded (13). Proxy SNPs were not available for our analysis. All genetic IVs used to proxy for SUA are listed in Supplementary Table S2.

2.3 Outcome data sources

Our outcomes included any stroke (AS), ischemic stroke (IS), intracranial hemorrhage (ICH), post-stroke functional outcome, and motor recovery. GWAS data for AS (39,818 cases, 271,817 controls), IS (10,551 cases, 202,223 controls), and ICH (3,749 cases, 339,914 controls) were obtained from the FinnGen Consortium (14). AS included any stroke, mainly IS, transient ischemic attack (TIA), hemorrhagic stroke, and subarachnoid hemorrhage. IS referred to any ischemic stroke excluding all hemorrhages, and ICH specifically denoted all cases of hemorrhage excluding IS and TIA. These diseases were principally defined based on ICD diagnosis codes at the time of discharge or death. We additionally obtained GWAS for AS (40,585 cases and 406,111 controls) and IS (34,217 cases and 406,111 controls) from the MEGASTROKE consortium, and ICH (1,545 cases and 1,481 controls) from the ISGC consortium (15, 16). GWAS summary data for functional outcome after ischemic stroke at 90d were derived from the Genetics of Ischemic Stroke Functional Outcome (GISCOME) network, which included 4,363 individuals of European ancestry (17). Functional outcome was assessed using the modified Rankin Scale (mRS) approximately 90 days after the stroke. The mRS score of 0–1 is defined as a good functional outcome (1,796 cases) and scores of 2–6 are considered poor functional outcomes (2,567 cases). Functional outcomes, adjusted for age, sex, ancestry, and baseline stroke severity as assessed by the National Institutes of Health Stroke Scale (NIHSS), were used for discovery analyses, while those unadjusted for baseline NIHSS were utilized for validation analyses. GWAS data for post-stroke motor recovery were obtained from further analysis of the Vitamin Intervention for Stroke Prevention

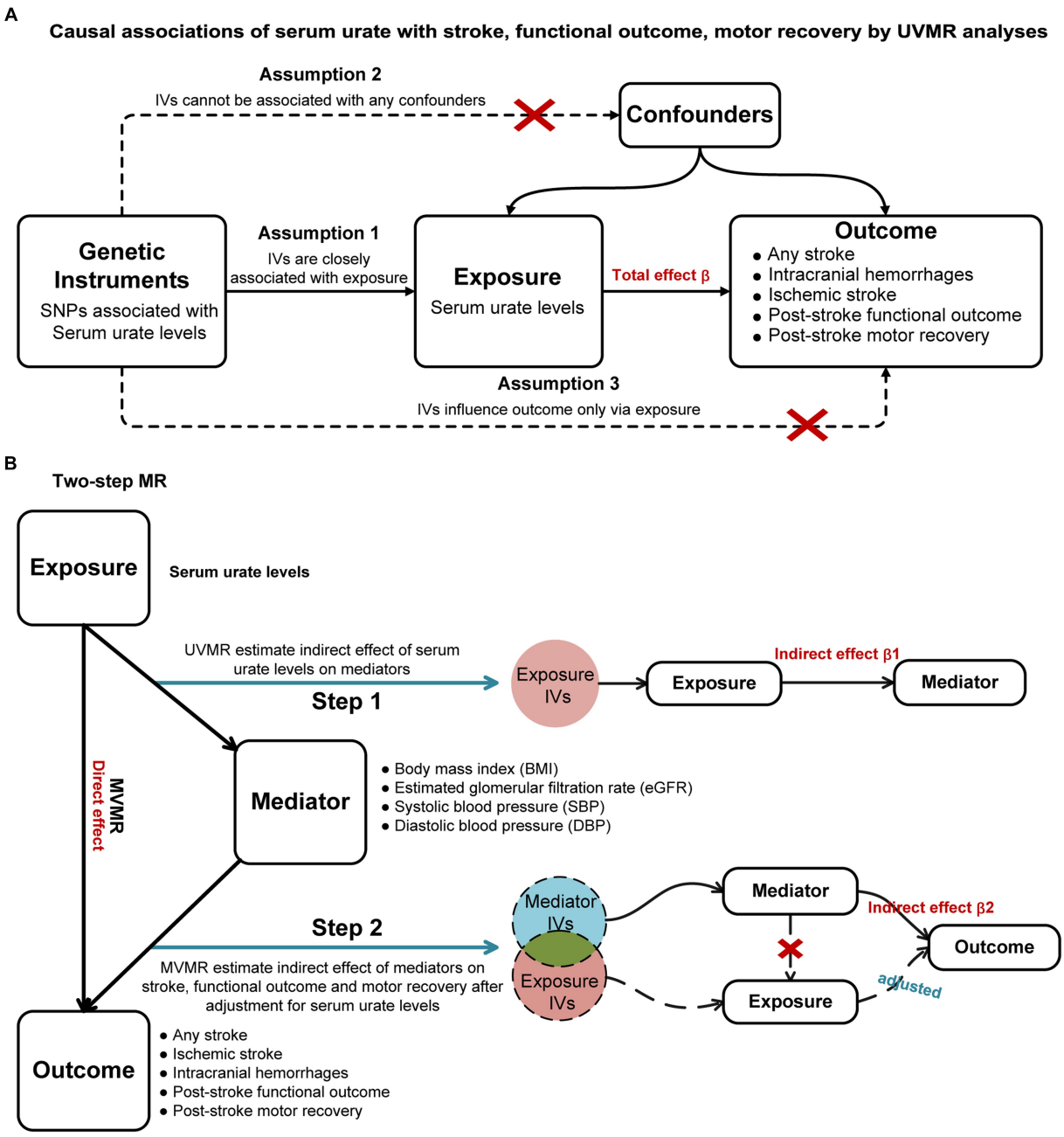

FIGURE 1
Study workflow overview. **(A)**: Causal associations of serum urate with stroke, functional outcome, motor recovery by UVMR analyses; **(B)**: Two-step MR. UVMR, univariable Mendelian randomization; MVMR, multivariable Mendelian randomization; IVs, instrumental variables.

(VISP) dataset by Aldridge CM et al., including 488 European individuals (18). This study applied the NIHSS subscores 5A/5B and 6A/6B to assess motor drift scores of limb motor weakness at six time points over 24 months. A drift score decrease of ≥1 vs. < 1 at each time point was taken as the study outcome. Detailed information on outcomes is presented in Supplementary Table S1.

2.4 Statistical analysis

We initially performed UVMR analyses, and the multiplicative random-effects inverse variance weighting (IVW) was adopted as our primary method to identify the causal associations of SUA on stroke, post-stroke functional outcome, and motor recovery, respectively. In the assumption that all IVs were valid, the IVW could provide the most robust estimate for MR (19). Complementary analyses to examine the consistency of the results included MR-Egger, weighted median, and MR pleiotropy residual sum and outlier (MR-PRESSO). MR-Egger regression incorporated an intercept term, which still yielded a reliable causal estimate even if all the IVs were invalid. Additionally, the weighted median method could provide a consistent estimate when the assumption of over 50% IVs validity was fulfilled. Cochran's Q statistical tests were utilized to detect heterogeneity in estimates among SNPs, while the

intercept derived from MR-Egger assessed horizontal pleiotropy. A significance level of $p < 0.050$ indicated the presence of heterogeneity or horizontal pleiotropy. Moreover, we performed the MR-PRESSO test to detect and correct horizontal pleiotropy outliers by removing them. To control for false-positive results due to multiple testing, the p-value for Bonferroni-corrected IVW was set at $p < 0.006$ (0.050/9 outcomes). The nominally significant p-value was defined as $0.006 \leq p < 0.050$, indicating suggestive evidence for potential causality. We further utilized the online tool[1] to estimate the statistical power for various outcomes. A higher power value indicates a greater certainty in detecting significant effects.

For significant causality in UVMR, we applied the random-effects IVW model within the MVMR analysis. This approach adjusted for potential confounders such as BMI, eGFR, SBP, and DBP, enabling us to estimate a direct causal effect. To further ensure the reliability of our findings, we conducted sensitivity analyses using MR-Egger and weighted median methods. These analyses were particularly important due to the close metabolic relationship between hyperuricemia, BMI, and eGFR, as well as the fact that elevated SUA levels independently contribute to high blood pressure, a significant risk factor for cardiovascular disease. To explore the potential effects of mediators in this causal pathway, we further performed a two-step MR analysis. In step 1, UVMR was performed to estimate the indirect effects of SUA on the mediators (β1), and in step 2, we conducted MVMR to estimate the indirect effects of mediators on stroke, post-stroke functional outcome, and motor recovery after adjusting for SUA (β2). Finally, we estimated the significance of mediating effects (β1*β2) using the delta method, and then, their proportion in the total effect was calculated as proportion% = (β1*β2)/β*100%, where β was the total causal effect of SUA on stroke, post-stroke functional outcome, or motor recovery.

All analyses were conducted by using the "TwoSampleMR (version 0.5.6)," "MR-PRESSO (version 1.0)," "MVMR," and "MendelianRandomization (version 0.8.0)" packages in R (version 4.3.1; The R Foundation for Statistical Computing).

3 Results

3.1 Univariable MR analysis

We performed UVMR to identify the causal associations between genetically predicted SUA and stroke, functional outcome after ischemic stroke at 90d, and motor recovery within 24 months after stroke, as well as to estimate their total causal effects. As shown in Figure 2 and Supplementary Table S3, the primary random-effects IVW in the UVMR analysis showed credible evidence that genetically predicted higher SUA levels were associated with increased risk of AS and IS, the results from the FinnGen and MEGASTROKE consortiums were highly consistent, and further meta-analysis of their IVW results indicated that each 1-SD increase in genetically predicted SUA was associated with a 9% higher risk of developing AS (OR = 1.09, 95% CI = 1.04–1.13, $p = 3.69e\text{-}05$; $I^2 = 25\%$, $p_{heterogeneity} = 0.250$) and IS (OR = 1.10, 95% CI = 1.01–1.19, $p = 0.021$; $I^2 = 56\%$, $p_{heterogeneity} = 0.130$). However, no significant causal association between SUA and ICH was shown in the FinnGen and ISGC consortiums, nor their meta-analysis (OR = 0.99, 95% CI = 0.90–1.10, $p = 0.910$; $I^2 = 0\%$, $p_{heterogeneity} = 0.700$). Significantly, we found that higher SUA levels were negatively linked to poor functional outcome after ischemic stroke at 90d, with each 1-SD increase in genetically predicted SUA levels being linked to a 19% lower risk of poor functional outcome (OR = 0.81, 95% CI = 0.72–0.90, $p = 1.79e\text{-}04$), and this result was consistent with the unadjusted NIHSS data (OR = 0.82, 95% CI = 0.73–0.91, $p = 1.72e\text{-}04$). Additionally, our results also indicated a positive correlation between higher SUA levels and motor recovery within 24 months after stroke, with each 1-SD increase in genetically predicted SUA levels associated with a 42% improvement in motor recovery (OR = 1.42, 95% CI = 1.23–1.64, $p = 2.15e\text{-}06$).

Sensitivity analysis methods, including MR-Egger, weighted median, and MR-PRESSO, were conducted to assess the robustness of the results. Although some of the sensitivity analysis methods did not yield significance estimates consistent with IVW, particularly MR-Egger, we noted the direction of causal estimates for the majority of them that were consistent with IVW (Figure 2 and Supplementary Table S3). Notably, no evidence of horizontal pleiotropy was found in any of the MR-Egger intercept tests, all of which were above 0.05 (Figure 2 and Table 1). In addition, we further performed MR-PRESSO analysis and found some outliers (Supplementary Table S3). Following excluding these outliers, UVMR analyses were repeated to obtain the final estimates. Finally, we performed reverse UVMR analyses, wherein no evidence of bidirectional causal associations of SUA levels with AS, IS, ICH, poststroke functional outcomes, or motor recovery were detected (Supplementary Table S4).

3.2 Multivariable MR analysis

After adjusting for BMI and eGFR using MVMR, the causal effect of SUA on AS and IS remained significant, but the estimates were attenuated or no longer significant after adjusting for SBP and DBP. Furthermore, after adjusting for BMI, eGFR, SBP, and DBP, the causal effect of SUA on functional outcome and motor recovery was no longer significant (Figure 3 and Supplementary Table S5).

3.3 Mediation analysis

Two-step MR was utilized to conduct mediation analyses aimed at investigating whether the identified causal effect of SUA on stroke (FinnGen data), post-stroke functional outcomes (adjusted for NIHSS), and motor recovery could be mediated by SBP, DBP, BMI, or eGFR. Of note, our study revealed that SBP and DBP exerted proportionally mediating effects on the causal associations of SUA with AS and IS. Specifically, SBP was found to mediate 52.4% (95% CI: 45.8–74.4%, $p = 1.67e\text{-}08$) and 34.5% (95% CI: 32.0–46.4%, $p = 1.45e\text{-}04$) of the causal effects of SUA on AS and IS, respectively, while DBP mediated 28.5% (95%CI: 27.3–32.4%, $p = 3.80e\text{-}05$) and 23.4% (95%CI: 22.5–23.6%, $p = 0.003$) of the causal effects on AS and IS, respectively (Figure 4 and Supplementary Table S6).

4 Discussion

To investigate the causal associations and mechanisms of SUA on stroke, post-stroke functional outcome, and motor recovery, we performed this MR study utilizing large-scale, publicly available

1 https://sb452.shinyapps.io/power

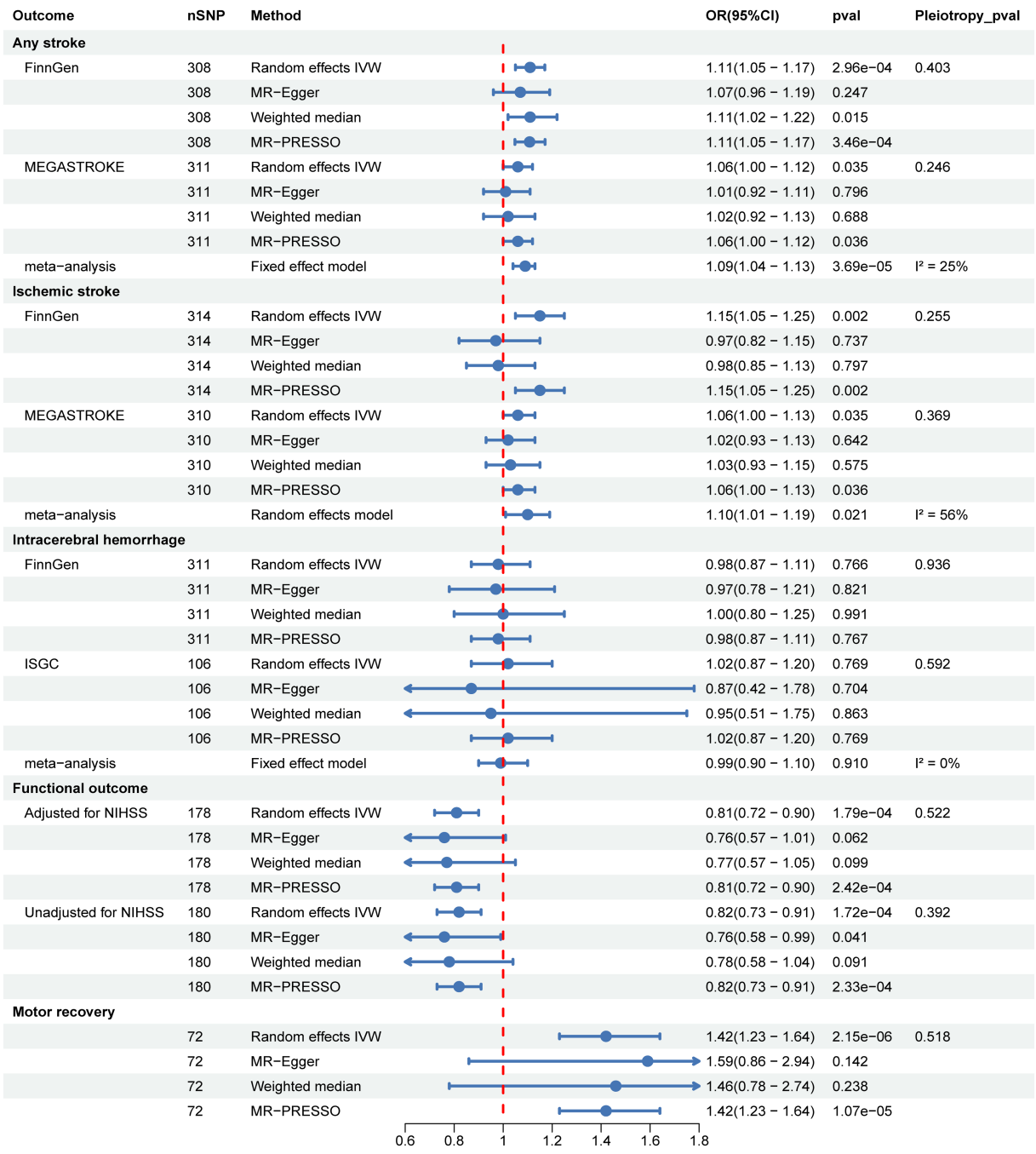

FIGURE 2
Two-sample univariable MR to identify the causal associations of SUA with stroke, post-stroke functional outcome, and motor recovery.

GWAS summary data. Four critical findings emerged from our analysis: (1) Genetically predicted elevated SUA levels were significantly causally associated with an increased risk of AS and IS, and these associations remained significant even after adjusting for BMI and eGFR. (2) SBP and DBP were identified as critical mediators in the causal pathways linking SUA to AS and IS. (3) Elevated SUA levels were found to lower poor functional outcomes after 90d of ischemic stroke and also contributed to motor recovery within 24 months after stroke. (4) There was no evidence of a significant causal association between SUA and ICH. Additionally, sensitivity analyses suggested consistent estimates and effect directions for almost all outcomes, and no horizontal pleiotropy was found.

Previous observational studies have explored the link between SUA and stroke but yielded conflicting conclusions (6, 20, 21). Epidemiologic studies often struggle to fully exclude confounders and address reverse causality, which may be key drivers of inconsistent conclusions. MR using genetic variants as IVs to proxy for different phenotypes contributes to maximizing control for confounders and avoids reverse causality interference, thus providing more reliable causal inferences. A recent MR study suggested that higher SUA levels would increase AS risk, with each 1-SD (80.3 μmol/L) increase in genetically predicted SUA levels being associated with an 11% increase in the risk of developing AS (22). Our MR analyses using GWAS data from different sources yielded similar results. The subsequent

TABLE 1 Heterogeneity and horizontal pleiotropy in the causal associations of SUA with stroke, post-stroke functional outcome, and motor recovery as detected using IVW and MR-Egger.

Outcome	nSNP	Heterogeneity (IVW)		Pleiotropy (MR-Egger)		R^2 sums	*F*-statistic mean	Power (%)
		Cochran's Q	*p*-value	Intercept	*p*-value			
Finngen_AS	308	432.378	3.01E-06	0.001	0.403	0.063	89.323	99.8
MEGASTROKE_AS	311	364.981	0.017	0.001	0.246	0.072	101.626	83.5
Finngen_IS	314	351.563	0.066	0.005	0.255	0.065	89.940	95.6
MEGASTROKE_IS	310	357.255	0.030	0.001	0.369	0.072	101.838	83.5
Finngen_ICH	311	289.661	0.791	0.000	0.936	0.073	102.223	4.8
ISGC_ICH	106	17.331	1.000	0.006	0.592	0.032	131.441	3.3
Functional outcome adjusted NIHSS	178	45.992	1.000	0.004	0.522	0.105	263.976	62.0
Functional outcome unadjusted NIHSS	180	49.019	1.000	0.005	0.392	0.105	262.607	56.5
Motor recovery	72	5.836	1.000	−0.012	0.518	0.087	541.893	20.4

SUA, serum urate; Finngen_AS, Finngen for any stroke; MEGASTROKE_AS, MEGASTROKE for any stroke; Finngen_IS, Finngen for ischemic stroke; MEGASTROKE _IS, MEGASTROKE for ischemic stroke; Finngen_ICH, Finngen for intracranial hemorrhage; ISGC_ICH, ISGC for intracranial hemorrhage; NIHSS, National Institute of Health Stroke Scale.

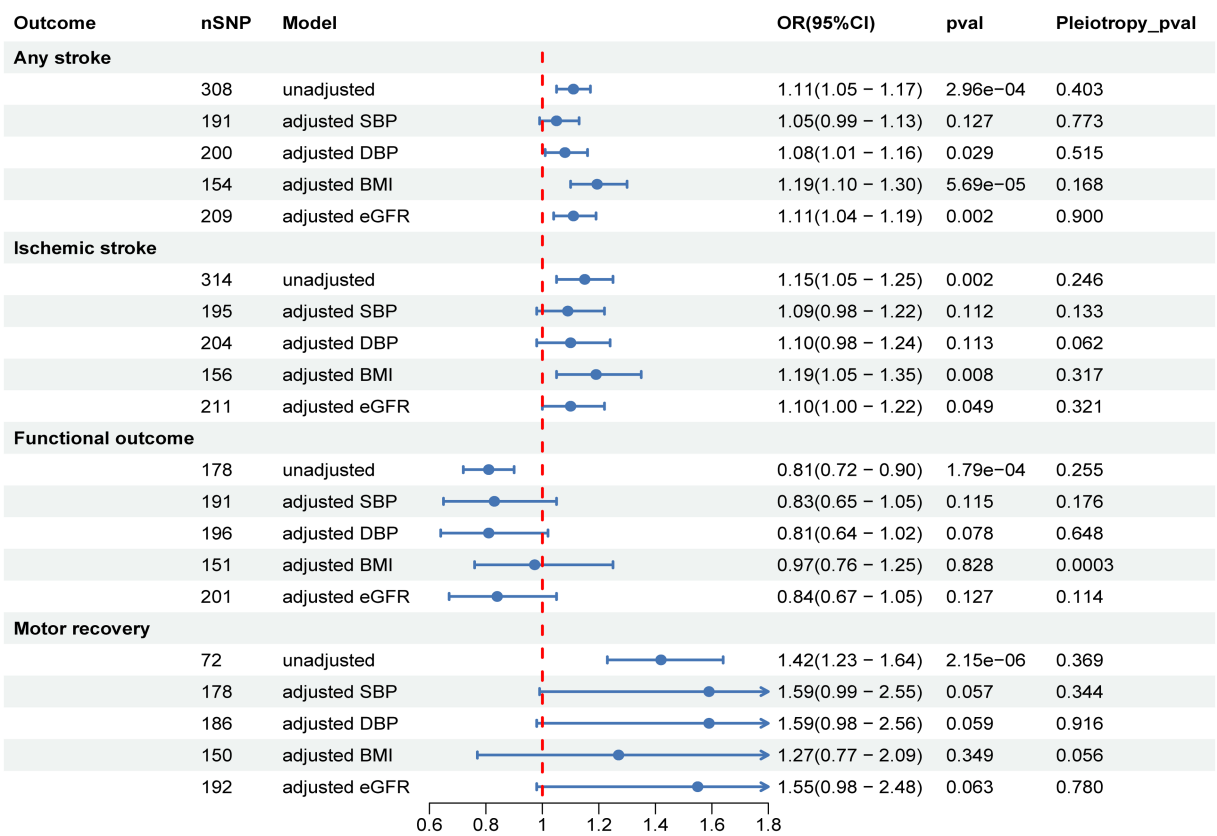

FIGURE 3
Multivariable MR to analyze the causal effects of SUA on stroke, post-stroke functional outcome, and motor recovery after adjusting for confounders and to estimate their direct effects. SBP, systolic blood pressure; DBP, diastolic blood pressure; BMI, body mass index; eGFR, estimated glomerular filtration rate.

meta-analysis of the IVW estimates derived from these analyses obtained a more significant OR estimate and a narrower 95% confidence interval. IS is the primary subtype of AS, and evidence from two previous MR studies involving SUA and IS did not support a causal association among them (23, 24). These were contradictory to our findings. Given that our MR extracted more eligible IVs (310–314 vs. 28 SNPs) and employed GWAS summary data only from European ancestry, this enhances the reliability of our findings. Additionally, the study further indicated that there was no causal association between SUA and ICH. Therefore, a previous observational

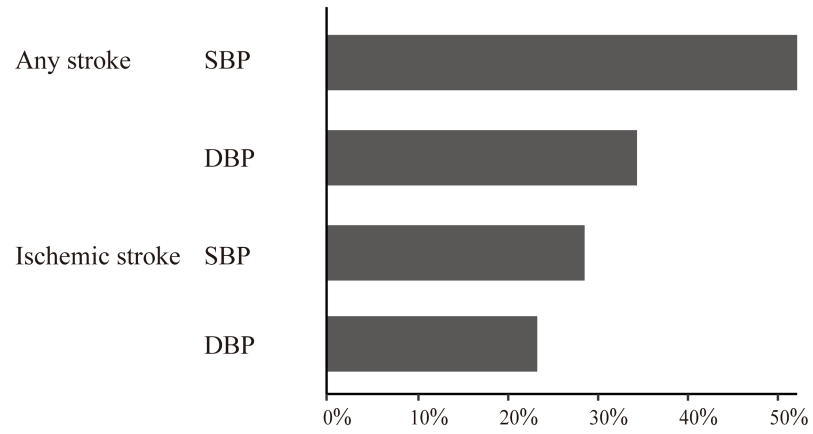

FIGURE 4
Two-step MR estimates of causal effect proportions mediated by SBP and DBP in SUA on any stroke and ischemic stroke pathways.

study reported that a positive relationship of stable high SUA with ICH risk but not with IS may have been coincidental (21).

Currently, there is a lack of consensus on the exact role of SUA in stroke prognosis (25, 26). In a recent MR study, SUA was not found to be causally associated with poor functional prognosis (mRS > 2) at 90d after ischemic stroke (27). However, our MR analysis, using GWAS data defining mRS > 1 as poor functional outcome, identified a significant and negative causal association between SUA and poor functional prognosis in ischemic stroke patients at 90d. Prior meta-analysis suggested a non-linear (U-shaped) association between SUA and the risk of poor functional outcomes after ischemic stroke (28). This complex relationship between SUA and post-stroke functional prognosis may be the key factor contributing to this contradictory result. Additionally, our MR analyses found a positive causal association between SUA and motor recovery within 24 months after stroke. This is consistent with previous findings that SUA exerted antioxidant properties and potential neuroprotective effects (29). However, further studies are still required to fully grasp the complexity and potential non-linear relationship between SUA and post-stroke prognosis.

Through this study, we have found that SUA has dual effects, with elevated SUA being a risk factor for AS and IS, while also exerting a protective effect on post-stroke functional outcome and motor recovery. However, the exact mechanism between them remains ambiguous. Numerous studies suggest that hyperuricemia plays an important role in the etiology of hypertension, which is the leading risk factor for stroke (30, 31). Our further mediation analyses identified SBP and DBP as key mediators lying on the SUA to AS and IS are causal pathways, which is consistent with the result previously reported by Chaudhary NS et al. (31). Additionally, blood pressure is the primary driver of maintaining cerebral perfusion. Sustaining appropriate blood pressure in the early stages of ischemic stroke is beneficial for cerebral perfusion and aids in neurological function recovery. These factors, in turn, positively influence stroke prognosis (32). Of note, although we failed to detect the mediating effect of blood pressure in the pathway of SUA on stroke prognosis, the influence of SUA on post-stroke functional outcome and motor recovery became non-significant after adjusting for SBP and DBP using MVMR. This evidence provided insights into the role of SUA in the pathogenesis and rehabilitation of stroke and may benefit future research and clinical practice.

Overweight is also a well-known risk factor for stroke. Our analyses revealed that BMI did not act as a mediator or attenuate the impact of SUA on AS and IS, suggesting that SUA increases the stroke risk and may be independent of BMI. It is important to note that being overweight is not always detrimental. Some studies have suggested that being overweight indicated the presence of more nutritional reserves, which could potentially help counteract post-stroke hypermetabolic depletion, thus translating into a protective factor against poor functional outcomes (33, 34). This might be a potential explanation for our finding that the causal effect of SUA on post-stroke functional outcome and motor recovery became non-significant after adjusting for BMI. Additionally, impaired kidney function is an independent risk factor for stroke and is linked to more severe stroke and worse outcomes (35). In our analysis, we also found that eGFR attenuated the causal effect and significance of SUA on IS. Although further mediation analysis failed to yield a significant mediating effect, it still implied that the improvement of post-stroke functional outcome and the promotion of motor recovery by SUA may rely on favorable renal function.

Our study holds several strengths as follows. First, the study employed MR to investigate the causal association between SUA and stroke risk and prognosis, which minimized bias from confounders and reverse causality, thus providing credible causal inferences. Second, our efforts identified the dual effects of SUA on stroke risk and prognosis, and a series of replication analyses, GWAS meta-analyses, and sensitivity analyses observed similar results, ensuring the robustness of the findings. Finally, potential mechanisms of stroke risk factors in causal pathways were explored by MVMR and mediation analyses, and this insight may guide the development of targeted intervention and prevention strategies.

The study also has some limitations. First, the potential pleiotropy is an inherent limitation of MR analysis. Despite performing strict selection criteria for genetic IVs and examining for outliers and horizontal pleiotropy, pleiotropy may still be present and could

introduce bias into our results. Second, it is necessary to point out the genetic variation differences that exist among different races, which may introduce heterogeneity into the causal estimates. Although the incidence of stroke is also high in the Asian region (36–38), considering that our study mainly involves participants of European descent, this may limit the generalization of our findings to other races and populations. Third, in this study, we noted a 43.6% sample overlap in SUA and eGFR GWAS datasets, potentially impacting the accuracy of MVMR and mediation analysis. Due to the absence of independent GWAS datasets excluding UK Biobank, we evaluated the robustness of our findings by estimating potential bias and type I error rate. The finding indicates that a 43.6% overlap might cause a bias ranging from 0.007 to 0.008 and increase type I error rates between 0.19 and 0.27. Although the bias suggests a somewhat reliable result, the elevated type I error rates, substantially above the 5% standard threshold, indicate a heightened risk of false positives. Future studies with non-overlapping samples are required to corroborate and reinforce our conclusions. Finally, limited by the GWAS data, we were unable to stratify SUA levels or explore trend relationships between SUA and stroke risk and prognosis. In future studies, a more comprehensive collection of SUA data and more in-depth analysis will contribute to further insight into the potentially complex associations between them.

In conclusion, our MR study supports a dual role for genetically predicted SUA in increasing the risk of stroke, especially ischemic stroke, and in improving post-stroke poor functional outcome and motor recovery. Moreover, we provide credible genetic evidence that SBP and DBP mediate considerable proportions of the causal effects of SUA on AS and IS. These findings contribute to a deeper understanding of the underlying mechanisms that link SUA to stroke risk and prognosis.

Data availability statement

The original contributions presented in the study are included in the article/Supplementary material, further inquiries can be directed to the corresponding author.

Ethics statement

Ethical review and approval was not required for the study on human participants in accordance with the local legislation and institutional requirements. Written informed consent for participation was not required for this study in accordance with the national legislation and the institutional requirements.

Author contributions

SC: Conceptualization, Funding acquisition, Methodology, Writing – original draft. ZC: Data curation, Visualization, Writing – original draft. QX: Data curation, Writing – original draft. XJ: Formal analysis, Validation, Writing – original draft. CL: Formal analysis, Writing – original draft. JJ: Conceptualization, Funding acquisition, Methodology, Writing – original draft.

Funding

The author(s) declare that no financial support was received for the research, authorship, and/or publication of this article.

Acknowledgments

The authors thank FinnGen, MEGASTROKE, ISGC, GISCOME, ICBP, GIANT, CKDGen, and UK Biobank consortium and Aldridge CM et al., Barton AR et al., Mbatchou J et al., and Stanzick KJ et al. for making publicly available GWAS summary statistics for SUA, AS, IS, ICH, functional outcome after ischemic stroke, motor recovery, SBP, DBP, BMI, and eGFR involved in the study.

Conflict of interest

The authors declare that the research was conducted in the absence of any commercial or financial relationships that could be construed as a potential conflict of interest.

Publisher's note

All claims expressed in this article are solely those of the authors and do not necessarily represent those of their affiliated organizations, or those of the publisher, the editors and the reviewers. Any product that may be evaluated in this article, or claim that may be made by its manufacturer, is not guaranteed or endorsed by the publisher.

Supplementary material

The Supplementary material for this article can be found online at: https://www.frontiersin.org/articles/10.3389/fneur.2024.1359292/full#supplementary-material

References

1. Zhu HY, Zhao SZ, Zhang ML, Wang Y, Pan ZM, Cheng HR, et al. Elevated serum uric acid increases the risk of ischemic stroke recurrence and its inflammatory mechanism in older adults. *Front Aging Neurosci*. (2022) 14:822350. doi: 10.3389/fnagi.2022.822350

2. Wu SS, Kor CT, Chen TY, Liu KH, Shih KL, Su WW, et al. Relationships between serum uric acid, malondialdehyde levels, and carotid intima-media thickness in the patients with metabolic syndrome. *Oxidative Med Cell Longev*. (2019) 2019:6859757–9. doi: 10.1155/2019/6859757

3. Bo S, Gambino R, Durazzo M, Ghione F, Musso G, Gentile L, et al. Associations between serum uric acid and adipokines, markers of inflammation, and endothelial dysfunction. *J Endocrinol Investig*. (2008) 31:499–504. doi: 10.1007/BF03346397

4. Kubota Y, McAdams-DeMarco M, Folsom AR. Serum uric acid, gout, and venous thromboembolism: the atherosclerosis risk in communities study. *Thromb Res*. (2016) 144:144–8. doi: 10.1016/j.thromres.2016.06.020

5. Kuwabara M. Hyperuricemia, cardiovascular disease, and hypertension. *Pulse (Basel)*. (2016) 3:242–52. doi: 10.1159/000443769

6. Shi X, Yang J, Wang L, Zhao M, Zhang C, He M, et al. Prospective study of serum uric acid levels and stroke in a Chinese hypertensive cohort. *Clin Exp Hypertens*. (2017) 39:527–31. doi: 10.1080/10641963.2017.1281938

7. Hashimoto H, Takeuchi M, Kawakami K. Association between urate-lowering therapy and cardiovascular events in patients with asymptomatic hyperuricemia. *Clin Rheumatol*. (2023) 42:3075–82. doi: 10.1007/s10067-023-06710-9

8. Chamorro A, Amaro S, Castellanos M, Gomis M, Urra X, Blasco J, et al. Uric acid therapy improves the outcomes of stroke patients treated with intravenous tissue plasminogen activator and mechanical Thrombectomy. *Int J Stroke*. (2017) 12:377–82. doi: 10.1177/1747493016684354

9. Wang Z, Lin Y, Liu Y, Chen Y, Wang B, Li C, et al. Serum uric acid levels and outcomes after acute ischemic stroke. *Mol Neurobiol*. (2016) 53:1753–9. doi: 10.1007/s12035-015-9134-1

10. Wu H, Jia Q, Liu G, Liu L, Pu Y, Zhao X, et al. Decreased uric acid levels correlate with poor outcomes in acute ischemic stroke patients, but not in cerebral hemorrhage patients. *J Stroke Cerebrovasc Dis*. (2014) 23:469–75. doi: 10.1016/j.jstrokecerebrovasdis.2013.04.007

11. Bowden J, Holmes MV. Meta-analysis and Mendelian randomization: a review. *Res Synth Methods*. (2019) 10:486–96. doi: 10.1002/jrsm.1346

12. Barton AR, Sherman MA, Mukamel RE, Loh PR. Whole-exome imputation within UK Biobank powers rare coding variant association and fine-mapping analyses. *Nat Genet*. (2021) 53:1260–9. doi: 10.1038/s41588-021-00892-1

13. Burgess S, Thompson SGCollaboration CCG. Avoiding bias from weak instruments in Mendelian randomization studies. *Int J Epidemiol*. (2011) 40:755–64. doi: 10.1093/ije/dyr036

14. Kurki MI, Karjalainen J, Palta P, Sipila TP, Kristiansson K, Donner KM, et al. Finngen provides genetic insights from a well-phenotyped isolated population. *Nature*. (2023) 613:508–18. doi: 10.1038/s41586-022-05473-8

15. Malik R, Chauhan G, Traylor M, Sargurupremraj M, Okada Y, Mishra A, et al. Multiancestry genome-wide association study of 520,000 subjects identifies 32 loci associated with stroke and stroke subtypes. *Nat Genet*. (2018) 50:524–37. doi: 10.1038/s41588-018-0058-3

16. Woo D, Falcone GJ, Devan WJ, Brown WM, Biffi A, Howard TD, et al. Meta-analysis of genome-wide association studies identifies 1q22 as a susceptibility locus for intracerebral hemorrhage. *Am J Hum Genet*. (2014) 94:511–21. doi: 10.1016/j.ajhg.2014.02.012

17. Soderholm M, Pedersen A, Lorentzen E, Stanne TM, Bevan S, Olsson M, et al. Genome-wide association meta-analysis of functional outcome after ischemic stroke. *Neurology*. (2019) 92:e1271–83. doi: 10.1212/WNL.0000000000007138

18. Aldridge CM, Braun R, Keene KL, Hsu FC, Worrall BB. Single nucleotide polymorphisms associated with motor recovery in patients with nondisabling stroke: GWAS study. *Neurology*. (2023) 101:e2114–25. doi: 10.1212/WNL.0000000000207716

19. Pierce BL, Burgess S. Efficient design for Mendelian randomization studies: subsample and 2-sample instrumental variable estimators. *Am J Epidemiol*. (2013) 178:1177–84. doi: 10.1093/aje/kwt084

20. Jimenez MC, Curhan GC, Choi HK, Forman JP, Rexrode KM. Plasma uric acid concentrations and risk of ischaemic stroke in women. *Eur J Neurol*. (2016) 23:1158–64. doi: 10.1111/ene.12998

21. Wang A, Tian X, Zuo Y, Chen S, Mo D, Zhang L, et al. Effect of changes in serum uric acid on the risk of stroke and its subtypes. *Nutr Metab Cardiovasc Dis*. (2022) 32:167–75. doi: 10.1016/j.numecd.2021.09.017

22. Gill D, Cameron AC, Burgess S, Li X, Doherty DJ, Karhunen V, et al. Urate, blood pressure, and cardiovascular disease: evidence from Mendelian randomization and meta-analysis of clinical trials. *Hypertension*. (2021) 77:383–92. doi: 10.1161/HYPERTENSIONAHA.120.16547

23. Keenan T, Zhao W, Rasheed A, Ho WK, Malik R, Felix JF, et al. Causal assessment of serum urate levels in cardiometabolic diseases through a Mendelian randomization study. *J Am Coll Cardiol*. (2016) 67:407–16. doi: 10.1016/j.jacc.2015.10.086

24. Efstathiadou A, Gill D, McGrane F, Quinn T, Dawson J. Genetically determined uric acid and the risk of cardiovascular and neurovascular diseases: a Mendelian randomization study of outcomes investigated in randomized trials. *J Am Heart Assoc*. (2019) 8:e012738. doi: 10.1161/JAHA.119.012738

25. Liu H, Reynolds GP, Wang W, Wei X. Lower uric acid is associated with poor short-term outcome and a higher frequency of posterior arterial involvement in ischemic stroke. *Neurol Sci*. (2018) 39:1117–9. doi: 10.1007/s10072-018-3307-4

26. Liu Y, Liu X, Jia J, Guo J, Li G, Zhao X. Uric acid and clinical outcomes in young patients with ischemic stroke. *Neuropsychiatr Dis Treat*. (2022) 18:2219–28. doi: 10.2147/NDT.S373493

27. Zhong J, Cai H, Zhang Z, Wang J, Xiao L, Zhang P, et al. Serum uric acid and prognosis of ischemic stroke: cohort study, meta-analysis and Mendelian randomization study. *Eur Stroke J*. (2023) 9:23969873231209620:235–43. doi: 10.1177/23969873231209620

28. Zhang W, Cheng Z, Fu F, Zhan Z. Serum uric acid and prognosis in acute ischemic stroke: a dose-response meta-analysis of cohort studies. *Front Aging Neurosci*. (2023) 15:1223015. doi: 10.3389/fnagi.2023.1223015

29. Sun Z, Feng J, He M, Wang M, Zhang Y, Wang N, et al. Higher uric acid is associated with better discharge recovery and short-term outcome in stroke patients treated with thrombolysis. *Neurol Sci*. (2021) 42:3225–31. doi: 10.1007/s10072-020-04919-z

30. Xu W, Huang Y, Li L, Sun Z, Shen Y, Xing J, et al. Hyperuricemia induces hypertension through activation of renal epithelial sodium channel (ENaC). *Metabolism*. (2016) 65:73–83. doi: 10.1016/j.metabol.2015.10.026

31. Chaudhary NS, Bridges SL Jr, Saag KG, Rahn EJ, Curtis JR, Gaffo A, et al. Severity of hypertension mediates the Association of Hyperuricemia with stroke in the regards case cohort study. *Hypertension*. (2020) 75:246–56. doi: 10.1161/HYPERTENSIONAHA.119.13580

32. He M, Cui B, Wu C, Meng P, Wu T, Wang M, et al. Blood pressures immediately following ischemic strokes are associated with cerebral perfusion and neurologic function. *J Clin Hypertens (Greenwich)*. (2018) 20:1008–15. doi: 10.1111/jch.13310

33. Zhao L, Du W, Zhao X, Liu L, Wang C, Wang Y, et al. Favorable functional recovery in overweight ischemic stroke survivors: findings from the China National Stroke Registry. *J Stroke Cerebrovasc Dis*. (2014) 23:e201–6. doi: 10.1016/j.jstrokecerebrovasdis.2013.10.002

34. Saini M, Saqqur M, Shuaib A, Collaborators V. Body mass index and acute ischemic stroke outcomes. *Int J Stroke*. (2014) 9:618–23. doi: 10.1111/ijs.12168

35. Smyth A, Judge C, Wang X, Pare G, Rangarajan S, Canavan M, et al. Renal impairment and risk of acute stroke: the interstroke study. *Neuroepidemiology*. (2021) 55:206–15. doi: 10.1159/000515239

36. Choi Y, Lee SJ, Spiller W, Jung KJ, Lee JY, Kimm H, et al. Causal associations between serum bilirubin levels and decreased stroke risk: a two-sample Mendelian randomization study. *Arterioscler Thromb Vasc Biol*. (2020) 40:437–45. doi: 10.1161/ATVBAHA.119.313055

37. Wang W, Jiang B, Sun H, Ru X, Sun D, Wang L, et al. Prevalence, incidence, and mortality of stroke in China: results from a nationwide population-based survey of 480 687 adults. *Circulation*. (2017) 135:759–71. doi: 10.1161/CIRCULATIONAHA.116.025250

38. Lee SJ, Jee YH, Jung KJ, Hong S, Shin ES, Jee SH. Bilirubin and stroke risk using a Mendelian randomization design. *Stroke*. (2017) 48:1154–60. doi: 10.1161/STROKEAHA.116.015083

frontiers | Frontiers in Neurology

TYPE Original Research
PUBLISHED 25 April 2024
DOI 10.3389/fneur.2024.1327873

Check for updates

OPEN ACCESS

EDITED BY
Shubham Misra,
Yale University, United States

REVIEWED BY
Cyprien Rivier,
Yale Medicine, United States
Sun Ha Jee,
Yonsei University, Republic of Korea
Canfei Zhang,
The First Affiliated Hospital of Henan University of Science and Technology, China

*CORRESPONDENCE
Wenbao Wu
✉ wuwenbao1983@163.com

†These authors share first authorship

RECEIVED 25 October 2023
ACCEPTED 15 April 2024
PUBLISHED 25 April 2024

CITATION
Wu W, Fan D, Que B, Chen Y and Qiu R (2024) Investigation on the relationship between hemoglobin concentration and stroke risk: a bidirectional Mendelian randomization study. *Front. Neurol.* 15:1327873. doi: 10.3389/fneur.2024.1327873

COPYRIGHT
© 2024 Wu, Fan, Que, Chen and Qiu. This is an open-access article distributed under the terms of the Creative Commons Attribution License (CC BY). The use, distribution or reproduction in other forums is permitted, provided the original author(s) and the copyright owner(s) are credited and that the original publication in this journal is cited, in accordance with accepted academic practice. No use, distribution or reproduction is permitted which does not comply with these terms.

Investigation on the relationship between hemoglobin concentration and stroke risk: a bidirectional Mendelian randomization study

Wenbao Wu[1*†], Daofeng Fan[2†], Binfu Que[1], Yangui Chen[2] and Rui Qiu[1]

[1]Department of Acupuncture and Moxibustion, Longyan First Hospital Affiliated to Fujian Medical University, Longyan, China, [2]Department of Neurology, Longyan First Hospital Affiliated to Fujian Medical University, Longyan, China

Background: The relationship between hemoglobin concentration and stroke has garnered significant interest in the research community. However, findings from published observational epidemiological studies on this relationship have been inconclusive. By using publicly available genome-wide association study (GWAS) aggregated statistics, a two-sample Mendelian randomization analysis is conducted to explore the causal relationship between hemoglobin concentration and stroke.

Methods: Summary statistics data from UK Biobank for hemoglobin concentration and from the FinnGen R9 and MEGASTROKE consortium for stroke are used. A series of quality control steps are taken to select eligible instrumental SNPs closely related to exposure. In order to make the conclusion more robust and reliable, several robust analysis methods are employed including inverse variance weighted, weighted median, MR-Egger regression, which are based on different assumptions of two-sample MR Analysis. Meanwhile, sensitivity analyses such as pleiotropy test and MR-Egg regression, are performed to mitigate horizontal pleiotropy and heterogeneity.

Results: The two-sample Mendelian randomized study indicates a negative association between hemoglobin concentration and stroke, suggesting that hemoglobin concentration acts as a protective factor against stroke. From the FinnGen database, there is a negative association between hemoglobin concentration and stroke, with an odds ratio (OR) of 0.82 and a 95% confidence interval (CI) of 0.73–0.92, $p = 0.0006$. Similarly, the MEGASTROKE database findings reinforce this observation. The negative association between hemoglobin concentration and stroke (OR: 0.91, 95%CI: 0.83–1.00, $p = 0.040$), ischemic stroke (OR: 0.87, 95%CI: 0.79–0.96, $p = 0.004$), and cardiogenic stroke (OR: 0.82, 95% CI: 0.69–0.99, $p = 0.039$) further suggests that higher hemoglobin levels might confer a protective effect against these conditions.

Conclusion: Hemoglobin concentration serves as a protective factor against stroke, and managing abnormal hemoglobin levels can effectively reduce the incidence of stroke.

KEYWORDS

two-sample Mendelian randomization, hemoglobin concentration, ischemic stroke, stroke, Cardioembolic stroke

1 Introduction

Stroke, a leading causes of death and long-term disability, continues to pose a significant global health burden. Although advancements in secondary stroke prevention and diagnostic and treatment protocols have contributed to minimizing acute ischemic stroke occurrences, the incidence of stroke remains high (1). Effective interventions targeting stroke risk factors have proven successful in reducing stroke incidence (2). Traditionally, various cardiovascular risk factors, such as hypertension, diabetes, and hyperlipidemia have been closely associated with the development of stroke (3). However, with the advancement of research as well as technology, new biomarkers have attracted the attention of scientists, including hemoglobin concentration.

The relationship between hemoglobin concentration and stroke is still of interest, but it remains uncertain. Observational studies have demonstrated a complex relationship between hemoglobin concentration and stroke (4). High hemoglobin concentration is seen in conditions like polycythemia vera (5), chronic obstructive pulmonary disease (6) and plateau erythrocytosis (7). Numerous studies have shown that high hemoglobin concentrations increased the blood clotting tendencies and thrombosis risk. Clinical evidence has linked polycythemia vera to thrombosis, including stroke (8), suggesting that high hemoglobin concentration is a risk factor for stroke. Hemoglobin is a key oxygen-carrying molecule in the blood, the relationship between stroke and anemia can be partially explained by a direct link between the central nervous system, blood supply, and oxygen delivery to tissues (9). Consequently, anemia is also a risk factor for ischemic stroke and is associated with a higher mortality rate after hospitalization (10). The relationship between anemia and increased mortality or disability in patients with various types of stroke, including ischemic stroke, cerebral hemorrhage, and subarachnoid hemorrhage, has been investigated (11). However there is inconclusive evidence regarding the correlation, positive or negative, between hemoglobin concentration and stroke.

Randomized controlled Trails (RCTs) are the gold standard for establishing causal relationships in epidemiological studies. However, due to medical ethical restrictions and high costs, conducting certain RCTs can be challenging. In contrast, observational studies are widely used in initial causal exploration due to their relatively simple design and ease of implementation. However, confounding factors and inversion of causality often limit the ability to infer causality. Mendelian randomization (MR) principles address these challenges by utilizing genotypes as instrumental variables to investigate genetic traits and their associations, thereby allowing for the study of genetic interactions and causal inference (12). Therefore, genotypes can be used as instrumental variables to study intermediate phenotypes to infer causal associations with disease states, avoiding the influence of confounding factors and reverse causal associations (13). The rapid development of genome-wide association studies (GWAS) has led to the increasing application of MR analysis, using single nucleotide polymorphisms (SNPs) that are strongly correlated with phenotypes as instrumental variables (12).

In the present study, MR analyses are performed to elucidate whether hemoglobin concentration has a causal effect on stroke. Specifically, correlational MR analyses are conducted to investigate the relationship between hemoglobin concentration and stroke, utilizing hemoglobin concentration as an exposure tool for genetic variation and stroke as the outcome. The aim was to obtain causal estimates and determine whether hemoglobin concentration is negatively or positively associated with stroke.

2 Methods

2.1 Study design

A two-sample MR approach is employed using summary statistics data from UK Biobank for hemoglobin concentration, and from the FinnGen R9 and MEGASTROKE consortium for stroke. The use of these datasets was in accordance with appropriate patient consent and ethical approval. The present study was approved by the ethics committee of Longyan First Hospital (Ethics number: 2022022). The specific process is illustrated in the Figure 1.

2.2 Outcome data sources

Summary-level data for stroke were obtained from the FinnGen R9 and MEGASTROKE, FinnGen R9 consortium which including a total of 306,377 individuals of European ancestry, consisting of 39,818 stroke cases and 271,817 controls (13). Moreover, in the MEGASTROKE Consortium's meta-analysis of genome-wide association study (GWAS) data, stroke data were collected, which included stroke subtypes and stroke information in Europeans (40,585 cases, 406,111 controls) (14). The sources and detailed information of this data are presented in Table 1.

2.3 Instrumental variable selection

Hemoglobin concentration as exposure data (containing 13,791,467 SNPs) in a population of 350,474 European ancestry is selected from the UK Biobank dataset (15). Among these SNPs, 71,104 SNPs are identified robustly associated with hemoglobin concentration ($p < 5\times10–8$) (16). To ensure the independence of the hemoglobin concentration instrumental variables, we applied clumping with an r2 threshold<0.001 and a clump window of 10,000 kb based on the 1,000 genomes linkage disequilibrium (LD) reference panel of only Europeans (17). After implementing the correlation settings, we identified 287 SNPs that were used as instrumental variables for the exposure. We calculated the F-statistics of these 287 SNPs to assess the strength of genetic variation, and all F-statistics were found to be more than 10. Details of the SNPs associated with the hemoglobin concentration are presented in Supplementary Table S1. 255 and 275 exposure SNPs were obtained from the instrumental variables for stroke outcome data in Supplementary Tables S2, S3. After conducting a harmonize check, we removed some SNPs due to palindromic alleles and compatibility issues with other alleles. After the above operations, we obtained SNPS suitable for MR analysis, which are detailed in Supplementary Tables S4, S5.

2.4 Pleiotropy assessment

To identify and exclude possible pleiotropic associations between instrumental variables and other phenotypes, all SNPs are searched

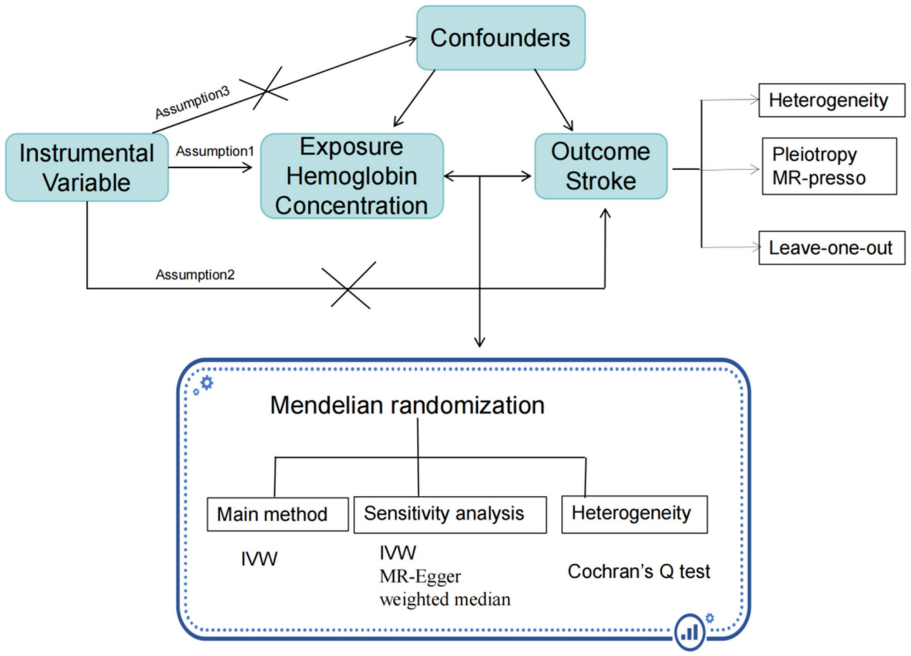

FIGURE 1
The study flow chart.

TABLE 1 Stroke subtypes and data sources.

Outcome	Sample size (cases/controls)	Ancestry	Significance level	Data sources
Stroke	39818/27181	European	5e−8	https://www.finngen.fi/fir9.finngen.fi
Stroke	40585/406111	European	5e−8	MEGASTROKE Consortium (ebi-a-GCST005838)
Ischemic stroke	34217/406111	European	5e−8	MEGASTROKE Consortium (ebi-a-GCST005843)
Cardioembolic stroke	7193/406111	European	5e−8	MEGASTROKE Consortium (ebi-a-GCST005842)
Large artery stroke	4373/406111	European	5e−8	MEGASTROKE Consortium (ebi-a-GCST005840)
Small vessel stroke	5386/192662	European	5e−8	MEGASTROKE Consortium (ebi-a-GCST005841)

using the human genotype–phenotype association database (PhenoScanner V2)[1] to detect possible pleiotropy (18). Through this analysis, it's found that that some of the SNPs related to hemoglobin concentration were also associated with various stroke risk factors, including hypertension, diabetes, dyslipidemia, heart disease, smoking, alcohol consumption, overweight or obesity, platelet aggregation, etc. By controlling for confounding factors that may affect stroke outcomes, specific SNPs can be identified to serve as instrumental variables. Detailed information regarding these SNPs can be found in Supplementary Tables S6–S11.

2.5 Statistical analysis

To assess the associations between hemoglobin concentration and stroke, multiple statistical methods including inverse variance weighted (IVW), MR-Egger regression, weighted median approaches were used to examine the potential causal association. The IVW method uses a meta-analysis approach combined with Wald estimates for each SNP, to estimate the causal relationship between hemoglobin concentration and stroke (12). In the absence of horizontal pleiotropy, the IVW method provides unbiased results. The weighted median method weights the estimates of causal effects at each locus of genetic variation and enhance the accuracy and robustness of causal inference (19). The MR-Egger regression method corrects for horizontal pleiotropy by estimating

1 http://www.phenoscanner.medschl.cam.ac.uk

the bias weight, which enhances the accuracy and reliability of Mendelian randomization analysis (20). We employed both the MR-Egger method and outlier (MR-PRESSO) method to test for horizontal pleiotropy. Furthermore, a 'leave one out' analysis was conducted to examine whether the causal relationship between exposure and outcome was influenced by a single SNP. Odds ratios (ORs) for stroke were calculated per one standard deviation (SD) increase in genetically predicted hemoglobin concentration in all analyses. All SNPs that had a significant effect on hemoglobin concentration at the genome-wide significance levels were used for sensitivity analysis. All statistical analyses were two-sided and performed in R 4.3.0 software (R Foundation for Statistical Computing, Vienna, Austria). MR analyses were performed using the TwosampleMR (version 0.5.7), Mendelian Randomization (version 0.5.7), and MR-PRESSO (version 1.0) packages. $P < 0.05/5$ (with Bonferroni corrections) was statistically significant with p-value between 0.05 and 0.01 as suggestively significant. We interpreted the results not solely based on p-values but also considered the strengths of the associations and the consistency across sensitivity analyses.

3 Results

3.1 Exploration of the causal relationship between hemoglobin concentration and stroke

The associations between hemoglobin concentration and stroke are shown in Figure 2. This study found a negative association between genetically predicted hemoglobin concentration and stroke, including ischemic stroke and cardiogenic stroke. Significant causal relationships were identified using the Inverse Variance Weighted (IVW) method. The results from different MR methods are as follows: Firstly, data from FinnGen demonstrated a significant negative association between hemoglobin concentrations and stroke, with an odds ratio (OR) of 0.82 (95% confidence interval [CI]: 0.73 to 0.92) and a p-value of 0.0006. Secondly, findings from MEGASTROKE also reveal a negative correlation between hemoglobin concentration and stroke (OR: 0.91, 95% CI: 0.83–1.00, $p = 0.040$). This association is observed for both ischemic stroke (OR: 0.87, 95% CI: 0.79–0.96, $p = 0.004$) and cardiogenic stroke (OR: 0.82, 95% CI: 0.69–0.99, $p = 0.039$) (detail in Supplementary Table S12). Notably, even after applying Bonferroni correction, hemoglobin concentration remains significantly negatively correlated with ischemic stroke. Thus, it's revealed that hemoglobin concentration can reduce the incidence of stroke, suggesting that hemoglobin concentration is a protective factor against stroke. The scatter plot indicates that the hemoglobin concentration is negatively correlated with any stroke, ischemic stroke and cardiogenic stroke in the MEGASTROKE database (shown in Figure 3). The funnel plot indicates no heterogeneity between hemoglobin concentration and different stroke subgroups. The leave-one-out plot also indicates the stability of this study model. When hemoglobin concentration is analyzed against stroke in the FinnGen R9 database, there is heterogeneity ($Q = 181.427$, $p < 0.05$),suggesting that our MR-Egger method did not outperform the inverse variance weighting method (16), as is shown in Figure 4.

3.2 Exploration of the causal relationship between stroke and hemoglobin concentration

To establish a causal relationship between hemoglobin concentration and stroke, a reverse Mendelian randomization (MR) study is conducted. The reverse MR results indicate no significant association between hemoglobin concentration and the various types of stroke (available in the Supplementary Tables S13–S18). Based on the IVW results, it can be concluded that there is no causal relationship between hemoglobin concentration and different subtypes of stroke. The specific findings are as follows: Any stroke: OR 1.13, 95% CI: 0.90–1.41, $p = 0.288$;Ischemic stroke: OR 1.01, 95% CI: 0.80–1.27, $p = 0.922$;Large artery stroke: OR 0.99, 95% CI: 0.98–1.00, $p = 0.421$; Cardioembolic stroke: OR 1.11, 95% CI: 0.91–1.35, $p = 0.312$. For the Small vessel stroke subtype, an MR analysis was conducted without SNP after applying a strong correlation threshold of $p <$ 5e-08. Subsequently, an MR analysis is performed between Small vessel stroke and hemoglobin concentration, setting a p-value threshold of $p <$ 5e-06. The results of this analysis also show that there is no causal relationship between the two variables (OR: 1.00, 95% CI: 0.99–1.01, $p = 0.671$). These results indicate that there is no significant evidence to suggest a causal relationship between hemoglobin concentration and these specific stroke subtypes. Furthermore, employing bidirectional MR analysis, it is observed that hemoglobin concentration exhibits a negative correlation with stroke, particularly ischemic stroke.

4 Discussion

The present MR study of hemoglobin concentration and stroke makes use of the summary statistics of hemoglobin concentration from the UK Biobank consortium, and from the FinnGen R9 and MEGASTROKE consortium for stroke. A two-sample MR analysis is carried out to investigate the potential causal association between these two factors. Novel findings demonstrate a negative causal relationship between hemoglobin concentration and stroke, particularly ischemic stroke. Additionally, the results suggest that hemoglobin concentration acts as a protective factor against stroke, providing the first indication of its potential role in stroke prevention.

A large number of observational studies have examined the relationship between hemoglobin concentration and stroke, but there is no uniform interpretation of their relationship (21). Previous studies have suggested that hospitalized patients with high hemoglobin concentration are more likely to have a stroke than those with low hemoglobin concentration (22). Lee et al. found that an elevation in Hb concentration from the normal range to high levels was associated with an increased risk of stroke (hazard ratio [95% confidence interval]: 1.10 [1.02–1.35]) (23). The increased risk is attributed to high hemoglobin levels causing elevated blood viscosity and a higher propensity for thrombosis. Excess hemoglobin can also damage the endothelium of blood vessels, leading to artery walls thickening and an increased risk of arterial narrowing, all contributing factors to the stroke risk. On the other hand, low hemoglobin concentration can cause anemia, insufficient oxygen supply to the brain and some cardiovascular and cerebrovascular problems. Observational studies have shown an association between low hemoglobin concentrations

outcome	method	nsnp	pval	OR	OR_lci95	OR_uci95	OR95%CI
stroke	MR Egger	187	0.7015	0.96	0.79	1.17	0.96(0.79to1.17)
stroke	Weighted median	187	0.0938	0.89	0.77	1.02	0.89(0.77to1.02)
stroke	Inverse variance weighted	187	0.0401	0.91	0.84	1.00	0.91(0.84to1.00)
stroke	Simple mode	187	0.7642	0.94	0.63	1.41	0.94(0.63to1.41)
stroke	Weighted mode	187	0.0771	0.80	0.63	1.02	0.80(0.63to1.02)
ischemic stroke	MR Egger	203	0.3828	0.91	0.73	1.13	0.91(0.73to1.13)
ischemic stroke	Weighted median	203	0.0188	0.82	0.69	0.97	0.82(0.69to0.97)
ischemic stroke	Inverse variance weighted	203	0.0038	0.87	0.79	0.96	0.87(0.79to0.96)
ischemic stroke	Simple mode	203	0.3940	0.84	0.55	1.26	0.84(0.55to1.26)
ischemic stroke	Weighted mode	203	0.0563	0.78	0.61	1.01	0.78(0.61to1.01)
large artery stroke	MR Egger	207	0.1041	1.58	0.91	2.73	1.58(0.91to2.73)
large artery stroke	Weighted median	207	0.5556	1.13	0.75	1.71	1.13(0.75to1.71)
large artery stroke	Inverse variance weighted	207	0.2203	0.86	0.68	1.09	0.86(0.68to1.09)
large artery stroke	Simple mode	207	0.9650	1.02	0.36	2.94	1.02(0.36to2.94)
large artery stroke	Weighted mode	207	0.7222	1.12	0.60	2.07	1.12(0.60to2.07)
cardioembolic stroke	MR Egger	214	0.0793	0.69	0.46	1.04	0.69(0.46to1.04)
cardioembolic stroke	Weighted median	214	0.0936	0.78	0.58	1.04	0.78(0.58to1.04)
cardioembolic stroke	Inverse variance weighted	214	0.0389	0.82	0.69	0.99	0.82(0.69to0.99)
cardioembolic stroke	Simple mode	214	0.5273	0.78	0.36	1.69	0.78(0.36to1.69)
cardioembolic stroke	Weighted mode	214	0.0880	0.67	0.42	1.06	0.67(0.42to1.06)
small vessel stroke	MR Egger	189	0.4478	0.80	0.45	1.42	0.80(0.45to1.42)
small vessel stroke	Weighted median	189	0.3863	0.82	0.51	1.29	0.82(0.51to1.29)
small vessel stroke	Inverse variance weighted	189	0.1253	0.83	0.65	1.05	0.83(0.65to1.05)
small vessel stroke	Simple mode	189	0.9876	0.99	0.32	3.06	0.99(0.32to3.06)
small vessel stroke	Weighted mode	189	0.5550	0.83	0.44	1.55	0.83(0.44to1.55)
R9−stroke	MR Egger	135	0.5310	0.91	0.69	1.21	0.91(0.69to1.21)
R9−stroke	Weighted median	135	0.0067	0.80	0.69	0.94	0.80(0.69to0.94)
R9−stroke	Inverse variance weighted	135	0.0006	0.82	0.73	0.92	0.82(0.73to0.92)
R9−stroke	Simple mode	135	0.2634	0.78	0.51	1.20	0.78(0.51to1.20)
R9−stroke	Weighted mode	135	0.1703	0.77	0.54	1.11	0.77(0.54to1.11)

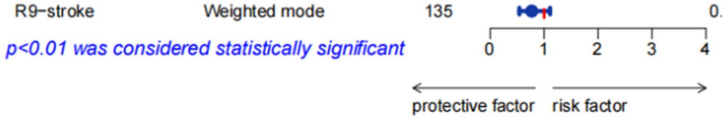

FIGURE 2
MR estimates from different methods for assessing the causal effect of hemoglobin concentration on stroke (pval was the value pval after MRpresso).

and a higher likelihood of stroke occurrence (8). Therefore, it is very necessary to elucidate the causal relationship between hemoglobin concentration and stroke. This two-sample Mendelian randomization study shows that hemoglobin concentration is negatively correlated with stroke, challenging the previous view that high hemoglobin concentration is more likely to cause stroke.

Anemia, characterized by low hemoglobin levels, a prevalent condition and recognized as the fifth major cardiovascular risk factor. It affects individuals across all age groups, including children, adults, and the elderly. The relationship between anemia and stroke has been extensively discussed in clinical practice and research, with studies exploring this relationship even in pediatric populations. For example, studies have indicated that low hemoglobin concentration is a major risk factor for increased stroke risk in children with sickle cell anemia (24). Maguire et al. have demonstrated that iron deficiency anemia was a significant risk factor for stroke in otherwise healthy young children (25). The youth population can experience both hypoproliferative anemia and hyperproliferative anemia, which are linked to cerebrovascular diseases. These diseases range from transient ischemic attacks to ischemic stroke and hemorrhagic stroke (26). In adults, low hemoglobin levels have been associated with an increased risk of stroke in both men and women, irrespective of their gender. Panwar et al. demonstrated that the likelihood of stroke in women increased by a factor of 0.59 for every unit decrease in hemoglobin levels (4). The study also indicates that a gradual decline in hemoglobin levels over time may elevate stroke risk, with a Hazard Ratio (HR) of 4.12 (95% Confidence Interval: 1.50, 11.28) in men (27). In the study investigating the connection between chronic kidney disease and stroke, it is found that individuals with anemia had a significantly higher risk of stroke compared to those without anemia (HR 5.43; 95% CI 2.04 to 14.41) (28). Research conducted on the elderly population has demonstrated a negative correlation between hemoglobin levels and stroke. Additionally, it has been found that low hemoglobin status is an independent predictor of both short-term and long-term mortality (29). Another study also shows that decreased in-hospital hemoglobin is

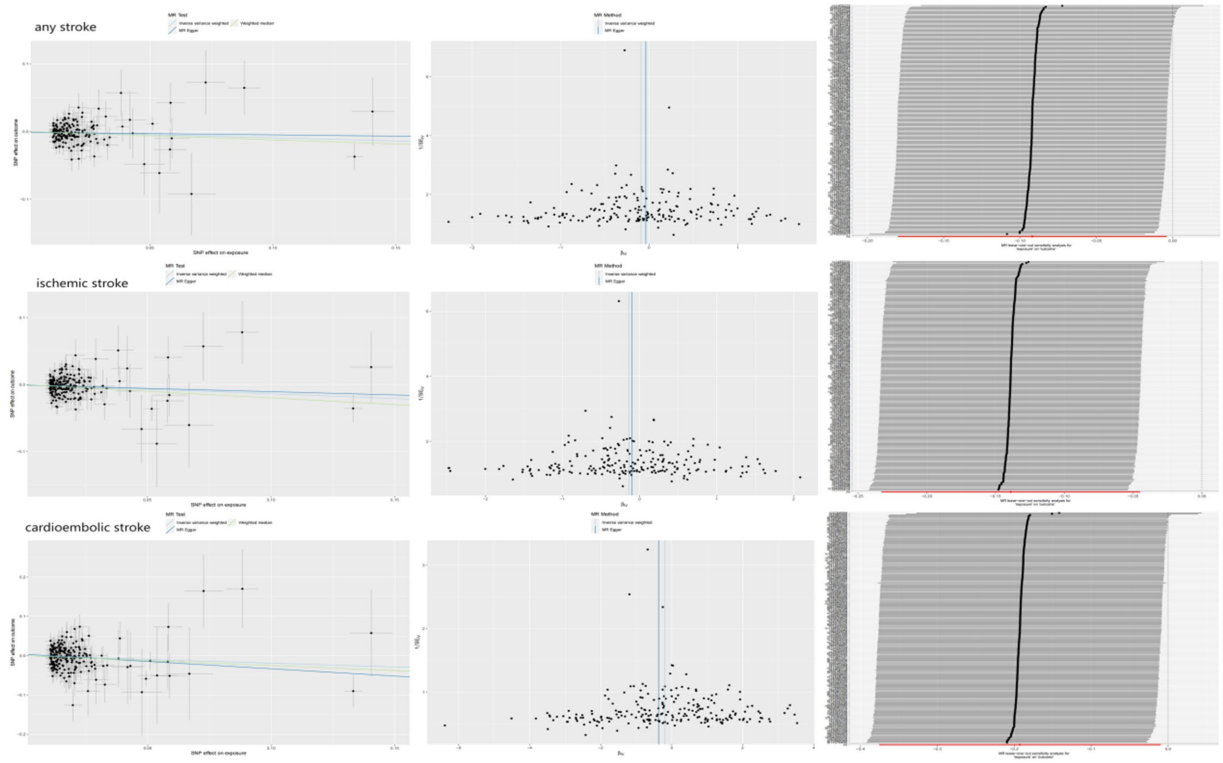

FIGURE 3
The causal effect of hemoglobin concentration on stroke (MEGASTROKE).

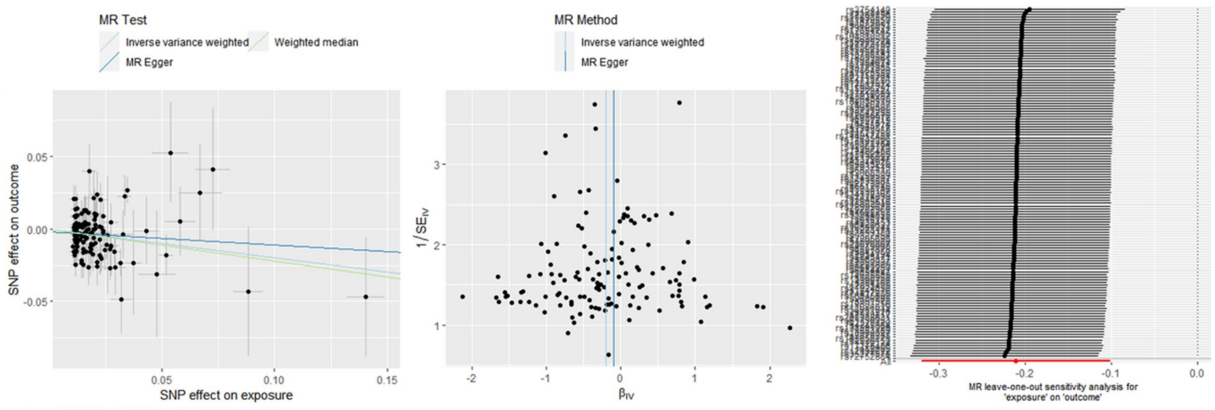

FIGURE 4
The causal effect of hemoglobin concentration on stroke (FinnGen R9).

independently associated with increased stroke events in older patients (30). The aforementioned study on low hemoglobin concentration and stroke risk further supports the claim that our two-sample Mendelian randomization indicates a negative correlation between hemoglobin concentration and stroke. Raphae S Barlas et al. conducted a meta-analysis on the relationship between anemia and stroke, the study found strong evidence that anemia patients had a higher risk of stroke, with a negative correlation between hemoglobin concentration and stroke incidence (31).

The relationship between hemoglobin concentration and stroke has been observed to exhibit a J or U-shaped curve. This means that the risk of stroke tends to increase at both low and high hemoglobin levels (32–34). However, the present Mendelian randomization study demonstrates that hemoglobin concentration is a protective factor against stroke. Similarly, increasing hemoglobin concentration to the normal range in cases of anemia may also reduce the occurrence of stroke. Earlier studies have also indicated that reducing hemoglobin concentrations from the high range to the normal range reduces the risk of stroke (hazard ratio [95% confidence interval]: 0.80 [0.60–0.97]), and improving anemia to the normal range also reduces the risk of all-cause stroke (hazard ratio [95% confidence interval]: 0.81 [0.69–0.94]) (23).

This study provides a significant advantage as it is the first to establish a causal relationship between hemoglobin concentration and stroke using MR Analysis. Furthermore, it is the first time that hemoglobin concentration is used as a protective factor against stroke. This approach

allows doctors to eliminate the influence of confounding factors and establish a reverse causal reasoning. To ensure the reliability of our findings, genetic variation data is collected from the largest available UK Biobank meta-analysis on hemoglobin concentration and from the FinnGen R9 and MEGASTROKE consortium for stroke. The selection of instrumental variables strengthens the MR Analysis. Measures are also taken to detect and exclude horizontal pleiotropy through MR-Egger regression intercept item tests. Additionally, a two-sample MR Design is employed, using non-overlapping exposures and summarizing results at a level data to minimize bias and increase the validity of the conclusions.

There are some limitations of the MR analysis that need to be considered. This study considers the heterogeneity of the included population, taking into account factors such as education level, cultural background, and living habits that may impact the experimental results. Further investigation is needed to explore the causal relationship between education level, living habits, and stroke. Additionally, since the study only includes European individuals, it is important to examine the potential causal relationship between racial differences and stroke, which should be a focus of future research.

5 Conclusion

This study conducted a two-sample MR Study and successfully identified a causal relationship between hemoglobin concentration and stroke. Then, with stroke as the exposure factor and Hb as the outcome, we reevaluated the causal relationship between them. The findings indicate a potential protective effect of higher hemoglobin levels against stroke. However, further large sample multi-center randomized clinical studies are needed to validate these results. The study also highlights the importance of considering the impact of hemoglobin concentration on stroke, particularly in the management of anemia patients. This highlights the need for increased attention to hemoglobin levels in the context of stroke prevention and treatment.

Data availability statement

The datasets presented in this study can be found in online repositories. The names of the repository/repositories and accession number(s) can be found in the article/Supplementary material.

Ethics statement

The studies involving humans were approved by the Ethics Committee of Longyan First Hospital. The studies were conducted in accordance with the local legislation and institutional requirements. The participants provided their written informed consent to participate in this study. Written informed consent was obtained from the individual(s) for the publication of any potentially identifiable images or data included in this article.

Author contributions

WW: Funding acquisition, Project administration, Writing – original draft. DF: Data curation, Writing – original draft. BQ: Investigation, Writing – original draft. YC: Writing – review & editing. RQ: Writing – review & editing.

Funding

The author(s) declare financial support was received for the research, authorship, and/or publication of this article. This project was funded by the Special Project on Traditional Chinese Medicine of Fujian Provincial Health Commission (No. 2021zylc55).

Acknowledgments

Thanks to all the staff of UK Biobank, FinnGen and MEGASTROKE database for their efforts on this study.

Conflict of interest

The authors declare that the research was conducted in the absence of any commercial or financial relationships that could be construed as a potential conflict of interest.

Publisher's note

All claims expressed in this article are solely those of the authors and do not necessarily represent those of their affiliated organizations, or those of the publisher, the editors and the reviewers. Any product that may be evaluated in this article, or claim that may be made by its manufacturer, is not guaranteed or endorsed by the publisher.

Supplementary material

The Supplementary material for this article can be found online at: https://www.frontiersin.org/articles/10.3389/fneur.2024.1327873/full#supplementary-material

References

1. Hankey GJ. Secondary stroke prevention. *Lancet Neurol.* (2014) 13:178–94. doi: 10.1016/S1474-4422(13)70255-2

2. Diener HC, Easton JD, Hart RG, Kasner S, Kamel H, Ntaios G. Review and update of the concept of embolic stroke of undetermined source. *Nat Rev Neurol.* (2022) 18:455–65. doi: 10.1038/s41582-022-00663-4

3. Benesch C, Glance LG, Derdeyn CP, Fleisher LA, Holloway RG, Messé SR, et al. Perioperative neurological evaluation and management to lower the risk of acute stroke in patients undergoing noncardiac, nonneurological surgery: a scientific statement from the American Heart Association/American Stroke Association. *Circulation.* (2021) 143:e923–46. doi: 10.1161/CIR.0000000000000968

4. Panwar B, Judd SE, Warnock DG, McClellan WM, Booth JN III, Muntner P, et al. Hemoglobin concentration and risk of incident stroke in community-living adults. *Stroke.* (2016) 47:2017–24. doi: 10.1161/STROKEAHA.116.013077

5. Gordeuk VR, Stockton DW, Prchal JT. Congenital polycythemias/erythrocytoses. *Haematologica.* (2005) 90:109–16.

6. Yasuda H, Yamaya M, Nakayama K, Ebihara S, Sasaki T, Okinaga S, et al. Increased arterial carboxyhemoglobin concentrations in chronic obstructive pulmonary disease. *Am J Respir Crit Care Med*. (2005) 171:1246–51. doi: 10.1164/rccm.200407-914OC

7. Jiang C, Chen J, Liu F, Luo Y, Xu G, Shen HY, et al. Chronic mountain sickness in Chinese Han males who migrated to the Qinghai-Tibetan plateau: application and evaluation of diagnostic criteria for chronic mountain sickness. *BMC Public Health*. (2014) 14:701. doi: 10.1186/1471-2458-14-701

8. Marchioli R, Finazzi G, Specchia G, Cacciola R, Cavazzina R, Cilloni D, et al. Cardiovascular events and intensity of treatment in polycythemia vera. *N Engl J Med*. (2013) 368:22–33. doi: 10.1056/NEJMoa1208500

9. Rees DC, Williams TN, Gladwin MT. Sickle-cell disease. *Lancet*. (2010) 376:2018–31. doi: 10.1016/S0140-6736(10)61029-X

10. Valentijn TM, Hoeks SE, Martienus KA, Bakker EJ, van de Luijtgaarden KM, Verhagen HJ, et al. Impact of haemoglobin concentration on cardiovascular outcome after vascular surgery: a retrospective observational cohort study. *Eur J Anaesthesiol*. (2013) 30:664–70. doi: 10.1097/EJA.0b013e328362a5fd

11. Ohene-Frempong K, Weiner SJ, Sleeper LA, Miller ST, Embury S, Moohr JW, et al. Cerebrovascular accidents in sickle cell disease: rates and risk factors. *Blood*. (1998) 91:288–94.

12. Carter AR, Sanderson E, Hammerton G, Richmond RC, Davey Smith G, Heron J, et al. Mendelian randomisation for mediation analysis: current methods and challenges for implementation. *Eur J Epidemiol*. (2021) 36:465–78. doi: 10.1007/s10654-021-00757-1

13. Chen C, Liu Q, Li Y, Yu J, Wang S, Liu L. Impact of immune cells on stroke limited to specific subtypes: evidence from Mendelian randomization study. *Neurol Ther*. (2024). doi: 10.1007/s40120-024-00592-y

14. Malik R, Chauhan G, Traylor M, Sargurupremraj M, Okada Y, Mishra A, et al. Multiancestry genome-wide association study of 520,000 subjects identifies 32 loci associated with stroke and stroke subtypes. *Nat Genet*. (2018) 50:524–37. doi: 10.1038/s41588-018-0058-3

15. Mbatchou J, Barnard L, Backman J, Marcketta A, Kosmicki JA, Ziyatdinov A, et al. Computationally efficient whole-genome regression for quantitative and binary traits. *Nat Genet*. (2021) 53:1097–103. doi: 10.1038/s41588-021-00870-7

16. Linden AB, Clarke R, Hammami I, Hopewell JC, Guo Y, Whiteley WN, et al. Genetic associations of adult height with risk of cardioembolic and other subtypes of ischemic stroke: a mendelian randomization study in multiple ancestries. *PLoS Med*. (2022) 19:e1003967. doi: 10.1371/journal.pmed.1003967

17. Chen L, Peters JE, Prins B, Persyn E, Traylor M, Surendran P, et al. Systematic Mendelian randomization using the human plasma proteome to discover potential therapeutic targets for stroke. *Nat Commun*. (2022) 13:6143. doi: 10.1038/s41467-022-33675-1

18. Wu F, Huang Y, Hu J, Shao Z. Mendelian randomization study of inflammatory bowel disease and bone mineral density. *BMC Med*. (2020) 18:312. doi: 10.1186/s12916-020-01778-5

19. Davies NM, Holmes MV, Davey SG. Reading Mendelian randomisation studies: a guide, glossary, and checklist for clinicians. *BMJ*. (2018) 362:k601. doi: 10.1136/bmj.k601

20. Burgess S, Thompson SG. Interpreting findings from Mendelian randomization using the MR-egger method. *Eur J Epidemiol*. (2017) 32:377–89. doi: 10.1007/s10654-017-0255-x

21. Park YH, Kim BJ, Kim JS, Yang MH, Jang MS, Kim N, et al. Impact of both ends of the hemoglobin range on clinical outcomes in acute ischemic stroke. *Stroke*. (2013) 44:3220–2. doi: 10.1161/STROKEAHA.113.002672

22. Di Mascio R, Marchioli R, Vitullo F, Tognoni G. A positive relation between high hemoglobin values and the risk of ischemic stroke. Progetto 3A investigators. *Eur Neurol*. (1996) 36:85–8. doi: 10.1159/000117214

23. Lee G, Choi S, Kim K, Yun JM, Son JS, Jeong SM, et al. Association between changes in hemoglobin concentration and cardiovascular risks and all-cause mortality among young women. *J Am Heart Assoc*. (2018) 7:e008147. doi: 10.1161/JAHA.117.008147

24. DeBaun MR, Sarnaik SA, Rodeghier MJ, et al. Associated risk factors for silent cerebral infarcts in sickle cell anemia: low baseline hemoglobin, sex, and relative high systolic blood pressure. *Blood*. (2012) 119:3684–90. doi: 10.1182/blood-2011-05-349621

25. Maguire JL, deVeber G, Parkin PC. Association between iron-deficiency anemia and stroke in young children. *Pediatrics*. (2007) 120:1053–7. doi: 10.1542/peds.2007-0502

26. Fonseca AC, Silva DP, Infante J, Ferro JM. Cerebrovascular complications of Anemia. *Curr Neurol Neurosci Rep*. (2021) 21:51. doi: 10.1007/s11910-021-01141-y

27. Dayimu A, Qian W, Fan B, Wang C, Li J, Wang S, et al. Trajectories of Haemoglobin and incident stroke risk: a longitudinal cohort study. *BMC Public Health*. (2019) 19:1395. doi: 10.1186/s12889-019-7752-7

28. Abramson JL, Jurkovitz CT, Vaccarino V, Weintraub WS, McClellan W. Chronic kidney disease, anemia, and incident stroke in a middle-aged, community-based population: the ARIC study. *Kidney Int*. (2003) 64:610–5. doi: 10.1046/j.1523-1755.2003.00109.x

29. Milionis H, Papavasileiou V, Eskandari A, D'Ambrogio-Remillard S, Ntaios G, Michel P. Anemia on admission predicts short- and long-term outcomes in patients with acute ischemic stroke. *Int J Stroke*. (2015) 10:224–30. doi: 10.1111/ijs.12397

30. Damluji AA, Macon C, Fox A, Garcia G, al-Damluji MS, Marzouka GR, et al. The association between in-hospital hemoglobin changes, cardiovascular events, and mortality in acute decompensated heart failure: results from the ESCAPE trial. *Int J Cardiol*. (2016) 222:531–7. doi: 10.1016/j.ijcard.2016.07.264

31. Wei CC, Zhang ST, Tan G, Zhang SH, Liu M. Impact of anemia on in-hospital complications after ischemic stroke. *Eur J Neurol*. (2018) 25:768–74. doi: 10.1111/ene.13595

32. Gagnon DR, Zhang TJ, Brand FN, Kannel WB. Hematocrit and the risk of cardiovascular disease—the Framingham study: a 34-year follow-up. *Am Heart J*. (1994) 127:674–82. doi: 10.1016/0002-8703(94)90679-3

33. Kim MY, Jee SH, Yun JE, Baek SJ, Lee DC. Hemoglobin concentration and risk of cardiovascular disease in Korean men and women - the Korean heart study. *J Korean Med Sci*. (2013) 28:1316–22. doi: 10.3346/jkms.2013.28.9.1316

34. Chang YL, Hung SH, Ling W, Lin HC, Li HC, Chung SD. Association between ischemic stroke and iron-deficiency anemia: a population-based study. *PLoS One*. (2013) 8:e82952. doi: 10.1371/journal.pone.0082952

frontiers | Frontiers in Neurology

TYPE Original Research
PUBLISHED 28 May 2024
DOI 10.3389/fneur.2024.1405108

Check for updates

OPEN ACCESS

EDITED BY
Shubham Misra,
Yale University, United States

REVIEWED BY
Anna Stanisławska-Sachadyn,
Gdansk University of Technology, Poland
He Li,
Tianjin Huanhu Hospital, China
Si Cao,
Reproductive and Genetic Hospital of CITIC-Xiangya, China

*CORRESPONDENCE
Xiaokai Yang
yakeworld@wmu.edu.cn

RECEIVED 22 March 2024
ACCEPTED 13 May 2024
PUBLISHED 28 May 2024

CITATION
Hu H, Zhou M, Zhao Y, Mao J and Yang X (2024) Effects of immune cells on ischemic stroke and the mediating roles of metabolites.
Front. Neurol. 15:1405108.
doi: 10.3389/fneur.2024.1405108

COPYRIGHT
© 2024 Hu, Zhou, Zhao, Mao and Yang. This is an open-access article distributed under the terms of the Creative Commons Attribution License (CC BY). The use, distribution or reproduction in other forums is permitted, provided the original author(s) and the copyright owner(s) are credited and that the original publication in this journal is cited, in accordance with accepted academic practice. No use, distribution or reproduction is permitted which does not comply with these terms.

Effects of immune cells on ischemic stroke and the mediating roles of metabolites

Haoxiang Hu, Mi Zhou, Yunhan Zhao, Jiesheng Mao and Xiaokai Yang*

Postgraduate Training Base Alliance of Wenzhou Medical University, Third Affffliated Hospital of Shanghai University (Wenzhou People's Hospital), Wenzhou, China

Objective: Previous studies have not shown an association between IgD-CD24- B-cell absolute count (IgD-CD24-AC) and ischemic stroke (IS). Our study aimed to assess the causal effect of IgD-CD24-AC on IS and to explore the role of ascorbic acid 2-sulfate (AA2S) as a potential mediator.

Methods: Our study was based on the largest available genome-wide association study (GWAS). Inverse variance weighting (IVW), MR–Egger, weighted median (WMN), simple mode, and weighted mode methods were used to assess causal effects, with IVW as the primary outcome. Subsequently, we further performed a two-step MR analysis to evaluate whether AA2S mediated this causal effect. In addition, several sensitivity analyses were conducted to evaluate heterogeneity, including Cochran's Q test, the MR–Egger intercept test, the MR-PRESSO global test, and the leave-one-out analysis.

Results: Using the IVW approach, the risk ratio of IgD-CD24-AC to IS was estimated to be 1.216 (95% CI=1.079–1.371, p=0.001). This result was supported by the WMN method (OR=1.204, 95% CI=1.020–1.421, p=0.028) and the MR–Egger method (OR=1.177, 95% CI=0.962–1.442, p=0.133). We also observed the same trend with the simple model and weighted model. Furthermore, the proportion of genetically predicted IgD-CD24-AC mediated through AA2S levels was 3.73%.

Conclusion: Our study revealed a causal relationship between IgD-CD24-AC and IS, a small part of which was mediated by AA2S. These findings offer critical insights for developing immune-targeted therapies in the future and lay a strong foundation for advancements in precision medicine.

KEYWORDS

Mendelian randomization, ischemic stroke, IgD-CD24-AC, AA2S, metabolite, immunology

1 Introduction

Ischemic stroke (IS) is caused by an obstruction, generally from a blood clot, in the brain's blood vessels (1). It is characterized not only by its high prevalence and mortality rates but also by being a significant contributor to disability and mortality among middle-aged and elderly populations, representing a formidable global health challenge (2–5). IS has been demonstrated to induce the release of inflammatory mediators, subsequently eliciting an immune response (6). IS can induce neuroinflammation characterized by impaired immune cell function,

highlighting the pivotal role of immune responses in the outcomes of IS (7, 8). Furthermore, the effects of various immune cells on ischemic strokes are complex and exhibit contradictory aspects (9). B cells play an important role in this process among the various immune cells. Following an ischemic event, there is a notable accumulation of B cells in the affected area, where they actively engage in the immune response (10, 11). A previous Mendelian randomization (MR) study revealed that distinct B-cell subtypes exhibit differential impacts on IS, and this study posits that specific B-cell phenotypes, such as CD24+ B-cell phenotypes, potentially confer neuroprotection, in contrast to IgD+CD24-B cells, which may predispose individuals to a heightened risk of IS (12). Although this investigation offers preliminary insights, the intricate interplay and roles of IgD and CD24 phenotypes within the context of IS have yet to be comprehensively delineated, underscoring the critical necessity for this research.

The IgD-CD24-B-cell absolute count (IgD-CD24-AC) reflects the absolute count of B cells that are devoid of surface expression of both immunoglobulin D (IgD) and CD24 proteins. IgD, a marker protein on the surface of B cells, is usually associated with the immune response (13). CD24, an additional surface marker, is generally related to B-cell energy metabolism and selective developmental processes (14, 15). In recent years, a large number of scholars have focused on the function of the IgD and CD24 proteins on the surface of B cells in neurological diseases. Recent MR studies demonstrated that the absence of IgD protein in B cells elevates the risk for small-vessel stroke (16), with IgD protein negativity also displaying a positive correlation with the incidence of large-vessel and large-vessel atherosclerotic stroke (LAS) (17). Furthermore, an immunological analysis of individuals suffering from traumatic brain injury (TBI) revealed a universal increase in the number of IgD-CD24-B cells across all examined patients (18). In a cross-sectional study, investigators observed a significant increase in IgD- and CD24-expressing B cells among individuals diagnosed with myalgic encephalomyelitis/chronic fatigue syndrome (ME/CFS) (19). Moreover, contemporary Mendelian randomization (MR) studies have furnished compelling evidence, notably one such study illustrating that IgD+CD24-B cells significantly amplify the risk associated with the onset of Alzheimer's disease (20). Similarly, an additional recent MR investigation revealed an increased risk for Parkinson's disease development in the presence of IgD-CD24-B cells (21). Although these findings do not directly address the specific effects of IgD and CD24 deficiency on IS, they highlight the complexity of immune responses mediated through the IgD and CD24 proteins and their potential impact on neurological disorders.

Previous studies have shown that metabolites act as mediators that can reveal the relationship between genetic variation and disease, leading to a deeper understanding of the biological pathogenesis of human disease (22). Ascorbic acid 2-sulfate (AA2S), a phase II metabolite of ascorbic acid, is synthesized catalytically by sulfotransferases originating from the liver, exhibiting widespread distribution in the body (23), and is excreted mainly in the urine (24). Consequently, the concentration of AA2S could serve as an indicator of the metabolic processing of ascorbic acid (AA) (25). AA has a variety of physiological functions in the body, such as preventing the formation of oxygen free radicals, regulating inflammatory factors, reducing inflammatory cell infiltration, reversing endothelial dysfunction, enhancing microcirculation, and relieving microinflammatory conditions (26). Regarding the immune system, AA is a powerful first-line antioxidant with multifaceted roles. For example, it regulates the function of both innate and adaptive immune cells (27). It improves plasma cell differentiation by altering epigenetic patterns (28). It also acts as a cofactor in various biosynthetic pathways and influences redox pathways in the immune system (29, 30). Previous studies have shown that AA lowers the risk of IS by protecting the cardiovascular system against atherosclerosis through its anti-inflammatory, antioxidant, and endothelium-protective effects. In contrast, elevated levels of AA2S may suggest excessive AA depletion, which in turn increases the risk of IS (31, 32). Earlier Mendelian randomization studies revealed causal effects of AA2S levels on 26 disease traits across 12 categories in humans (33). However, this study did not identify a relationship between AA2S levels and IS. Accordingly, based on these findings, we postulate that the levels of AA2S could mediate the relationship between IgD-CD24-AC and IS.

Conventional observational epidemiological studies have numerous limitations in studying etiology and inferring causality due to confounding factors such as reverse causality and potential confounders (34). Therefore, a new design is needed to avoid or minimize these biases. Similar to randomized controlled trials (RCT), Mendelian randomization (MR) is a novel method for exploring causal relationships between exposures and outcomes (35). As a powerful statistical tool, it is used to infer causal relationships between exposures and outcomes (36). It provides a novel approach to exploring the relationship between IgD-CD24-AC and IS and its underlying mechanisms by exploiting genetic variability. The MR study design follows the Mendelian "random assignment of parental alleles to offspring," which avoids the interference of reverse causation bias and potential confounding factors, allowing us to make more robust causal inferences (37, 38). Previous studies have assessed the causal effects of various types of biomarkers (including circulating markers, cerebrospinal fluid markers, and gut microbiota markers) on neurological diseases through MR analysis (39–41). Moreover, with the increasing abundance of genome-wide association study (GWAS) data, MR analysis methods will be a key driver of progress in the field of neurology (42). Thus, it was essential to use the MR method to explore the effects of immune cells and metabolites on IS. The objectives of our study were (i) to determine whether IgD-CD24-AC is causally associated with IS and (ii) to assess the extent to which AA2S mediates the effect of IgD-CD24-AC on IS by mediation analysis.

2 Methods

2.1 Study design

A convincing Mendelian randomization (MR) design must meet three basic assumptions to ensure its scientific validity and effectiveness: (1) a significant association exists between the genetic instrumental variable and the exposure variable; (2) the genetic instrumental variable is independent of confounders, and (3) the genetic instrumental variable affects the outcome only through the exposure (43). Among these assumptions, the first hypothesis represents the causal hypothesis, while the second and third hypotheses collectively refer to pleiotropy (44), which can be tested using a range of statistical methods. In our study, we initially analyzed the effects of immune cells and metabolites on IS. Subsequently,

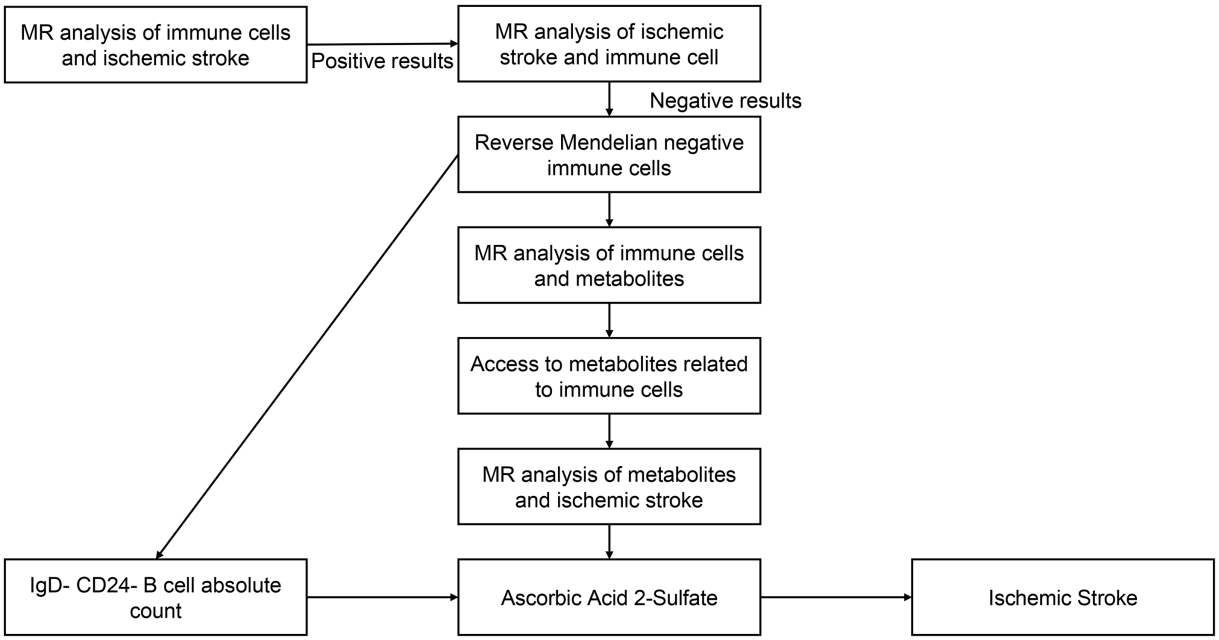

FIGURE 1
The flowchart of our MR analysis. IgD-CD24-AC, IgD-CD24-B-Cell absolute count, AA2S, Ascorbic Acid 2-Sulfate.

we explored the mutual causality between IgD-CD24-AC, AA2S, and IS by screening single nucleotide polymorphisms (SNPs) from 731 immune cells, 1,400 metabolites, and the FinnGen database using Mendelian randomization. These SNPs were defined as instrumental variables (IVs) (45). Figure 1 illustrates the flowchart of our analyses.

2.2 GWAS summary data sources

Data on IgD-CD24-AC were procured from a 2020 investigation conducted by Orrù et al. (46). The inquiry meticulously scrutinized 731 immunophenotypes, encompassing an array of parameters: 192 relative cell counts (RC), 32 morphometric attributes (MP), 118 absolute cell counts (AC), and 389 instances of median fluorescence intensity (MFI), the latter delineating the magnitude of surface antigen presence. Overall, this research revealed 122 substantial independent association signals distributed across 70 genetic loci, revealing 53 hitherto undiscovered loci and elucidating the molecules and mechanisms involved in the regulation of 459 cellular attributes. Furthermore, flow cytometry was used to determine 118 absolute cell counts (ACs), 389 median fluorescence intensities (MFIs) indicative of surface antigen levels, 32 morphological parameters (MPs), and 192 relative cell counts (RCs). The MFI indicates protein expression levels in designated cell subpopulations and reflects the median fluorescence emitted by a targeted protein. For example, the trait "IgD-CD24-B-cell" represents a negative B-cell for both IgD and CD24. These GWAS data include 3,757 nonoverlapping European individuals, including 22 million SNPs, and were tested for correlations after controlling for covariates such as age, age^2, and sex.

Our data on AA2S come from the study by Chen (47), the most comprehensive survey of genetic loci for blood metabolites to date. Chen conducted a series of large GWASs, including the testing of 1,091 metabolites and 309 metabolite ratios in 8,299 individuals from the Canadian Longitudinal Study of Aging (CLSA) cohort. Of the 1,091 metabolites tested, 850 had known properties in eight super pathways (i.e., lipids, amino acids, xenobiotics, nucleotides, cofactors and vitamins, carbohydrates, peptides, and energy). The residual cohort of 241 molecular entities was categorized as either unknown or possessing partial characterization. These metabolites were subjected to stringent Bonferroni correction and adjusted for the total number of metabolites tested ($p < 5 \times 10^{-8}/1{,}091 = 4.58 \times 10^{-11}$). AA2S is metabolized via the super-pathway of vitamin C. The metabolism of AA2S was also determined by Bonferroni correction ($p < 5 \times 10^{-8}/1{,}091 = 4.58 \times 10^{-11}$).

To minimize sample overlap, we utilized IS data from the FinnGen consortium (Round 10)[1] as our outcomes. A total of 374,631 controls and 1,485 patients with IS were included in our research; all of the participants were of European descent. The FinnGen study is a large-scale genomics initiative that has analyzed over 500,000 Finnish biobank samples and correlated genetic variation with health data to understand disease mechanisms and predispositions. The project involves collaboration between research organizations and biobanks in Finland and international industry partners (48).

2.3 Instrumental variable selection and data harmonization

For MR analyses, the genetic variants utilized must be representative of the characteristics of IgD-D24-AC and

1 https://www.finngen.fi/en

AA2S. Based on previous similar studies (49, 50), we selected single nucleotide polymorphisms (SNPs) with p values less than (1×10^{-5}) as instrumental variables (IVs) to make them more informative. Furthermore, SNPs that exhibited a linkage disequilibrium (LD) coefficient (r^2) of less than 0.001 and those positioned more than 10,000 kilobases apart were chosen to ensure independence. To quantify the strength of the IV, we calculated the F value using the genetic variance (R^2), total sample size (N), and number of IVs (k) with the formula $F = R^2(N - k - 1)/k(1 - R^2)$, where the genetic variance is considered weak when the F statistic is less than 10, which may bias the results (51, 52). Due to the binary nature of the outcomes being investigated, ratio estimates had to be transformed to produce the appropriate odds ratios (OR) and 95% confidence intervals (53).

2.4 Statistical analysis

All analyses were conducted using R version 4.3.2.[2] The "Two Sample MR package" (54) (version 0.5.9) was used for the analyses. Additionally, the MR-Pleiotropy RESidual Sum and Outlier (MR-PRESSO) and robust adjusted profile score (MR. RAPS) methods were applied using the R packages "MRPRESSO" and "MR.raps." Moreover, the statistical power for MR was calculated using mRnd.[3]

2.5 Mediation analyses

Figure 2 presents an analysis schematic. We conducted two-sample bidirectional Mendelian randomization to evaluate the reciprocal causality between IgD-CD24-AC and the IS (Figure 2A), which was referred to as the total effect (beta. all).

The causal relationship between IgD-CD24-AC and IS was assessed through a suite of methods: inverse variance weighting (IVW) (35), weighted median (WMN) (55), MR-Egger (56), and simple model and weighted model (57). Employing the IVW approach, which aggregates Wald ratio estimates of each instrumental SNP through a meta-analysis-like methodology, allowed for precise effect estimation. The results are reported as beta values with 95% confidence intervals (CIs) for standard errors and odds ratios (ORs) for continuous outcomes. For binary outcomes, $p < 0.05$ was considered nominally significant. The MR–Egger method, complemented by weighted median, weighted modal, and simple modal analyses, was used to assess multivariate validity as a Supplementary Method to bolster the reliability of IVW findings. A principal advantage of the weighted median approach lies in its ability to yield consistent causality estimates, even when more than 50% of the instrumental variables are invalidated (55).

An investigation into whether AA2S mediated the causal pathway from IgD-CD24-AC to IS outcomes (Figure 2B), which was involved in conducting mediation analyses, was performed using a two-step MR. The overall effect can be broken down into indirect (mediated) and direct effects (58). Therefore, the impact of IgD-CD24-AC on IS was divided into two components: (1) the direct effect of IgD-CD24-AC on IS (direct effect in Figure 2B) and (2) the indirect effect of IgD-CD24-AC on IS mediated by AA2S (beta1 × beta2 in Figure 2B). Subsequently, we calculated the percentage of mediated effects by dividing the indirect effect by the total effect. Additionally, we used the delta method to calculate 95% confidence intervals (59).

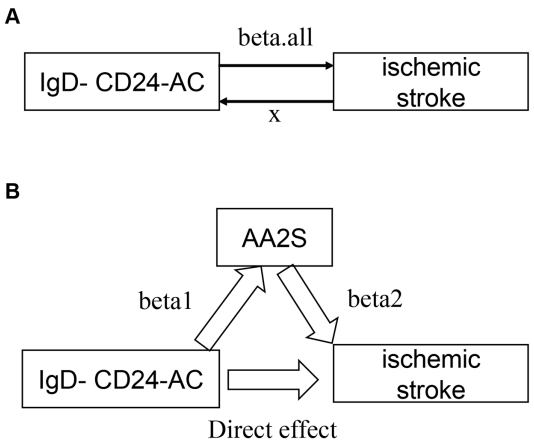

FIGURE 2
Graphs illustrate the associations examined in this study. **(A)** Total effect "beta. All" of IgD-CD24-AC with ischemic stroke. **(B)** Total effect de-composed as (i) mediated effect using a two-step approach "beta12" = beta1 × beta2 (where "beta1" is the total effect of IgD-CD24-AC on AA2S and "beta2" is the effect of AA2S on ischemic stroke effect) (ii) direct effect = "total effect" – "mediated effect" (beta. All-beta12). The mediated ratio is the indirect effect divided by the total effect. IgD-CD24-AC, IgD-CD24-B Cell absolute count, AA2S, Ascorbic Acid 2-Sulfate.

2.6 Sensitivity analyses

Heterogeneity markers from the IVW and MR–Egger approaches (Cochran Q-derived $p < 0.05$) were utilized as indicators of potential pleiotropy (60–62). By contrasting the Egger intercept term with the null result, MR–Egger analysis was able to evaluate directional pleiotropy (55). In addition, the MR-PRESSO test was used to assess the total pleiotropy of the studies and to identify any SNPs that were unusual or showed horizontal pleiotropy. To ensure the robustness of the effects, the MR analysis included an assessment before and after the removal of outlier SNPs (56, 62). If an outlier SNP was detected ($p < 0.05$), it was excluded, and the causal and sensitivity analyses were reconducted using a random-effects model to ensure the reliability of the results.

3 Results

3.1 Primary results

Among 731 immune cells and 1,400 metabolites, 30 immune cell features were initially identified as being associated with IS by the IVW method (Supplementary Figure S1), as well as 36 metabolites (Supplementary Figure S2). After performing a two-step MR analysis (Figure 1) and sensitivity analyses, it was finally determined that IgD-CD24-AC was associated with IS and that AA2S acted as its mediator.

2 https://www.r-project.org/

3 https://cnsgenomics.shinyapps.io/mRnd/

3.2 Association of IgD-CD24-AC with IS

Characteristics of significant SNPs with genome-wide associations in Supplementary Table S2. All SNPs used to measure IgD-CD24-AC exposure had *F* values greater than 10. We identified 18 SNPs as instrumental variables. Our results revealed a causal effect of IgD-CD24-AC on IS. As shown in Figures 3A, 4, the positive correlation between IgD-CD24-AC and the IS was broadly and consistently demonstrated across all five MR analysis methods. Employing the IVW approach, the risk ratio of IgD-CD24-AC to IS was estimated to be 1.216 (95% CI = 1.079–1.371, $p = 0.001$). This result was supported by both the weighted median method (OR = 1.204, 95% CI = 1.020–1.421, $p = 0.028$) and the MR–Egger method (OR = 1.177, 95% CI = 0.962–1.442, $p = 0.133$). The same trend was also observed in the simple and weighted models. The detailed results are displayed in Figure 5.

3.3 Association of IgD-CD24-AC with AA2S

Supplementary Table S4 contains Characteristics of significant SNPs with genome-wide associations and the F-statistics for all SNPs utilized in MR studies that were larger than 10. Figure 3B shows that genetically predicted IgD-CD24-AC was positively linked and trended consistently with AA2S risk using the five MR analysis methods., we discovered that genetically predicted IgD-CD24-AC was positively

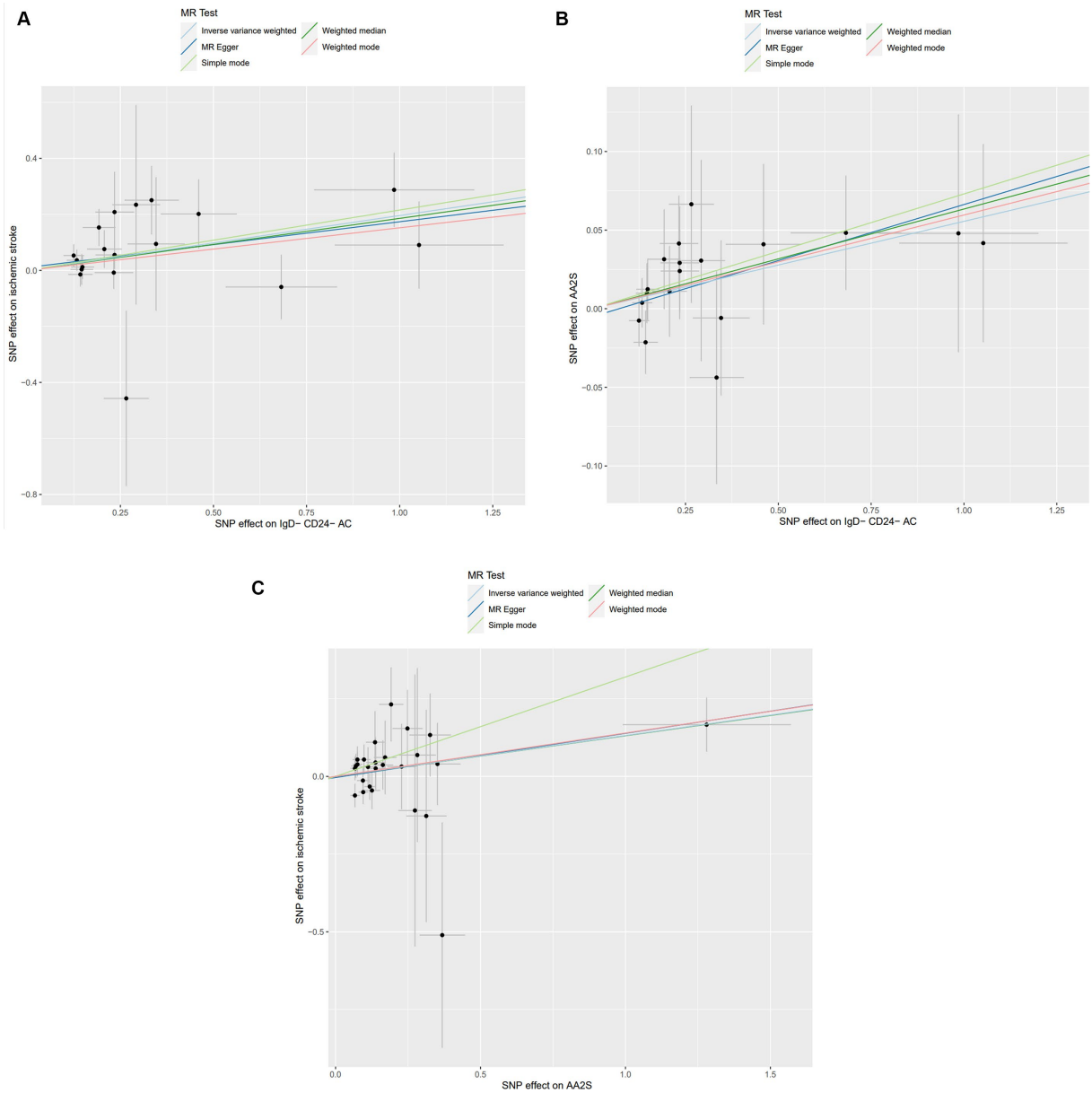

FIGURE 3
Scatter plot of genetic association between IgD-CD24-AC, AA2S, and IS. **(A)** Association of IgD-CD24-AC with IS; **(B)** Association of IgD-CD24-AC with AA2S; **(C)** Association of AA2S with IS. The slope and direction of the straight line represent the magnitude and direction of the causal relationship. IgD-CD24-AC, IgD-CD24-B Cell absolute count, AA2S, Ascorbic Acid 2-Sulfate.

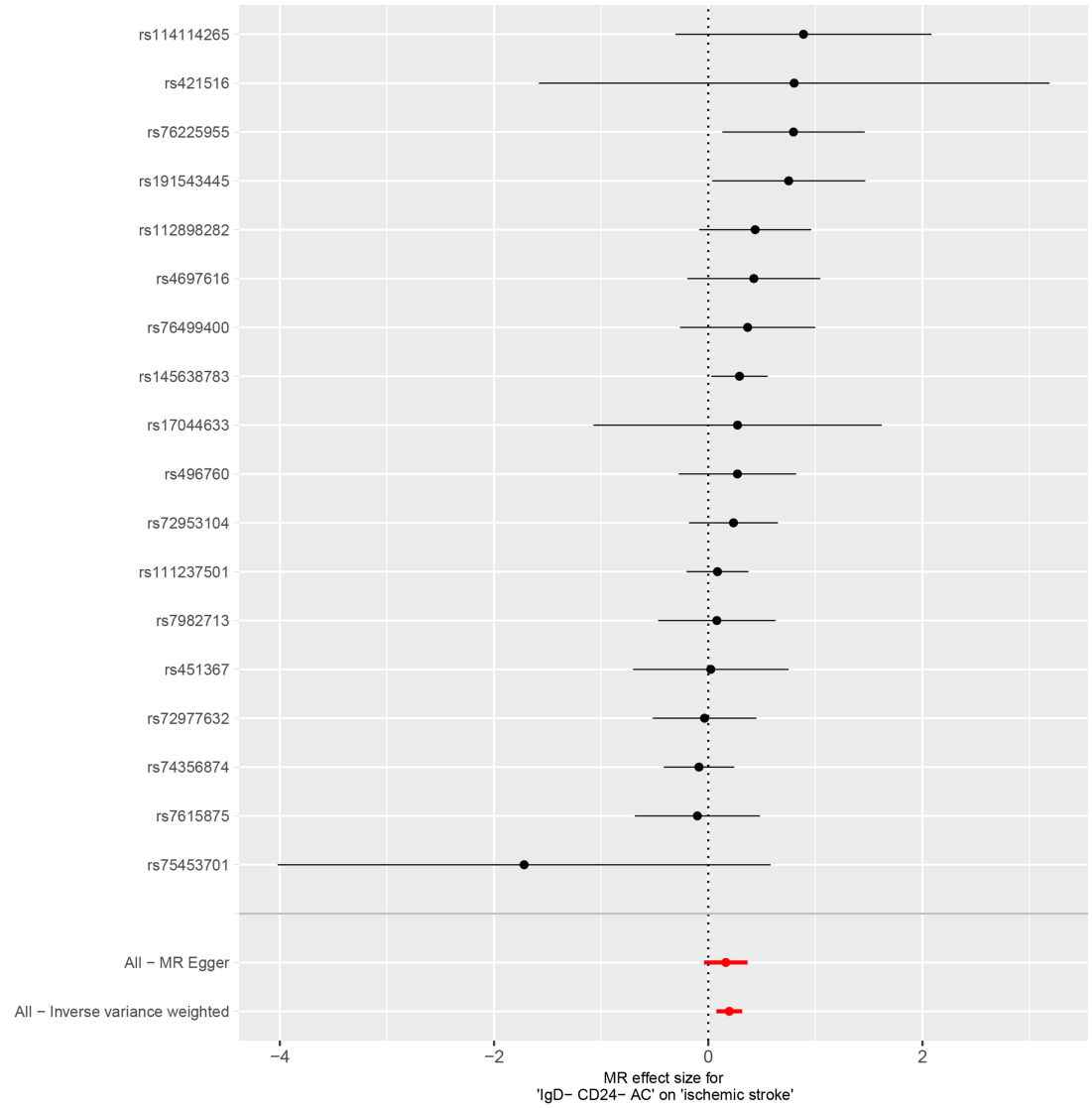

FIGURE 4
Forest plot of genetic association between IgD-CD24-AC and IS.

linked and trended consistently with AA2S risk using the five MR analysis methods. Specifically, the IVW method estimated the ratio of initial IgD-CD24-AC to IS risk to be 1.057 (95% CI = 1.006–1.111, $p = 0.028$). The weighted median (OR = 1.065, 95% CI = 0.998–1.137, $p = 0.057$) and MR–Egger (OR = 1.074, 95% CI = 0.990–1.165, $p = 0.106$) estimates were consistent. The detailed results are shown in Figure 5.

3.4 Association of AA2S with IS

The SNP data can be found in Supplementary Table S5. Every genetic tool linked to AA2S is listed here at the genome-wide significance level ($p < 5 \times 10^{-5}$). The results from the genetic prediction using the IVW method showed a strong positive association between AA2S and IS (OR = 1.140, 95% CI, 1.020–1.275; $p = 0.021$). As shown in Figure 3C, all four of the remaining methods had consistent estimation directions. Figure 5 shows the detailed results.

3.5 Proportion of the association between IgD-CD24-AC and IS mediated by AA2S

The link between IgD-CD24-AC and the IS is mediated by AA2S. According to our research, AA2S was responsible for 3.73% of the elevated risk of IS linked to IgD-CD24-AC (mediator ratio: 3.73%; −3.88, 11.3%). Figure 6 displays the results.

3.6 Sensitivity analysis

We performed a series of sensitivity analyses to identify and address the existence of heterogeneity and pleiotropy in causality estimation. Neither the Cochran's Q test nor the MR-Egger intercept showed evidence of heterogeneity in causality between these SNPs. We assessed potential horizontal pleiotropy in our study, which showed no horizontal pleiotropy. In addition, no influential SNPs were

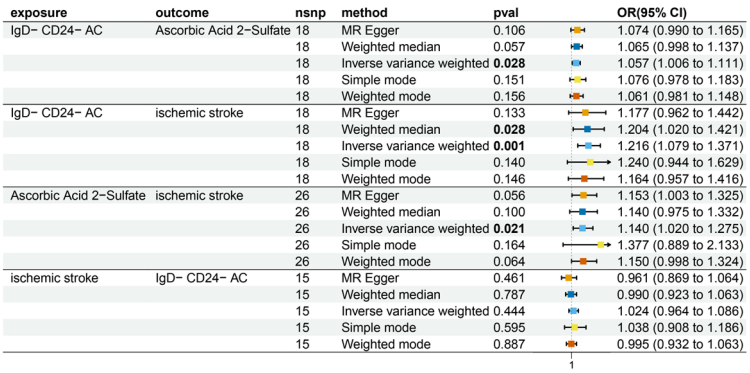

FIGURE 5
Forest plot to visualize the causal effects of AA2S with IgD-CD24-AC and ischemic stroke. IgD-CD24-AC, IgD-CD24-B Cell absolute count, AA2S, Ascorbic Acid 2-Sulfate.

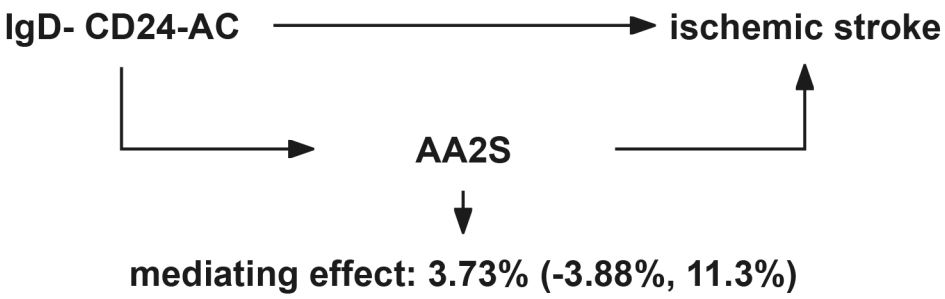

FIGURE 6
Schematic diagram of the AA2S mediation effect. IgD-CD24-AC, IgD-CD24-B Cell absolute count, AA2S, Ascorbic Acid 2-Sulfate.

detected in the "leave-one-out" analysis when any of the SNPs were excluded sequentially. The distribution of the funnel plots was also symmetrical. These results indicate that all SNPs were significant for causality and that there was no heterogeneity or pleiotropy (Supplementary Table S6; Supplementary Figures S3, S4).

4 Discussion

In this study, we primarily identified 30 immune cells and 36 metabolites associated with IS. Then we used available genome-wide association study (GWAS) data with MR analysis to investigate the association between IgD-CD24-AC and IS and examined whether this causality was mediated through AA2S. The results showed that genetically predicted IgD-CD24-AC levels were significantly associated with an increased risk of IS (a 21.6% increase in AA2S risk for every 1 SD increase in IgD-CD24-AC) and that 3.73% of this effect was mediated through AA2S. This study represents a pioneering effort to systematically delineate the causal relationship between IgD-CD24-AC and IS and to confirm the role of AA2S as a mediator.

One of the vital pathological mechanisms of acute IS is the dysregulation of inflammatory and adaptive immune responses (63, 64). The immune response is frequently associated with oxidative stress (65), which is a state of cellular damage resulting from the overproduction of reactive oxygen species (ROS). When ROS concentrations exceed the ability of antioxidants to maintain redox balance, cellular and vascular damage occurs (66). Abnormalities in energy metabolism and brain tissue infarction caused by IS increase ROS levels in the affected area, causing the release of inflammatory factors, which stimulate an immune response (67–69). Previous studies have suggested that a compromised blood–brain barrier after an IS may facilitate the entry of B cells and other peripheral immune cells into damaged brain tissue (10, 11). However, the specific effects of the absence of IgD and CD24 proteins on the surface of B cells on IS and the underlying mechanisms are unclear, suggesting the need to explore further the nuanced roles of IgD and CD24 in IS. Previous research has indicated that CD24 functions as a growth-promoting factor and can trigger adenosine monophosphate kinase (AMPK) activation via phosphorylation, which is one of the critical signals in the overall metabolic pathway (70). Cells can activate this pathway under hypoxic conditions to boost ATP production and maintain energy balance. Furthermore, research has shown that when this enzyme is deactivated, CD24 expression decreases (15). IgD is crucial for regulating both innate and adaptive immune responses (13). If IgD

is not present on the B-cell surface, it can lead to maladaptive immunity. Research has demonstrated that dysfunctional immune processes can result in a greater likelihood of experiencing stroke (63). In addition, IgD transmits regulatory signals at the B-cell receptor (BCR) to promote the formation of protective immunoglobulins, which helps to prevent autoimmune reactions and prevent early apoptosis (71). Studies in mouse models have highlighted the role of IgD in preventing premature differentiation of B cells into short-lived plasma cells (72). Thus, CD24 is crucial for B-cell selection and development (14). B cells that do not express CD24 and IgD not only have a weaker immune response but also a shorter lifespan. This study confirmed that the risk of IS increases with an increase in the number of IgD-CD24-B cells. One possible mechanism is the impaired energy metabolism of immune cells and reduced immune response capacity due to the absence of CD24 and IgD, which consequently elevates the risk of IS.

The strength of our study lies in the utilization of comprehensive, up-to-date data on 731 immune cells, 1,400 metabolites, and various IS datasets from multiple databases. Through magnetic resonance analysis, we hypothesize that the presence of IgD and CD24 on B immune cells elevates the risk of IS. AA2S, a metabolite of AA, has been shown in early animal experiments to possess weaker antioxidant properties compared to AA (73). Some experiments suggest that AA may mediate the interaction between immune cells and disease through complex mechanisms (31, 32). However, research on the correlation between AA2S and immune cells remains limited. Our findings indicate that the antioxidant effect of AA2S diminishes as its levels increase, thus elevating the risk of IS. This aligns with the correlation between IgD-CD24-AC and IS. Further mediation analyses have demonstrated that AA2S leads to increased levels of IgD-CD24-AC, heightening the risk of IS by 3.73%. Although the percentage is relatively small and other mediators that have not yet been investigated may also have a role, this is still clinically significant. This study provides theoretical support for strategies to prevent, reverse, and mitigate IS. It also highlights the dual role of AA2S in increasing IS risk, both directly and mediated by IgD-CD24-AC. These insights are crucial for the development of targeted immune therapies and for establishing a solid foundation for the advancement of precision medicine.

There are several limitations in this study. Our findings should be interpreted cautiously when applying them to ethnicities other than European populations due to the limited SNP data available. Second, despite our attempts to identify and remove abnormal variations, we cannot entirely exclude the potential influence of pleiotropy on our findings. In our study, we utilized summary-level statistics instead of individual-level data. Hence, we could not investigate causal relationships between subgroups such as females and males in more depth. The genetic prediction rate of IS mediated by AA2S levels in our study was 3.73%, indicating a very low level of prediction. More research is needed to investigate and measure more potential mediators in the future.

5 Conclusion

Our study identified a causal relationship between the Absolute Count of IgD-CD24-B cells and IS, a small part of which is mediated by AA2S levels. These findings offer critical insights for developing immune-targeted therapies in the future and lay a strong foundation for advancements in precision medicine.

Data availability statement

The datasets presented in this study can be found in online repositories. The names of the repository/repositories and accession number(s) can be found in the article/Supplementary material.

Ethics statement

Ethical review and approval was not required for the study on human participants in accordance with the local legislation and institutional requirements. Written informed consent from the patients/participants or patients/participants' legal guardian/next of kin was not required to participate in this study in accordance with the national legislation and the institutional requirements.

Author contributions

HH: Conceptualization, Data curation, Formal analysis, Writing – original draft, Writing – review & editing. MZ: Conceptualization, Data curation, Writing – original draft. YZ: Conceptualization, Writing – original draft. JM: Conceptualization, Data curation, Writing – original draft, Writing – review & editing. XY: Conceptualization, Data curation, Methodology, Writing – original draft, Writing – review & editing.

Funding

The author(s) declare that no financial support was received for the research, authorship, and/or publication of this article.

Acknowledgments

The authors sincerely want to acknowledge the participants and investigators of the FinnGen study, as well as the associated consortiums and the original GWASs for managing and sharing the summary statistics.

Conflict of interest

The authors declare that the research was conducted in the absence of any commercial or financial relationships that could be construed as a potential conflict of interest.

Publisher's note

All claims expressed in this article are solely those of the authors and do not necessarily represent those of their affiliated organizations, or those of the publisher, the editors and the reviewers. Any product that may be evaluated in this article, or claim that may be made by its manufacturer, is not guaranteed or endorsed by the publisher.

Supplementary material

The Supplementary material for this article can be found online at: https://www.frontiersin.org/articles/10.3389/fneur.2024.1405108/full#supplementary-material

References

1. Zhao Y, Zhang X, Chen X, Wei Y. Neuronal injuries in cerebral infarction and ischemic stroke: from mechanisms to treatment (review). *Int J Mol Med*. (2022) 49:15. doi: 10.3892/ijmm.2021.5070

2. Hasan TF, Hasan H, Kelley RE. Overview of acute ischemic stroke evaluation and management. *Biomedicines*. (2021) 9:1486. doi: 10.3390/biomedicines9101486

3. Feske SK. Ischemic stroke. *Am J Med*. (2021) 134:1457–64. doi: 10.1016/j.amjmed.2021.07.027

4. O'Donnell MJ, Chin SL, Rangarajan S, Xavier D, Liu L, Zhang H, et al. Global and regional effects of potentially modifiable risk factors associated with acute stroke in 32 countries (INTERSTROKE): a case-control study. *Lancet*. (2016) 388:761–75. doi: 10.1016/S0140-6736(16)30506-2

5. Feigin VL, Stark BA, Johnson CO, Roth GA, Bisignano C, Abady GG, et al. Global, regional, and national burden of stroke and its risk factors, 1990–2019: a systematic analysis for the global burden of disease study 2019. *Lancet Neurol*. (2021) 20:795–820. doi: 10.1016/S1474-4422(21)00252-0

6. Wang Z, Pan J, Yuan R, Chen M, Guo X, Zhou S. Shell-sheddable polymeric micelles alleviate oxidative stress and inflammation for enhanced ischemic stroke therapy. *Nano Lett*. (2023) 23:6544–52. doi: 10.1021/acs.nanolett.3c01567

7. Lv M, Zhang Z, Cui Y. Unconventional T cells in brain homeostasis, injury and neurodegeneration. *Front Immunol*. (2023) 14:1273459. doi: 10.3389/fimmu.2023.1273459

8. Wang H, Zhang S, Xie L, Zhong Z, Yan F. Neuroinflammation and peripheral immunity: focus on ischemic stroke. *Int Immunopharmacol*. (2023) 120:110332. doi: 10.1016/j.intimp.2023.110332

9. Zhang Z, Lv M, Zhou X, Cui Y. Roles of peripheral immune cells in the recovery of neurological function after ischemic stroke. *Front Cell Neurosci*. (2022) 16:1013905. doi: 10.3389/fncel.2022.1013905

10. Malone MK, Ujas TA, Britsch DRS, Cotter KM, Poinsatte K, Stowe AM. The immunopathology of B lymphocytes during stroke-induced injury and repair. *Semin Immunopathol*. (2023) 45:315–27. doi: 10.1007/s00281-022-00971-3

11. Pattarabanjird T, Li C, McNamara C. B cells in atherosclerosis: mechanisms and potential clinical applications. *JACC Basic Transl Sci*. (2021) 6:546–63. doi: 10.1016/j.jacbts.2021.01.006

12. Deng X, Hou S, Wang Y, Yang H, Wang C. Genetic insights into the relationship between immune cell characteristics and ischemic stroke: a bidirectional mendelian randomization study. *Eur J Neurol*. (2024) 31:e16226. doi: 10.1111/ene.16226

13. Gutzeit C, Chen K, Cerutti A. The enigmatic function of IgD: some answers at last. *Eur J Immunol*. (2018) 48:1101–13. doi: 10.1002/eji.201646547

14. Mensah FFK, Armstrong CW, Reddy V, Bansal AS, Berkovitz S, Leandro MJ, et al. CD24 expression and B cell maturation shows a novel link with energy metabolism: potential implications for patients with myalgic encephalomyelitis/chronic fatigue syndrome. *Front Immunol*. (2018) 9:2421. doi: 10.3389/fimmu.2018.02421

15. Zhou J, Huang W, Tao R, Ibaragi S, Lan F, Ido Y, et al. Inactivation of AMPK alters gene expression and promotes growth of prostate cancer cells. *Oncogene*. (2009) 28:1993–2002. doi: 10.1038/onc.2009.63

16. Chen C, Liu Q, Li Y, Yu J, Wang S, Liu L. Impact of immune cells on stroke limited to specific subtypes: evidence from mendelian randomization study. *Neurol Ther*. (2024). doi: 10.1007/s40120-024-00592-y

17. Wang M, Zhang X, Fan R, Zhang L. Causal role of immune cell traits in stroke: a mendelian randomization study. *J Stroke Cerebrovasc Dis*. (2024) 33:107625. doi: 10.1016/j.jstrokecerebrovasdis.2024.107625

18. Magatti M, Pischiutta F, Ortolano F, Pasotti A, Caruso E, Cargnoni A, et al. Systemic immune response in young and elderly patients after traumatic brain injury. *Immun Ageing*. (2023) 20:41. doi: 10.1186/s12979-023-00369-1

19. Mensah F, Bansal A, Berkovitz S, Sharma A, Reddy V, Leandro MJ, et al. Extended B cell phenotype in patients with myalgic encephalomyelitis/chronic fatigue syndrome: a cross-sectional study. *Clin Exp Immunol*. (2016) 184:237–47. doi: 10.1111/cei.12749

20. Liao J, Zhang Y, Tang Z, Liu P, He L. Causal relationships between peripheral immune cells and alzheimer's disease: a two-sample mendelian randomization study. *Neurol Sci*. (2024). doi: 10.1007/s10072-024-07324-y

21. Song J, Qin Y, Wang L, Quan W, Xu J, Li J, et al. Exploring the causal relationship between B lymphocytes and parkinson's disease: a bidirectional, two-sample mendelian randomization study. *Sci Rep*. (2024) 14:2783. doi: 10.1038/s41598-024-53287-7

22. Gieger C, Geistlinger L, Altmaier E, Hrabé De Angelis M, Kronenberg F, Meitinger T, et al. Genetics meets metabolomics: a genome-wide association study of metabolite profiles in human serum. *PLoS Genet*. (2008) 4:e1000282. doi: 10.1371/journal.pgen.1000282

23. Fluharty AL, Stevens RL, Miller RT, Shapiro SS, Kihara H. Ascorbic acid-2-sulfate sulfhohydrolase activity of human arylsulfatase a. *Biochim Biophys Acta*. (1976) 429:508–16. doi: 10.1016/0005-2744(76)90298-9

24. Tsujimura M, Fukuda T, Kasai T. Studies on the excretion of ascorbic acid 2-sulfate and total vitamin C into human urine after oral administration of ascorbic acid 2-sulfate. *J Nutr Sci Vitaminol*. (1982) 28:467–76. doi: 10.3177/jnsv.28.467

25. Yin X, Li J, Bose D, Okamoto J, Kwon A, Jackson AU, et al. Metabolome-wide mendelian randomization characterizes heterogeneous and shared causal effects of metabolites on human health. *medRxiv* [Preprint]. (2023).

26. Nosewicz J, Spaccarelli N, Roberts KM, Hart PA, Kaffenberger JA, Trinidad JC, et al. The epidemiology, impact, and diagnosis of micronutrient nutritional dermatoses part 1: zinc, selenium, copper, vitamin a, and vitamin C. *J Am Acad Dermatol*. (2022) 86:267–78. doi: 10.1016/j.jaad.2021.07.079

27. Maity J, Majumder S, Pal R, Saha B, Mukhopadhyay PK. Ascorbic acid modulates immune responses through jumonji-C domain containing histone demethylases and ten eleven translocation (TET) methylcytosine dioxygenase. *BioEssays*. (2023) 45:e2300035. doi: 10.1002/bies.202300035

28. Chen H-Y, Almonte-Loya A, Lay F-Y, Hsu M, Johnson E, González-Avalos E, et al. Epigenetic remodeling by vitamin C potentiates plasma cell differentiation. *eLife*. (2022) 11:e73754. doi: 10.7554/eLife.73754

29. Linster CL, Van Schaftingen E, Vitamin C. Biosynthesis, recycling and degradation in mammals. *FEBS J*. (2007) 274:1–22. doi: 10.1111/j.1742-4658.2006.05607.x

30. Munteanu C, Schwartz B. The relationship between nutrition and the immune system. *Front Nutr*. (2022) 9:1082500. doi: 10.3389/fnut.2022.1082500

31. Zhong S, Li L, Shen X, Li Q, Xu W, Wang X, et al. An update on lipid oxidation and inflammation in cardiovascular diseases. *Free Radic Biol Med*. (2019) 144:266–78. doi: 10.1016/j.freeradbiomed.2019.03.036

32. Tang X, Liu H, Xiao Y, Wu L, Shu P. Vitamin C intake and ischemic stroke. *Front Nutr*. (2022) 9:935991. doi: 10.3389/fnut.2022.935991

33. Tang H-Y, Huang J-E, Tsau M-T, Chang C-J, Tung Y-C, Lin G, et al. Metabolomics assessment of volume overload-induced heart failure and oxidative stress in the kidney. *Metabolites*. (2023) 13:1165. doi: 10.3390/metabo13111165

34. Smith GD, Ebrahim S. "Mendelian randomization": can genetic epidemiology contribute to understanding environmental determinants of disease? *Int J Epidemiol*. (2003) 32:1–22. doi: 10.1093/ije/dyg070

35. Burgess S, Small DS, Thompson SG. A review of instrumental variable estimators for mendelian randomization. *Stat Methods Med Res*. (2017) 26:2333–55. doi: 10.1177/0962280215597579

36. Paternoster L, Tilling K, Davey SG. Genetic epidemiology and mendelian randomization for informing disease therapeutics: conceptual and methodological challenges. *PLoS Genet*. (2017) 13:e1006944. doi: 10.1371/journal.pgen.1006944

37. Larsson SC. Mendelian randomization as a tool for causal inference in human nutrition and metabolism. *Curr Opin Lipidol*. (2021) 32:1–8. doi: 10.1097/MOL.0000000000000721

38. Sekula P, Del Greco MF, Pattaro C, Köttgen A. Mendelian randomization as an approach to assess causality using observational data. *J Am Soc Nephrol*. (2016) 27:3253–65. doi: 10.1681/ASN.2016010098

39. Zeng Y, Cao S, Yang H. Circulating sex hormone-binding globulin levels and ischemic stroke risk: a mendelian randomization study. *Postgrad Med J*. (2023) 99:1272–9. doi: 10.1093/postmj/qgad083

40. Zeng Y, Guo R, Cao S, Liu C, Yang H. CSF N-acylethanolamine acid amidase level and parkinson's disease risk: a mendelian randomization study. *Parkinsonism Relat Disord*. (2024) 123:106953. doi: 10.1016/j.parkreldis.2024.106953

41. Zeng Y, Cao S, Yang H. Roles of gut microbiome in epilepsy risk: a mendelian randomization study. *Front Microbiol*. (2023) 14:1115014. doi: 10.3389/fmicb.2023.1115014

42. Gagnon E, Daghlas I, Zagkos L, Sargurupremraj M, Georgakis MK, Anderson CD, et al. Mendelian randomization applied to neurology: promises and challenges. *Neurology*. (2024) 102:e209128. doi: 10.1212/WNL.0000000000209128

43. Boef AGC, Dekkers OM, le Cessie S. Mendelian randomization studies: a review of the approaches used and the quality of reporting. *Int J Epidemiol*. (2015) 44:496–511. doi: 10.1093/ije/dyv071

44. Emdin CA, Khera AV, Kathiresan S. Mendelian Randomization. *JAMA*. (2017) 318:1925–6. doi: 10.1001/jama.2017.17219

45. Davey Smith G, Hemani G. Mendelian randomization: genetic anchors for causal inference in epidemiological studies. *Hum Mol Genet*. (2014) 23:R89–98. doi: 10.1093/hmg/ddu328

46. Orrù V, Steri M, Sidore C, Marongiu M, Serra V, Olla S, et al. Complex genetic signatures in immune cells underlie autoimmunity and inform therapy. *Nat Genet*. (2020) 52:1036–45. doi: 10.1038/s41588-020-0684-4

47. Chen Y, Lu T, Pettersson-Kymmer U, Stewart ID, Butler-Laporte G, Nakanishi T, et al. Genomic atlas of the plasma metabolome prioritizes metabolites implicated in human diseases. *Nat Genet*. (2023) 55:44–53. doi: 10.1038/s41588-022-01270-1

48. Kurki MI, Karjalainen J, Palta P, Sipilä TP, Kristiansson K, Donner KM, et al. FinnGen provides genetic insights from a well-phenotyped isolated population. *Nature*. (2023) 613:508–18. doi: 10.1038/s41586-022-05473-8

49. Wang C, Zhu D, Zhang D, Zuo X, Yao L, Liu T, et al. Causal role of immune cells in schizophrenia: Mendelian randomization (MR) study. *BMC Psychiatry*. (2023) 23:590. doi: 10.1186/s12888-023-05081-4

50. Guo M-N, Hao X-Y, Tian J, Wang Y-C, Li J-D, Fan Y, et al. Human blood metabolites and lacunar stroke: a mendelian randomization study. *Int J Stroke*. (2023) 18:109–16. doi: 10.1177/17474930221140792

51. Burgess S, Thompson SGCRP CHD Genetics Collaboration. Avoiding bias from weak instruments in Mendelian randomization studies. *Int J Epidemiol*. (2011) 40:755–64. doi: 10.1093/ije/dyr036

52. Palmer TM, Lawlor DA, Harbord RM, Sheehan NA, Tobias JH, Timpson NJ, et al. Using multiple genetic variants as instrumental variables for modifiable risk factors. *Stat Methods Med Res*. (2012) 21:223–42. doi: 10.1177/0962280210394459

53. Burgess S, Labrecque JA. Mendelian randomization with a binary exposure variable: interpretation and presentation of causal estimates. *Eur J Epidemiol*. (2018) 33:947–52. doi: 10.1007/s10654-018-0424-6

54. Yavorska OO, Burgess S. MendelianRandomization: an R package for performing mendelian randomization analyses using summarized data. *Int J Epidemiol*. (2017) 46:1734–9. doi: 10.1093/ije/dyx034

55. Bowden J, Davey Smith G, Haycock PC, Burgess S. Consistent estimation in Mendelian randomization with some invalid instruments using a weighted median estimator. *Genet Epidemiol*. (2016) 40:304–14. doi: 10.1002/gepi.21965

56. Burgess S, Thompson SG. Interpreting findings from mendelian randomization using the MR-egger method. *Eur J Epidemiol*. (2017) 32:377–89. doi: 10.1007/s10654-017-0255-x

57. Hartwig FP, Davey Smith G, Bowden J. Robust inference in summary data mendelian randomization via the zero modal pleiotropy assumption. *Int J Epidemiol*. (2017) 46:1985–98. doi: 10.1093/ije/dyx102

58. Carter AR, Sanderson E, Hammerton G, Richmond RC, Davey Smith G, Heron J, et al. Mendelian randomisation for mediation analysis: current methods and challenges for implementation. *Eur J Epidemiol*. (2021) 36:465–78. doi: 10.1007/s10654-021-00757-1

59. Leal SM. Genetics and analysis of quantitative traits. *Am J Hum Genet*. (2001) 68:548–9. doi: 10.1086/318209

60. Greco MFD, Minelli C, Sheehan NA, Thompson JR. Detecting pleiotropy in mendelian randomisation studies with summary data and a continuous outcome. *Stat Med*. (2015) 34:2926–40. doi: 10.1002/sim.6522

61. Burgess S, Bowden J, Fall T, Ingelsson E, Thompson SG. Sensitivity analyses for robust causal inference from mendelian randomization analyses with multiple genetic variants. *Epidemiology*. (2017) 28:30–42. doi: 10.1097/EDE.0000000000000559

62. Verbanck M, Chen C-Y, Neale B, Do R. Detection of widespread horizontal pleiotropy in causal relationships inferred from mendelian randomization between complex traits and diseases. *Nat Genet*. (2018) 50:693–8. doi: 10.1038/s41588-018-0099-7

63. Endres M, Moro MA, Nolte CH, Dames C, Buckwalter MS, Meisel A. Immune pathways in etiology, acute phase, and chronic sequelae of ischemic stroke. *Circ Res*. (2022) 130:1167–86. doi: 10.1161/CIRCRESAHA.121.319994

64. Iadecola C, Buckwalter MS, Anrather J. Immune responses to stroke: mechanisms, modulation, and therapeutic potential. *J Clin Invest*. (2020) 130:2777–88. doi: 10.1172/JCI135530

65. Sierra C, Coca A, Schiffrin EL. Vascular mechanisms in the pathogenesis of stroke. *Curr Hypertens Rep*. (2011) 13:200–7. doi: 10.1007/s11906-011-0195-x

66. Allen CL, Bayraktutan U. Oxidative stress and its role in the pathogenesis of ischaemic stroke. *Int J Stroke*. (2009) 4:461–70. doi: 10.1111/j.1747-4949.2009.00387.x

67. Wang Z, Zhao Y, Hou Y, Tang G, Zhang R, Yang Y, et al. A thrombin-activated peptide-templated nanozyme for remedying ischemic stroke via thrombolytic and neuroprotective actions. *Adv Mater*. (2023) 36:e2210144. doi: 10.1002/adma.202210144

68. Bigham NP, Wilson JJ. Metal coordination complexes as therapeutic agents for ischemia-reperfusion injury. *J Am Chem Soc*. (2023) 145:9389–409. doi: 10.1021/jacs.3c01984

69. Ma X, Zhang B, Ma N, Liu C, Miao Y, Liang X, et al. Unveiling the mechanism of alleviating ischemia reperfusion injury via a layered double hydroxide-based nanozyme. *ACS Appl Mater Interfaces*. (2023):acsami.2c19570. doi: 10.1021/acsami.2c19570

70. Frasca D, Diaz A, Romero M, Blomberg BB. Human peripheral late/exhausted memory B cells express a senescent-associated secretory phenotype and preferentially utilize metabolic signaling pathways. *Exp Gerontol*. (2017) 87:113–20. doi: 10.1016/j.exger.2016.12.001

71. Dirks J, Andres O, Paul L, Manukjan G, Schulze H, Morbach H. IgD shapes the pre-immune naïve B cell compartment in humans. *Front Immunol*. (2023) 14:1096019. doi: 10.3389/fimmu.2023.1096019

72. Noviski M, Mueller JL, Satterthwaite A, Garrett-Sinha LA, Brombacher F, Zikherman J. IgM and IgD B cell receptors differentially respond to endogenous antigens and control B cell fate. *eLife*. (2018) 7:e35074. doi: 10.7554/eLife.35074

73. Takebayashi J, Kaji H, Ichiyama K, Makino K, Gohda E, Yamamoto I, et al. Inhibition of free radical-induced erythrocyte hemolysis by 2-O-substituted ascorbic acid derivatives. *Free Radic Biol Med*. (2007) 43:1156–64. doi: 10.1016/j.freeradbiomed.2007.07.002

frontiers | Frontiers in Neurology

TYPE Original Research
PUBLISHED 12 June 2024
DOI 10.3389/fneur.2024.1399345

Check for updates

OPEN ACCESS

EDITED BY
Shubham Misra,
Yale University, United States

REVIEWED BY
Marta Kopańska,
University of Rzeszow, Poland
Yuhua Ji,
Jinan University, China

*CORRESPONDENCE
Bartosz Karaszewski
✉ bartosz@karaszewski.org

RECEIVED 11 March 2024
ACCEPTED 21 May 2024
PUBLISHED 12 June 2024

CITATION
Stańczak M, Wyszomirski A, Słonimska P, Kołodziej B, Jabłoński B, Stanisławska-Sachadyn A and Karaszewski B (2024) Circulating miRNA profiles and the risk of hemorrhagic transformation after thrombolytic treatment of acute ischemic stroke: a pilot study. *Front. Neurol.* 15:1399345. doi: 10.3389/fneur.2024.1399345

COPYRIGHT
© 2024 Stańczak, Wyszomirski, Słonimska, Kołodziej, Jabłoński, Stanisławska-Sachadyn and Karaszewski. This is an open-access article distributed under the terms of the Creative Commons Attribution License (CC BY). The use, distribution or reproduction in other forums is permitted, provided the original author(s) and the copyright owner(s) are credited and that the original publication in this journal is cited, in accordance with accepted academic practice. No use, distribution or reproduction is permitted which does not comply with these terms.

Circulating miRNA profiles and the risk of hemorrhagic transformation after thrombolytic treatment of acute ischemic stroke: a pilot study

Marcin Stańczak[1,2], Adam Wyszomirski[3], Paulina Słonimska[4], Barbara Kołodziej[3], Bartosz Jabłoński[1,2], Anna Stanisławska-Sachadyn[5,6] and Bartosz Karaszewski[1,2,3]*

[1]Department of Adult Neurology, Faculty of Medicine, Medical University of Gdańsk, Gdańsk, Poland, [2]Department of Adult Neurology, University Clinical Center, Gdańsk, Poland, [3]Brain Diseases Centre, Medical University of Gdańsk, Gdańsk, Poland, [4]Laboratory for Regenerative Biotechnology, Department of Biotechnology and Microbiology, Gdańsk University of Technology, Gdańsk, Poland, [5]Department of Biotechnology and Microbiology, Gdańsk University of Technology, Gdańsk, Poland, [6]BioTechMed Center, Gdańsk University of Technology, Gdańsk, Poland

Background: Hemorrhagic transformation (HT) in acute ischemic stroke is likely to occur in patients treated with intravenous thrombolysis (IVT) and may lead to neurological deterioration and symptomatic intracranial hemorrhage (sICH). Despite the complex inclusion and exclusion criteria for IVT and some useful tools to stratify HT risk, sICH still occurs in approximately 6% of patients because some of the risk factors for this complication remain unknown.

Objective: This study aimed to explore whether there are any differences in circulating microRNA (miRNA) profiles between patients who develop HT after thrombolysis and those who do not.

Methods: Using qPCR, we quantified the expression of 84 miRNAs in plasma samples collected prior to thrombolytic treatment from 10 individuals who eventually developed HT and 10 patients who did not. For miRNAs that were downregulated (fold change (FC) <0.67) or upregulated (FC >1.5) with $p < 0.10$, we investigated the tissue specificity and performed KEGG pathway annotation using bioinformatics tools. Owing to the small patient sample size, instead of multivariate analysis with all major known HT risk factors, we matched the results with the admission NIHSS scores only.

Results: We observed trends towards downregulation of miR-1-3p, miR-133a-3p, miR-133b and miR-376c-3p, and upregulation of miR-7-5p, miR-17-3p, and miR-296-5p. Previously, the upregulated miR-7-5p was found to be highly expressed in the brain, whereas miR-1, miR-133a-3p and miR-133b appeared to be specific to the muscles and myocardium.

Conclusion: miRNA profiles tend to differ between patients who develop HT and those who do not, suggesting that miRNA profiling, likely in association with other omics approaches, may increase the current power of tools predicting thrombolysis-associated sICH in acute ischemic stroke patients. This study represents a free hypothesis-approach pilot study as a continuation from our previous work. Herein, we showed that applying mathematical analyses to extract information from raw big data may result in the identification of new pathophysiological pathways and may complete standard design works.

KEYWORDS

microRNA, miR, ischemic stroke, hemorrhagic transformation, thrombolysis, biomarker

1 Introduction

Ischemic stroke was found to have an incidence of 7.6 million individuals worldwide in 2019, resulting in 63.48 million disability-adjusted life years (DALYs) and 3.29 million deaths. Ischemic stroke is a devastating neurological condition characterized by brain tissue damage caused by sudden obstruction of blood flow in the cerebral arteries (1, 2). Treatment in the acute phase aims to restore blood flow through intravenous thrombolysis and mechanical thrombectomy. The former method, which is used in up to 25% of patients, involves the administration of tissue-type plasminogen activator (rtPA), which promotes the formation of plasmin, a proteolytic enzyme. Plasmin breaks the crosslinks between fibrin molecules, leading to thrombus dissolution and restoration of blood flow (3, 4).

Hemorrhagic transformation (HT), which involves the extravasation of blood across a disrupted blood–brain barrier into the brain parenchyma, is one of the most common complications of ischemic stroke (5). According to the European Cooperative Acute Stroke Study (ECASS), HT can be categorized based on its intensity and radiological features into small petechial hemorrhagic infarction (HI1), confluent petechial hemorrhagic infarction (HI2), small parenchymal hemorrhage (PH1) (<30% infarct, mild mass effect), and large parenchymal hemorrhage (PH2, >30% infarct, marked mass effect) (6). Depending on its severity, HT may remain asymptomatic; however, if it is sufficiently large to exert a mass effect on brain tissue outside the infarct, it may cause neurological deterioration (7). Autopsy studies revealed hemorrhagic transformations in 18–42% of patients with acute ischemic stroke, and clinical assessment indicated symptomatic intracerebral hemorrhage after intravenous thrombolysis in approximately 6% of patients (8, 9).

Several studies aim at pinpointing reliable predictors of hemorrhagic transformation. The established clinical risk factors include baseline National Institutes of Health Stroke Scale (NIHSS) score, systolic and diastolic blood pressure, atrial fibrillation, antiplatelets use, age, and time from onset to treatment and hyperglycemia among others (10, 11). Radiological determinants of increased risk of hemorrhagic transformation include a large infarct size, early ischemic changes visible on computed tomography (CT), and absent or poor collaterals (10, 12). Among identified blood biomarkers, matrix metalloproteinase-9 (MMP-9), ferritin, and cellular fibronectin (c-Fn), as well as the neutrophil-to-lymphocyte ratio (NLR) and high-density lipoprotein (HDL), have been extensively studied across multiple experiments (13, 14).

Recent advances in artificial intelligence (AI) and omics have fostered their application in the search for novel HT biomarkers and predictive models. Machine learning methods have been used to develop predictive models based on clinical data and laboratory test results (15). In our previous study, we explored a hypothesis-free approach using MS proteomic data to identify new biomarkers (16). In that study, 15 proteins detected in the blood collected prior to rtPA treatment were unique to patients who developed HT.

MicroRNAs (miRNAs) are small non-coding RNA molecules composed of approximately 22 nucleotides that are known for their regulatory roles in various biological processes, mainly through the post-transcriptional regulation of gene expression (17). Their stability and detectability in various tissues, including blood, have attracted significant attention in the last decade, leading to their exploration as potential diagnostic and prognostic biomarkers, particularly in oncology (18). Circulating miRNAs have also emerged as valuable tools in stroke medicine. Numerous studies have identified miRNAs as diagnostic markers for ischemic stroke, with hsa-let-7e-5p, hsa-miR-124-3p, hsa-miR-17-5p, and hsa-miR-185-5p showing consistent differential expression (19). Furthermore, the combination of miR-124-3p, miR-125b-5p, and miR-192-5p expression has been shown to predict the extent of neurological deterioration in ischemic stroke patients treated with rtPA (20). In another study, miR-21-5p, miR-206, and miR-3123 were implicated in predicting the risk of hemorrhagic transformation in patients with cardioembolic stroke (21). Additionally, the assessment of RNA markers, including miRNA-23a, miRNA-193a, miRNA-128, miRNA-99a, miRNA-let-7a, miRNA-494, miRNA-424, and the long non-coding (lnc)RNA H19, has been shown to improve the prediction of symptomatic intracranial hemorrhage (sICH) after rtPA (22).

The findings of the above studies suggest that quantitative miRNA and proteomic data may increase the current power of the tools for predicting thrombolysis-associated sICH in patients with acute ischemic stroke [as we showed in our previous study (16)]. However, the main objective of the presented studies is to demonstrate a methodology for and the feasibility of such an approach. This pilot study only aimed to identify potential miRNAs indicative of an increased risk of HT occurrence.

2 Methods

2.1 Study population

This research is a continuation of our previous study on biomarkers of rtPA-associated intracranial hemorrhage in acute ischemic stroke (16). Participants were recruited between March 2019 and April 2022 from among patients at the Stroke Comprehensive Center of the Department of Adult Neurology, University Clinical Center, Medical University of Gdansk.

Before recruitment, approval was obtained from The Independent Bioethics Committee for Scientific Research at the Medical University of Gdańsk in Poland. This study was conducted in accordance with the principles outlined in the World Medical Association Declaration of Helsinki. All subjects were informed of the purpose and course of the study and signed an informed consent form.

For patients with acute stroke, a pretreatment MRI protocol (described in Section 2.2) was performed, in addition to the collection of two blood samples: plasma in an EDTA-coated tube and serum in

a silica clot activator (Becton Dickinson Vacutainer). However, only plasma samples were used for further analyses. Upon confirmation of ischemic stroke diagnosis and patient adherence to thrombolysis inclusion criteria according to the stroke guidelines, alteplase was administered intravenously at a standard dose of 0.9 mg/kg. Subsequently, patients were assigned to either the HT or control group, based on follow-up MRI scans on day 5–9 after the treatment. In the initial cohort of 94 patients admitted for acute stroke, 56 received intravenous rtPA, met the standard inclusion and exclusion criteria, and had no contraindications for MRI. Due to limited funding during this phase of the study, 10 patients with HT were selected for further analysis and matched with 10 non-HT controls based on comparable risk factors for hemorrhagic transformation (NIHSS score, Oxfordshire Community Stroke Project classification) and similar miRNA profiles (age and sex).

The Propensity Score Matching method, which incorporates the k-nearest neighbor (k-NN) algorithm without replacement, was used to select a well-matched control group (non-HT) with a distribution of baseline characteristics similar to that of the HT group. The analysis was conducted using the MatchIt library in R software (23).

2.2 Brain imaging

Pretreatment MRI was performed using a Siemens Healthcare GOBrain application on a 1.5 T MRI-scanner (Siemens Magnetom Aera), comprising axial T2-weighted fluid attenuation inversion recovery, axial diffusion-weighted imaging (*b*-values 0,800 s/mm) with apparent diffusion coefficient maps, axial T2*-weighted, and sagittal T1-weighted images. These scans were used to assess the infarct volume and were analyzed by radiologists using the syngo.via software. The follow-up MRI scan was taken using the same 1.5 T Siemens device, but the protocol was expanded compared to the initial one and additionally included the following sequences: axial susceptibility-weighted imaging, sagittal T2-weighted, axial diffusion tensor imaging, and 3D axial T1-weighted sequences.

2.3 miRNA quantification

Plasma samples previously stored at deep-freezing temperatures (−80°C) were used for miRNA quantification. Briefly, plasma miRNAs were isolated using the miRNeasy Serum/Plasma Advanced Kit (Cat. no. 217204; Qiagen, Hilden, Germany). cDNA was synthesized using a miRCURY LNA RT Kit (Cat. no. 339340; Qiagen, Hilden, Germany). Each sample contained miRNA corresponding to 16 µL of plasma sample, 1 x buffer, 1 x miRCURY RT Enzyme mix, synthetic RNA spike-ins. All cDNA samples were synthesized from a master mix of reagents. Samples were incubated for 60 min at 42°C followed by incubation for 5 min at 95°C. The efficiency of miRNA isolation and cDNA synthesis was evaluated by PCR analysis of exogenous synthetic miRNAs (Cat. no. 339390; Qiagen, Hilden, Germany). DNA isolation and cDNA synthesis were successful in all samples.

The quantification of 84 miRNAs was performed using the Serum/Plasma Small Focus miRCURY LNA Panel (cat. no. 339325; Qiagen), which comprised 84 human miRNAs curated by the manufacturer based on their highest expression in serum and plasma samples obtained from healthy individuals and those afflicted with various conditions. The LC96 Roche platform was used. The same panel was used to determine the occurrence of hemolysis. The determinant that indicated an increased risk of hemolysis exceeded the value of dCq = 7, which was the difference between the value of miR-23a, which is constant in the blood, and the value of miR-451a, which is specific to red blood cells. The miRNA analyses were performed at the Department of Molecular Biotechnology and Microbiology of Gdansk University of Technology.

2.4 Statistical analysis and results exploration

Normalized miRNA expression was calculated as $2^{-(Cq(miRNA) - Cq(mean\ of\ references))}$. The fold change was calculated for each miRNA as the quotient of the mean normalized expression in the HT and non-HT groups.

The Yuen–Welch t-test permutation was applied to compare the trimmed means of the two study groups. The number of permutations was set to 1,000 with a random seed of 123 in the R program. A 10%-trimmed mean value was established. To address the issue of multiple hypothesis testing, *p*-values were adjusted using the Benjamini-Hochberg correction method. All statistical analyses were performed using R software version 3.6.3.

A multifactor analysis allowed us to control for confounding factors. However, the sample size in the present study was too small to achieve statistical validity; (24) therefore, we limited our single-factor analysis.

To assess miRNA tissue/organ specificity, we utilized the TissueAtlas (24). Subsequently, the significant miRNAs were subjected to functional analysis using DIANA mirPath v.3 (25). To identify miRNA target genes, we selected TarBase v.7.0, a database of experimentally validated miRNA-gene interactions (26). The tool was set to annotate target genes to Kyoto Encyclopedia of Genes and Genomes (KEGG) pathways, with results merging set to a pathway union (27).

3 Results

3.1 Patients' characteristic

Of 75 patients with acute ischemic stroke treated with intravenous thrombolysis, 25 were excluded because of incomplete data. Among the remaining 50 patients, HT was detected in 10. All patients with HT experienced stroke in the anterior circulation territory and none had lacunar strokes. As this was only the pilot phase of the study, HT was not differentiated into symptomatic or asymptomatic. Ten patients with anterior circulation and non-lacunar stroke who developed HT were matched with 10 patients without HT, as described in the Methods section. The clinical and demographic characteristics of the patients selected for further investigation are presented in Table 1. The complete dataset is shown in Supplementary Table S1.

3.2 miRNA isolation and cDNA synthesis

To estimate the RNA isolation efficiency, UniSp2, UniSp4, and UniSp5 spike-ins were added to the plasma samples, which allowed for

TABLE 1 Demographical and clinical characteristics of patients selected for miRNA analysis.

	Patients with HT (n = 10)	Patients without HT (n = 10)
Age, median (IQR)	77.5 (60.75–86.25)	80 (76.00–85.5)
Sex, female /male, n (%)	3 (30%) / 7 (70%)	5 (50%) / 5 (50%)
NIHSS on admission, median (IQR)	8 (4.25–11.00)	5 (4.25–10.75)
Stroke subtype according to OCSP, n (%)		
PACS	7 (70%)	7 (70%)
TACS	3 (30%)	3 (30%)
Baseline infarct volume (IQR)	12.14 (0.0–19.35)	25.92 (11.30–42,52)
Systolic blood pressure on admission, median (IQR)	159.5 (150.00–165.25)	167 (150.5–179.50)
Diastolic blood pressure on admission, median (IQR)	79 (71.25–90.00)	82.5 (74.5–90.00)
Comorbidities, n (%)		
Atrial Fibrillation	1 (10%)	4 (40%)
Diabetes	2 (20%)	1 (10%)
Hypertension	9 (90%)	8 (80%)
Hyperlipidemia	9 (90%)	4 (40%)
Antiplatelets use	4 (40%)	6 (60%)
Active smoking	3 (30%)	4 (40%)
Type of HT according to ECASS, n (%)		
HI1	7 (70%)	–
HI2	2 (20%)	–
PH1	1 (10%)	–
PH2	0 (0%)	–
NIHSS on discharge, median (IQR)	1.5 (0–2.75)	0.5 (0–1.75)

IQR, interquartile range; OCSP, oxfordshire community stroke project (classification); PACS, partial anterior circulation stroke; TACS, total anterior circulation stroke; ECASS, European cooperative acute stroke study (classification); HI1, hemorrhagic infarction type 1; HI2, hemorrhagic infarction type 2; PH1, parenchymal hematoma type 1.

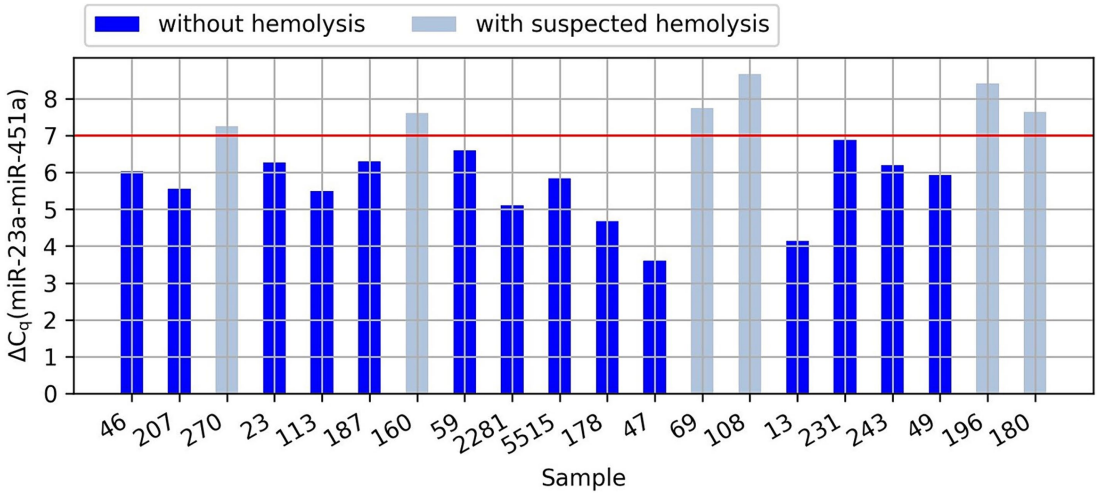

FIGURE 1
Graph showing the difference in the Cq values of miR-23a and miR-451a (dCq) in the analyzed samples. The red line indicates the value of dCq above which there is an increased risk of hemolysis.

the comparison of RNA isolation between samples after RT-qPCR. RNA isolation efficiency remained stable across all samples, with UniSp2 presenting a minimum quantification cycle (Cq) value of 22.01 and a maximum Cq value of 19.47 for samples 108 and 160, respectively. In addition, UniSp4 (present at a 100-fold lower concentration than UniSp2) and UniSp5 (present at a 100-fold lower concentration than

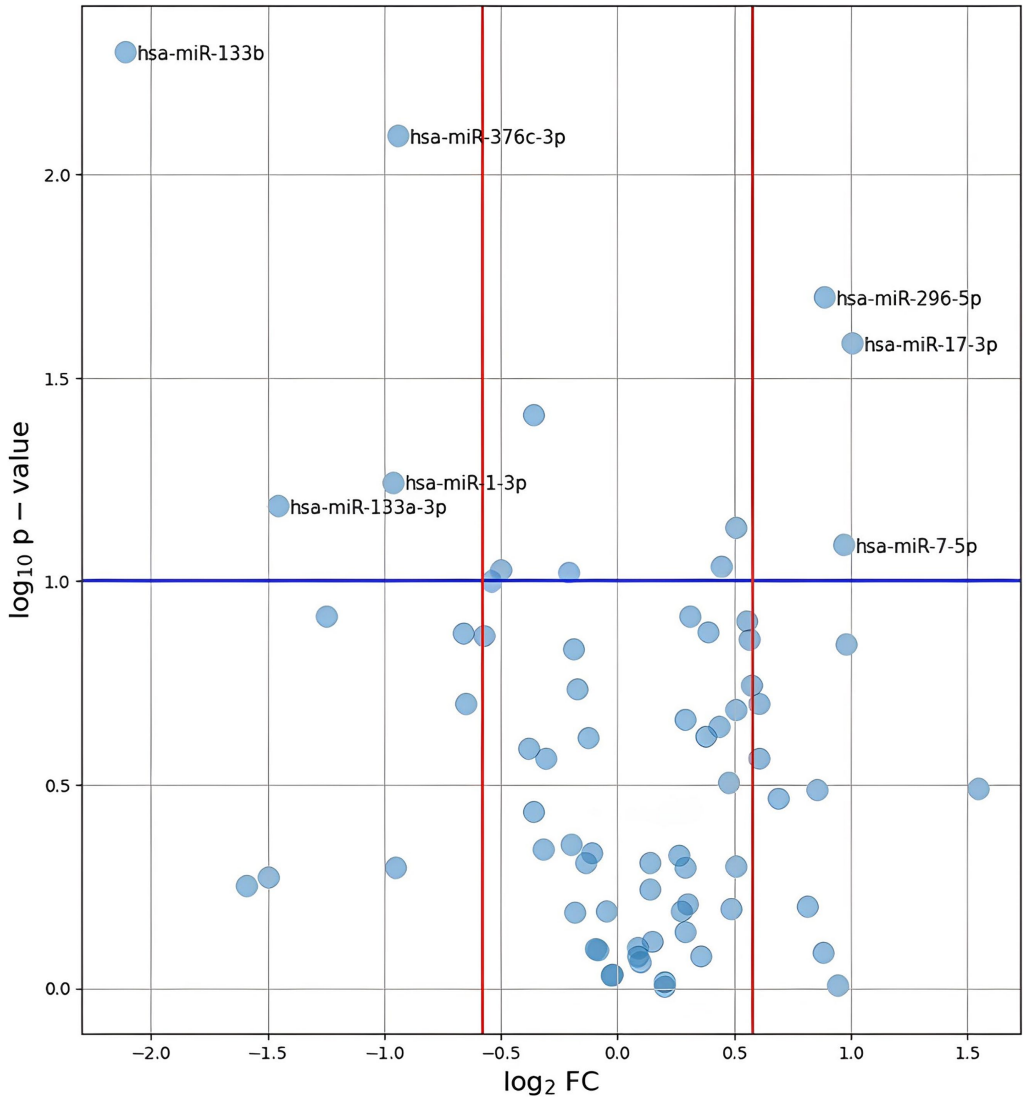

FIGURE 2
Plot of log2(FC) against −log10(*p*-value) for all analyzed miRNAs. The values presented on the plot were calculated using the *p*-values obtained after performing Permutation Yuen-Welch *t* test. A blue line represents the level of *p*-value = 0.1. Red lines indicate the range of FC < 0, 67 or > 1, 5.

UniSp4) were detected in all samples. Similarly, cDNA synthesis efficiency was assessed using the UniSp6 spike-in, which was amplified with the min Cq value of 19.11 and max Cq value of 18.56 among all samples.

3.3 Hemolysis in samples

Based on the analysis of the differences in the Cq values of miR-23a and miR-451a, it was noticed that in six samples, the probability of hemolysis increased (the dCq value was higher than 7). In four samples we observed the hemolysis marker at values between 7.26 and 7.76 and in two samples at values of 8.43 and 8.68 (the exact values of dCq for each sample are presented in the Figure 1). However, since low levels of hemolysis are difficult or impossible to eliminate in clinical practice and we cannot determine the degree of hemolysis based on these results, while our samples were not highly hemolyzed, we decided to continue the research using these samples.

3.4 miRNA differential expression

The miRNAs hsa-miR-30c-5p, hsa-miR-103a-3p, and hsa-miR-23a-3p were selected as reference miRNAs to calculate the relative expression of plasma miRNAs. Normalized results of miRNA quantification are provided in Supplementary Table S2. When the mean Cq of the reference miRNAs was calculated, sample no. 47 was found to be an outlier. The mean Cq value for the reference miRNAs was 34.67, while the lowest mean Cq value among the other samples was 30.03. Thus, the levels of miRNAs in this sample were notably lower, which resulted in the lack of detection of several plasma miRNAs. This led us to exclude sample 47 from further analyses.

Of the 84 assessed miRNAs, 12 were excluded from further analyses due to missing data in more than 50% of the samples and one was excluded due to non-specific amplification. In our study, "missing data," referred to situations in which the concentration of genetic material was so low that we were unable to detect it. Following normalization of miRNA levels, differential expression was calculated. The results are

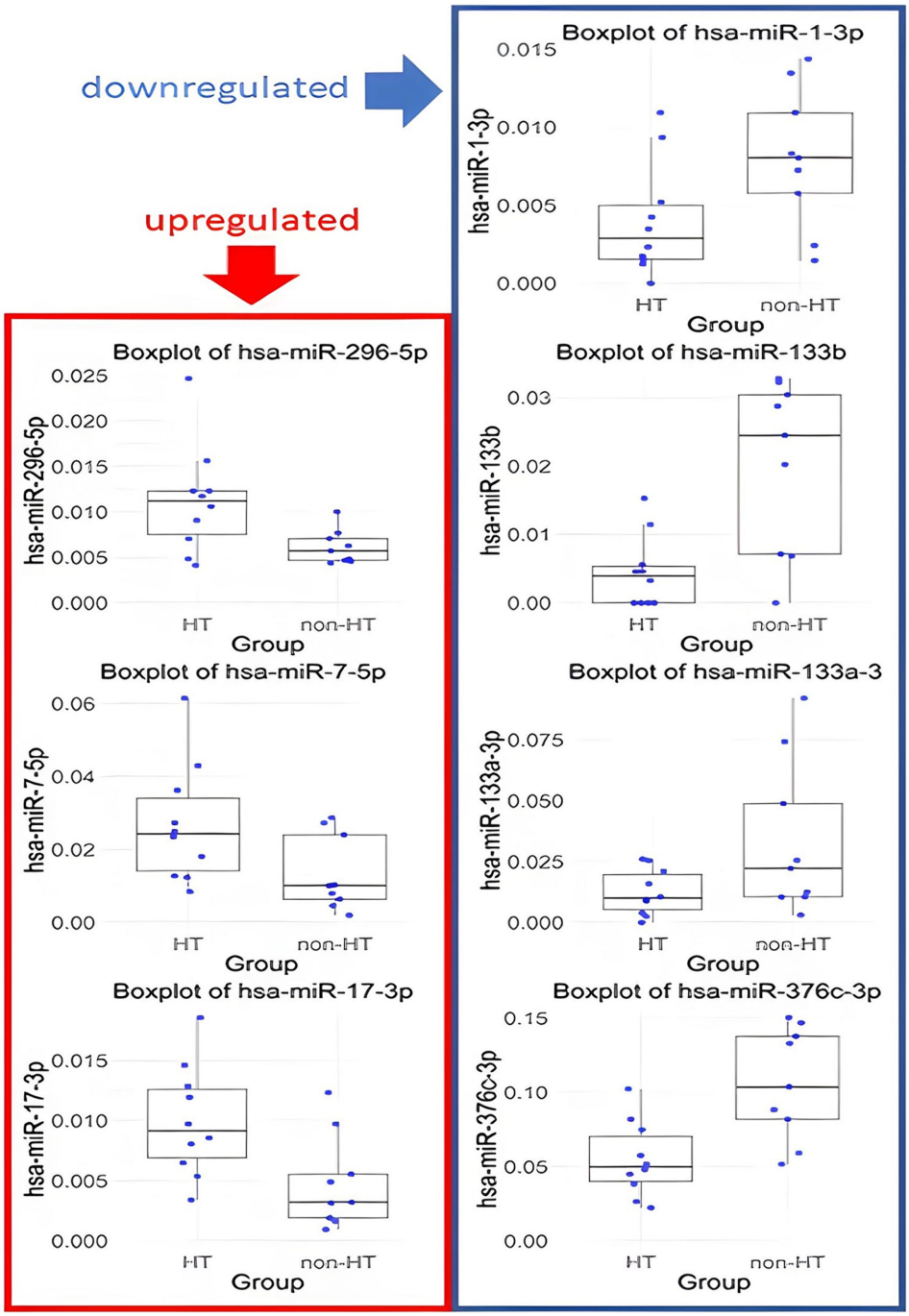

FIGURE 3
Box plots of miRNA expression in HT and non-HT group. Only results with $p < 0.1$ and FC >1.5 or < 0.67 are presented.

shown in Figure 2. Thirteen miRNAs reached a Permutation Yuen-Welch *t*-test *p*-value <0.10, with five having a p-value <0.05. However, after Benjamini and Hochberg correction for multiple testing problems, none of the analyzed miRNAs had a p-value <0.05.

Regarding the magnitude of difference between the HT and non-HT groups, miRNAs with a fold change (FC) in relative expression (FC) <0.67 were considered downregulated in HT, while miRNAs with FC >1.5 were deemed upregulated. Owing to the nature of the pilot study, the level of significance was set to 0.10. Using the commonly encountered value of 0.05 could potentially result in the pilot study being underpowered (28). The results of the statistical analysis of all miRNAs with a complete set of data are provided in Supplementary Table S3. Sources for the analysis are avaliable in online repository: https://github.com/barbara-kolodziej-gumed/Circulating-miRNA-profiles-and-the-risk-of-HT-after-rtPA.

The analysis included two previously described stroke biomarkers, hsa-miR-124-3p and hsa-miR-17-5p. The concentration of hsa-miR-124-3p was so low in 12 samples that quantitative determination was not possible. For hsa-miR-17-5p, no statistically significant differences were found between the HT and non-HT groups.

MiRNAs with *p*-values <0.1 and FC <0.67 or > 1.5 are listed in Table 2. Specifically, hsa-miR-133b, hsa-miR-376c-3p, hsa-miR-133a-3p, and hsa-miR-1-3p were downregulated, whereas

TABLE 2 miRNAs with $p < 0.05$ and FC >1.5 or < 0.67.

miRNA	FC in relative expression of miRNAs in HT compared to non-HT	Permutation Yuen-Welch *t* test *p*-value	Adjusted *p*-value
hsa-miR-133b	0.23	0.005	0.284
hsa-miR-376c-3p	0.52	0.008	0.284
hsa-miR-296-5p	1.85	0.020	0.462
hsa-miR-17-3p	2.01	0.026	0.462
hsa-miR- 1-3p	0.51	0.057	0.474
hsa-miR-133a-3p	0.36	0.065	0.474
hsa-miR-7-5p	1.96	0.081	0.474

Downregulated miRNAs are marked in blue, upregulated ones in red.

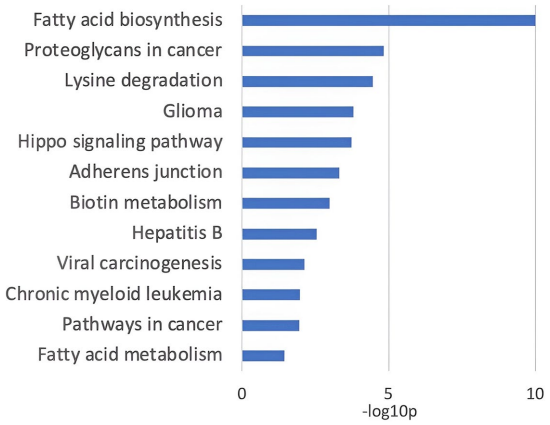

FIGURE 4
KEGG pathways annotated to the 7 investigated miRNAs.

hsa-miR-17-3p, hsa-miR-296-5p and hsa-miR-7-5p were upregulated in the ICH group. The distributions of their values in the HT and non-HT groups are shown in Figure 3.

Next, the TissueAtlas was used to determine whether these seven miRNAs exhibited specificity to any organ or tissue. Specifically, miR-133b, miR-1-3p, and miR133a-5p appeared to be predominantly present in muscles and myocardium, miR-7-5p was found to be abundant in the brain, miR-376c-3p in the brain, bone, and tunica albuginea, and miR-17-3p in muscle and thyroid tissues, whereas miR-296-5p levels were uniform across all the investigated tissues (Supplementary Table S4).

Subsequently, the DIANA miR path tool was used to assess the potential functional roles of the seven miRNAs. The KEGG pathways significantly associated with the investigated miRNAs are shown in Figure 4. These pathways include those associated with cell adhesion molecules, fatty acid synthesis, and metabolism, as well as those associated with signal transduction, amino acid metabolism, and pathways explored in carcinogenesis.

4 Discussion

This pilot study highlighted the differences in circulating miRNA profiles between patients who developed HT and those who did not. We hypothesized that miRNA profiling and other omic approaches may increase the predictive power of thrombolysis-associated sICH in acute ischemic stroke; however, this requires further investigation. This study was a free hypothesis-approach pilot study based on previous work from our group, in which we showed that applying mathematical analyses to extract information from raw big data may result in the identification of new pathophysiological pathways and may complete standard design work.

Despite the low number of patients investigated in this study and the restricted miRNA panel, to the best of our knowledge, this study still reveals the broadest panel of miRNAs that might play a role in hemorrhagic transformation associated with the thrombolytic treatment of acute ischemic stroke.

The miRNAs miRNA-1, −133a and −133b, which were downregulated in HT patients, are known to be present in abundance in both skeletal and cardiac muscle (29). They have further been reported to be elevated in the circulation following a myocardial infarction (30). Notably, miR-133b alone has been found to be a risk factor for cardiovascular disease (31). Another miRNA downregulated in HT, miR-376c, has been extensively studied as a cancer modulator, with evidence supporting a role in both cancer suppression and progression (32). In neonatal hypoxic–ischemic encephalopathy, miR-376c demonstrates protective effects against oxygen–glucose deprivation-induced cell injury (33). One of the upregulated miRNAs, miR-296-5p, has previously been found to be present at high levels in deep venous thrombosis patients. Interestingly, in a mouse model, its elevation inhibited deep venous thrombosis by suppressing S100A4 expression, which influences the release of prothrombosis-related factors (34). Therefore, the observed increase in the level of this miRNA in patients with HT after intravenous thrombolysis in our study is of particular interest. MiR-17-3p is a member of the miR-17/92 cluster and plays a role in cell cycle regulation, proliferation, and apoptosis. It is frequently dysregulated in cardiovascular, immune, and neurodegenerative diseases (35). Notably, in a mouse model, miR-17-3p overexpression suppressed cardiomyocyte apoptosis induced by oxygen–glucose deprivation and reperfusion (36).

The last upregulated miRNA, miR-7-5p, is highly expressed in the brain and is involved in cerebral cortex development. It has also been shown to play a role in neurodegenerative diseases, neuroinflammation, and mental disorders (37). In rodent models, miR-7-5p expression was found to be downregulated in the brain following focal ischemia. Interestingly, administration of miR-7 mimic resulted in smaller infarct volume and better functional recovery, supposedly by repressing α-synuclein (38). Among the imRNAs excluded from the differential expression analysis due to low signal intensity, hsa-miR-124-3p was identified as potentially important. This miRNA is downregulated in ischemic stroke (39), which could explain its undetectable expression in our samples.

The detected trends in miRNA expression aligned with patterns observed in various cardiovascular diseases and the pathophysiological mechanisms associated with ischemic stroke. Implementing our proposed methodology in a large-scale study could facilitate the identification of significant biomarkers indicative of the risk of hemorrhagic transformation. Broadening the spectrum of analyzed miRNAs through either an expanded qPCR panel or small RNA sequencing would further enrich the study and potentially deepen our understanding of the pathophysiology of hemorrhagic transformation.

4.1 Limitations

In this miRNA analysis, owing to the small sample size, a multiple regression model that included the baseline characteristics of the patients used in the matching process was not calculated. The small size of the recruited study group resulted in none of the adjusted *p*-values being <0.1. Therefore, based on the obtained results, it is not possible to definitively determine which miRNAs may serve as markers of HT after rtPA treatment for stroke. This article is a pilot study and primarily serves as a description of miRNA measurement methods in clinical practice. It should also be noted that the quality of the results may also be influenced by hemolysis, which was observed in six samples. However, in clinical practice, the risks of suboptimal collection and handling of biological materials must be considered. Therefore, these samples were included in our analysis.

5 Conclusion

The quantitative determination of miRNA expression in HT and non-HT patients serves as a complement to our previous analysis (16) and may potentially expand the predictive power of currently used calculators for thrombolysis-associated HT in acute ischemic stroke based on clinical and neuroimaging data; however, further studies are needed to verify this idea. We found differences in the blood concentrations of seven miRNAs, and further analysis of the available miRNA databases revealed that miR-296-5p was most directly linked to the occurrence of HT. However, owing to the small sample size, these results may only be considered as a pilot for any major study. Overall, this study shows that analyzing datasets for a sufficiently large number of patients using a hypothesis-free approach could be used to identify complex pathophysiological associations that may be unachievable in standard-design studies.

Data availability statement

The datasets presented in this study can be found in online repositories. The names of the repository/repositories and accession number(s) can be found in the article/Supplementary material.

Ethics statement

The studies involving humans were approved by The Independent Bioethics Committee for Scientific Research at the Medical University of Gdańsk, Poland. The studies were conducted in accordance with the local legislation and institutional requirements. The participants provided their written informed consent to participate in this study.

Author contributions

MS: Formal analysis, Investigation, Project administration, Resources, Visualization, Writing – original draft. AW: Formal analysis, Writing – original draft. PS: Investigation, Writing – review & editing. BKo: Project administration, Visualization, Writing – original draft. AS-S: Writing – original draft, Formal analysis, Investigation, Methodology. BKa: Conceptualization, Funding acquisition, Methodology, Supervision, Writing – review & editing. BJ: Writing – review & editing, Data curation.

Funding

The author(s) declare that financial support was received for the research, authorship, and/or publication of this article. This research was Funded by Siemens Helthineers (research grant for the Medical University of Gdansk, PI—BKa, 2018; Contract Number C00229230), by the Excellence Initiative – Research University program at the Medical University of Gdansk and by the Medical University of Gdansk.

Conflict of interest

The authors declare that the research was conducted in the absence of any commercial or financial relationships that could be construed as a potential conflict of interest.

Publisher's note

All claims expressed in this article are solely those of the authors and do not necessarily represent those of their affiliated organizations, or those of the publisher, the editors and the reviewers. Any product that may be evaluated in this article, or claim that may be made by its manufacturer, is not guaranteed or endorsed by the publisher.

Supplementary material

The Supplementary material for this article can be found online at: https://www.frontiersin.org/articles/10.3389/fneur.2024.1399345/full#supplementary-material

SUPPLEMENTARY TABLE S1
Clinical and neuroimaging data of 20 stroke patients with and without hemorrhagic transformation.

SUPPLEMENTARY TABLE S2
Normalized results of miRNA quantification.

SUPPLEMENTARY TABLE S3
MicroRNA comparison between study groups.

SUPPLEMENTARY TABLE S4
Expression of selected miRNAs in various organs according to the TissueAtlas.

References

1. Feigin VL, Stark BA, Johnson CO, Roth GA, Bisignano C, Abady GG, et al. Global, regional, and national burden of stroke and its risk factors, 1990–2019: a systematic analysis for the global burden of disease study 2019. *Lancet Neurol*. (2021) 20:795–820. doi: 10.1016/S1474-4422(21)00252-0

2. Kuriakose D, Xiao Z. Pathophysiology and treatment of stroke: present status and future perspectives. *Int J Mol Sci*. (2020) 21:1–24. doi: 10.3390/ijms21207609

3. Bivard A, Lin L, Parsons MW. Review of stroke Thrombolytics. *J Stroke*. (2013) 15:90. doi: 10.5853/jos.2013.15.2.90

4. Van Wijngaarden JDH, Dirks M, Huijsman R, Niessen LW, Fabbricotti IN, Dippel DWJ. Hospital rates of thrombolysis for acute ischemic stroke: the influence of organizational culture. *Stroke*. (2009) 40:3390–2. doi: 10.1161/STROKEAHA.109.559492

5. Spronk E, Sykes G, Falcione S, Munsterman D, Joy T, Kamtchum-Tatuene J, et al. Hemorrhagic transformation in ischemic stroke and the role of inflammation. *Front Neurol*. (2021) 12:661955. doi: 10.3389/fneur.2021.661955

6. Fiorelli M, Bastianello S, Von Kummer R, Del Zoppo GJ, Larrue V, Lesaffre E, et al. Hemorrhagic transformation within 36 hours of a cerebral infarct relationships with early clinical deterioration and 3-month outcome in the European cooperative acute stroke study I (ECASS I) cohort. *Stroke*. (1999) 30:2280–4. doi: 10.1161/01.STR.30.11.2280

7. Mazya M, Egido JA, Ford GA, Lees KR, Mikulik R, Toni D, et al. Predicting the risk of symptomatic intracerebral hemorrhage in ischemic stroke treated with intravenous alteplase: safe implementation of treatments in stroke (SITS) symptomatic intracerebral hemorrhage risk score. *Stroke*. (2012) 43:1524–31. doi: 10.1161/STROKEAHA.111.644815

8. Hong JM, Kim DS, Kim M. Hemorrhagic transformation after ischemic stroke: mechanisms and management. *Front Neurol*. (2021) 12:703258. doi: 10.3389/fneur.2021.703258

9. Charbonnier G, Bonnet L, Biondi A, Moulin T. Intracranial bleeding after reperfusion therapy in acute ischemic stroke. *Front Neurol*. (2021) 11:629920. doi: 10.3389/fneur.2020.629920

10. Van Kranendonk KR, Treurniet KM, Boers AMM, Berkhemer OA, Van Den Berg LA, Chalos V, et al. Clinical and imaging markers associated with hemorrhagic transformation in patients with acute ischemic stroke. *Stroke*. (2019) 50:2037–43. doi: 10.1161/STROKEAHA.118.024255

11. Hao Y, Zhou H, Pan C, Xie G, Hu J, Zhang B, et al. Prediction factors and clinical significance of different types of hemorrhagic transformation after intravenous thrombolysis. *Eur J Med Res*. (2023) 28:509. doi: 10.1186/s40001-023-01503-x

12. Whiteley WN, Slot KB, Fernandes P, Sandercock P, Wardlaw J. Risk factors for intracranial hemorrhage in acute ischemic stroke patients treated with recombinant tissue plasminogen activator. *Stroke*. (2012) 43:2904–9. doi: 10.1161/STROKEAHA.112.665331

13. Krishnamoorthy S, Singh G, Jose KJ, Soman B, Foerch C, Kimberly WT, et al. Biomarkers in the prediction of hemorrhagic transformation in acute stroke: a systematic review and Meta-analysis. *Cerebrovasc Dis*. (2022) 51:235–47. doi: 10.1159/000518570

14. Liu J, Wang Y, Jin Y, Guo W, Song Q, Wei C, et al. Prediction of hemorrhagic transformation after ischemic stroke: development and validation study of a novel multi-biomarker model. *Front Aging Neurosci*. (2021) 13:667934. doi: 10.3389/fnagi.2021.667934

15. Xu Y, Li X, Wu D, Zhang Z, Jiang A. Machine learning-based model for prediction of hemorrhage transformation in acute ischemic stroke after Alteplase. *Front Neurol*. (2022) 13:897903. doi: 10.3389/fneur.2022.897903

16. Karaszewski B, Gójska-Grymajło A, Czaplewska P, Jabłoński B, Lewandowska AE, Ossowska D, et al. SWATH-MS for prospective identification of protein blood biomarkers of rtPA-associated intracranial hemorrhage in acute ischemic stroke: a pilot study. *Sci Rep*. (2021) 11:18765. doi: 10.1038/s41598-021-97710-9

17. O'Brien J, Hayder H, Zayed Y, Peng C. Overview of microRNA biogenesis, mechanisms of actions, and circulation. *Front Endocrinol*. (2018) 9:402. doi: 10.3389/fendo.2018.00402

18. Zhang C, Sun C, Zhao Y, Wang Q, Guo J, Ye B, et al. Overview of MicroRNAs as diagnostic and prognostic biomarkers for high-incidence cancers in 2021. *Int J Mol Sci*. (2022) 23:11389. doi: 10.3390/ijms231911389

19. Wang Y, Su X, Leung GHD, Ren B, Zhang Q, Xiong Z, et al. Circulating microRNAs as diagnostic biomarkers for ischemic stroke: evidence from comprehensive analysis and real-world validation. *Int J Med Sci*. (2023) 20:1009–23. doi: 10.7150/ijms.83963

20. He XW, Shi YH, Liu YS, Li GF, Zhao R, Hu Y, et al. Increased plasma levels of miR-124-3p, miR-125b-5p and miR-192-5p are associated with outcomes in acute ischaemic stroke patients receiving thrombolysis. *Atherosclerosis*. (2019) 289:36–43. doi: 10.1016/j.atherosclerosis.2019.08.002

21. Zheng L, Xiong Y, Liu J, Yang X, Wang L, Zhang S, et al. MMP-9-related microRNAs as prognostic markers for hemorrhagic transformation in Cardioembolic stroke patients. *Front Neurol*. (2019) 10:945. doi: 10.3389/fneur.2019.00945

22. Han Z, Li L, Tao Z, Wang R, Zhao H, Zheng Y, et al. Neutrophilic noncoding RNAs predict outcomes of acute ischemic stroke patients treated with recombinant tissue plasminogen activator. *Front Pharmacol*. (2022) 13:1003806. doi: 10.3389/fphar.2022.1003806

23. Stuart E, King G, Imai K, Ho D. MatchIT: nonparametric preprocessing for parametric causal inference. *J Stat Softw*. (2011) 42:1–28. doi: 10.18637/jss.v042.i08

24. Harrell FE. *Regression modeling strategies: With applications to linear models, logistic and ordinal regression, and survival analysis*. Cham, Switzerland: Springer International Publishing (2015).

25. Keller A, Gröger L, Tschernig T, Solomon J, Laham O, Schaum N, et al. miRNATissueAtlas2: an update to the human miRNA tissue atlas. *Nucleic Acids Res*. (2022) 50:D211–21. doi: 10.1093/nar/gkab808

26. Vlachos IS, Zagganas K, Paraskevopoulou MD, Georgakilas G, Karagkouni D, Vergoulis T, et al. DIANA-miRPath v3.0: deciphering microRNA function with experimental support. *Nucleic Acids Res*. (2015) 43:W460–6. doi: 10.1093/nar/gkv403

27. Vlachos IS, Paraskevopoulou MD, Karagkouni D, Georgakilas G, Vergoulis T, Kanellos I, et al. DIANA-TarBase v7.0: indexing more than half a million experimentally supported miRNA:mRNA interactions. *Nucleic Acids Res*. (2015) 43:D153–9. doi: 10.1093/nar/gku1215

28. Lee EC, Whitehead AL, Jacques RM, Julious SA. The statistical interpretation of pilot trials: should significance thresholds be reconsidered? *BMC Med Res Methodol*. (2014) 14:41. doi: 10.1186/1471-2288-14-41

29. Townley-Tilson WHD, Callis TE, Wang D. MicroRNAs 1, 133, and 206: critical factors of skeletal and cardiac muscle development, function, and disease. *Int J Biochem Cell Biol*. (2010) 42:1252–5. doi: 10.1016/j.biocel.2009.03.002

30. Dimmeler S, Zeiher AM. Circulating microRNAs: novel biomarkers for cardiovascular diseases? *Eur Heart J*. (2010) 31:2705–7. doi: 10.1093/eurheartj/ehq221

31. Gacoń J, Badacz R, Stępień E, Karch I, Enguita FJ, Zmudka K, et al. Diagnostic and prognostic micro-RNAs in ischaemic stroke due to carotid artery stenosis and in acute coronary syndrome: a four-year prospective study. *Kardiol Pol*. (2018) 76:362–9. doi: 10.5603/KP.a2017.0243

32. Zhao F, Zhong M, Pei W, Tian B, Cai Y. miR-376c-3p modulates the properties of breast cancer stem cells by targeting RAB2A. *Exp Ther Med*. (2020) 20:1. doi: 10.3892/etm.2020.9196

33. Zhang H, Zhou J, Zhang M, Yi Y, He B. Upregulation of miR-376c-3p alleviates oxygen–glucose deprivation-induced cell injury by targeting ING5. *Cell Mol Biol Lett*. (2019) 24:67. doi: 10.1186/s11658-019-0189-2

34. Pan Z, Zhang Y, Li C, Yin Y, Liu R, Zheng G, et al. MiR-296-5p ameliorates deep venous thrombosis by inactivating S100A4. *Exp Biol Med*. (2021) 246:2259–68. doi: 10.1177/15353702211023034

35. Mogilyansky E, Rigoutsos I. The miR-17/92 cluster: a comprehensive update on its genomics, genetics, functions and increasingly important and numerous roles in health and disease. *Cell Death Differ*. (2013) 20:1603–14. doi: 10.1038/cdd.2013.125

36. Shi J, Bei Y, Kong X, Liu X, Lei Z, Xu T, et al. miR-17-3p contributes to exercise-induced cardiac growth and protects against myocardial ischemia-reperfusion injury. *Theranostics*. (2017) 7:664–76. doi: 10.7150/thno.15162

37. Zhao J, Zhou Y, Guo M, Yue D, Chen C, Liang G, et al. MicroRNA-7: expression and function in brain physiological and pathological processes. *Cell Biosci*. (2020) 10:77. doi: 10.1186/s13578-020-00436-w

38. Kim TH, Mehta SL, Morris-Blanco KC, Chokkalla AK, Chelluboina B, Lopez M, et al. The microRNA miR-7a-5p ameliorates ischemic brain damage by repressing-synuclein. *Sci Signal*. (2018) 11:eaat4285. doi: 10.1126/scisignal.aat4285

39. Kanehisa M, Sato Y, Kawashima M, Furumichi M, Tanabe M. KEGG as a reference resource for gene and protein annotation. *Nucleic Acids Res*. (2016) 44:D457–62. doi: 10.1093/nar/gkv1070

frontiers | Frontiers in Neurology

TYPE Original Research
PUBLISHED 19 June 2024
DOI 10.3389/fneur.2024.1361888

Check for updates

OPEN ACCESS

EDITED BY
Pradeep Kumar,
All India Institute of Medical Sciences, India

REVIEWED BY
Mingchao Fan,
The Affiliated Hospital of Qingdao University, China
Yu Li,
The First Affiliated Hospital of Kunming Medical University, China
Yunlin Chen,
Second Affiliated Hospital of Chongqing Medical University, China

*CORRESPONDENCE
Jianguo Xu
✉ xujg@scu.edu.cn
Min He
✉ hemin19910306@wchscu.cn

RECEIVED 27 December 2023
ACCEPTED 24 May 2024
PUBLISHED 19 June 2024

CITATION
Wang R, Rong J, Xu J and He M (2024) A prognostic model incorporating the albumin-corrected anion gap in patients with aneurysmal subarachnoid hemorrhage. *Front. Neurol.* 15:1361888. doi: 10.3389/fneur.2024.1361888

COPYRIGHT
© 2024 Wang, Rong, Xu and He. This is an open-access article distributed under the terms of the Creative Commons Attribution License (CC BY). The use, distribution or reproduction in other forums is permitted, provided the original author(s) and the copyright owner(s) are credited and that the original publication in this journal is cited, in accordance with accepted academic practice. No use, distribution or reproduction is permitted which does not comply with these terms.

A prognostic model incorporating the albumin-corrected anion gap in patients with aneurysmal subarachnoid hemorrhage

Ruoran Wang[1], Juan Rong[2], Jianguo Xu[1]* and Min He[3]*

[1]Department of Neurosurgery, West China Hospital, Sichuan University, Chengdu, Sichuan, China, [2]West China Centre of Excellence for Pancreatitis, Institute of Integrated Traditional Chinese and Western Medicine, West China Hospital, Sichuan University, Chengdu, Sichuan, China, [3]Department of Critical Care Medicine, West China Hospital, Sichuan University, Chengdu, Sichuan, China

Background: Aneurysmal subarachnoid hemorrhage (aSAH) patients typically have poor prognoses. The anion gap (AG) has been proven to correlate with mortality in various critically ill patients. However, hypoalbuminemia can lead to underestimations of the true anion gap levels. This study was conducted to verify the prognostic value of single AG and albumin-corrected anion gap (ACAG) among aSAH patients.

Methods: Significant factors in the univariate logistic regression analysis were included in the multivariate logistic regression analysis to explore the risk factors for mortality in aSAH patients and to confirm the independent relationship between ACAG and mortality. The restricted cubic spline (RCS) was used to visually show the relationship between ACAG level and mortality risk of aSAH patients. The predictive model for mortality was developed by incorporating significant factors into the multivariate logistic regression analysis. The prognostic value of ACAG and the developed model was evaluated by calculating the area under the receiver operating characteristics curve (AUC).

Results: Among 710 aSAH patients, a 30-day mortality was observed in 20.3% of the cases. A positive relationship was demonstrated between the ACAG level and mortality in aSAH patients using the RCS curve. The multivariate logistic regression analysis helped discover that only six factors were finally and independently related to mortality of aSAH patients after adjusting for confounding effects, including the Hunt–Hess scale score ($p = 0.006$), surgical options ($p < 0.001$), white blood cell count ($p < 0.001$), serum chloride levels ($p = 0.023$), ACAG ($p = 0.039$), and delayed cerebral ischemia ($p < 0.001$). The AUC values for the AG, albumin, and ACAG in predicting mortality among aSAH patients were 0.606, 0.536, and 0.617, respectively. A logistic regression model, which includes the Hunt–Hess scale score, surgical options, white blood cell count, serum chloride levels, ACAG, and delayed cerebral ischemia, achieved an AUC of 0.911 for predicting mortality.

Conclusion: The ACAG is an effective prognostic marker for aSAH patients. A prognostic model incorporating ACAG could help clinicians evaluate the risk of poor outcomes among aSAH patients, thereby facilitating the development of personalized therapeutic strategies.

KEYWORDS

serum anion gap, albumin, aneurysmal subarachnoid hemorrhage, prognosis, marker

1 Introduction

With a reported annual incidence of 9.1 per 100,000 people in the world, aneurysmal subarachnoid hemorrhage (aSAH) is a type of hemorrhagic stroke with mortality ranging from 8.3% to 66.7% (1, 2). The high mortality of aSAH patients is attributable to both the initial severity of hemorrhage and the subsequent complications during hospitalizations (3). Acid-base disturbance and electrolyte disorder are prevalent among aSAH patients and correlate with the prognosis of aSAH patients (4–6). Evaluating the risk and severity of these disturbances is helpful for clinicians in the risk stratification of aSAH patients and for correcting these disturbances.

As an index for diagnosing and distinguishing metabolic acidosis, the anion gap (AG) is a comprehensive and readily available marker of acid-base balance calculated based on the following formula: AG = $[Na^+$ (mmol/L) + K^+ (mmol/L)] – $[Cl^-$(mmol/L) + HCO_3^- (mmol/L)]. The AG has been considered a marker of tissue hypoperfusion and has been confirmed to be associated with mortality due to various diseases, including acute pancreatitis, acute myocardial infarction, congestive heart failure, and sepsis (7–11). However, AG levels can be underestimated with hypoalbuminemia. To address this, the albumin-corrected anion gap (ACAG) was developed to more accurately reflect true AG levels by accounting for the influence of albumin on measuring the true level of AG. Although some studies have explored the value of AG in risk stratification for stroke patients, including those diagnosed with ischemic stroke, intracerebral hemorrhage, or intracerebral infarction (12–14), only two studies have confirmed that AG is effective in the risk stratification of subarachnoid hemorrhage patients. These studies did not evaluate the accurate prognostic value of ACAG or establish a prognostic model incorporating it (15, 16). Therefore, we conducted this study to compare the different prognostic values between AG and ACAG and to develop a prognostic model for aSAH patients using ACAG.

2 Materials and methods

2.1 Patients

Patients confirmed with ruptured aneurysms and those receiving treatments in the West China Hospital, Sichuan University, between 1 January 2017 and 31 June 2019 were enrolled in this observational study. Some aSAH patients were excluded from this study to ensure the reliability of the conclusions: (1) patients transferred from other medical centers or admitted to our hospital 48 h after the onset of typical symptoms for aneurysm rupture (n = 8) and (2) patients without a history of albumin, AG, or other needed laboratory values (n = 27). A total of 710 aSAH patients were eventually enrolled in the study after screening (Figure 1). This observational study was conducted with the approval of the ethical review board of West China Hospital (2021–1684) and abided by the Declaration of Helsinki.

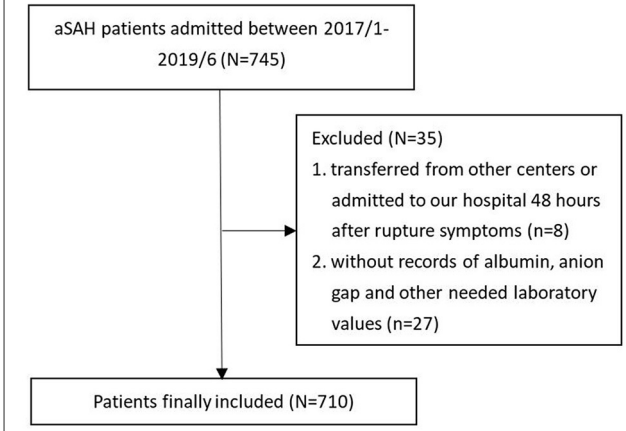

FIGURE 1
Process of aSAH patients screening.

2.2 Data collection

Demographical information, including age, gender, history of smoking, history of alcoholism, and history of comorbidities such as diabetes mellitus and hypertension, was recorded. Initial blood pressure on admission and conventional clinical scores specified on aSAH patients, including the World Federation Neurosurgical Society (WFNS) score, the Hunt–Hess scale score, and the modified Fisher (mFisher) scale score, were collected. Information such as the location of the aneurysm, the presence of multiple aneurysms, and the occurrence of intraventricular hemorrhage was confirmed based on radiological findings. The values of white blood cell count, hemoglobin, albumin, serum creatinine, blood urea nitrogen, serum sodium, serum potassium, serum chloride, serum calcium, and serum AG were collected from laboratory records analyzing the first blood sample after admission (within 6 h after admission). Delayed cerebral ischemia was diagnosed based on the following process: the existence of a new focal functional defect (hemiplegia, aphasia, apraxia, hemianopsia, or neglect) or a decrease in the Glasgow Coma Scale (GCS) by at least two points, excluding other causes of secondary neurological deterioration such as fever, infectious complications, hydrocephalus, seizures, respiratory failure, or electrolyte disorders. The primary outcome of this study was 30-day mortality. The follow-up using telephone interviews lasted until 1 month after the aneurysm rupture.

2.3 Statistical analysis

Continuous variables were shown as mean ± standard deviation (normally distributed variables) and median (interquartile range) (non-normally distributed variables). Categorical variables were shown as counts (percentages). Patients were divided into two groups (survivors and non-survivors) based on their 30-day survival. Differences in the variables between these two groups were compared using χ^2 tests or the Fisher test (categorical variables), the Independent Student's t-test

TABLE 1 Baseline characteristics of included aSAH patients.

Variables	Overall patients ($n = 710$)	Survivors ($n = 566$, 79.7%)	Non-survivors ($n = 144$, 20.3%)	p
Age (year)	55 (49–65)	55 (48–64)	61 (51–69)	0.003
Male gender (%)	245 (34.5%)	196 (34.6%)	49 (34.0%)	0.892
Smoking (%)	125 (17.6%)	104 (18.4%)	21 (14.6%)	0.286
Alcoholism (%)	107 (15.1%)	89 (15.7%)	18 (12.500%)	0.334
Diabetes mellitus (%)	34 (4.8%)	29 (5.1%)	5 (3.5%)	0.407
Hypertension (%)	306 (43.1%)	251 (44.3%)	55 (38.2%)	0.183
Systolic blood pressure (mmHg)	146 (129–166)	147 (129–165)	141 (126–168)	0.491
Diastolic blood pressure (mmHg)	85 (76–95)	85 (76–95)	86 (78–95)	0.318
WFNS	2 (2–4)	2 (1–4)	4 (4–5)	<0.001
Hunt Hess	2 (2–3)	2 (2–3)	4 (3–4)	<0.001
mFisher	4 (2–4)	3 (2–4)	4 (3–4)	<0.001
Location (%)				0.091
Anterior circulation	655 (92.3%)	527 (93.1%)	128 (88.9%)	
Posterior circulation	55 (7.7%)	39 (6.9%)	16 (11.1%)	
Multiple aneurysm (%)	68 (9.6%)	50 (8.8%)	18 (12.5%)	0.182
Laboratory examination				
White blood cell ($10^{9/L}$)	10.34 (7.99–13.52)	9.90 (7.71–12.48)	13.20 (9.70–17.25)	<0.001
Hemoglobin (mg/L)	125 (110–136)	125 (110–135)	125 (111–138)	0.530
Albumin (mg/dL)	3.97 (3.50–4.28)	3.99 (3.54–4.28)	3.94 (3.38–4.25)	0.182
Serum creatinine (mg/L)	57 (49–70)	56 (48–66)	68 (55–81)	<0.001
Blood urea nitrogen (mg/L)	4.33 (3.50–5.50)	4.30 (3.40–5.40)	4.50 (3.67–5.84)	0.027
Sodium (mol/L)	139.6 (137.3–142.9)	139.5 (137.3–142.1)	140.8 (137.3–146.2)	0.002
Potassium (mol/L)	3.76 (3.50–4.08)	3.76 (3.51–4.07)	3.78 (3.43–4.11)	0.757
Chloride (mol/L)	101.9 (98.5–105.6)	101.7 (98.5–105.0)	103.5 (99.2–110.4)	<0.001
Calcium (mol/L)	2.16 ± 0.13	2.16 ± 0.12	2.15 ± 0.15	0.621
AG (mol/L)	19.63 ± 3.55	19.32 ± 3.27	20.85 ± 4.26	<0.001
ACAG (mol/L)	20.78 (18.65–23.00)	20.60 (18.40–22.58)	21.85 (19.35–24.68)	<0.001
Intraventricular hemorrhage (%)	309 (43.5%)	232 (41.0%)	77 (53.5%)	0.007
Delayed cerebral ischemia (%)	117 (16.5%)	68 (12.0%)	49 (34.0%)	<0.001
Surgical options				<0.001
None	113 (15.9%)	44 (7.8%)	69 (47.9%)	
Clip	524 (73.8%)	463 (81.8%)	61 (42.4%)	
Coil	73 (10.3%)	59 (10.4%)	14 (9.722)	
Length of ICU stay (day)	3 (0–9)	3 (0–9)	4 (0–10)	0.119
Length of hospital stay (day)	12 (9–19)	13 (10–19)	7 (3–13)	<0.001

WFNS, World Federation of Neurosurgical Societies; mFisher, modified Fisher; AG, anion gap; ACAG, albumin corrected anion gap.

(normally distributed variables), and the Mann—Whitney U-test (non-normally distributed variables). The restricted cubic spline (RCS) was used to visually demonstrate the relationship between the ACAG level and the mortality risk of aSAH patients. The multivariate logistic regression analysis included significant factors in the univariate logistic regression analysis to explore risk factors for mortality in aSAH patients and to confirm the independent relationship between ACAG and mortality. The predictive model for mortality was developed by incorporating significant factors into the multivariate logistic regression analysis. The prognostic value of ACAG and the developed model was evaluated by calculating the area under the receiver operating characteristics curve (AUC). The Z test was used to compare the AUC between the model and other scores.

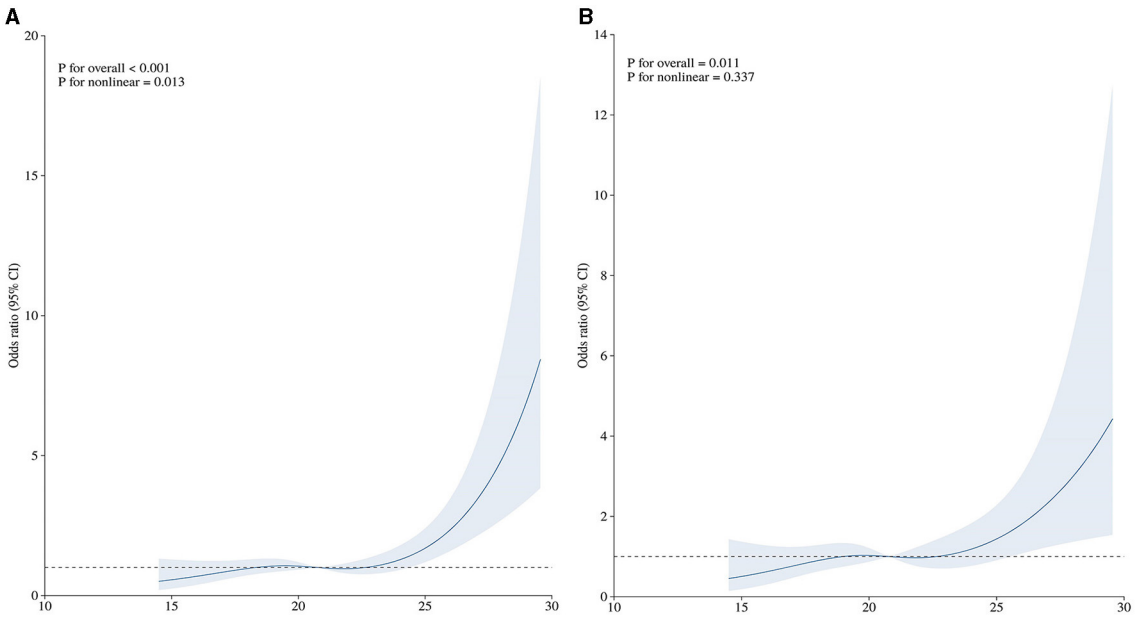

FIGURE 2
(A) Unadjusted association between ACAG and the mortality of aSAH patients. **(B)** Adjusted association between ACAG and the mortality of aSAH patients.

A two-sided $p < 0.05$ was defined as statistically significant. Analyses were performed using SPSS 22.0 Windows software (SPSS, Inc., Chicago, IL) and R software (Version 3.6.1).

3 Results

3.1 Baseline comparison between survivors and non-survivors

A total of 144 aSAH patients experienced 30-day mortality, including 710 patients with a mortality rate of 20.3% (Table 1). Non-survivors had older age ($p = 0.003$), higher WFNS score ($p < 0.001$), higher Hunt-Hess score ($p < 0.001$), and higher mFisher score ($p < 0.001$) than survivors. Compared to the survivors, laboratory examinations showed that white blood cell count ($p < 0.001$), serum creatinine ($p < 0.001$), blood urea nitrogen ($p = 0.027$), serum sodium ($p = 0.002$), serum chloride ($p < 0.001$), AG ($p < 0.001$), and ACAG ($p < 0.001$) were all higher in the non-survivors. In contrast, the albumin level did not show statistical significance between the survivors and the non-survivors. Compared to the survivors, the non-survivors had a higher incidence of intraventricular hemorrhage ($p = 0.007$), delayed cerebral ischemia ($p < 0.001$), and a longer length of hospital stay ($p < 0.001$).

3.2 Association between ACAG and the mortality of aSAH patients

The positive relationship between the ACAG level and the mortality of aSAH patients is demonstrated using the unadjusted RCS curve shown in Figure 2A. The univariate logistic regression indicated that age ($p = 0.001$), WFNS score ($p < 0.001$), Hunt–Hess scale score ($p < 0.001$), mFisher scale score ($p < 0.001$), white blood cell count ($p < 0.001$), serum creatinine ($p = 0.007$), blood urea nitrogen ($p = 0.046$), serum sodium ($p < 0.001$), serum chloride ($p < 0.001$), ACAG ($p < 0.001$), intraventricular hemorrhage ($p = 0.007$), delayed cerebral ischemia ($p < 0.001$), surgical options ($p < 0.001$) were significantly correlated with the mortality of aSAH patients (Table 2). The multivariate logistic regression discovered that only six factors were finally and independently related to the mortality of aSAH patients after adjusting for confounding effects, including Hunt-Hess scale score ($p = 0.006$), surgical options ($p < 0.001$), white blood cells ($p < 0.001$), serum chloride ($p = 0.023$), ACAG ($p = 0.039$), and delayed cerebral ischemia ($p < 0.001$). After adjusting for the other five significant factors, the relationship between the ACAG level and the mortality of aSAH patients was still positive, as shown in Figure 2B.

3.3 Prognostic value of ACGA in aSAH patients

The AUC values for the AG, albumin, and ACAG in predicting the mortality of aSAH patients were 0.606, 0.536, and 0.617, respectively (Figure 3A; Table 3). The AUC values for conventional scoring systems, including the WFNS, Hunt–Hess, and mFisher scale scores, were 0.804, 0.817, and 0.616. A logistic regression model composed of the Hunt–Hess scale score, mFisher scale score, white blood cell count, serum chloride levels, ACAG, and delayed cerebral ischemia achieved an AUC

TABLE 2 Univariate and multivariate logistic regression analysis of risk factors for mortality in aSAH patients.

	Unadjusted analysis			Adjusted analysis		
	OR	95% CI	*P*-value	OR	95% CI	*P*-value
Age	1.026	1.01–1.043	0.001	1.019	0.996–1.043	0.110
Male gender	0.974	0.662–1.432	0.892			
Smoking	0.758	0.456–1.262	0.287			
Alcoholism	0.766	0.445–1.318	0.335			
Diabetes mellitus	0.666	0.253–1.752	0.410			
Hypertension	0.776	0.533–1.128	0.184			
Systolic blood pressure	0.998	0.991–1.006	0.676			
Diastolic blood pressure	1.008	0.995–1.020	0.221			
WFNS	2.749	2.289–3.301	<0.001	1.079	0.684–1.704	0.744
Hunt Hess	3.925	3.098–4.973	<0.001	2.277	1.275–4.114	0.006
mFisher	1.646	1.334–2.032	<0.001	1.340	0.923–1.967	0.129
Location						
Anterior circulation	1.000	Reference				
Posterior circulation	1.689	0.915–3.118	0.094			
Multiple aneurysm	1.474	0.831–2.614	0.184			
White blood cell	1.177	1.129–1.228	<0.001	1.127	1.065–1.196	<0.001
Hemoglobin	1.002	0.994–1.011	0.621			
Serum creatinine	1.008	1.002–1.013	0.007	1.004	0.992–1.012	0.515
Blood urea nitrogen	1.064	1.001–1.132	0.046	0.905	0.773–1.023	0.199
Sodium	1.076	1.045–1.107	<0.001	0.984	0.896–1.078	0.725
Potassium	1.384	0.973–1.969	0.070			
Chloride	1.073	1.046–1.100	<0.001	1.101	1.015–1.198	0.023
Calcium	0.666	0.159–2.784	0.577			
ACAG	1.158	1.097–1.222	<0.001	1.088	1.006–1.181	0.039
Intraventricular hemorrhage	1.655	1.145–2.390	0.007	1.016	0.502–2.07	0.966
Delayed cerebral ischemia	3.777	2.463–5.794	<0.001	4.571	2.517–8.398	<0.001
Surgical options						
None	1.000	Reference				
Clip	0.084	0.053, 0.133	<0.001	0.075	0.039–0.14	<0.001
Coil	0.151	0.076, 0.303	<0.001	0.122	0.046–0.298	<0.001

WFNS, World Federation of Neurosurgical Societies; mFisher, modified Fisher; ACAG, albumin corrected anion gap.

of 0.911, which was significantly higher than that of the WFNS score ($Z = 6.305$, $p < 0.001$), the Hunt–Hess scale score ($Z = 6.028$, $p < 0.001$), the mFisher scale score ($Z = 12.212$, $p < 0.001$), and single ACAG ($Z = 10.466$, $p < 0.001$). The nomogram and calibration plot for this model are shown in Figures 3B, C.

4 Discussion

The prevalence of delayed cerebral ischemia and mortality was 16.5% and 20.3%, which was similar to the recently reported incidence (17–20). The high mortality rate makes risk evaluation crucial. As a readily available marker of acid-base balance, AG

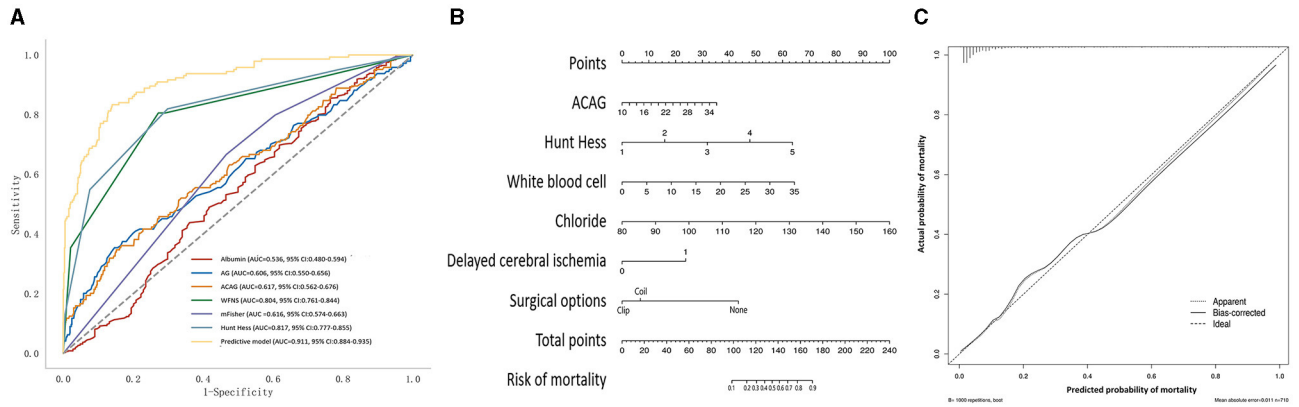

FIGURE 3
(A) The receiver operating characteristic curve of the prognostic model for the mortality of aSAH patients. **(B)** Nomogram of the prognostic model for the mortality of aSAH. **(C)** Calibration plot of the prognostic model for the mortality of aSAH.

TABLE 3 Value of the predictive model and ACAG for predicting the mortality of aSAH patients.

	30-day mortality					
	AUC	95% CI	Sensitivity	Specificity	Youden index	Cut off
Anion gap	0.606	0.551–0.662	0.354	0.853	0.208	22.6
Albumin	0.536	0.480–0.592	0.855	0.236	0.091	32.6
ACAG	0.617	0.563–0.670	0.347	0.848	0.195	23.8
WFNS	0.804	0.760–0.848	0.806	0.728	0.533	4
Hunt Hess	0.817	0.774–0.859	0.819	0.701	0.521	3
mFisher	0.616	0.567–0.664	0.667	0.534	0.200	4
Predictive model	0.911	0.884–0.935	0.833	0.860	0.694	0.208

AUC, area under the receiver operating characteristic curve; CI, confidence interval; WFNS, World Federation of Neurosurgical Societies; ACAG, albumin corrected anion gap.
The predictive model was composed of Hunt Hess, surgical options, white blood cell, serum chloride, ACAG, delayed cerebral ischemia.

may be beneficial for the risk evaluation of prognoses among aSAH patients. The results of this study showed that, among aSAH patients, the non-survivors had higher levels of AG and ACAG than the survivors. The accuracy of ACAG in predicting the mortality of aSAH patients was higher than that of the original AG. As a marker identifying metabolic acidosis, the AG increased due to the overproduction of organic acids or the reduced renal excretion of anion (21). It is worth noting that aSAH leads to acidosis through multiple mechanisms, including hypoxia of cerebral tissue, accumulation of acidic metabolites, and other electrolyte disorders such as hypokalemia and hypocalcemia (4–6). Additionally, impaired renal function, which is commonly observed among aSAH patients, causes the accumulation of acidic metabolites (22–24). Therefore, the increased AG after aSAH may comprehensively reflect the abnormal metabolic state and renal dysfunction and thus contribute to the higher risk of mortality. Additionally, it could be deduced that elevated serum sodium levels cause an increase in AG based on the following formula: AG = $[Na^+$ (mmol/L) + K^+ (mmol/L)] – $[Cl^-$(mmol/L) + HCO_3^- (25). The detrimental effect of hypernatremia on the prognosis of aSAH patients has been proven by several studies (6, 26–28). Finally, high serum AG levels have been found to be related to a high level of inflammatory biomarkers, including white blood cells and C-reactive protein (29). The inflammatory response after aSAH plays an important role in the pathophysiological process of brain injury and extracranial organ dysfunction (30–33).

Although many studies have explored the prognostic value of AG in various diseases, including acute pancreatitis, acute myocardial infarction, congestive heart failure, and sepsis, they have not compared the distinct impacts of single AG vs. ACAG (7–11). AG levels are often underestimated in cases of hypoalbuminemia, which commonly occurs during hospitalizations of aSAH patients (34). This underestimation may obscure the actual effect of acidosis on the prognosis of aSAH patients. Moreover, two recent studies that used AG for risk stratification in subarachnoid hemorrhage patients did not explore the supplementary effect of albumin correction or develop a prognostic model using ACAG (15, 16). The prognostic value of the ACAG was higher than that of the single AG in our study. When the measured AG is at the same level, a lower albumin level indicates a higher ACAG. This finding indicates that a high ACAG also partially reflects the effect of hypoalbuminemia on the prognosis of aSAH patients. Previous studies showed that hypoalbuminemia is associated with poor prognosis and complications after aSAH, including pneumonia, cerebral vasospasm, and delayed cerebral ischemia (35–38).

In addition to the AG, blood gas analysis could also be used to evaluate acid-base disturbances. The result of the blood gas

analysis could be disturbed by compensatory respiratory alkalosis. Compared with the blood gas analysis needing arterial puncture, the AG is less expensive and more easily available in situations with limited resources (39). After being corrected using the albumin, the ACAG is useful for clinicians when evaluating the risk of poor prognosis among aSAH patients with relatively fewer resources.

Some limitations of this study should be noted. First, only the ACAG at admission was recorded, and any changes in ACAG were not tracked over time, so we could not evaluate the prognostic value of ACAG at different time points or ACAG changes among aSAH patients. Second, the record of blood lactate levels in our patient cohort was not complete, limiting our ability to compare the different values of lactate and ACAG. Third, only the survival outcome (30-day mortality) was analyzed; however, no other outcomes, including functional status and long-term cognitive status, were analyzed. The association between functional outcome and ACAG has been analyzed in our preliminary study, but we found that ACAG was not effective in predicting the functional outcome and thus did not include these results. Fourth, some confounders influencing the level of AG were not analyzed, including renal excretory function, the intravenous infusion volume, and the use of dehydration drugs. Fifth, some aneurysm-related morphological information, such as aneurysm size and aneurysm shape, was not collected. Our developed model may be improved after adding these variables. Finally, this study was conducted using the data from a single medical center in the southwestern region of China, highlighting the need for future studies in other regions and with larger sample sizes to validate our findings.

5 Conclusion

The ACAG is a prognostic marker for aSAH patients and could guide clinicians in correcting acid-base imbalances. A prognostic model incorporating ACAG could help clinicians evaluate the risk of poor outcomes among aSAH patients, thereby facilitating the development of personalized therapeutic strategies.

Data availability statement

The raw data supporting the conclusions of this article will be made available by the authors, without undue reservation.

Ethics statement

The studies involving humans were approved by the Ethics Committee of West China Hospital. The studies were conducted in accordance with the local legislation and institutional requirements. The participants provided their written informed consent to participate in this study.

Author contributions

RW: Conceptualization, Data curation, Formal analysis, Writing – original draft. JR: Data curation, Formal analysis, Writing – original draft. MH: Writing – review & editing. JX: Writing – review & editing.

Funding

The author(s) declare that financial support was received for the research, authorship, and/or publication of this article. This study was funded by 1.3.5 project for disciplines of excellence-Clinical Research Incubation Project, West China Hospital, Sichuan University (2020HXFH036), Knowledge Innovation Program of the Chinese Academy of Sciences (JH2022007), General Program of the National Natural Science Foundation of China (82173175), and Sichuan Science and Technology Program (24QYCX0411 and 2024YFHZ0070).

Conflict of interest

The authors declare that the research was conducted in the absence of any commercial or financial relationships that could be construed as a potential conflict of interest.

Publisher's note

All claims expressed in this article are solely those of the authors and do not necessarily represent those of their affiliated organizations, or those of the publisher, the editors and the reviewers. Any product that may be evaluated in this article, or claim that may be made by its manufacturer, is not guaranteed or endorsed by the publisher.

References

1. de Rooij NK, Linn FH, van der Plas JA, Algra A, Rinkel GJ. Incidence of subarachnoid haemorrhage: a systematic review with emphasis on region, age, gender and time trends. *J Neurol Neurosurg Psychiatr.* (2007) 78:1365–72. doi: 10.1136/jnnp.2007.117655

2. Nieuwkamp DJ, Setz LE, Algra A, Linn FH, de Rooij NK, et al. Changes in case fatality of aneurysmal subarachnoid haemorrhage over time, according to age, sex, and region: a meta-analysis. *Lancet Neurol.* (2009) 8:635–42. doi: 10.1016/S1474-4422(09)70126-7

3. Li R, Lin F, Chen Y, Lu J, Han H, Yan D, et al. In-hospital complication-related risk factors for discharge and 90-day outcomes in patients with aneurysmal subarachnoid hemorrhage after surgical clipping and endovascular coiling: a propensity score-matched analysis. *J Neurosurg.* (2021) 137:1–12. doi: 10.3171/2021.10.JNS211484

4. Alimohamadi M, Saghafinia M, Alikhani F, Danial Z, Shirani M, Amirjamshidi A, et al. Impact of electrolyte imbalances on the outcome of aneurysmal subarachnoid hemorrhage: a prospective study. *Asian J Neurosurg.* (2016) 11:29–33. doi: 10.4103/1793-5482.154978

5. Langer T, Zadek F, Carbonara M, Caccioppola A, Brusatori S, Zoerle T, et al. Cerebrospinal fluid and arterial acid-base equilibrium of spontaneously breathing patients with aneurismal subarachnoid hemorrhage. *Neurocrit Care.* (2022) 37:102–10. doi: 10.1007/s12028-022-01450-1

6. Qureshi AI, Suri MF, Sung GY, Straw RN, Yahia AM, Saad M, et al. Prognostic significance of hypernatremia and hyponatremia among patients with aneurysmal subarachnoid hemorrhage. *Neurosurgery.* (2002) 50:749–55. doi: 10.1097/00006123-200204000-00012

7. Mohr NM, Vakkalanka JP, Faine BA, Skow B, Harland KK, Dick-Perez R, et al. Serum anion gap predicts lactate poorly, but may be used to identify sepsis patients at risk for death: a cohort study. *J Crit Care.* (2018) 44:223–28. doi: 10.1016/j.jcrc.2017.10.043

8. Hu T, Zhang Z, Jiang Y. Albumin corrected anion gap for predicting in-hospital mortality among intensive care patients with sepsis: a retrospective propensity score matching analysis. *Clin Chim Acta.* (2021) 521:272–77. doi: 10.1016/j.cca.2021.07.021

9. Jian L, Zhang Z, Zhou Q, Duan X, Xu H, Ge L, et al. Association between albumin corrected anion gap and 30-day all-cause mortality of critically Ill patients with acute myocardial infarction: a retrospective analysis based on the mimic-IV database. *BMC Cardiovasc Disord.* (2023) 23:211. doi: 10.1186/s12872-023-03200-3

10. Lu J, Zhong L, Yuan M, Min J, Xu Y. Association between serum anion gap and all-cause mortality in patients with acute myocardial infarction: a retrospective study based on mimic-IV database. *Heliyon.* (2023) 9:e17397. doi: 10.1016/j.heliyon.2023.e17397

11. Li P, Shi L, Yan X, Wang L, Wan D, Zhang Z, et al. Albumin corrected anion gap and the risk of in-hospital mortality in patients with acute pancreatitis: a retrospective cohort study. *J Inflamm Res.* (2023) 16:2415–22. doi: 10.2147/JIR.S412860

12. Liu X, Feng Y, Zhu X, Shi Y, Lin M, Song X, et al. Serum anion gap at admission predicts all-cause mortality in critically ill patients with cerebral infarction: evidence from the mimic-III database. *Biomarkers.* (2020) 25:725–32. doi: 10.1080/1354750X.2020.1842497

13. Jhou HJ, Chen PH, Yang LY, Chang SH, Lee CH. Plasma anion gap and risk of in-hospital mortality in patients with acute ischemic stroke: analysis from the mimic-IV database. *J Pers Med.* (2021) 11:10004. doi: 10.3390/jpm11101004

14. Shen J, Li DL, Yang ZS, Zhang YZ. Anion gap predicts the long-term neurological and cognitive outcomes of spontaneous intracerebral hemorrhage. *Eur Rev Med Pharmacol Sci.* (2022) 26:3230–36. doi: 10.26355/eurrev_202205_28741

15. Ji L, Tong X, Wang K, Jiang Z, Liu A. Plasma anion gap and risk of in-hospital mortality in patients with spontaneous subarachnoid hemorrhage. *Front Neurol.* (2022) 13:1008030. doi: 10.3389/fneur.2022.1008030

16. Zhong C, Ye M, Hu L, Liu J. Association between high serum anion gap and all-cause mortality in non-traumatic subarachnoid hemorrhage: a retrospective analysis of the mimic-IV database. *Front Neurol.* (2022) 13:922099. doi: 10.3389/fneur.2022.922099

17. Labib H, Tjerkstra MA, Coert BA, Post R, Vandertop WP, Verbaan D, et al. Sodium and its impact on outcome after aneurysmal subarachnoid hemorrhage in patients with and without delayed cerebral ischemia. *Crit Care Med.* (2024) 52:752–63. doi: 10.1097/CCM.0000000000006182

18. Chikh K, Tonon D, Triglia T, Lagier D, Buisson A, Alessi MC, et al. Early metabolic disruption and predictive biomarkers of delayed-cerebral ischemia in aneurysmal subarachnoid hemorrhage. *J Proteome Res.* (2024) 23:316–28. doi: 10.1021/acs.jproteome.3c00575

19. Balança B, Bouchier B, Ritzenthaler T. The management of delayed cerebral ischemia after aneurysmal subarachnoid hemorrhage. *Rev Neurol.* (2022) 178:64–73. doi: 10.1016/j.neurol.2021.11.006

20. Han W, Yi HJ, Shin DS, Kim BT. Pan-immune-inflammation value predict delayed cerebral ischemia in patients with aneurysmal subarachnoid hemorrhage. *J Clin Neurosci.* (2024) 121:47–52. doi: 10.1016/j.jocn.2024.02.003

21. Kraut JA, Madias NE. Serum anion gap: its uses and limitations in clinical medicine. *Clin J Am Soc Nephrol.* (2007) 2:162–74. doi: 10.2215/CJN.03020906

22. Guillemin L, Goronflot T, Desal H, Rozec B, Lakhal K. Early acute kidney injury in patients with non-traumatic subarachnoid hemorrhage who undergo catheter angiography: incidence, associated risk factors and impact on outcome. *J Stroke Cerebrovasc Dis.* (2022) 31:106488. doi: 10.1016/j.jstrokecerebrovasdis.2022.106488

23. Tujjar O, Belloni I, Hougardy JM, Scolletta S, Vincent JL, Creteur J, et al. acute kidney injury after subarachnoid hemorrhage. *J Neurosurg Anesthesiol.* (2017) 29:140–49. doi: 10.1097/ANA.0000000000000270

24. Eagles ME, Powell MF, Ayling OG, Tso MK, Macdonald RL. Acute kidney injury after aneurysmal subarachnoid hemorrhage and its effect on patient outcome: an exploratory analysis. *J Neurosurg.* (2019) 133:1–8. doi: 10.3171/2019.4.JNS19103

25. Miller PM, Dufour DR. Extreme hypernatremia with markedly increased anion gap. *Clin Chem.* (2015) 61:1422. doi: 10.1373/clinchem.2015.242313

26. Kumar AB, Shi Y, Shotwell MS, Richards J, Ehrenfeld JM. Hypernatremia is a significant risk factor for acute kidney injury after subarachnoid hemorrhage: a retrospective analysis. *Neurocrit Care.* (2015) 22:184–91. doi: 10.1007/s12028-014-0067-8

27. Jin D, Jin S, Liu B, Ding Y, Zhou F, Jin Y, et al. Association between serum sodium and in-hospital mortality among critically ill patients with spontaneous subarachnoid hemorrhage. *Front Neurol.* (2022) 13:1025808. doi: 10.3389/fneur.2022.1025808

28. Liu J, Li J, Zhang Q, Wang L, Wang Y, Zhang J, et al. Association between serum sodium levels within 24 h of admission and all-cause mortality in critically ill patients with non-traumatic subarachnoid hemorrhage: a retrospective analysis of the mimic-IV database. *Front Neurol.* (2023) 14:1234080. doi: 10.3389/fneur.2023.1234080

29. Farwell WR, Taylor EN. Serum anion gap, bicarbonate and biomarkers of inflammation in healthy individuals in a national survey. *Cmaj.* (2010) 182:137–41. doi: 10.1503/cmaj.090329

30. Wu F, Liu Z, Li G, Zhou L, Huang K, Wu Z, et al. Inflammation and oxidative stress: potential targets for improving prognosis after subarachnoid hemorrhage. *Front Cell Neurosci.* (2021) 15:739506. doi: 10.3389/fncel.2021.739506

31. Nie Z, Lin F, Li R, Chen X, Zhao Y, A. Pooled analysis of preoperative inflammatory biomarkers to predict 90-day outcomes in patients with an aneurysmal subarachnoid hemorrhage: a single-center retrospective study. *Brain Sci 13.* (2023). doi: 10.3390/brainsci13020257

32. Peng L, Li X, Li H, Zhong Y, Lian J, Gao H, et al. Relationship between peripheral blood inflammatory factors and prognosis of subarachnoid hemorrhage: a meta-analysis. *Eur Neurol.* (2023) 86:193–206. doi: 10.1159/000530208

33. Rostgaard N, Olsen MH, Capion T, MacAulay N, Juhler M. Inflammatory markers as predictors of shunt dependency and functional outcome in patients with aneurysmal subarachnoid hemorrhage. *Biomedicines 11.* (2023). doi: 10.3390/biomedicines11040997

34. Behrouz R, Godoy DA, Topel CH, Birnbaum LA, Caron JL, Grandhi R, et al. Early hypoalbuminemia is an independent predictor of mortality in aneurysmal subarachnoid hemorrhage. *Neurocrit Care.* (2016) 25:230–6. doi: 10.1007/s12028-016-0259-5

35. Shang F, Zhao H, Cheng W, Qi M, Wang N, Qu X, et al. Predictive value of the serum albumin level on admission in patients with spontaneous subarachnoid hemorrhage. *Front Surg.* (2021) 8:719226. doi: 10.3389/fsurg.2021.719226

36. Wang P, Zhang Y, Wang X, Peng L, Jia L, Li T, et al. Association between serum albumin and hospital-acquired infections after aneurysmal subarachnoid hemorrhage. *Neurocrit Care.* (2022) 37:424–34. doi: 10.1007/s12028-021-01421-y

37. Dicpinigaitis AJ, Galea VP, Sursal T, Al-Shammari H, Feldstein E, Ali S, et al. Low serum albumin as a risk factor for delayed cerebral ischemia following aneurysmal subarachnoid hemorrhage: eicu collaborative research database analysis. *J Neurosurg Sci.* (2022). doi: 10.23736/S0390-5616.22.05604-1

38. Chen L, Jin Y, Wang L, Wei K, Li X, Jiang T, et al. Impact of human serum albumin level on symptomatic cerebral vasospasm in patients with aneurysmal subarachnoid hemorrhage. *Neurol Sci.* (2024) 45:213–22. doi: 10.1007/s10072-023-07014-1

39. Glasmacher SA, Stones W. Anion gap as a prognostic tool for risk stratification in critically ill patients - a systematic review and meta-analysis. *BMC Anesthesiol.* (2016) 16:68. doi: 10.1186/s12871-016-0241-y

Frontiers in Neurology

Explores neurological illness to improve patient care

The third most-cited clinical neurology journal explores the diagnosis, causes, treatment, and public health aspects of neurological illnesses. Its ultimate aim is to inform improvements in patient care.

Discover the latest Research Topics

See more →

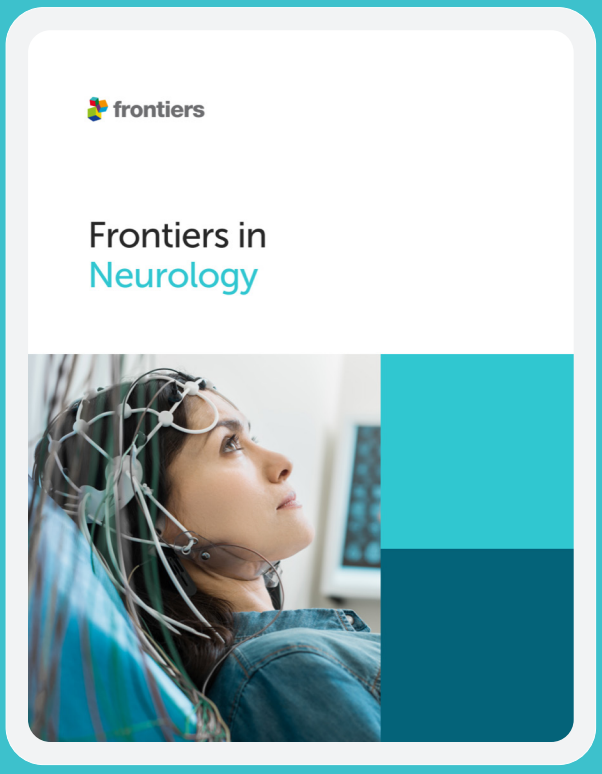

Frontiers

Avenue du Tribunal-Fédéral 34
1005 Lausanne, Switzerland
frontiersin.org

Contact us

+41 (0)21 510 17 00
frontiersin.org/about/contact